Identification of Potent and Selective Inhibitors of the Epithelial Sodium Channel δ

A thesis submitted to the University of Sussex for the degree of Doctor of Philosophy

Victoria Miller

September 2018

I hereby declare that this thesis has not been and will not be, submitted in whole or in part to another University for the award of any other degree.

Signature: ……..

Summary:

Members of the DEG/ENaC family have been recently implicated in the neurodegeneration associated with a number of CNS disease states. More specifically the neuronally-expressed ENaC δ channel has been linked to the integration of ischemia-related signals in inflamed and hypoxic tissues (Ji, et al., 2000; Ji & Benos, 2004). Although a recent study reported clinical efficacy of the prototypical ENaC inhibitor amiloride in multiple sclerosis (Friese, et al., 2007; Vergo, et al., 2011), this drug was optimised for the non-CNS ENaC variant (αβγ). To date, a small number of compounds are described in the literature as ENaC blockers but all share a structural similarity to amiloride. These amiloride analogues all exhibit activity at multiple ion channels and have poor pharmacokinetic properties with respect to CNS penetration.

As such our aim is to identify novel potent and selective inhibitors of the ENaC δ channel which could be used to probe channel function. A heterologous expression system was developed to overexpress the ENaC δβγ channel in a Human Embryonic Kidney (HEK) 293 cell line. This implemented a BacMam baculoviral delivery system to transiently express ENaC δ subunit in HEK293 cell which stably expressed ENaC β and γ subunits, reconstituting channel function. This expression system has been used to establish both a novel membrane potential-based fluorescence assay and an automated electrophysiological-based assay to screen for regulators of ENaC δ channel function. Primary hits have been subsequently triaged using conventional whole cell patch clamp electrophysiology. This has been used to support an SAR-based approach to improve

potency and selectivity in the development of a tool compound to investigate the ENaC δβγ channel.

Key words:- ENaC, neurodegeneration, inhibitor, BacMam, membrane potential, electrophysiology, SAR

Acknowledgements:

This thesis is an account of original work carried out in the laboratories of the Sussex Drug Discovery Centre, School of Life Sciences, Sussex University. The investigation was funded by an MRC Case Award and MRC Confidence in Concept Grant, for which I am extremely grateful.

First and foremost, I would like to thank my supervisors, Prof. Martin Gosling and Prof. John Atack. This work would not have been possible without their guidance and continuous support of my Ph.D research. Their patience, motivation, and immense knowledge have been invaluable. In addition, I would like to thank the other members of the Sussex Drug Discovery Centre, including my fellow Ph.D students, for stimulating discussions, the sharing of knowledge, and all the fun we have had along the way.

My sincere thanks also goes to Dr. Michael Morton, who provided me with the opportunity to work with his team at ApconiX Ltd., giving me access to their laboratory and research facilities. Without his support it would not be possible to conduct the final stages of my research.

Last but not the least, I would like to thank my family- my parents, my brother and my sister- for always encouraging me to embrace new challenges and supporting me throughout writing this thesis. In particular, I will forever be thankful to my partner and biggest cheerleader in life, Jav. He inspires me every day, and I thank him for his mutual recognition that the greatest accompaniment to each celebration or commiseration along my Ph.D journey has been a good bottle of wine.

Contents:

List of Figures:

Figure:

36. Potency of three analogues of UoS-00017907, which were still able to inhibit the ENaC δ channel.
37. Effect of mutating the WYHFHY motif of the ENaC δ subunit on the potency of amiloride, benzamil and UoS-00017907.
38. Effect of mutating the serine residue at position 533 of the ENaC δ subunit on the potency of amiloride, benzamil and UoS-00017907.

Chapter 6.

39. Comparison of extracellular buffers used on the IonWorks platform with the HEK293-ENaC β*γ* cell line.
40. The effect of titrating the baculoviral MOI on the performance of the cell line on the IonWorks platform.
41. The effect of the scanning parameters of the IonWorks on the data reproducibility across the PatchPlate™.
42. Recording in single- hole (HT) mode and Population Patch Clamp™ (PPC) mode.
43. The effect of the cell density in the cell bath on the IonWorks assay.
44. DMSO tolerance of the IonWorks assay.
45. The effect of compound incubation time on pharmacology.
46. Pharmacological validation of IonWorks assay.
47. Data from the IonWorks screen of compounds at 40 µM against the ENaC δβ*γ* channel, analysed using both compound additions for normalisation of each well.
48. Data from the IonWorks screen of compounds at 40 µM against the ENaC δβ*γ* channel, analysed using just the first test compound addition.
49. Correlation of inhibition (%) for each compound from the CUTE Ion Channel library screened using the MP assay and the IonWorks assay.
50. Pharmacological validation of the QPatch assay using the QPatch 16, ApconiX Ltd.

51. Pharmacological validation of the QPatch assay using the QPatch 16, SDDC.
52. Example of instability of assay, observed across both the QPatch 16 and QPatch HTX, SDDC.
53. Hit validation using conventional patch clamp.

List of Tables:

Table:

List of Abbreviations:

+/+	with calcium and magnesium
ABD	amiloride binding domain
ADH	anti-diuretic hormone
Amp	ampicillin
AmpR	amipicillin resistance
BBB	blood-brain barrier
bp	base pairs
cAMP	cyclic adenosine monophosphate
CCD	charge-coupled device
cDNA	complementary deoxyribonucleic acid
CF	cystic fibrosis
CFTR	cystic fibrosis transmembrane conductance regulator
CHO	chinese hamster ovary
cRNA	complementary ribonucleic acid
DEG	degenerin
dH_2O	distilled water
DiBAC4	bis-(1,3-dibutylbarbituric acid)trimethine oxonol
DMSO	dimethyl sulfoxide
DNA	deoxyribonucleic acid
DPBS	Dulbecco's phosphate-buffered saline
EC_{50}	half maximal effective concentration
ECS	extracellular solution
EIPA	5-(n-ethyl-n-isopropyl)amiloride
ENaC	epithelial sodium channel
E_{rev}	reversal potential
E_vB	Evans Blue
FLIPR	fluorescence imaging plate reader
FRET	fluorescence resonance energy transfer
GDSC	genome damage and stability centre
GFP	green fluorescent protein
GOI	gene of interest
HBEC	human bronchial epithelial cells
HEK	human embryonic kidney
HT	high throughput
HTS	high throughput screening
IC_{50}	half maximal inhibitory concentration
ICS	intracellular solution
Kan	kanamycin
KanR	kanamycin resistance

LB	Luria-Bertani
LC-MS	liquid chromatography–mass spectrometry
LTP	long term potentiation
MOI	multiplicity of infection
MS	multiple sclerosis
Murr1	mouse u2af1-rs1 region
Na_v	voltage-gated sodium channel
NCE	new chemical entities
NMDAR	n-methyl-d-aspartate receptor
PBS	phosphate buffered saline
PCR	polymerase chain reaction
pfu	plaque forming units
PHA-1	pseudohypoaldosteronism type 1
PKA	protein kinase a
PMT	photomultiplier
P_o	open probability
PPC	population patch clamp™
ppFEV$_1$	percentage predicted forced expiratory volume in the first second
RT	room temperature
S.O.C	super optimal broth
SAR	structure-activity relationship
SD	standard deviation
SDDC	Sussex Drug Discovery Centre
SEM	standard error of the mean
SGK	serum- and glucocorticoid- induced protein kinase
SPLUNC1	short palate lung and nasal epithelial clone 1
SV40	polyomavirus simian virus 40
TGN	trans golgi network
T_m	melting temperature
TM1/2	transmembrane domain ½
tRNA	transfer ribonucleic acid
TSA	trichostatin A
v/v	volume/volume
VGIC	voltage-gated ion channel
VSV-G	glycoprotein of the vesicular stomatitis virus
w/v	weight/volume
WPRE	Woodchuck hepatitis virus (WHP) posttranscriptional regulatory element
wt	wild type
Z'	S prime
β-ME	β-mercaptoethanol

GENERAL INTRODUCTION

Chapter 1

1.1. Ion channels in the plasma membrane:

Evolution of life on earth can be much attributed to the emergence of genetic and metabolic systems. The appearance of membranes may be given less accreditation but the barrier created via the lipid bilayer of a cell is essential to both of these systems. A membrane enables the cell's distinction from the surrounding environment and its integrity to mediate interactions with it (Monnard & Deamer, 2002).

The unique microenvironment formed at the interface of water and non-polar membrane components, for example lipids, serves a number of purposes. Firstly, it aids the self-assembly and folding of peptides (Phorille, 2002) whilst concentrating reactive species for more efficient progression of chemical reactions (Berry, 2002). Furthermore, the membrane provides anchorage for macromolecular complexes which can interact with specific intra- and extra-cellular components to convey a cellular response to changing conditions (Deamer, et al., 2002). Finally, its role as a permeability barrier to protons and sodium ions underpins the establishment of an electrochemical gradient across a membrane. This yields free energy, which can be chemically stored and used to drive the production of ATP, fundamental to energy metabolism (Berry, 2002).

The most abundant lipid in the membrane bilayer is the phospholipid. It is the amphipathic nature of this molecule, with a polar phosphate-containing head group and hydrophobic fatty acid tails, which provides an impenetrable barrier to other polar species. Only a few solute ions will cross the lipid bilayer every minute, and whilst many cellular processes demand a bidirectional flux of ions, the rate of passive ion movement across the barrier is insufficient to meet this demand (Deamer, et al.,

2002). Subsequently, specialised proteins at the membrane act as passive or active transporters of ionic species**.** One such protein macromolecule, the ion channel, is a membrane-embedded facilitator of diffusive ion transport. Ion channels create a hydrophilic pathway through the hydrophobic bilayer to permit the movement of ions down an electrochemical or osmotic gradient (Hille, 1992). They are not exclusive to the cellular membrane but can also be located in the membranes of intracellular organelles.

1.1.1. The ion channel concept:

The ion channel field is a longstanding area of research that has progressed as a direct result of the advancement in enabling technologies. The ion channel developed as a concept in the late 1800s when initial work by Ringer (1983) and Nernst (1888) suggested there was an ionic origin of bioelectric potentials, observed as the electrical phenomena in cells. The following century saw the transformation of theory to fact. Bernstein (1902) described the resting membrane potential of a cell as a diffusion potential, and attempted to decipher the mechanism underlying the action potential. He attributed action potentials to the breakdown of the potassium ion (K^+) selectivity of the membrane. This was then revised by Hodgkin & Huxley (1939) when they successfully recorded the propagation of an action potential directly in the squid giant axon. From this recording, they were able to observe a reversal in membrane potential at the peak of the action potential. Although this suggested that the large and sudden change in membrane potential during an action potential was not caused by a breakdown in the membrane's K^+ selectivity, it could not provide enough information to provide an alternative explanation. Technological advancements over

the next decade, which allowed the experimenter to control the membrane potential through voltage clamp, became fundamental to decoding the changes in membrane conductance (Cole, 1949). With this, Hodgkin and Huxley were able to conclude that ionic conductance was not due to changes in the properties of the lipid bilayer itself, but was controlled at very specific and discrete sites (Hodgkin & Huxley, 1952), which we now know to be ion channels.

The introduction of the patch clamp technique gave rise to the first measurement of single channel recordings (Neher & Sakmann, 1976), verifying the discrete nature of a channel. This method was able to isolate a small patch of membrane with minimal leak, and therefore could discriminate channel current from background noise. It has since been applied to measurements of macroscopic currents in whole cell, and intact tissue recordings, providing valuable information regarding ion channels' physiological functions and regulation. In addition, the first atomically-detailed protein structure of an ion channel was published in 1998 (Doyle, et al., 1998), which has accelerated the delineation of structure-function relationships.

1.1.2 Ionic origin of bioelectric potentials:

Ion channels help to establish and control voltage potential across cell membranes through three key features: the conductance of ions, the selectivity for an ionic species, and the regulation of channel gating by external cues (Aidley & Standfield, 1996; Hille, 1992).

Ion channel conductance of the permeant species occurs at high rates analogous to their rate of diffusion in free solution, often in excess of 10^6 ions s^{-1}. It does not require the coupling to an energetic input, for example ATP hydrolysis, but promotes

the rapid transport of ions necessary for numerous physiological processes, including neuronal excitability (Catterall, 1984). A pure phospholipid bilayer has a conductance near to zero, but the conductance of biological membranes is several orders of magnitude higher, a summation of the conductance of the ion channels present. Single-channel conductance may vary widely among different types of channels, but typically ranges between 0.01 and 100 pS (Hodgkin & Huxley, 1952).

The selectivity of an ion channel refers to the ability of channels to discriminate among ions and dictates the rates at which they are able to permeate the channel pore. It is prescribed through conserved signature sequences of amino acids which form a structural unit called the selectivity filter. The channel may be selective for either cations or anions, and then exhibit additional selectivity within these two species (Hille, 1992). Channels are typically named after the type of ion they permit (Hodgkin & Huxley, 1952), and the diversity in ion selectivity is necessary to independently regulate various signalling pathways in both time and space.

Regulation via external signals determines whether an ion is able to pass through a channel or not. Put simply, an ion channel can be thought of existing in three states: open activated, inactivated or refractory, and closed inactivated. The mechanism which transitions a channel between the three is termed ‘gating’. It can occur as a result of cues such as a change in membrane potential, ligand binding, or mechanical activation (Hille, 1992; Zhorov & Tikhonov, 2004). The sensing of a stimulus is conveyed to the ‘gating’ domain via a sequence of structural changes in the channel which ultimately lead to the gate opening or closing. The proximity of these sensing

and gating domains is not important; they can exist in distinct regions of the ion channel.

Channels which open in response to a change in membrane potential are known as voltage-gated ion channels (VGICs). These are the largest superfamily of ion channels, playing a fundamental role in neuronal excitability and cell homeostasis (Catterall, 1993). They are formed from a tetrameric arrangement of either four homologous subunits or four domains of a single protein (Figure 1.). Each subunit or domain has six transmembrane regions (S1-6), encompassing a voltage sensing domain (S1-4), a gating domain and a pore-forming domain (S5-loop-S6; (Hille, 1992). A voltage-induced conformational change in the protein is induced through the movement of charged amino acids located in the four voltage sensors, arranged laterally in the membrane (Catterall, 1993). Rotation of the S1-4 region is relayed to the S5-loop-S6 region which exposes a central, and now open, water-filled pore for the passage of ionic species, for example Na^+, K^+, Ca^{2+} or Cl^-.

Ligand-gated ion channels are opened, or gated, by the direct binding of a chemical messenger to an orthosteric site of channel protein. As with VGICs, a conformational change is necessary for the channel to transition into its conducting state. Prominent amongst these are those channels that mediate fast chemical synaptic transmission: the cysteine-loop (Cys-loop) channels (Figure 2.a) and the ionotropic glutamate receptors (iGluR; Figure 2.b). The Cys-loop subfamily includes the nicotinic acetylcholine receptor, sometimes referred to as the endplate channel due to its presence in vertebrate neuromuscular junctions. This is a widely studied channel, and was the first to have its unitary conductance measured using the patch clamp

technique (Neher & Sakmann, 1976). Other Cys-loop channels include the ionotropic gamma-aminobutyric acid ($GABA_A$) and serotonin (5-HT) receptors. These are pentameric channels formed of homologous subunits and are capable of mediating both inhibitory and excitatory synaptic transmission (Figure 2.a). The ionotropic glutamate receptors (iGluR) have a distinct subunit stoichiometry, formed of only four homologous subunits with a large extracellular domain for glutamate binding (Figure 2.b). The central pore permits the passage of small cations, exhibiting little selectivity between each but conveying excitatory synaptic transmission in the order of milliseconds (Olsen & Sieghart, 2008).

There are additional ligand-gated ion channels which act much more slowly due to activation via ligand binding to a protein distinct from the channel. One example of this is the inositol 1,4,5-trisphosphate (IP_3) receptor, which is responsible for the release of intracellular stores of Ca^{2+}, a wide-acting second messenger molecule, from the endoplasmic reticulum (Yamamoto-Hino, et al., 1994). Channel opening relies on the transduction of a signal from a receptor at the cell's surface, for example a G-protein-coupled receptor (GPCR), which results in the formation of IP_3, leading to activation of intracellular channels. As G-protein activation is associated with more than one signal transduction pathway, it allows for a much more complex and prolonged physiological response.

Finally, a less studied and smaller class of ion channels are those that respond to mechanical stimuli through the interpretation of membrane tension (Guharay & Sachs, 1984). Changes along the plane of the membrane have been implicated in osmotic stress, touch, hearing etc. In this instance the protein conformation is intrinsically

coupled to the surrounding membrane, as the channel acts as a mechano-electrical molecular switch, converting an external mechanical force into an intracellular electrical or biochemical signal. For example, its function may be to ensure cellular viability during osmotic stress (Nakayama, et al., 2012). It is unclear, however, whether the opening of the channels is a result of intrinsic tension within the bilayer, or extrinsic tension applied by extracellular or intracellular elements e.g. the cytoskeleton.

To add to this complexity, some ion channels exhibit activation by more than one of these three processes. For example, hyperpolarization-activated, cyclic nucleotide-gated (HCN) channels are both voltage-gated and ligand-gated (Robinson & Siegelbaum, 2003). They structurally resemble the voltage-gated K^+ channel with a six transmembrane domain topology, however they show selectivity for Na^+ as the permeating ion. At normal resting membrane potential they have a low level of constitutive activity which is thought to contribute significantly to resting membrane conductance of the cell. Unusually their activation is increased upon both binding of cyclic nucleotides (cAMP, cGMP, cCMP), which lowers the threshold potential of these channels, and membrane hyperpolarisation, more specifically upon repolarisation following action potential firing (Robinson & Siegelbaum, 2003).

1.2. Ion channels as therapeutic targets:

The highly regulated opening and closing events of an ion channel underpin numerous fundamental physiological processes (Hille, 1992), highlighting their essential roles in the physiology of all cells. Inherently, ion channels have a profound involvement in a wide range of pathologies. Defects in their functions give rise to the heterogeneous

group of disorders called “channelopathies”, comprising over 60 identified congenital diseases. These span all major therapeutic areas including the cardiovascular, neuronal, neuromuscular, musculoskeletal, metabolic, and respiratory systems (Ashcroft, 2006).

As therapeutic targets, ion channels are modulated by a range of currently prescribed drugs. Given the central functional role that the ion channel superfamily (Figure 3.) plays in human physiology, the diverse tissue distribution across members of the family, and a channel’s membrane localisation, it is unsurprising they are an attractive target class for drug discovery. Approximately 13.4% of known drugs have their primary therapeutic action at ion channels (Overington, et al., 2006): Benzodiazepines, for example, are a class of drugs that act selectively on $GABA_A$ receptors in the brain to enhance the GABA-mediated inhibitory pathways. Generally, they are used as sedatives, hypnotics, anxiolytics, anticonvulsants and muscle relaxants. These found popularity in the 1960s, becoming the most commonly prescribed drugs by the 1970s, and were worth nearly $3 billion worldwide by the following decade. In 2010, worldwide sales of ion channel drugs were estimated to be in excess of $12 billion (Clare, 2010). Despite this, ion channels as targets have been particularly resistant to high throughput approaches for drug discovery.

1.2.1. Difficulties facing ion channel drug discovery:

Most of the current ion channel drugs were developed empirically by traditional pharmacology, without prior knowledge of their precise molecular target. These drugs were profiled in animal models of disease states to inform compound optimisation, and despite the ambiguity of their precise mechanisms of action, the successful

therapeutics have been invaluable research tools. Such tools have permitted the purification of ion channel proteins and characterisation of their gating mechanisms in conjunction with unravelling the downstream pathways involved in their signal transduction (Garcia & Kaczorowski, 2005).

An example of a drug discovered empirically is amiloride. This was first synthesised by the Merck Sharp and Dohme Research laboratories in the 1960s for the purpose of an extensive screen to identify compounds with an ability to reverse the effects of mineralocorticoids e.g. aldosterone *in vivo* (Cragoe, et al., 1967). Whereas aldosterone promotes resorption of sodium ions, the screen identified amiloride as being capable of causing natriuresis without associated potassium excretion. Since then, amiloride has been shown to be a potent inhibitor of passive transepithelial Na^+ transport at the apical membrane. Amiloride and its analogues have proved invaluable in the identification and elucidation of transport mechanisms, including the roles of the ENaC αβγ channel, and other Na^+ transport processes including Na^+-H^+ and Na^+-Ca^{2+} exchange (reviewed by Kleyman (1988)).

More recently there has been a shift away from these traditional methods towards a molecular target-based paradigm steering drug discovery programs. This has been the outcome of a mutual increase in understanding of the cellular and molecular basis of ion channel function, facilitated by whole genome sequencing across multiple organisms, and in technological capabilities of automated electrophysiology platforms. Molecular-based approaches first identify and characterise a target associated with disease. New chemical entities are then assessed in high throughput screening assays

for their interaction with the target. Subsequent hits may form the starting point for a novel tool compound or drug.

Disappointingly, this approach has yielded very low rates of new drug approvals with lead compounds failing to advance through the drug discovery process. Poor chemical tractability can be attributed to problematic validation of new channel targets and generation of high throughput and high fidelity assays, and chemical libraries which are largely populated with chemotypes that are deemed unacceptable medicinal chemistry leads (Bagal, et al., 2013; Scannell & Bosley, 2016). It is without doubt, however, that improvements in these early stages can have the biggest impact on time and financial deficits incurred in the drug discovery process by preventing the continuation of unsuitable targets and small molecule leads.

Firstly, the complexity and diversity of the ion channel structure and function presents major challenges for molecular drug discovery in terms of target identification (Clare, 2010). In many cases, the exact subunit composition of the target channel in the tissue of interest is only poorly characterised and uncertainties surrounding the predictive nature of animal models for human pathophysiology (Kaczorowski, et al., 2008) may cast doubt over the exact target. Implementing a rigorous approach that combines comprehensive *in vitro* and *in vivo* studies, for example human genetic studies and gene ablation in rodents, is essential. This practice has been key to the identification of a number of new ion channel targets e.g. the voltage-gated sodium channel, $Na_v1.7$, for the treatment of pain (Dib-Hajj, et al., 2007). Despite the genetic validation of this channel target, there is still no specific $Na_v1.7$ channel blocker in late stage clinical trials. One of the main obstacles has been that the human loss of $Na_v1.7$ function,

characteristic of the genetic syndrome Congenital Indifference to Pain (CIP), is not replicated in mice (Nassar, et al., 2005). This indicates the possibility of compensatory changes in genetically derived disease models, highlighting the value of pharmacological tools to ratify a target in an animal model which emulates human physiology.

Secondly, identifying and characterising small molecule leads for a validated target has proven even more arduous. This commands sensitive and robust biologically relevant assays that have a sufficient capacity for high-throughput screening to confirm hits from large compound libraries (Herrington, et al., 2005; Garcia & Kaczorowski, 2006). High throughput screens often require the cloning of the target protein, which then must be abundantly expressed in a heterologous system (Garcia & Kaczorowski, 2016). Challenges caused by the structural complexity and stability of these proteins can impede the expression of an ion channel in a form that is closely representative to that in its native setting (Tapper & George Jr, 2003). In addition, this can be commonly hindered by toxicity issues of overexpression of these channels. One example of a cell-based screening technology that enables an HTS approach to ion channel drug discovery is the use of ion-specific or membrane-sensitive fluorescent dyes. This platform allows for monitoring of ionic flux in cells grown in a multiwall format and can even be used to define some mechanisms of action of a blocker in a time- and cost-effective manner (McManus, 2014). For example, this method can outline if a drug is a state-dependent blocker, which changes affinity for the ion channel subject to its precise gating state, or a use-dependent blocker, whereby its affinity for the ion channel is proportional to the activity of that channel. However, such hit finding

techniques are prone to high false positive/negative rates, accounting for a history of limited success in high-throughput screening attempts to identify potent and selective hits.

In the past gold-standard electrophysiology has been too low throughput for the interrogation of large chemical libraries. Routinely, conventional patch clamp, which demands time and high levels of speciality, is instead used to validate primary screening hits. Innovations over the last couple of decades have revived the ion channel drug discovery potential by way of automated electrophysiology, which facilitates high throughput patch clamp and removes the need for highly skilled operators (Dunlop, et al., 2008). The first commercially available platform was the IonWorks (Molecular Devices, USA) (Schroeder, et al., 2003). This took advantage of a planar multiwell chip design to allow for multiple parallel recordings and the screening of small compound libraries (John, et al., 2007). It was a breakthrough for drug discovery as screening chemical libraries was unimaginable by conventional patch clamp. However, the IonWorks' main drawback is the inability to recapitulate the tight gigaohm (GΩ) seal quality typical of manual recordings. A second series of platforms, including the QPatch (Sophion Bioscience, Denmark), were developed and these compromised the number of parallel recordings to just 16, for GΩ quality seals comparable to those seen in conventional patch clamp. More recently, the introduction of a 48-channel QPatch system married GΩ seals with a high throughput capacity. This platform is capable of providing high levels of functional information on the direct effect of large numbers of compounds on a specific channel, including selectivity and mechanistic information (McManus, 2014). Application of

these technologies can often be met with a lengthy and expensive optimisation process. However, their unprecedented screening capability now places them at the forefront of ion channel drug discovery programs, as the preferred primary and secondary screening platform.

Final obstacles prohibiting the progression of identified and validated hits include the assessment of whether they possess desirable chemical properties that qualify them for medicinal chemistry exploration (MacCoss & Baillie, 2004) and whether they have any toxicological liabilities at a number of known targets. This is applicable to lead compounds in any drug discovery program regardless of their target, and is fundamental for compound prioritisation, and to inform projects at the point of new compound design.

1.3. Sodium Ion Channels:

Sodium channels refer to all integral membrane proteins comprising a Na^+ permeable pore that traverses the membrane to allow for ion flux. These can be broadly divided into two categories: the voltage-gated sodium (Na_v) channels and the epithelial sodium channels (ENaCs).

1.3.1. Voltage-gated sodium (Na_v) channel family:

As briefly referred to in Section 1.1.2, Na_v channels are a type of VGIC that are activated upon membrane depolarisation and function as key mediators of cell excitability through the initiation and propagation of action potentials. They are formed of one α subunit (~260 kDa), containing four homologous domains (I-IV) of six-transmembrane spanning α helices (S1-6), in close association with an auxiliary β

subunit (~35 kDa). Although not necessary for functional expression, the β subunits are able to modify the biophysical properties of the ion channel, for example the kinetics and voltage-dependence of channel gating (Catterall, 1993; Isom, 2001). They are also implemented in ion channel localisation, bridging the gap between the α subunit and cytoskeletal molecules (Isom, 2001). The nine mammalian sodium channel isoforms that have been identified are defined by this α subunit. All are greater than 50% identical in amino acid sequence in the transmembrane and extracellular domains, but exhibit sequence divergence elsewhere. The α subunits contain all the binding domains for pharmacological agents, for example neurotoxins (e.g. tetrodotoxin (TTX)) and local anaesthetics (Cestèle & Catterall, 2000; Catterall, 2000).

The bacterial voltage-gated sodium channel (Na_vAb) architecture has been solved by x-ray crystallography at high resolution (2.7 Å; (Payandeh, et al., 2011; Payandeh, et al., 2012) and more recently the eukaryotic Na_v channel has had its structure solved by cryo-electron microscopy (Shen, et al., 2017). Both have promoted understanding of the molecular basis for ion conductance and voltage-dependent activation. The inner cavity of the pore is formed by the four S5 and S6 transmembrane segments, with an additional pore loop located between the two, which lines the outer entry to the pore. The pore itself has a large external vestibule, with a narrower ion selectivity filter with a specific sequence of amino acids, and then a large central, water-filled cavity. The selectivity filter contains four highly conserved glutamate residues and two ion coordination sites formed by backbone carbonyls. These coordination sites are too far

apart to bind Na^+ alone, but instead bind Na^+ with up to four planar waters of hydration.

The S1-4 regions contain the voltage-sensing capability and are symmetrically arranged around the outer rim of the pore. Specifically, S4 contains charged amino acids, usually arginine, at every third position of the primary sequence. At normal resting membrane potential it is predicted that this S4 is pulled towards the intracellular side of the membrane by electrostatic forces which are removed upon depolarisation allowing for the movement of S4 regions across the membrane to initiate a conformational change in the protein and channel activation. Between domain III and IV, there is a short intracellular loop which has the ability to fold toward the channel and block the pore, upon inactivation as a result of prolonged exposure to a depolarising stimulus.

1.3.2. ENaC/degenerin (DEG) ion channel family:

The second group of sodium channels, the ENaC channels, is the focus of this investigation, and is discussed in more detail in all subsequent sections.

These ion channels are an example of how the incorporation of methodological advancements in molecular cloning techniques throughout the 1980s and 90s, enabled the determination of novel classes of proteins. Pivotal to characterising members of the ENaC/DEG family, was the initial identification of two degenerin genes from a genetic screen of the *Caenorhabditis elegans* mechanosensory pathway (Chalfie & Wolinsky, 1990; Driscoll & Chalfie, 1991). These genes, *deg-1* and *mec-4*, are named such after the dominant cellular mutant phenotype, which saw the selective

*deg*eneration of sensory neurons associated with *mec*hanosensation. These nerves are subject to a cell death distinct from programmed cell death (PCD), whereby they first exhibit swelling of neuronal cell bodies followed by degeneration. This suggested that *deg-1* and *mec-4* are involved in ionic balance regulation via ion channel or transport systems, and that mutations in these genes result in the disruption of membrane integrity (Driscoll & Chalfie, 1991; Driscoll & Chalfie, 1992). Simultaneous to this genetic screen, was the successful cloning of a functional α-subunit of the amiloride-sensitive epithelial Na^+ channel (ENaC), isolated in *Xenopus laevis* oocytes (Canessa, et al., 1991).

The ENaC proteins similarly contribute to ion transport and had already been known to form functional sodium channels that play a role in the aldosterone-modulated electrogenic sodium reabsorption in tight epithelia, for example in the distal region of the kidney tubule (Koefoed-Johnsen & Ussing, 1958; Crabbé, 1961; Murer, et al., 1976). ENaC proteins show considerable sequence homology to the degenerins and together these became the founders of a new family of ion channels, termed the ENaC/DEG family.

The first sequences of these ENaC proteins were based on cDNAs cloned from rat or human tissues (Canessa, et al., 1994; Waldmann, et al., 1995). Since the cloning of three ENaC α, β and γ subunits, genetically related proteins have been identified through homology screening and characterised by functional studies (Kellenberger & Schild, 2002). One of these includes a fourth ENaC δ subunit.

1.3.2.1. Chromosome location and intron-exon organisation of ENaC genes:

The human genome contains nine genes that can be assigned to the ENaC/DEG family. These can be grouped into two subfamilies: non-voltage gated sodium channels, composed of four genes, *SCNN1A-D,* encoding the ENaC α, β, γ and δ subunits; and the acid-sensing ion channels (ASICs), composed of five genes, *ACCN1-5*, encoding the ASIC1-5 subunits. The gene abbreviations were assigned by the Human Genome Organisation (HUGO) Gene Nomenclature Committee (hhtp://www.genenames.org/).

Figure 4. shows some of the additional members in this gene family including: the BASICs (bile acid–sensitive ion channel), which are activated by bile acids (Wiemuth, et al., 2012; Lefèvre, et al., 2014) and formerly known as the mammalian hiNaC (human intestine Na^+ channel) after their main site of expression (Sakai, et al., 1999); the FMRF-amide-gated ion channel (FaNaC) cloned from the mollusc *Helix aspersa* (Lingueglia, et al., 1995) and in the cnidarian *Hydra* (Golubovic, et al., 2007); and the various *DEG/MEC/UNC* genes found in invertebrate Metazoan species. Despite the mere ~15-20% sequence identity across members of the family, all operate within sensory modalities encoding proteins in mechano- or chemosensory transduction pathways (Coscoy & Barbry, 2004). There is a higher homology seen between different subgroups within the family, for example ~30% between the different ENaC subunits, and anything between 45–75% between the four ASIC subunits, ASIC1, ASIC2, ASIC3, and ASIC4 (Kellenberger & Schild, 2002). The ASIC5 subunit has a lower level of homology with the other ASIC genes (~25%) and lacks the proton-sensing domain possessed by the other four members as inferred by their name (Coscoy & Barbry, 2004).

ENaC/DEG genes are only present in metazoa, which possess organs that enable complex functions such as coordination and digestion. In fact, they exist in the genome of all sequenced metazoans, and it has therefore been suggested that they were present in ancestors of metazoa. A study by Studer et al. (2011) found that the ASIC and ENaC genes in the mammalian genome were generated by two rounds of whole genome duplication at the origin of vertebrates. As there are no mammalian orthologs of the *C. elegans* and *Drosophila* ENaC/DEG members (Zelle, et al., 2013), it is proposed that there was an early divergence in evolution of the different ENaC/DEG subfamilies. As a result there was a massive diversification of the genes and sequences of these proteins within this family. An example of this is variation in the extracellular loop domain of each subunit (Zelle, et al., 2013), which commands their interaction with the surrounding environment. For these reasons, there is a great difficulty in studying any physiological or functional homology of these channels across distant species. Nevertheless, there is an 85% homology between human and rat orthologs for the ENaC α, β and γ subunits, in addition to almost 100% homology for ASIC1, -2, and -4 and 83% for ASIC3 (Kellenberger & Schild, 2002).

The chromosomal locations of all four ENaC subunits in the human genome is summarised in Table 1. Initially only the three canonical ENaC subunits were cloned, but in 1995 a fourth δ subunit was identified in human tissues (Waldmann, et al., 1995). There are two distinct branches within the ENaC subfamily: the α- and δ-subunit branch, and the β- and γ-subunit branch, with each pair sharing the highest level of homology with each other. Interestingly, ENaC β and γ subunits are in adjacent location on the same chromosome, and the juxtaposition of these genes is also true of

the corresponding *Scnn1b* and *Scnn1g* in the mouse genome (Brooker, et al., 1995). This provides evidence of two rounds of gene duplication events, first forming two ancestral genes, which then underwent a second local gene duplication event.

ENaC subunit	Gene Name	Chromosome	Length	Exons	Coding exons
α	SCNN1A	12p	669	13	12
β	SCNN1B	16p	640	13	12
γ	SCNN1G	16p	649	13	12
δ	SCNN1D	1p	638	16	13

Table 1. Details of the chromosomal location, length and exon organisation of the ENaC genes. Taken from Hanukoglu and Hanukoglu (2016).

The published cDNA sequence of the human *SCNN1D* is assigned to human chromosome 1p36.3-p36.2 with a sequence ID, NC_000001.11. It covers 18.03 kb, from 1280415...1292029 (NCBI, March 2015), on the direct strand (Gregory, et al., 2006). To date, the ENaC genes have been cloned across different species, and 31 gene orthologs of *SCNN1D* have been deposited to the Ensembl database, most of which are vertebrates. The orthologs all exhibit high sequence identity and include those from *Pan troglodytes* (located on chromosome 1, NC_006468.3), *Canis lupus familiaris* (chromosome 5, NC_006587.2), *Bos taurus* (chromosome 6, NC_007314.3), and *Gallus gallus* (chromosome 21, NC_006108.2). All three canonical ENaC subunits have been identified in mice but the DNA encoding the δ-subunit has not (Giraldez, et al., 2012). This is despite the human genes neighbouring *SCNN1D (UBE2J2* and *ACAP3)* having both been identified in mice adjacent to each other on Chromosome 4. It is therefore thought to be a pseudogene in rodents (Giraldez, et al., 2012), prohibiting the study of this subunit in this popular model system.

The intron-exon organisation across *SCNN1A*, *SCNN1B and SCNN1G* is conserved, with genes including 13 exons, from which 12 of these are protein-coding sequences (Table 1. (Ludwig, et al., 1998; Saxena, et al., 1998; Thomas, et al., 1996)). The introns lay at identical positions within these coding regions (Saxena, et al., 1998). The *SCNN1D* gene maintains the intron locations that exist in the other three genes, but the gene structure differs somewhat. There are thought to be at least 16 exons, of which only 13 are translated. The introns, although in the same locations, are much smaller: prior to splicing the nucleotide sequence of *SCNN1D* is 10,806 nt, which is much smaller than *SCNN1B*, for example, at 70,030 nt long.

Both ENaC and ASIC genes have different splice variants; transcription of the *SCNN1D* gene is predicted to produce 15 different mRNAs, of which 14 are alternatively spliced variants, and one is the unspliced form. ENaC δ splice variants include two, named δ1 and δ2, which have been studied by several groups (Giraldez, et al., 2007; Zhao, et al., 2012). These are 638 and 704 amino acids long respectively, with the δ2 variant containing a longer NH_2 terminus (Zhao, et al., 2012). This is speculated to modulate channel trafficking to the membrane (Wesch, et al., 2012) and/or single-channel conductance and ion selectivity (Zhao, et al., 2012).

1.3.2.2. Tissue expression profile:

As the name suggests, the ENaC channel is most prominently studied for its physiological roles in epithelial tissue. ENaC α, β and γ subunits together form this functional channel at the apical membrane of tight epithelia, which has been well described for its role as the rate limiting step in sodium ion reabsorption in the distal tubule of the kidney nephron. Studies on tissue localisation of these subunits report

highest levels of expression in the kidney, lung and colon. These were performed using immunohistochemical techniques or in-situ hybridisation (Duc, et al., 1994; Tousson, et al., 1989). The EMBL-EBI Expression Atlas database of gene expression (http://www.ebi.ac.uk/gxa/home) shows results of large-scale microarray studies and RNA sequencing to investigate the tissue specificity of these subunits' expression.

The ENaC δ subunit has a distinct pattern of tissue distribution and the physiological relevance is not well characterised. It was first studied by Waldman, et al. (1995) using northern-blots of mRNA samples from 16 tissue types, and then by dot-blot (Yamamura, et al., 2004) almost a decade later. Despite slight variations, data are concurrent in the predominant expression of *SCNN1D* in the heart, liver, brain, and lung (Figure 5.). In the brain, the ENaC δ subunit is the most prominently expressed of all ENaC proteins (Waldmann, et al., 1995; Yamamura, et al., 2004; Giraldez, et al., 2012) but contrary to this is a relatively weak level of expression in the spinal cord. It was shown to be expressed in 16 areas of the brain, excluding the frontal lobe, medulla oblongata, accumbens nucleus, thalamus, and corpus callosum (Yamamura, et al., 2006). Furthermore, its expression was found to be exclusively neuronal, including pyramidal neurons in layers II to VI and the frontal and temporal cortices (Giraldez, et al., 2007). Pyramidal neurons were shown to express either ENaC δ1 or δ2 dependent on the cortical region. For example, quantitative PCR (qPCR) analysis showed that δ1 transcript levels were 2.5-fold that of δ2 ENaC in human cerebral cortex (Wesch, et al., 2012). Overall ENaC δ was seen to occur in a development-dependent manner with lower expression levels in equivalent foetal tissue (Yamamura, et al., 2004). These

studies are consistent with the results on the Expression Atlas database (http://www.ebi.ac.uk/gxa/home).

1.4. Structure of the ENaC channel:

The ENaC/DEG proteins exhibit large diversity in their primary sequence and can range from ~530 to ~740 amino acids in length. However all members of the family share a common structural topology, enabling the formation of non-voltage gated cation channels. Much is known about the primary structure of the ENaC subunits and functions of conserved domains, but in the absence of a crystal structure, the channel's subunit stoichiometry was long disputed. Of the structures that have been determined by X-ray crystallography, the closest family member is the homotrimeric chicken ASIC1a ion channel (PDB ID: 2QTS; Figure 6. (Jasti, et al., 2007) and PDB ID: 4NYK (Gonzales, et al., 2009)). Hydrophobicity plots and sequence homology to the ASIC1a channel, predicts that the ENaC channel has a similar overall topology. However, strongest lines of evidence indicate that it is a heterotrimer composed of either an α or δ subunit, with both β and γ subunits (Staruschenko, et al., 2005; Stockand, et al., 2008). Each subunit has relatively short intracellular amino and carboxyl termini and two transmembrane domains (TM1 and TM2) linked by an extracellular loop, which is structurally unique to this ion channel family (Jasti, et al., 2007).

1.4.1. Homology to the Acid Sensing Ion Channel 1:

Difficulties in determining crystal structures of ion channels arise from inherent problems in efficiently expressing these proteins in heterologous expression systems, in addition to the transmembrane nature of these proteins. Nevertheless, the Gouaux

group determined two different X-ray crystallographic structures of a close family member to ENaC, the homotrimeric chicken ASIC1 ion channel.

The first crystal structure of ASIC1 (PDB ID: 2QTS; Figure 6.) was determined at pH 5.6 using a truncated protein variant, comprising of 438 amino acids (26–463; (Jasti, et al., 2007). Of those residues, only 42–457 (subunit A), 42–461 (subunit B) and 40–457 (subunit C) could be located in the electron density maps at 1.9 Å resolution (Jasti, et al., 2007). Furthermore, this incomplete protein variant does not exhibit proton-dependent gating, which is characteristic of the ASIC1 channel.

The second of these structures (PDB ID: 4NYK), comprising 406 amino acids (46-451), encompasses a construct that has the amino terminus, a region critical to the activation gating in both ASIC and ENaC channels. The protein is then truncated following the TM2 region at residue 466. This construct does retain the pH-dependent gating and sodium selectivity observed in a full length channel. It formed crystals at pH 6.5 and diffracted at 3 Å resolution, however N (2–45) and C (452–466) terminal residues were not seen in electron density maps (Gonzales, et al., 2009). Both structures were crystallised at low pH, and therefore represent the channel's desensitised state, whereby it is unresponsive to activation by protons. There is no analogous inactivated state of ENaC.

The ENaC proteins exhibit between 13% and 16% sequence homology with the ASIC1 protein, sharing an overall higher identity in the extracellular regions (Figure 7.). Nonetheless, the most peripheral regions of the extracellular domain actually show highest levels of sequence divergence, and it is here where direct interactions with extracellular factors, such as protons occurs (Gründer & Pusch, 2015). Furthermore,

the N- and C- termini are not well conserved, even among ENaC subunits, which is a feature true to most families of proteins. It is this divergence in key amino acid sequences that lie on both sides of the membrane which give a unique signature of protein interactions to each family member.

For these reasons, there is a limitation to the number of assumptions that can be made using these ASIC structures to create a homology model of the ENaC channel. The significant divergence in sequences, tissue expression patterns, functions, regulation, and species specificity all have implications and must be taken into consideration.

1.4.2. ENaC subunit stoichiometry:

To date, as many as three stoichiometric models have been proposed for the ENaC channel. These include: a heterotrimer, 1α1β1γ; a heterotetramer, 2α1β1γ; and a heteromer of nine subunits, 3α3β3γ (Berdiev, et al., 1998; Firsov, et al., 1998; Jasti, et al., 2007; Snyder, et al., 1998; Staruschenko, et al., 2005). However, after determination of the homotrimeric ASIC1 structure (Jasti, et al., 2007; Gonzales, et al., 2009), the general consensus is that the ENaC channel is also formed from three subunits. Hydrophobicity plots predict two transmembrane segments per subunit, and there is high sequence identity to ASIC1 in specific regions in the core of the extracellular domains and in the TM2 helices. However, functional studies suggest that the ENaC channel is most likely to assemble as a heterotrimer, formed of an α or δ subunit, in combination with β and γ subunits (Giraldez, et al., 2007).

Gene knock-out studies of the α, β and γ subunits have all shown to be fatal in mice (Hummler, et al., 1996; Barker, et al., 1998; Bonny & Hummler, 2000). In heterologous expression systems, all three α, β and γ subunits are required for ENaC currents, with

one or two subunits producing no detectable currents (Giraldez, et al., 2007). One exception to this is the δ subunit, which is believed to be capable of forming functional channels on its own. However, coexpression with β- and γ-subunits amplifies channel activity by up to two orders of magnitude (Ji, et al., 2012). ENaC α and δ subunits share a 37% sequence identity. A small variation in subunit composition reflects in pharmacological and biophysical distinctions between the ENaC δβγ and αβγ channels, (Bangel-Ruland, et al., 2010), in addition to differences in patterns of expression and regulation. Therefore, it may be inferred that ENaC δβγ channels have a similar but also functionally distinct physiological role to the ENaC αβγ channel that is yet to be defined.

1.5. Relating structure to function:

Knowledge of the primary structure of the ENaC subunits, including conserved sequences within its ion channel family, lends itself to an understanding of the functions of some key domains within the ion channel.

1.5.1. The ENaC pore:

The two transmembrane regions of the ENaC subunits are homologous to those of the ASIC1 channel (Figure 7.), specifically the TM2 segment where sequence identity is highest. The ASIC1 channel structure reveals that the TM1 and TM2 domains contributed by each subunit are organised in two concentric triads. The inner triads are made up of the TM2 domains and form the central pore, which is encircled by the outer TM1 triad (Li, et al., 2011). These outer TM1 domains all interact with their neighbouring subunits' transmembrane helices.

Ions can then move through this pore but, as yet, it is not known what path these ions take. The extracellular loops of each of the three subunits come together to form a funnel with rotational symmetry (Jasti, et al., 2007; Baconguis, et al., 2014) but the three subunits are not always in close proximity. Fenestrations are present between the subunits, which form a hollow space along the central axis of the rotational symmetry called the 'extracellular vestibule' (Baconguis, et al., 2014). This vestibule undergoes constriction and expansion if crystallised in different conditions (Baconguis, et al., 2014), suggesting a role in the regulation of the flow of ions through the pore. It is thought that the state of the vestibule is dictated through rotation of the TM1/2 domains. Conformational changes in the channel can be a result of various intra- and extra-cellular factors, for example changes in pH (Gründer & Pusch, 2015), or binding of second messenger proteins.

In all ENaC orthologs there is a stretch of two-three conserved Arg/Lys residues preceding the first transmembrane domain (TM1) on the cytoplasmic side of the membrane (Hanukoglu & Hanukoglu, 2016). These positively charged residues appear in much higher proportions on the intracellular portions of the proteins, particularly in regions in very close proximity to the lipid bilayer. The role of these is thought to be to provide a secure anchorage of the ENaC proteins within the membrane via interactions of the positive charges with the polar head groups of the membrane phospholipids (von Heijne, 1992; Pogozheva, et al., 2014). Furthermore, at the beginning of the TM1 region there is a conserved tryptophan residue. Aromatic residues like tryptophan or tyrosine are shown to be located at the membrane-water interface (Pogozheva, et al., 2014) to provide an additional degree of anchorage and positioning of the

transmembrane domains within the plasma membrane. Kashlan, et al. (2006) showed that mutations of this tryptophan at the TM1 segment altered channel activity and cation selectivity, as did mutations in a similar conserved tryptophan residue in the second transmembrane domain (TM2).

This TM2 segment is highly conserved in all ENaC subunits and its location was predicted via analysis of the subunits' hydrophobic profiles prior to resolution of the ASIC1 structure (Canessa, et al., 1994). These predictions revealed a stretch of hydrophobic residues preceding TM2 (Canessa, et al., 1994). In other known Na^+ -selective cation channels, a short hydrophobic segment preceding the most COOH-terminal transmembrane domain forms the outer pore of the channel with the receptor sites for external blockers (Tikhonov & Zhorov, 2017). It is therefore suggested that the pre-TM2 segment of ENaC subunits may contribute to the formation of the channel pore. Subsequent to the ASIC1 structure being solved, the 'pre-TM2 segment' is now considered to be encompassed within TM2 itself. Regardless, within the TM2 domain resides functional sites that are integral to the ENaC channel, for example, the channel gate, selectivity filter and the binding site for the prototypical blocker, amiloride. Functional studies have been used to confirm each of these three sites (Kellenberger, et al., 2002; Schild, et al., 1997).

1.5.1.1. Ion selectivity and single channel properties:

ENaC channels are defined as sodium selective channels, able to discriminate between cationic species. They have a Na^+/K^+ permeability ratio of >100, making them the most sodium selective of all mammalian ion channels (Gründer & Pusch, 2015). ASIC channels display a lower Na^+/K^+ selectivity ratio (PNa^+/PK^+<10). Less physiologically

relevant but still somewhat important to distinguish the two ENaC channels, is their ability to conduct Li^+ at similarly high rates to Na^+. On comparison, the ENaC δβγ channel has an increased permeability for Na^+ over Li^+ ions, which is the opposite for the α-containing channel (I_{Li}/I_{Na} = 0.6 vs. αβγ I_{Li}/I_{Na} = 2; (Waldmann, et al., 1995)), and in addition has a much higher single-channel Na^+ ion conductance (12 vs. 4 pS) with a longer opening time (0.27 ± 0.03 vs 0.0193 ± 0.006 ms; (Waldmann, et al., 1995; Kelly, et al., 2003).

The cation selectivity of ENaC is attributed to a well-conserved three amino acid motif, G/S-X-S, in the TM2 of each subunit on the cytosolic side of the membrane. Kellenberger, et al. (1999) showed that a single point mutation in this motif of the α subunit (S589D) induced a change of channel ion selectivity, allowing for an increased K^+ permeation. Additional mutations of acidic residues distal to this G/S-X-S tract residue have also been linked to ion selectivity. For example, mutations within the TM2 domain of the ENaC α subunit (D602K or D602A), and the equivalent site of the ENaC γ subunit (D562C), cause K^+ conductance, or significantly increase the Li^+/Na^+ current ratio, respectively (Sheng, et al., 2001). However, the difference in Na^+/Li^+ selectivity between the ENaC α and δ- containing channels may be due to non-conserved residues in this region.

On comparison of the ENaC δ1βγ and δ2βγ channels' cation permeability, it was found that they were both similar. Differences could be seen, however, between their unitary conductance and the estimated P_o value was greater for δ2βγ (Zhao, et al., 2012). Ion selectivity and single-channel conductance has been attributed to a hydrophobic domain in the δ subunit that forms part of the second transmembrane

domain (Ji, et al., 2000). However this region is conserved between the δ1βγ and δ2βγ channel. Owing to the fact that the only region where the two isoforms' primary structures do differ is their N-terminus, it could imply that this region may also contribute to the differences in their single-channel conductance.

1.5.1.2. Channel gating:

Channel gating has been linked to two distinct regions of the ENaC subunits. The first is the 'degenerin' site within the TM2 region, upstream of the suspected amiloride binding site. This contains a motif of four amino acids (L-L-S-N) and has been shown to modulate the open probability (P_o) of the channel (Kellenberger, et al., 2002). Replacement of the serine residue with larger residues increases the P_o and this is thought to be a result of destabilisation of the closed state of the channel (Kellenberger, et al., 2002). It is referred to as the degenerin site because replacement of the same serine with larger residues in the *C.elegans* ortholog induces neurodegeneration due to increased P_o (Garcia-Anoveros, et al., 1995).

The second identified region is located in the NH_2-terminal domain and is discussed in Section 1.5.4.

1.5.1.3. Amiloride binding:

Amiloride was developed as a potassium-sparing diuretic in the 1960s (Baer, et al., 1967). Inhibition by amiloride at the outer mouth of the ENaC channel is characteristic of both ENaC and ASIC channels, although at varying concentrations (ENaC αβγ channel: IC_{50} ~ 0.2 µM: ASIC channels: IC_{50} ~ 5 - 100 µM; (Kleyman & Cragoe, 1988; Kellenberger, et al., 2002; Diochot, et al., 2007; Ji, et al., 2012; Lingueglia & Lazdunski, 2013). Although its binding site was not known, observation of a voltage-dependency

of block at apical ENaC αβγ channels suggested that this block occurred within the pore (Schild, et al., 1997; Kellenberger, et al., 2001). Mutagenic studies using cloned mouse ENaC subunits led to the identification of a specific ENaC α serine residue (αS583) and equivalent ENaC β and γ glycine residues (βG525 and γG537) just upstream of the selectivity filter, which decreased the efficacy of amiloride when mutated (Schild, et al., 1997). The mutations in ENaC β and γ subunits had a much more profound effect than that of the ENaC α subunit, but all three mutations affected the voltage-dependence of block and pH-dependent rectification. Other groups observed that mutations within the selectivity filter itself (G/S-X-S) (Figure 7.b) also impacted amiloride efficacy (Waldmann, et al., 1995; Kellenberger, et al., 2001), which further supported the hypothesis that amiloride binds within the pore region. Further residues existing in the extracellular region have since been identified to be important in amiloride binding and are discussed in Section 1.5.2.5.

Amiloride block is conserved in δβγ channels, where it is less potent (IC_{50} ~ 2.6 μM) and has been found to exhibit higher voltage dependence (Ji & Benos, 2004; Waldmann, et al., 1995; Yamamura, et al., 2004). Varying data exists in regard to difference in the δ1βγ and δ2βγ channels' amiloride sensitivity, with reports of an increased sensitivity in δ2βγ channels (Zhao, et al., 2012), or no significant difference (Yamamura, et al., 2006). Again it has been suggested that if there is a difference, this may be indirectly related to the N-terminal tails of the δ-subunits.

1.5.2. Extracellular region:

Extracellular stimuli commonly regulate channels by altering two parameters: the number of channels at the membrane (N), and/or the single channel open probability

(P_o). As these two parameters operate on a continuous scale, the dynamic range of ENaC channel activity is very wide. The extracellular loop comprises the majority of the protein (~50 kDa) and has essential roles in ENaC channel regulation. For example, it is here that H^+-sensing residues are found on ASIC channels, which are involved in their activation (Hiroshi, 2011).

On observation of the ASIC1 structure (PDB: 2QTS; Figure 6.; (Jasti, et al., 2007)), the extracellular loop resembles an outstretched hand holding a ball. The core is formed from β-sheet domains (palm and β-ball) surrounded by α-helical domains (thumb, knuckle and finger), joined to the transmembrane region via two short connections (wrist). The palm and β ball domains exhibit higher levels of sequence conservation across the family of proteins. Conversely, poor conservation in sequence is found within the thumb, knuckle and finger domains, allowing for a divergence in interactions that the channel has with extracellular cues.

All identified ENaC proteins contain 16 conserved cysteine residues in their extracellular loop, probably forming eight disulphide bonds (Jasti, et al., 2007). These domains are likely to represent structural elements important for mediating interactions with extracellular structures through maintenance of the channel's tertiary structure. This domain functions as a sensor that is able to transduce environmental cues via the opening and closing of the channel. Several sites of posttranslational modification in this region include protease cleavage sites and glycosylation sites. Such processing defines both ENaC structure and function, through the regulation of membrane trafficking and P_o (Eldeheit, et al., 2014).

1.5.2.1. Proteolytic activation:

ENaC channels are activated by proteolytic cleavage of specific regions in the extracellular loop (Chraibi, et al., 1998). This activation is the result of an increase in P_o and occurs in two stages: first, in the trans-Golgi network (TGN); and subsequently at the plasma membrane, mediated by proteases such as trypsin or furin (Rossier & Stutts, 2009). Cleavage sites have been identified in ENaC α, δ and γ subunits, releasing inhibitory interactions (Kleyman, et al., 2009; Haerteis, et al., 2009) but, interestingly, these sites are missing in the ENaC β subunit. In the TGN it is most likely that furin, a serine protease that primarily localises there, cleaves the ENaC α subunit twice (R205 and R231 in the mouse sequence) and the γ subunit once (R143 in mouse) immediately following serine residues (Hughey, et al., 2004). At the cell surface, proteases further process these subunits to remove inhibitory tracts in the finger domains (Sheng, et al., 2006). For example, it is thought that GPI-anchored proteases, including plasmin and prostasin, further cleave the γ subunit (reviewed in (Kleyman, et al., 2009).

It has been shown that this proteolytic cleavage increases the P_o, without affecting single-channel conductance or ion selectivity. Cleavage of the inhibitory interactions in the γ subunit increases the P_o more than that of the α subunit, with removal of both having the greatest effect (Carattino, et al., 2008). Furthermore, peptides which correspond to those removed from the ENaC α and γ subunits, have been shown to be inhibitory (Carattino, et al., 2008). However, it is largely unknown how these peptides inhibit ENaC, as there is little conservation in these domains with the ASIC1 channel. Some lines of evidence, based of mutagenesis experiments, suggest it may be due to an interaction occurring between finger and thumb domains (Kashlan, et al., 2010).

Proteolytic cleavage is also observed with the ENaC δ channel. Exogenous application of chymotrypsin directly activates the channel, causing an increase in amiloride-sensitive Na^+ currents, although to a lesser extent as the ENaC α channel (Haerteis, et al., 2009). This may occur at the ENaC δβγ channels expressed in the gastro intestinal tract (Haerteis, et al., 2009) and in hippocampal and cerebral cortical neurons where these trypsin-like proteases are also expressed (Vukicevic, et al., 2006). The differences in the change of ENaC current between the α and δ channel may be explained by the presence of a dormant pool of the unprocessed form of these ENaC subunits (Haerteis, et al., 2009). The currents measured in oocytes expressing the ENaC δ channel is higher than those of the α channel, despite equivalent levels of channel expression. It is hypothesised that there is a smaller pool of unprocessed ENaC δ subunits, and therefore a larger number of active channels at the cell surface. On addition of chymotrypsin there are fewer unprocessed proteins to be cleaved, resulting in a smaller increase in current. The cleaved ENaC δ peptide was detectable using western-blot (Haerteis, et al., 2009).

1.5.2.2. Glycosylation sites:

Several asparagine (Asn) glycosylation sites on the ENaC proteins have been characterised: 6 for ENaC α, 12 for ENaC β, and 5 for ENaC γ (Kellenberger & Schild, 2002). Alignment of subunit sequences across different species showed that these are conserved in mammals and rats, but not lower species (Canessa, et al., 1994). Canessa, et al. (1994) used site-directed mutagenesis on N-linked glycosylation sites to further support that these transmembrane domains are linked by a large cysteine-rich extracellular loop and that the NH2- and COOH- termini are intracellular. Although not

fully characterised, it is predicted that the ENaC δ subunit also undergoes glycosylation. Haerteis, et al. (2009) showed that in oocytes expressing ENaC δ, two prominent bands could be detected using western blot at 75 and 86 kDa. They concluded that these were not cleavage products, but were in fact the glycosylated and nonglycosylated forms of the protein. This was supported by experiments which used the enzymes *N*-glycosidase F or endoglycosidase H_f to remove N-linked glycoproteins, and resulted in just one visible band at 75 kDa.

Removal of these glycosylation sites from the ENaC α subunit through mutating the Asn residues was shown to have no effect on ENaC currents, however complete blockade of N-linked glycosylation reduces channel activity (Haerteis, et al., 2009). Glycosylation, therefore, appears to be important for channel function and trafficking.

1.5.2.3. Inhibition of channel activity by extracellular Na^+:

Two mechanisms for channel inhibition by extracellular Na^+ have been described and are defined by their distinct kinetics and sites of action. The first of these is called Na^+ self-inhibition. This occurs over seconds in response to a rise in extracellular Na^+. Despite an initial increase in current due to the increase in electrochemical driving force, the current then declines to a steady state value (Sheng, et al., 2004) and is characterised by a decrease in P_o (Sheng, et al., 2006). This effect is greatest if the inhibitory tracts of ENaC subunits have not been cleaved during posttranslational modifications (Sheng, et al., 2006). It is believed to be a result of Na^+ binding to an allosteric site in the extracellular portion of the ENaC channel (Fuchs, et al., 1977; Sheng, et al., 2006). Na^+ self-inhibition has been observed in both ENaC α and δ channels expressed in oocytes, where whole-cell currents were measured on

application of higher Na^+ concentrations to the bath (Fuchs, et al., 1977). The self-inhibition time for the ENaC δβγ channel was over three-fold greater than of the ENaC αβγ channel (Ji, et al., 2006).

The second process of inhibition is called Na^+ feedback inhibition. This occurs over minutes in response to an increase in cytosolic Na^+. The observed reduction in the ENaC current is thought to be a result of a decrease in cell surface expression of the ENaC channels, mediated by the ubiquitin ligase Nedd4-2 (Anantharam, et al., 2006), and a decrease in single-channel activity, linked to diminished proteolytic cleavage (Knight, et al., 2008).

1.5.2.4. Proton sensing:

The ENaC δ channels are constitutively active; however extracellular acidification is thought to modulate the gating kinetics of ENaC δ channels by increasing the channels' P_o (Yamamura, et al., 2004), with an EC_{50} value of pH6.0 for proton activation (Zhao, et al., 2012). This acid-sensing capability is shared with ASIC channels, which have been studied much more extensively in terms of their physiological roles. In the brain, ASIC1a channels are activated by proteolytic cleavage at Arg-145, which is located in the N-terminal part of the extracellular loop (Vukicevic, et al., 2006). This residue falls within the domain implicated in the inactivation kinetics and pH dependence of gating. Proton activation of brain ASIC channels has been linked to hypoxia-induced neuronal damage with degenerative consequences (Siesjo, et al., 1995; Keung Tai & Truong, 2013).

Titration of important residues in the extracellular loop of the ENaC δ channel leads to a conformational change that increases the P_o of the channel through extended

opening time (Ji & Benos, 2004). The main difference between the acid-sensing component of the ASIC and ENaC δ channels is the time for activation and desensitisation kinetics in response to a decrease in extracellular pH. Whereas ASIC channel kinetics are fast, ENaC δ channel kinetics are very slow (Ji & Benos, 2004). It has been suggested that this feature of ENaC δ channels could aid acid sensing in situations of slow extracellular pH changes. For example, the channel may also be a key coordinator of oxidative stress in the ischaemic brain (Yamamura, et al., 2004).

1.5.2.5. Amiloride binding:

In addition to residues within the channel pore itself, Ismailov, et al. (1996) identified a tract in the extracellular domain of the rat ENaC α subunit (WYRFHY, residues 278-283; Figure 7.c), proposed to be a putative amiloride binding domain. Deletion of these residues in the α subunit caused over a 100-fold decrease in sensitivity to amiloride binding, both when expressed alone and with rat β and γ subunits (Ismailov, et al., 1996). Further interrogation using single-point mutations identified the importance of each residue individually. Other channel characteristics including cation selectivity and single-channel conductance were unchanged as a result of these mutations (Ismailov, et al., 1996).

This six amino-acid domain is conserved across all species of cloned ENaC α subunit, including in humans (residues 251-256 (Voilley, et al., 1994). This conservation extends to the human ENaC δ subunit, with a WYHFHY tract located in its extracellular domain at positions 232-237. The contribution of this domain to amiloride binding at the ENaC δ channel remains to be investigated.

1.5.3. The carboxyl terminus:

The balance of membrane channel trafficking, channel endocytosis and channel recycling directly impacts on the channel density at the membrane. The half-life for ENaC αβγ membrane residence is about 1h (Staub, et al., 1997) despite levels of the channel at membrane remaining relatively constant. Identifying key orchestrators of these processes becomes essential to understand the life cycle of ENaC δ channels.

A conserved region in ENaC α, β and γ proteins includes a proline-rich motif in the cytoplasmic COOH terminus (Figure 7.d). These PY motifs are unique to the ENaC subfamily and have the consensus sequence PPPXYXXL, located 65-70 residues after the end of TM2. These participate in protein-protein interactions (Eastwood & Goodwood, 2012), for example they are recognised by WW domains on Nedd4-2 for ubiquitination (Snyder, et al., 2004), or by the Serum- and Glucocorticoid Kinase (SGK) for phosphorylation (Diakov & Kormacher, 2004). Their close proximity to the intracellular side of the plasma membrane facilitates interactions with components of the lipid bilayer, and phosphoinositides located at the membrane (Di Paolo & De Camilli, 2006). The lack of this PY motif in ENaC δ deduces a divergence in protein-protein interactions.

It is currently accepted that all ENaC protein trafficking and membrane anchoring pathways depend on ubiquitination through Nedd4-2, an E3 ubiquitin ligase (Snyder, et al., 1995). In the context of the ENaC αβγ channels, two main hormonal pathways that converge on this enzyme are the anti-diuretic hormone (ADH) pathway and aldosterone pathway (Rossier, 2002). The net effect of each pathway is that Nedd4-2 is no longer able to ubiquitinate ENaC, which leads to a higher channel density at the membrane (Snyder, et al., 2004).

ADH is an important regulator of extracellular fluid volume. It increases intracellular cyclic-AMP (cAMP) levels, which augments the activity of cAMP dependent protein kinase-A (PKA). PKA has the ability to phosphorylate key residues in Nedd4-2 and specifically accelerates the endocytosis of β and γ subunits (Staub, et al., 1997). PKC has not yet been studied in the context of the ENaC δ channels.

Aldosterone release is dependent on Angiotensin and is able to elevate the intracellular serum and glucocorticoid kinase (SGK) levels. SGK inhibits the activity of Nedd4-2, via phosphorylation of key residues (Debonneville, et al., 2001). Aldosterone has also been shown to upregulate the rate of ENaC αβγ channel transcription (Verrey, 1999). More recently, studies have shown tissue specific coexpression of ENaC δ and SGK1.1, a novel isoform of SGK, which regulates the activity of ENaC δ in CNS (Wesch, et al., 2010). Inhibition of Nedd4-2 activity by SGK1.1, results in an amplification in ENaC current. This was observed in both hetero- and homo-trimeric ENaC δ channels. Nedd4-2 has previously been found to interact with α, β and γ subunits via the PY motif (Debonneville, et al., 2001), however ENaC δ is able to interact with Nedd4-2 via other unknown residues.

Analysis of the amino acid sequence of the C- and N-terminal domains of the ENaC δ subunit does reveal proline residues, which are particularly rich in the N terminus, and may provide binding sites for interacting proteins via WW or SH3 domains (Sudol, 1998). Biasio, et al. (2003) screened a human brain cDNA library with each-terminal domain to identify any interacting proteins. One protein found to interact with the ENaC δ C-terminal domain was Murr1 (mouse U2af1-rs1 region), which is a protein that has been implicated in copper transport (van De Sluis, et al., 2002). Murr1

additionally bound to the β and γ subunits, but not ENaC α. When it was coexpressed with either δ or α containing ENaC channels, there was no sodium current. This was reversed on the truncation of the C terminus of the ENaC δ subunit. This inhibition in ENaC current has been linked to a reduction in cell surface expression of the ENaC proteins and suggests that Murr1 plays a role in the recruitment of the subunits to the plasma membrane.

1.5.4. The Amino terminus:

In addition to the 'degenerin' site, the second identified region linked to channel gating is a His-Gly (HG) motif. This is located cytoplasmically in the NH2-terminal domain between a putative hydrophobic α-helix and the TM1 domain. Mutations within this motif are implicated in pseudohypoaldosteronism type I (PHA-1), a Na^+ wasting disorder characterised by unresponsiveness to aldosterone in ENaC expressing kidney cells (Hanukoglu, 1991). Genetic studies in patients with an autosomal recessive disorder have identified specific mutations in all ENaC subunits, excluding ENaC δ (Hanukoglu, 1991).

Within this HG motif, and its surrounding region, substitution of Ala, Ser or Gly residues to larger ones increases current as a result of longer opening times for each individual channel (Champigny, et al., 1998). A mutation in a corresponding Ala residue in *C.elegans* degenerins causes degeneration of touch receptor cells, which appears to be a consequence of cations leaking into the cells (Driscoll & Chalfie, 1991). This infers that cytosolic residues may be closely associated with the pore.

1.6. Physiological role of the ENaC δ channel in the brain:

Although the physiological role of the canonical ENaC αβγ channel is well documented, that of the ENaC δ channels is largely unclear. Some processes for which it has been described in the context of include: fluid absorption, mechano-sensing, salt taste and sour taste receptor signalling, and sperm motility and capacitation (Hernandez-Gonzalez, et al., 2006). Most interestingly, in neurons it has been proposed that the ENaC δ channel may have a role in the generation of an action potential.

ENaC δ channels exhibit constitutive channel activity, which permits a persistent influx of a depolarising Na^+ current into a cell. Studying the distribution of ENaC δ channels in the human brain has been shown that it is expressed in pyramidal neurons in the cerebral cortex (Wesch, et al., 2010). Gradual depolarisation of the resting membrane potential of such a cell can facilitate the generation of an action potential by amplifying the effect on synaptic potentials. As a result, stimuli which would not normally be large enough to raise the membrane potential above its threshold potential, would now be able to initiate an action potential.

The ASIC1a channel in the central nervous system has been implicated in synaptic plasticity, specifically in long-term potentiation (LTP). It was shown that by genetically deleting or blocking the ASIC1a channel with a pharmacological agent, LTP in the CA1 region of the mouse hippocampus was greatly reduced, in part due to N-methyl-D-aspartate receptor (NMDAR) -dependent mechanisms (Liu, et al., 2016). As with the ASIC1a channel, ENaC δ exhibits a proton sensitivity. This suggests that small fluxes in synaptic pH may also activate these channels, leading to postsynaptic plasticity involved in aspects of learning and memory (Bianchi & Driscoll, 2002; Wemmie, et al., 2002).

1.7. ENaC δ, disease and neurodegeneration:

The ENaC channel has been documented in the context of genetic and non-genetic diseases, however more commonly it is the α- containing channels for its role in PHA-1 (Schild, 1996). This is characterised by severe neonatal salt-wasting and an inability for sodium retention in the kidney, and is directly linked to the ENaC αβγ channel function due to the identification of mutations in the genes encoding its subunits. To date, this excludes the *SCNN1D* gene encoding the ENaC δ subunit. A missense mutation (G37S) of the conserved glycine residue of the HG motif in the N-terminus of the β-ENaC subunit has been shown to cause a loss-of-function of the channel. Despite no change in surface expression, this mutation disrupts channel gating, reducing the probability of the channel opening (Gründer, et al., 1997). Furthermore, PHA-1 has also been linked to interference with disulphide bridge formation. The extracellular loop contains cysteine-rich domains and the disulphide bridge C133–C305 in the human ENaC α subunit has been linked through studies on thermosensitive mutants (Gründer, et al., 1998).

Genetic links between the *SCNN1D* gene and disease are less clear. In the NCBI database, 404 single nucleotide polymorphisms of *SCNN1D* have been collected but corresponding phenotypes have not yet been identified. This gene is located on chromosome 1 and terminal distal nonlethal deletion, large enough that it leads to loss of this gene, is characteristic of some rare diseases. One of these, monosomy 1p36 deletion syndrome (Keppler-Noreuil, et al., 1995), is characterised by distinct craniofacial features, associated with mental retardation, hypotonia, muscle hypotrophy, seizures, brain abnormalities and heart diseases (Battaglia, 2005).

Additionally, in autism patients 1p36 can be truncated from 1.19 to 1.23 Mb (van der Zwaag, et al., 2009), which is a region encoding both *SCNN1D* and *UBE2J2* genes. On the other hand, gain of copies of the *SCNN1D* gene has been noted in cardiovascular diseases (Prakash, et al., 2010). The contribution of *SCNN1D* to these diseases, however, is undefined.

ENaC δ has also been linked to non- genetic diseases, including ischemic disorders. Owing to its acid-sensing capabilities, proton-activated ENaC δβγ currents have been shown to be regulated by hypo-osmolarity and EDTA. This indicates the channel may integrate ischemia-related signals in inflamed and hypoxic tissues (Ji & Benos, 2004; Ji, et al., 2006). During cardiac and brain ischemia, the production of acids, such as pyruvic acid, can result in acidosis within minutes (Silver & Erecinska, 1992). Facilitation of proton-activated currents by these acidic metabolites strongly indicates that ENaC δ is most likely involved in ischemic signal transduction. Although ASIC channels are thought to be activated to transduce ischemia-related signals, pH decrement generally requires minutes to develop. ASIC channel kinetics are much faster than those of ENaC δ channels: ASIC channels activate within a millisecond, and desensitise in less than a second (Waldmann, et al., 1991). ENaC δ is distinguished by very slow activation and desensitisation (Ji & Benos, 2004), which would allow time for ischemic cells to detect changes in proton concentration and osmolarity.

1.8. ENaC channel modulators:

As with any protein when designing a tool to inhibit its function, this can either be via a direct interaction with the protein itself, or by indirectly disrupting regulatory pathways that converge on the protein. Tool compounds tend to directly inhibit their

target at sub-micro molar concentrations. Here, a number of ENaC channel modulators are discussed.

1.8.1. Amiloride and its therapeutic potential:

The first and prototypical inhibitor of the ENaC channel was amiloride, a pyrazine-carbonyl-guanidine approved for use as a potassium-sparing diuretic. In a clinical setting it is often used as an adjunct to thiazide and loop diuretics, with its primary site of action is the distal tubule and collecting ducts of the nephron. Here, it selectively blocks sodium transport and inhibits sodium-potassium exchange independent of aldosterone (Vidt, 1981). Binding to and blocking of amiloride-sensitive sodium channels decreases the net negative potential of the tubular lumen and reduces both potassium and hydrogen secretion and their subsequent excretion. As amiloride is able to bind to and block both ENaC and ASIC channels, its use has been explored in different disease settings in which these channels are implicated in the pathology.

Even before the cloning of the ENaC subunits, and its target identified, amiloride was investigated as a therapeutic option in cystic fibrosis (CF) patients (App, et al., 1990). Amiloride-sensitive sodium currents exist in lung epithelia and an increase in the absorption of Na^+ has been implicated in the pathogenesis of CF. The Cystic fibrosis transmembrane regulator (CFTR) and ENaC channel are the principal rate-limiting steps for Cl^- secretion and Na^+ absorption by ciliated airway epithelia, opposing processes, which both determine the pericillary layer depth. This must be maintained within a range that permits mucocillary clearance and unimpeded gas flow in the airway lumen. Therefore the lack or decrease in CFTR activity or increase in ENaC activity leads to a decrease in mucocillary clearance, characteristic of CF patients

(Smith, et al., 1994). Although in clinical trials treating chronic CF patients with amiloride were unsuccessful due to its rapid clearance from the lungs (Knowles, et al., 1990; Graham, et al., 1993; Pons, et al., 2000), a murine model provided proof of concept for the use of an ENaC blocker in the treatment of CF. The model overexpresses the ENaC β subunit and shows many well-defined CF traits, including mucus obstruction, goblet cell metaplasia, airway inflammation, impaired clearance, and mortality (Mall, et al., 2004). Amiloride inhalation effectively reduced the overproduction of mucus, airway obstruction and inflammation. Experimental studies on transgenic mice that receive treatment with amiloride from birth also suggest that it may be of use as a preventative measure much earlier on in the disease, before other factors of chronic CF could impede the therapeutic benefits of a drug (Zhou, et al., 2008).

Amiloride has a further role in the prevention of neurodegeneration through targeting of the ASIC channels in the brain, namely the ASIC1a channel. Disruption of a continuous supply of oxygen to the brain can lead to hypoxia-induced neuronal damage. The mechanism underlying this was thought to involve excessive stimulation of NMDARs by the excitatory neurotransmitter, glutamate, evident by the high levels of glutamate present in the ischaemic brain (Choi & Rothman, 1990). Glutamate has also been seen to induce neuronal cell death via NMDARs in rodent models; however NMDAR antagonists have not yet been shown to have therapeutic benefit (Simon, et al., 1984). Another factor, now thought to contribute to this form of neuronal damage is acidosis, which aggravates brain injury during ischaemia (Siesjo, et al., 1995). Activation of ASIC channels via a low extracellular pH increases the inward movement

of Ca^{2+}, but Ca^{2+} overload can lead to cell death. Promisingly, amiloride has been shown to possess neuroprotective and anti-seizure properties in a rat model of cardiac arrest-induced global cerebral hypoxia and reperfusion (Keung Tai & Truong, 2013).

A final example of amiloride's therapeutic potential is in the treatment of the neurodegenerative aspect of primary progressive multiple sclerosis (MS), for which current immunomodulatory treatments are inadequate. Most treatments thus far have focused on white matter inflammatory lesions, despite a strong correlation between neuroaxonal loss and clinical impairment (Haines, et al., 2011). Studies in post-mortem patients with the disease show a large upregulation of the ASIC1 channels in axons and oligodendrocytes, responsible for harmful intracellular cation levels (Na^+ and Ca^{2+}; (Vergo, et al., 2011). Low pH in the MS brain allows for the opening of the ASIC channels and conductance of Na^+ and Ca^{2+} into the cell. By blocking ASIC1 with amiloride, neuroprotective and myeloprotective effects have been observed in both acute and chronic experimental models of multiple sclerosis (Friese, et al., 2007; Vergo, et al., 2011). Furthermore, studies in human patients with primary progressive MS examined ASIC1 expression in chronic brain lesions from post-mortem patients and used MRI markers of neurodegeneration as outcome measures of neuroprotection (Arun, et al., 2013). This was in alignment with the animal studies. In a cohort of 14 patients, over three years, Arun and colleagues (2013) showed ASIC1a to be a promising target for neurodegeneration.

1.8.2. Amiloride derivatives:

Due to the failure of amiloride to show efficacy in clinical trials in CF patients, subsequent derivatives of amiloride were investigated. Amiloride's affinity for the

ENaC αβγ channel is in the nanomolar range (IC_{50} ~ 200 nM; (Kleyman & Cragoe, 1988), and it also shows affinity for other transporters such as the Na^+/H^+ exchanger and the Na^+/Ca^{2+} antiporter in the micromolar range (Frelin, et al., 1988). However, the primary issue with amiloride's application in CF was its short retention time in the lungs. Amiloride has an extremely short half-life in the airways after inhalation, with *in* vitro data suggesting the half-life to be ~9 min (Tarran, et al., 2001). It is thought this may be caused by rapid absorption by organic cation transporters (Hirsh, et al., 2004). The aim for amiloride derivatives was to improve the retention time in the lungs, and therefore the overall efficacy. Systematic studies introducing substitutions in each of amiloride functional moieties led to the development of inhibitors with enhanced specificity towards ENaC. Two of these second generation analogues were benzamil and phenamil.

On comparison to amiloride, benzamil and phenamil have substituted benzyl and phenyl groups, respectively, on the terminal nitrogen atom of the guanidinium moiety of amiloride (Figure 8.a). They are much more potent than amiloride (amiloride IC_{50} ~300 nM; benzamil IC_{50} ~35nM; phenamil IC_{50} ~75 nM (Hirsh, et al., 2004)). However both have a decreased pK_a value (amiloride pK_a = 8.8; benzamil pK_a = 8.1; phenamil pK_a = 7.8; (Kleyman & Cragoe, 1988)) and therefore are more lipophilic at physiological pH (~7.2). Consequently, *in vitro* studies in cultured human and ovine bronchial epithelial cells showed that the increased lipophilicity counteracted the increased potency, and the efficacy of these compounds remained similar to that of amiloride (Hirsh, et al., 2004).

1.8.3. Other: pyrazinoyl quaternary amines:

A series of compounds that were chemically distinct from the prototypical ENaC blockers were later synthesised by Novartis (Hunt, et al., 2012). This new class of ENaC blocker attempted to address the pharmacodynamics properties of the amiloride derivatives, which had given rise to their fast clearance in the airway epithelium. Despite the absence of a crystal structure of the ENaC channel, it is acknowledged that the guanidinium moiety binds to the outer mouth of the selectivity filter and the pyrazine ring binds near the TM2 domain (Sheng, et al., 2004). The relative spatial arrangement of these two functional groups is essential for blockade of ENaC (Venanzi, et al., 1992), however reports suggested that the positively charged acylguanidinium functional group was replaceable (Figure 8.b (Li, et al., 1985; Russ, et al., 1992).

In search of a treatment of CF which could be administered by inhalation, this new series of compound, that lacked the pyrazinoyl guanidine moiety characteristic of amiloride, was pursued. Hunt and his colleagues (2012) speculated that if the acyl guanidine of amiloride was replaced by a group which ionized at physiological pH, that new group would represent a bioisostere and produce broadly similar biological properties to amiloride. The first of these bioisosteres was an amine group (Figure 8.c). The resulting compound showed the ability to block the ENaC channel, despite a 10-fold decrease in its potency. Further SAR efforts led to the understanding that the two-carbon linker between the amide and amine was optimal; that this amine could be substituted with small alkyl groups; but methylation of the amide N-H saw a large drop in potency.

Hunt, et al. (2012) went on to identify a quaternary amine, which had comparable activity to amiloride (IC_{50} ~ 200 nM) and allowed for enhanced solubility without

compromising cell permeability, making it more suitable for a nebuliser (Figure 8.d). Further research developed a α-branched derivative with an even higher affinity (IC_{50} ~ 12 nM), which proved to be highly efficacious *in vivo* (Figure 8.e) (Hunt, et al., 2012), demonstrating that bioisosteres can be a successful approach to drug discovery for novel classes of compounds.

1.8.4. Other: P-1037 and P-1055:

Parion Sciences is a development stage biopharmaceutical company dedicated to research, development and commercialization of treatments to improve and extend the lives of patients with innate mucosal surface defence deficiencies of the lung or eye. It is at the forefront of developing inhibitors of ENaC for the potential treatment of pulmonary diseases, for example cystic fibrosis. The company has a portfolio of novel and proprietary inhaled ENaC inhibitors, with an aim to hydrate mucus associated with respiratory disease. This, for example in a CF setting, would aid clearance of mucus build up along airway epithelium. Two such inhibitors, P-1037 and P-1055 (undisclosed structures), were a focus of further studies into the treatment of CF and other pulmonary diseases. Inhaled delivery of a small dose of a drug has the advantage of achieving a high local concentration, whilst minimising systemic adverse effects. This is an ideal scenario for drug targets located in airway epithelium e.g. the ENaC α, but not δ, channel.

In 2015 a collaboration was established between Parion Sciences and Vertex Pharmaceuticals Incorporated, a global biotechnology company with a broader range of disease area interests. The premise of this partnership was to commercialise these two inhibitors, through the provision of funding to complete the necessary clinical

trials. P-1037, or otherwise known as VX-371, as a monotherapy in a short Phase 2 CF study, failed to show any signs of efficacy. This may have been due to the short duration of the study (14 days) but it was also suggested that the efficacy of an ENaC blocker may be limited if there is inadequate anion secretion. Therefore in September 2017, a Phase 2 study was completed that aimed to test the safety and effectiveness of VX-371 in CF patients, who are homozygous for the F508del-CFTR mutation, and are taking Orkambi (lumacaftor/ivacaftor). 142 patients completed the 28 day study but it failed to meet its primary endpoints. Spirometry, as measured by a percentage predicted Forced Expiratory Volume in the first second ($ppFEV_1$) is a standardized assessment to evaluate lung function that is the most widely used endpoint in cystic fibrosis studies. In this study patients receiving hypertonic saline saw a decrease in $ppFEV_1$ of 0.1 percentage points, and those receiving VX-371 and hypertonic saline saw an increase in $ppFEV_1$ of only 0.1 percentage points. Currently there are no plans for further development of this drug in CF.

1.8.5. Other: SPLUNC1 and SPX-101:

Short palate lung and nasal epithelial clone 1 (SPLUNC1) is a secreted, innate defence protein of ~28 kDa, which has been shown to be an inhibitor of ENaC expressed in airway epithelia (Garcia-Caballero, et al., 2009). In healthy lungs, SPLUNC1 is secreted by airway epithelial cells as an autocrine regulator of ENaC to limit sodium and water absorption. However, this action is pH dependent. In CF lungs, the acidic environment prevents this ENaC regulation due to abnormal folding of SPLUNC1 at low pH (Tarran & Redinbo, 2014). This protein was found to prevent ENaC proteolysis and inhibited ENaC-mediated currents in both *Xenopus* oocytes and in human bronchial epithelial

cultures (Garcia-Caballero, et al., 2009). However, although it prevents ENaC proteolysis, SPLUNC1 does not inhibit protease activity but binds to ENaC, preventing it from being cleaved (Garcia-Caballero, et al., 2009).

The domain responsible for this interaction with ENaC was identified in the N terminus of SPLUNC1, consisting of 18–amino acids (S18). Unlike the full-length protein, S18 was found to regulate ENaC in a pH-independent manner (Hobbs, et al., 2013). Scott, et al. (2017) exploited this therapeutically by optimising the natural sequence of S18 to improve its stability and then delivering it via nebulisation into the lung. This new drug, SPX-101, was seen to induce internalisation of ENaC in normal and CF human bronchial epithelial cells (HBECs), representing a novel peptide promoter of ENaC internalisation. *In vivo* it was shown to increase hydration and mucociliary clearance in the lungs, which has the potential to serve as a new therapeutic treatment for CF.

1.8.6. Evans Blue:

Complications of *in* vivo studies of the ENaC δ channel in the standard models for physiological research arise due to the absence of this gene in rodents. Therefore, there is a heightened need for a pharmacological tool that is able to discriminate between the two ENaC channel forms, for which amiloride is not a suitable candidate. ENaC δ is less sensitive to amiloride block and although amiloride is more potent for the canonical ENaC α channel, it is not selective enough to inhibit just ENaC α without significantly affecting the ENaC δ channel.

Previous work by Yamamura and co-workers (2005) appeared to have identified a suitable candidate to be Evans Blue (EvB). They indicated that EvB inhibited the activity of the human ENaC δβγ, but not αβγ, channel. It has since been demonstrated

that EvB directly interacts with amiloride, and therefore suggests that previous findings had in fact been an artefact and not representative of ENaC blockade by EvB.

At physiological pH 7.4, the guanidinium functional group of amiloride is protonated, and this positive charge is required for ENaC block (Kleyman & Cragoe, 1988). The four sulfonic groups in EvB, however, carry negative charges at pH 7.4 (Figure 9.). Perniss et al. (2015) showed that ionic interactions between these two compounds resulted in their precipitation in aqueous solution which was observed in a concentration-dependent manner. This chemical interaction reduces the effective concentration of amiloride in experimental solutions, observed as a reduction in amiloride-sensitive ion currents. These findings were supported by electrophysiological data. Therefore, there still remains no known selective inhibitor of the ENaC δ channel.

1.9. Aims of this investigation:

To establish and characterise a heterologous expressions system that could be used across a range of ion channel screening platforms to identify novel pharmacological tools for the investigation of ENaC δ channel function.

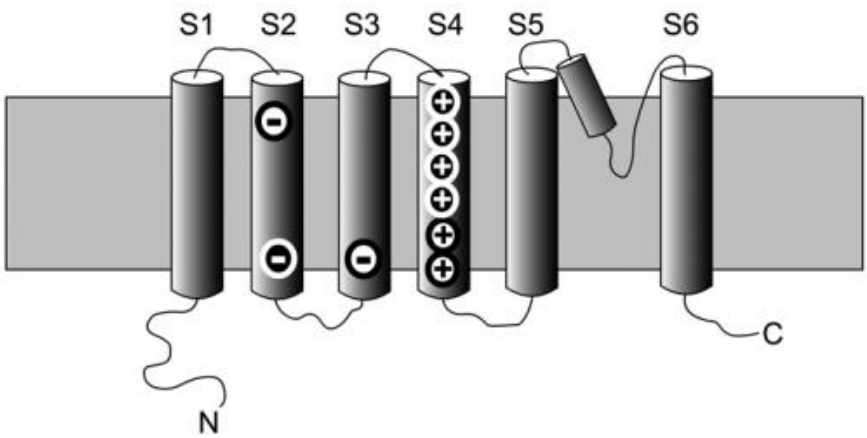

Figure 1. **Diagram of one voltage-gated ion channel (VGIC) subunit/domain.** Four separate protein subunits or domains of a single protein form one VGIC. Each subunit/domain has 6 membrane-spanning regions, named S1-S6, of which S1-S4 comprise the voltage sensing domain , with the S5-loop-S6 region containing the gating and pore-forming domains (Hille, 2001). Taken from Bezanilla (2005).

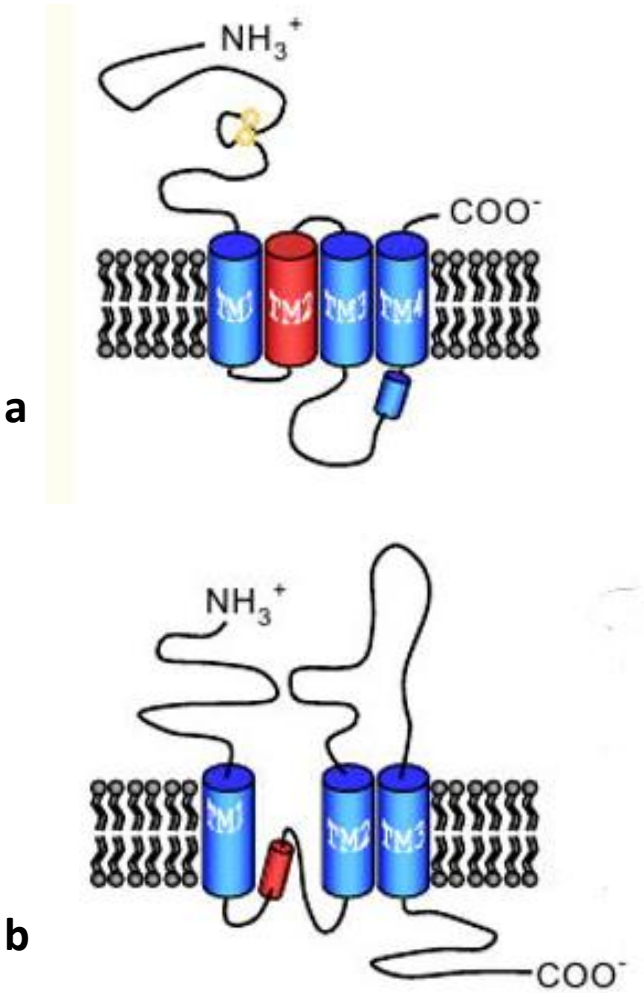

Figure 2. **Diagram of two ligand-gated ion channel subunits. a** One subunit of the pentameric cys-loop ion channel, with each subunit comprising 4 membrane-spanning domains. The second of the domain (TM2) plays roles in ion conduction/selectivity. The disulphide bridge, which lends to these ion channels name, is shown in yellow. **b** One subunit of the tetrameric ionotropic glutamate receptor, with each subunit comprising 4 membrane-spanning domains. Ion conduction/selectivity is mediated by a region between TM1 and TM2. Taken from Collingridge (2009).

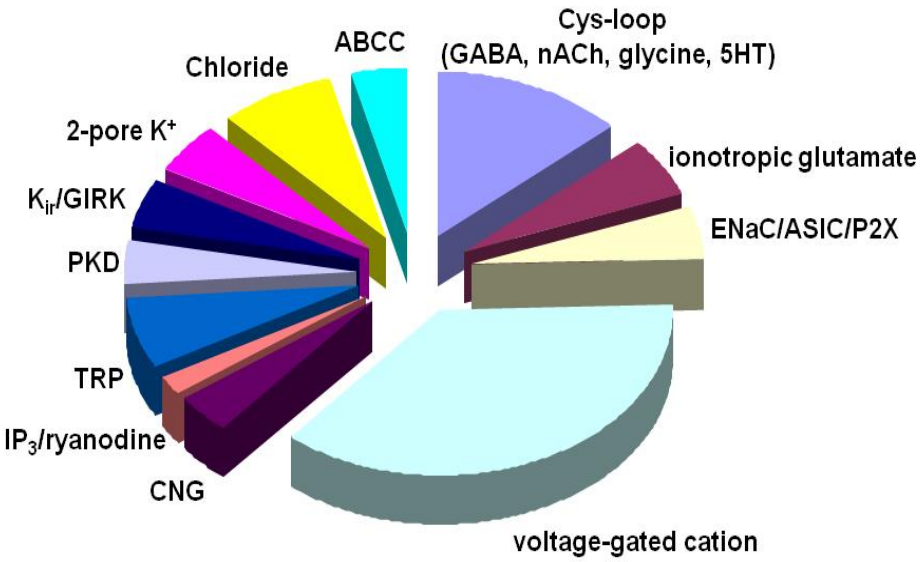

Figure 3. **Ion channel diversity.** The chart shows the major ion channel subfamilies. The sizes of the pies chart are a representation of the current understanding of the size of the subfamily in relation to others. Taken from Clare (2010).

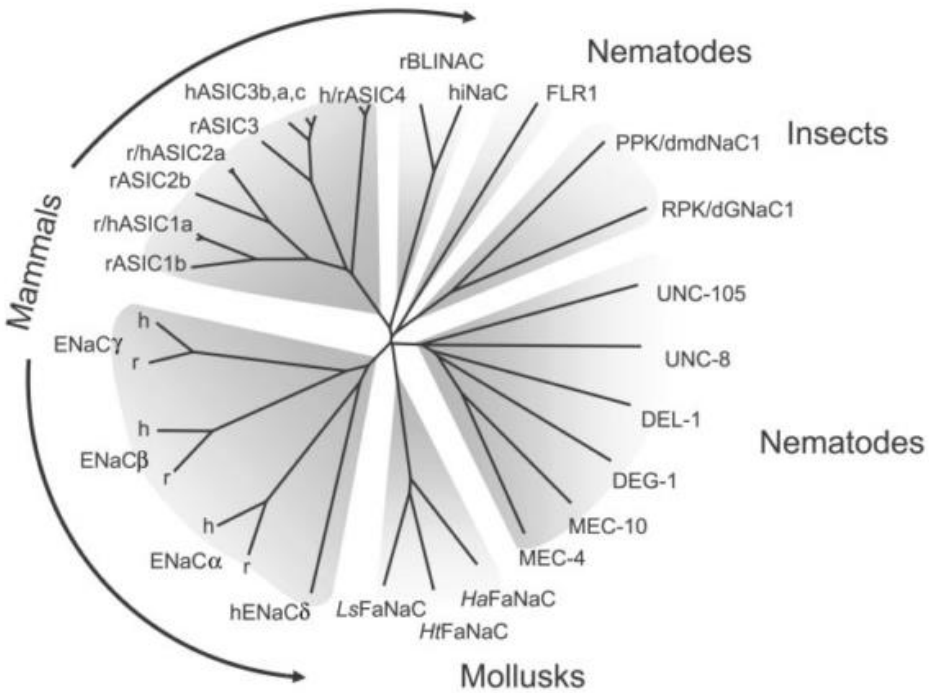

Figure 4. Phylogenetic tree of DEG/ENaC protein sequences. Members of the ENaC/DEG family have been identified in diverse species and ca be organised into subfamilies based on their sequences. Taken from Kellenberger & Schild (2002) who aligned the sequences with the ClustalW algorithm.

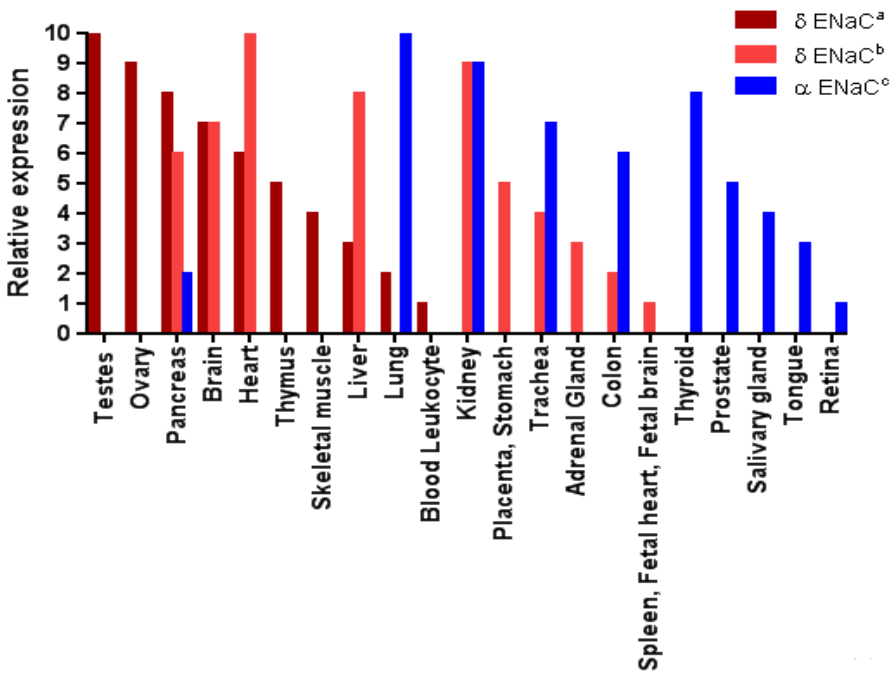

Figure 5. ENaC δ (*SCNN1D*) and ENaC α (*SCNN1A*) tissue expression profiles. Expression levels ranked 1-10, with 10 representing where the highest expression levels were found. [a]Data is taken from Waldmann, et al. (Waldmann, et al., 1995) from northern blots with mRNA samples of 16 different types of tissue. [b]Data is taken from Yamamura, et al. (Yamamura, et al., 2006) from dot-blot analysis from 73 patients and 73 different types of tissue.

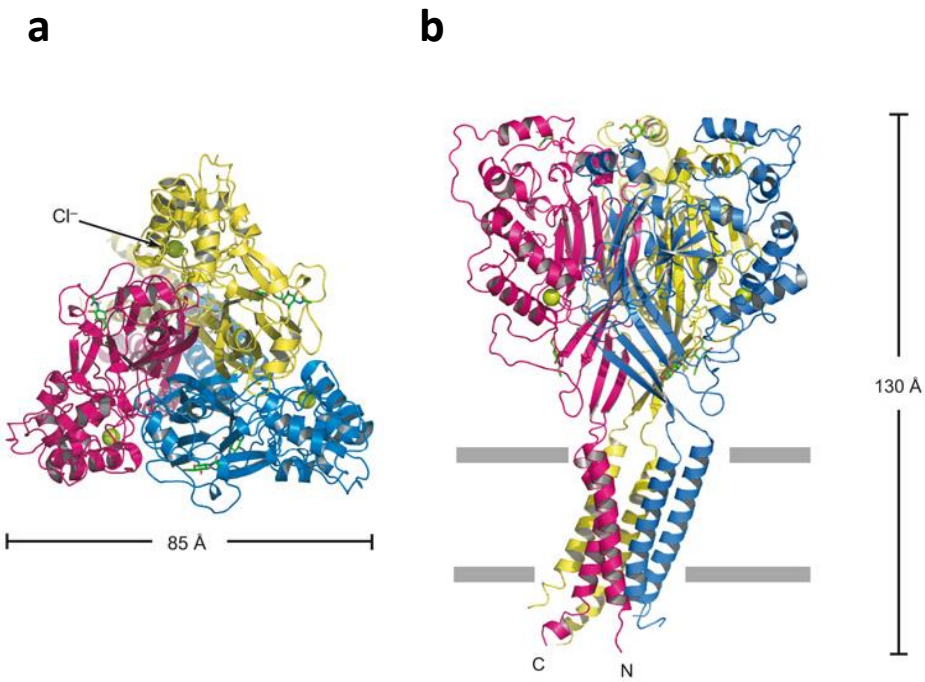

Figure 6. Crystal structure of an acid-sensing ion channel 1 at 1.9 A resolution and low pH. a View of the homotrimeric ASIC1 structure parallel to the molecular three-fold axis from the extracellular side of the membrane. Each crystallographically independent subunit is in a different colour, a single chloride ion per subunit is shown as a green sphere and N-linked carbohydrate is shown in stick representation. **b** Stereoview of the homotrimeric ASIC1 structure viewed parallel to the membrane plane. Taken from Jasti, et al.(2007).

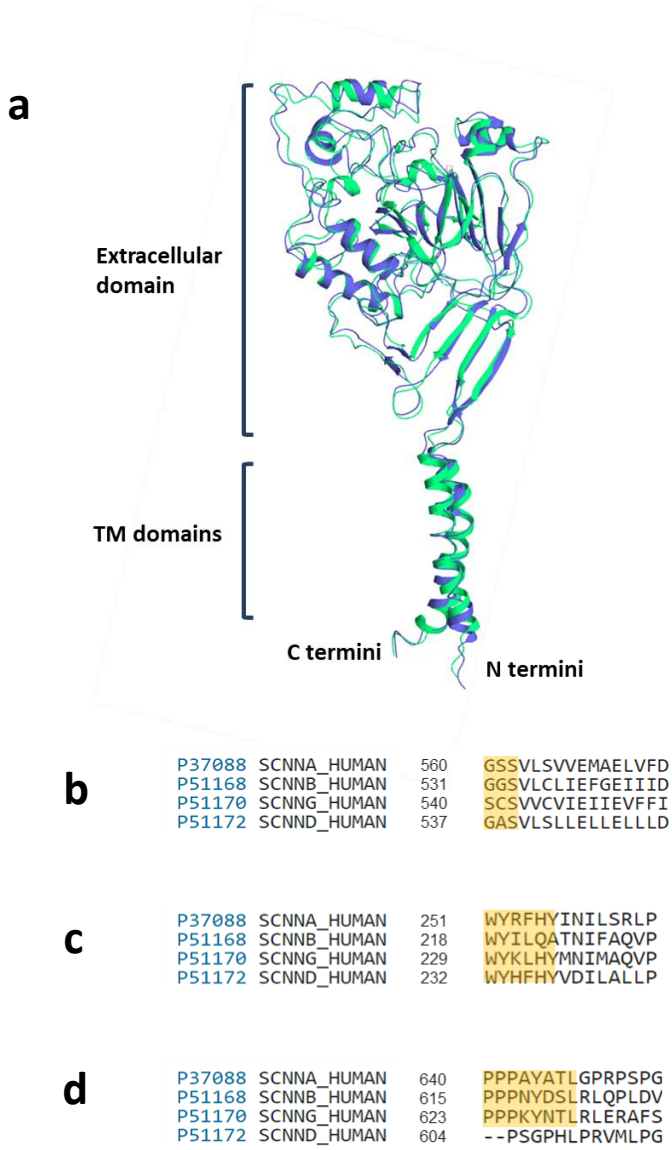

Figure 7. Homology model of the ENaC δ subunit based the ASIC 1 subunits from the crystal structure of the ASIC 1 channel from *Gallus gallus*, PDB: 2QTS. **a** Modelled using Maestro 10.6, showing TM domains, and extracellular domain (thumb, finger, knuckle, palm and β ball). Green= conserved regions. Blue= diverged regions (Jasti, et al., 2007). **b-d** Sequence alignment of the human ENaC α, β, γ, subunits, specifically the TM2 selectivity filter (**b**), the extracellular amiloride-binding domain (**c**) and the PY motif (**d**), which is not conserved in the ENaC δ subunit. Alignment were made using the UniProt alignment tool (www.uniprot.org/align).

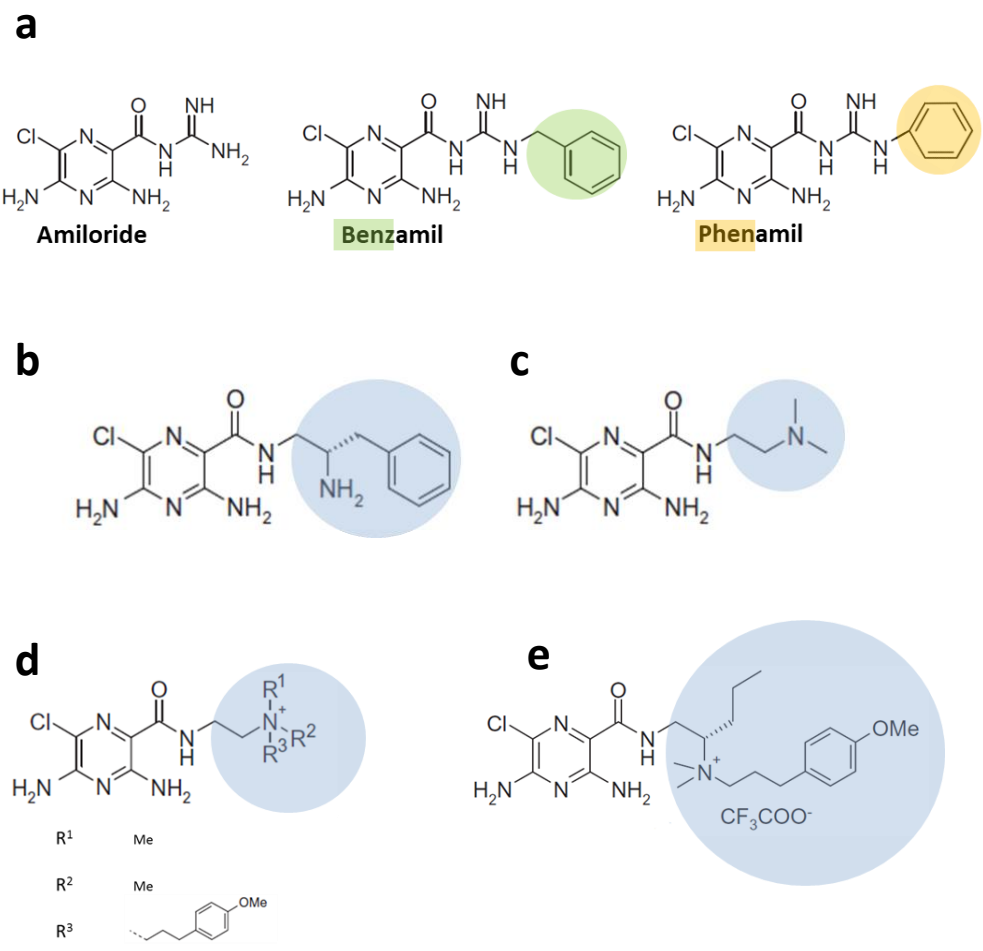

Figure 8. ENaC blockers. a Examples of pyrazinoyl guanidine ENaC blockers, Amiloride, Benzamil, and Phenamil. **b** Pyrazinoyl quaternary amine, whereby the positively charged acylguanidinium functional group was replaced (Russ, 1992) **c** Pyrazinoyl quaternary amine, whereby a bioisosteres approach was taken to change the acyl guanidine moiety for an amine group (Hunt, 2012). **d** A quaternary amine, which had comparable activity to amiloride which was more suitable for a nebuliser (Hunt, 2012). **e** An α-branched quaternary amine derivative with even higher affinity (Hunt, 2012).

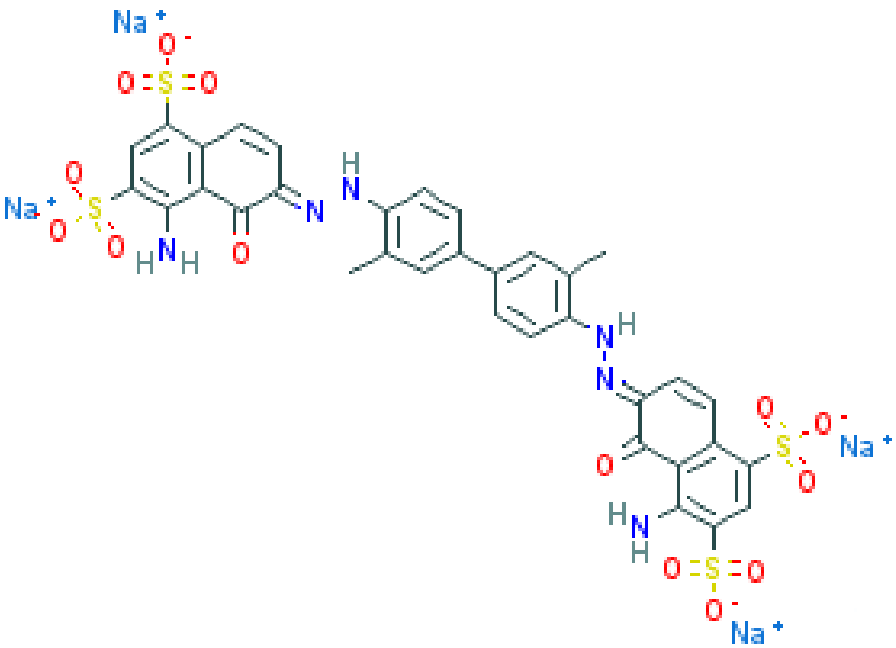

Figure 9. The chemical structure of Evans blue. The four sulfonic groups (yellow and red) carry negative charges,.

2

METHODS

Chapter 2

2.1. Materials:

2.1.1. DNA vectors:

2.1.1.1. ENaC δ gene construct:

Searches for ENaC δ primary protein structure was performed with the search tool at the UniProt Protein Knowledgebase (www.uniprot.org/), using the published ENaC δ, entry P51172 (Giraldez, et al., 2007). DNA sequence was determined using the Protein Sequence Back-translation (Backtranseq (EMBOSS)) tool at the EMBL European Bioinformatics Institute (http://www.ebi.ac.uk/Tools/st/). The construct was obtained from GenScript® via the OptimumGene™ Codon Optimisation Analysis service which optimised the codon sequences for expression in *Homo sapiens* (ENaC δ: Optimized Sequence Length: 1917, GC%:58.92) in a pUC57 vector (ampicillin resistance).

2.1.1.2. ENaC α gene construct:

The published ENaC α subunit, entry P37088 (www.uniprot.org/), contained within a pENTR™/D-TOPO® vector (Section 2.1.1.4.), was kindly donated by GSK, Stevenage, UK.

2.1.1.3. GFP-tagged constructs:

Vectors encoding GFP-tagged variants of the ENaC α and the ENaC δ1 subunits (Entry P37088 and P51172-1, respectively; www.uniprot.org/) were obtained via the GeneART Gene synthesis and subcloning service (Thermo Scientific™, Regensburg, Germany). The vectors (pCMV-DEST-SCNN1D-HRV3C-eGFP-6His and pCMV-DEST-SCNN1A-HRV3C-eGFP-6His) were designed so as the tags were added to the immediate C-terminus end of the gene sequence. The tag contained DNA encoding eGFP (714 bp) with a recognition and cleavage site for human rhinovirus 3C and

PreScission proteases (24 bp) at its N terminus, and a polyhistidine tag at its C terminus (16 bp), followed by a stop codon. These tagged sequences were codon-optimised for expression in *Homo sapiens*. These were first synthesised and cloned into the donor vector pDONR221 (4762 bp), before Gateway® cloning into the pCMV-DEST vector.

2.1.1.4. pENTR™/D-TOPO® vector:

The pENTR™/D-TOPO® vector was purchased as part of the pENTR™/D-TOPO™ Cloning Kit (Invitrogen™, #K240020). It contains a number of key elements, listed in Table 2. The *att*L1 and *att*L2 sites for site-specific recombination of the entry clone with a Gateway® destination vector.

2.1.1.5. pCMV-DEST vector:

The pCMV-DEST vector was purchased as part of the ViraPower™ BacMam Expression System (Invitrogen™, #A24227). It contains a number of key elements listed in Table 3.

2.1.1.6. Mutants:

The single-point mutations of the serine residues of the GFP-tagged ENaC α and δ genes at positions 556 and 533, respectively, were generated using the Genscript® Site-Directed Mutagenesis Service. The mutant *SCNN1A* and *SCNN1D* genes were cloned into the pCMV-DEST vector (Section 2.1.1.5.).

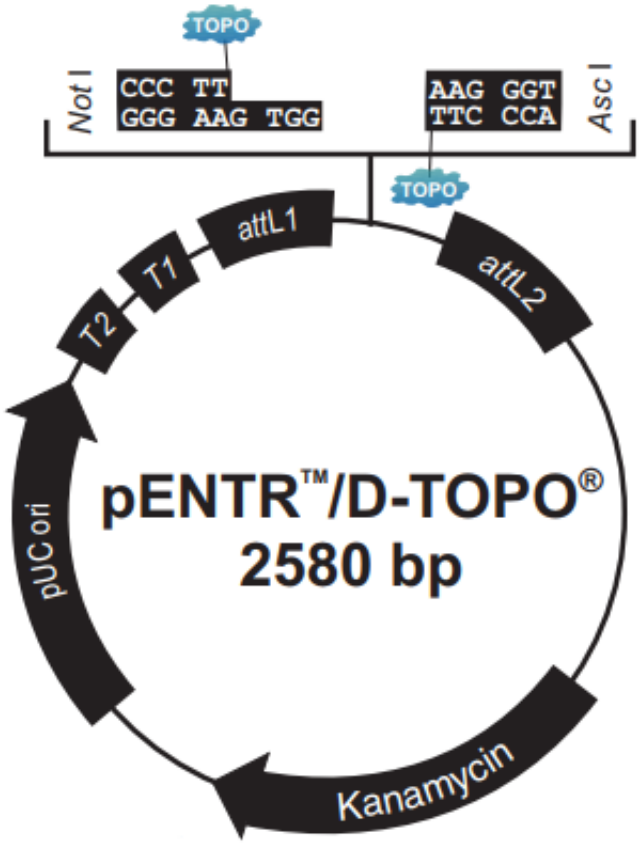

Bases	
268-295	*rrnB* T2 transcription termination sequence
427-470	*rrnB* T2 transcription termination sequence
537-552	M13 forward (-20) priming site
569-668	*att*L1
680-684	TOPO® recognition site 1
685-688	Overhang
689-693	TOPO® recognition site 2
705-804	*att*L2
821-840	T7 promotor/priming site
845-861	M13 reverse priming site
974-1783	Kanamycin resistance gene
1904-2577	pUC origin

Table 2. The pENTR™/D-TOPO® vector. Taken from Invitrogen™ user guide (Invitrogen, 2012).

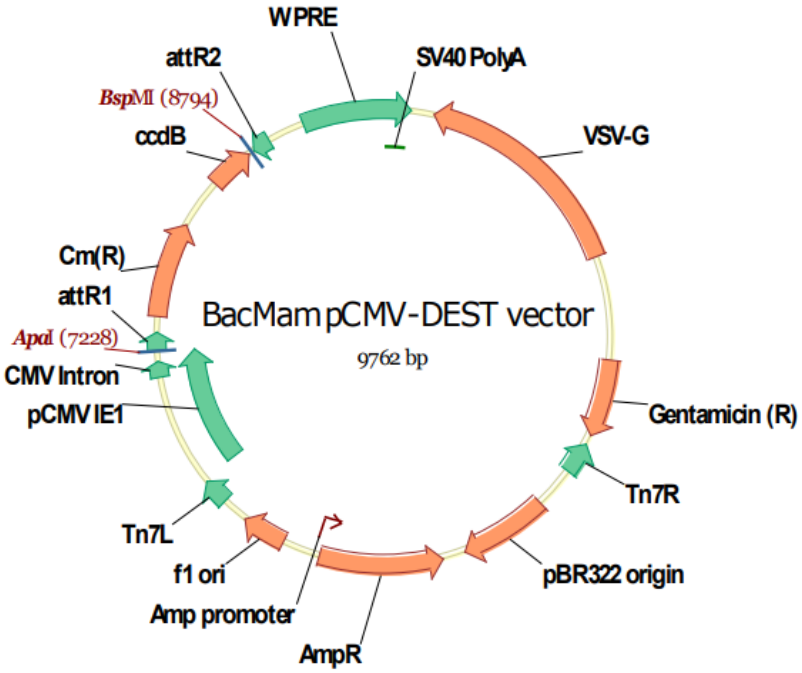

Bases	
1-138	SV40 PolyA transcription termination sequence
325-1860	VSV-G envelope glycoprotein
2582-3115	Gentamicin resistance gene
3182-3406	Tn7R transposon site
3694-4313	pBR322 origin
4468-5328	Ampicillin resistance gene
5591-5898	F1 origin of replication
6080-6264	Tn7L transposon site
6284-7227	pCMV IE1 promotor
7232-7356	*att*R2
74465-8124	Chloramphenicol resistance gene
8466-8771	ccdB gene
8812-8936	*att*R2
9195-167	WPRE posttranscriptional regulatory element

Table 3. The pCMV-DEST vector. Taken from Invitrogen™ user guide (Invitrogen, 2014).

2.1.2. Primers:

Table 4. details the primers used at various sloning step to amplify specific stretches of DNA from a vector for either use in subsequent cloning steps, generating mutants, or for verification that cloning steps have been successful.

Purpose	Primers	Supplier
To amplify the *SCNN1D* gene for TOPO® cloning	Forward: 5'- CACCATGGCAGAGCATAGAAGCATG-3' Reverse: 5'- TTAGGTGTCCAGTGTTTCCAG-3'	Eurofins Genomics
To verify presence of gene inserted into the pENTR™/D-TOPO® vector (M13 primer pair)	Forward: 5´-GTAAAACGACGGCCAG-3´ Reverse: 5´-CAGGAAACAGCTATGAC-3´	Thermo Scientific™
To verify presence of gene inserted into the bacmid (M13 (-40) primer pair)	Forward: 5'-GTT TTC CCA GTC ACG ACG-3' Reverse: 5´-CAGGAAACAGCTATGAC-3´	Thermo Scientific™
To introduce a deletion mutation into the *SCNN1A* amiloride binding site	Forward: 5'-GGATGCGGTGAGGGAGATCAACATCCTGTCGA-3' Reverse: 5'-TCGACAGGATGTTGATCTCCCTCACCGCATCC-3'	Eurofins Genomics
To introduce a deletion mutation into the *SCNN1D* amiloride binding site	Forward: 5'-GCCAGGATATCCACGTCCTGGACGGCTG-3' Reverse: 5'-CAGCCGTCCAGGACGTGGATATCCTGGC-3'	Eurofins Genomics

Table 4. Primers used for various cloning steps during cell line reagent generation and mutagenesis studies.

2.1.3. Cells:

2.1.3.1. Sf9 cells:

Sf9 cells, a clonal isolate of Spodoptera frugiperda Sf21 cells (IPLB-Sf21-AE), were obtained from the Genome and DNA Damage Centre (GDDC) at the University of Sussex.

2.1.3.2. HEK293 cell line:

Human Embryonic Kidney (HEK) 293 cells, stably expressing mutated forms of the ENaC β and γ subunits related to GenBank references NM_000336 and NM_001039 respectively, were kindly donated by GSK, Stevenage, UK. The ENaC β and γ subunits had been originally amplified from human kidney (ENaC β) or human brain (ENaC γ) marathon libraries before being subcloned into pBacMire (neomycin/geneticin resistance) and pBacMireHyg (hygromycin resistance) respectively, with the expression of both driven by a CMV promoter. After cotransfection with both constructs, stable cell lines had been established under selection of 0.5 mg/mL geneticin and 0.2 mg/mL hygromycin. Mutations in both subunits were created using the Strategene QuikChange XL Site-Directed Mutagenesis Kit (#200516) (ENaC β: from CCC-AAC-TAT to GCC-AAC-TTA, corresponding to P618A Y620L (β*); ENaC γ: from CCC to TAG, corresponding to P624Stop (γ*)).

2.1.4. Antibiotic selection plates:

Antibiotic stock solutions were prepared at the following concentrations: Ampicillin 10 mg/mL in water; Kanamycin 10 mg/mL in water; Tetracycline 10 mg/mL in water; Gentamicin 7 mg/mL in water. All stocks were filter-sterilised and stored at –20 °C, protected from light. For IPTG stocks, 2 g of IPTG was dissolved in 8 mL of sterile water and filter-sterilized with a 0.22 µm pore size. The volume of the solution was adjusted to 10 mL with sterile water and the stock solution (200 mg/mL) dispensed into 1 mL aliquots, stored at –20 °C. Bluo-gal was dissolved in dimethyl sulfoxide (DMSO) to make a 20 mg/mL stock solution and stored at –20 °C protected from light.

LB agar plates were poured with final concentration of 50 µg/mL ampicillin (Amp) or 50 µg/mL kanamycin (Kan) for transformations with the pUC57 (AmpR), pENTR™/D-TOPO® (KanR) and BacMam pCMV-DEST (AmpR) vectors. Once dry, plates were inverted and stored at 4 °C for up to one month.

LB agar plates for bacmid transposition were poured with final concentration of 50 µg/mL kanamycin, 7 µg/mL gentamicin, 10 µg/mL tetracycline, 100 µg/mL Bluo-gal and 40 µg/mL IPTG. Once dry, plates were inverted and stored at 4 °C for up to one month, protected from light.

2.1.5. Compounds:

2.1.5.1. Reference compounds:

Amiloride hydrochloride (Sigma-Aldrich, #1019701), benzamil hydrochloride (Sigma-Aldrich, #B2417) and 5-(N-Ethyl-N-isopropyl)amiloride (EIPA) (Sigma-Aldrich, #A3085) were prepared to 10 mM stocks in 100 % (v/v) DMSO. For viral transductions, amiloride was prepared to a 10 mM stock in dH_20.

2.1.5.2. CUTE Ion Channel library:

The CUTE Ion channel library (1491 compounds) from Life Chemicals Inc. (Niagara-on-the-Lake, Canada) was delivered in individual vials of liquid stocks at 10 mM in 100 % (v/v) DMSO. For hit validation studies, compounds were ordered from Life Chemicals Inc. in their powdered form, and prepared to 100 mM stocks at 10 mM in 100 % (v/v) DMSO. Compounds from original and reordered stocks were analysed using liquid chromatography-mass spectrometry (LC-MS) in a quality control step to assess stability and purity, and identity based on their mass. LCMS (MDAP) data was recorded on a Shimadzu Prominence Series coupled to a LCMS-2020 ESI and APCI mass spectrometer.

Samples were eluted through a Phenomenex Gemini 5 µ C18 110 Å 250 mm × 4.6 mm column, using water and acetonitrile acidified by 0.1% formic acid at 1 mL/min and detected at 254 nm. Vials and powders were stored at -80 °C until use.

2.1.5.3. Diverse 12k library:

The Diverse 12K compound set (12028 compounds) from BioAscent (BioCity Scotland, UK) was delivered pre-plated in 384-well v-bottomed plates, at 2 mM in 100 % (v/v) DMSO, in a total volume of 2 µL. For hit validation studies, compounds were ordered from BioAscent and delivered in a 384-well v-bottomed plate at 10 mM in 100 % (v/v) DMSO, in a total volume of 5.5 µL. All plates were stored at -80 °C until use.

2.1.5.4. Analogues:

Analogues were ordered from Ambinter (c/o Greenpharma, Orléans, France), or were synthesised in-house by Rosemery Huckvale (SDDC). All were prepared from powders to stocks at 100 mM in 100 % (v/v) DMSO and stored at -80 °C until use.

2.2. Methods:

2.2.1. Molecular biology techniques:

2.2.1.1. DNA transformation:

The process of bacterial transformation introduces foreign plasmid DNA into a bacterial cell, which allows for the bacteria to be used as the means for both storing and replicating plasmids. The plasmids are designed to carry both a bacterial origin of replication and an antibiotic resistance gene for use as a selectable marker in bacteria, even if it is to be used for subsequent mammalian cell expression.

2.2.1.1.1. One Shot® TOP10 chemically competent E. coli:

Transformations were performed using One Shot® TOP10 chemically competent *E. coli* (Life Technologies, #C4040-06,), unless otherwise stated. Into each 50 µL vial of competent cells, 2 µL of DNA (~50 ng) sample were added and tapped to mix. To test the efficiency of the competent cells, a control transformation was run in parallel adding 1 µL (10 pg) of the supercoiled pUC19 plasmid supplied with the kit to a vial of cells. The cells were incubated on ice for 30 min and then heat-shocked for 45 sec in a 42 °C waterbath. Cells were returned to ice for 2 min, and 250 µL of pre-warmed Super Optimal Broth (S.O.C medium; Life Technologies #15544-034) was then added to each vial. Cells were shaken at 37 ˚C, 225 rpm for I hr. This outgrowth step is necessary for the bacteria to generate the antibiotic resistance proteins encoded on the plasmid backbone. Two 10-fold serial dilutions of the cells were made to ensure separation of individual colonies on the plates. Each dilution (original, x 10^{-1}, x 10^{-2}) was spread onto pre-warmed agar plates and incubated at 37 ˚C, overnight. Agar plates had been prepared prior to transformation using LB agar (35 µg/mL) with antibiotics (50 µg/mL) on a sterile surface under flame.

The following morning, 1-2 colonies were inoculated in 5 mL Luria-Bertani medium (LB Broth) containing the antibiotic (50 µg/mL). These were shaken at 37 ˚C, 225 rpm for ~6-8 hr. The 5 mL culture was used to inoculate 250 mL LB Broth with antibiotic and shaken at 37 ˚C, 225 rpm, overnight. Cultures were centrifuged at 4500 rpm, 4 ˚C for 20 min, and cell pellets stored at -20 ˚C or used immediately to prepare DNA for subsequent cloning steps.

2.2.1.1.2. *One Shot® ccdB Survival™ T1R competent cells:*

Transformations of vectors containing the *ccdB* gene were performed using One Shot® *ccdB* Survival™ T1R Competent Cells (#A10460, Life Technologies). 100 µg of DNA was used in one vial of competent cells and tapped to mix. The subsequent transformation steps were identical to those using One Shot® TOP10 Chemically Competent *E. coli* (Section 2.2.1.1.1).

2.2.1.1.3. *MAX Efficiency® DH10Bac™ competent cells:*

Transformations for bacmid generation were performed using MAX Efficiency® DH10Bac™ competent cells (Gibco™, #10361012). To each vial of cells, 5 µg of the BacMam pCMV expression construct was added and tapped to mix before incubating on ice for 30 min. The cells were then heat-shocked for 45 sec in a 42 °C waterbath. Immediately the tubes were transferred to ice and chilled for 2 minutes. 900 µL of pre-warmed S.O.C medium was added and vials were shaken at 37 ˚C, 225 rpm for 4 hr. Following this, 3 x 10-fold serial dilutions of the cells (10^{-1}, 10^{-2}, 10^{-3}) were prepared with S.O.C medium for each BacMam pCMV transformation. Cells were spread on pre-warmed agar plates (50 µg/mL kanamycin, 7 µg/mL gentamicin, 10 µg/mL tetracycline, 100 µg/mL Bluo-gal and 40 µg/mL IPTG; Section 2.1.4.), inverted and incubated at 37°C, 48 hr.

Insertions of the mini-Tn7 into the mini-attTn7 attachment site on the bacmid disrupt the expression of the LacZα peptide, so colonies containing the recombinant bacmid are white in a background of blue colonies that harbour the unaltered bacmid. White colonies were selected for restreaking to avoid selecting false positives. The largest, most isolated white colonies were restreaked onto fresh plates, but colonies that

appeared grey in the centre were not as they were likely to contain a mixture of cells with empty bacmid and recombinant bacmid. Selected white colonies were resuspended in 200 µL fresh S.O.C medium and streaked onto fresh plates in discrete lines to ensure separation of new colonies. Plates were inverted and incubated at 37°C, 48 hr. A single colony, confirmed as having a white phenotype after restreaking, was used to inoculate 4 mL LB medium supplemented with 50 µg/mL kanamycin, 7 µg/mL gentamicin and 10 µg/mL tetracycline. This was shaken at 37 ˚C, 250 rpm for ~24 hr, until stationary growth phase had been achieved.

2.2.1.1.4. XL10-Gold® ultracompetent cells:

Mutagenesis reactions were transformed in XL10-Gold® ultracompetent Cells (Agilent, #200314). One vial of 100 µl of the ultracompetent cells was gently thawed on ice and 45 µl was aliquoted to a prechilled 14 mL BD Falcon polypropylene round-bottom tube per transformation reaction. To increase transformation efficiency of the cells, 2 µl of the β-Mercaptoethanol (β-ME) mix was added to each aliquot and mixed gently by inverting the tubes. Cells were incubated on ice before transferring 2 µl of the *Dpn* I-treated DNA from each sample reaction to separate aliquots of the ultracompetent cells. The transformation reactions were incubated on ice for 30 min. During this time, NZY+ broth (per litre: 10 g N-Z-Amine® A, from bovine milk, casein enzymatic hydrolysate (Sigma-Aldrich, #C0626), 5 g yeast extract and 5 g NaCl in dH_2O, pH 7.5 using NaOH, autoclaved), with 12.5 mL of 1 M $MgCl_2$, 12.5 mL of 1 M $MgSO_4$ and 20 mL of 20% (w/v) glucose, all filter-sterilized and added before use, was prewarmed in a 42 °C waterbath. The cells were transferred to a 42°C water bath for 30 sec, a step which is critical for obtaining the highest efficiencies, and returned to ice for a further 2 min.

0.5 mL of preheated S.O.C medium was added to each tube, and cells were incubated at 37 °C for 1 hr with shaking at 225–250 rpm. Cells were then plated on agar plates containing the appropriate antibiotic for the plasmid vector.

2.2.1.2. DNA preparation:

2.2.1.2.1. Plasmid DNA preparation:

Preparation of DNA constructs for PCR and subsequent cloning was performed using either the QIAGEN Plasmid Mini Kit (#12125) or the QIAGEN Plasmid Maxi Kit (#12165), dependent on the culture size and required yield of DNA. This was performed as per manufacturers' instructions, but briefly, they use a gravity-flow anion-exchange tip containing resin, which allows for the purification of up to 20 µg or 500 µg of high-copy DNA plasmids from culture. The yield is dependent on plasmid copy number, size of insert, host strain, and culture medium.

Cells containing DNA were harvested from culture by centrifugation at 6000 x g for 10 min at 4 °C. The pellet was resuspended, cells were lysed open, and unwanted cell material, including genomic DNA, was precipitated out of solution. After subsequent centrifugation at maximum speed, ≥20,000 g, 30 min, 4 °C, the supernatant, containing the required plasmid DNA was then collected in the resin-containing tip, under low salt conditions, and DNA eluted from the resin with a high salt buffer (Buffer QF: 1.25 M NaCl. 50 mM Tris-Cl, pH 8.5). The DNA was then precipitated out of solution with isopropanol before undergoing rounds of centrifugation at 13000 rpm, 4 ˚C in 70% (v/v) EtOH, to remove impurities. The DNA pellet was resuspended in 20 µL or 100 µL dH_20, and the yield quantified on a NanoDrop Lite (Thermo Scientific™), a

spectrophotometer that quantifies nucleic acid concentrations at 260 nm and purity using the 260/280 nm ratio.

2.2.1.2.2. Bacmid isolation:

Following transformation (Section 2.2.1.1.3.) the inoculated bacmid culture was monitored until it reached stationary growth phase. The culture was centrifuged at 13,000 g, 4 ˚C, 3 min and the pellet resuspended in 0.4 mL QIAGEN P1 Buffer (15 mM Tris-HCl, pH 8.0, 10 mM EDTA, 100µg/mL RNase A). On top of this, 0.4 mL P2 Buffer (0.2 N NaOH, 1% SDS) was added and gently mixed. This was incubated at RT, 5 min. Protein and *E. coli* genomic DNA were precipitated by the slow addition of 0.4 mL potassium acetate (3 M, pH 5.5). This was then incubated on ice, 5-10 min, before centrifugation at 14,000 x g, 15 min. The supernatant was then removed and added to 0.8 mL cold isopropanol, avoiding any white precipitate, and placed at -20 ˚C, 10 min or overnight. This was centrifuged again at 14,000 x g, 15 min. The supernatant was removed and 0.7 mL cold 70% ethanol added, followed by another spin at 14,000 x g, 15 min. Finally, as much of the supernatant was removed as possible, and the pellet left to air dry for 5-10 min, before resuspending in 40 µL dH_2O. The yield quantified using a NanoDrop Lite. Bacmid stocks were stored at 4 °C. It was advised against to store the purified bacmid DNA at –20°C as repeated freezing and thawing can shear the DNA.

2.2.1.3. Polymerase chain reaction (PCR):

2.2.1.3.1. Blunt-ended PCR:

For blunt-ended PCR, Platinum® *Pfx* DNA Polymerase (Invitrogen™, #11708013) was used. *Pfx* DNA Polymerase, from *Thermococcus kodakaraensis*, possesses

proofreading 3' to 5' exonuclease activity and is a highly processive enzyme with fast chain extension capability.

The PCR protocol was followed as per the manufacturer's instructions. Briefly, for each 50 µL reaction: 5 µL *Pfx* Amplification Buffer (10 x), 0.3 mM dNTP mixture, 1 mM $MgSO_4$, 0.3 µM forward primer, 0.3 µM reverse primer (Section 2.1.2.), 100 ng template and 1 unit Platinum Pfx DNA polymerase, made up to 50 µL with dH_2O, was mixed by brief centrifugation before thermocycling. Platinum® Pfx DNA Polymerase is provided in inactive form, due to specific binding of the Platinum® antibody. Polymerase activity was restored after a PCR denaturation step at 94 °C for 5 min. This provided an automatic "hot start" for increased specificity, sensitivity, and yield, and ensured the DNA template, regardless of GC content, was fully denatured. Thermocycling consisted of 15 sec denaturation step at 94 °C, 15 sec primer annealing step at 55 °C, and a primer extension step at 68 °C for 60 sec/Kb of template. Each PCR cycle was performed a total of 35 times.

2.2.1.3.2. Bacterial colony PCR:

PCR analysis was performed the morning after plating transformed *E. Coli* on agar plates using Maxima Hot start Taq DNA polymerase (Thermo Scientific™, #EP0601). 5-10 colonies were analysed per plate by removing ½ of each with a sterile pipette tip and submerging in 25 µL dH_20. To ensure lysis of cell membranes, this was vortexed thoroughly and heated to 94°C, 10 min. Briefly, for each 60 µL PCR reaction, 1 µL Maxima Hot Start Taq Buffer (10 x), 0.2 mM dNTP, 0.1 µg M13 (-20) forward primer, 0.1 µg M13 reverse primer (Section 2.1.2.), 2 mM $MgCl_2$, 1.5 unit Maxima Hot start

Taq DNA polymerase, made up to 60 µL with dH_20, was added to the vial containing the lysed clone. This was transferred to a PCR tube before thermocycling.

Thermocycling consisted of a 60 sec denaturation step at 95 °C, 60 sec primer annealing step at 55 °C, and a primer extension step at 72 °C for 60 sec/Kb of template. Each PCR cycle was performed a total of 35 times.

2.2.1.3.3. Bacmid PCR analysis:

Bacmid clones were analysed by PCR using Phusion Flash High-Fidelity PCR Master Mix (Thermo Scientific™, #F548S). The mix includes the Phusion Flash II DNA Polymerase, which is a modified proofreading DNA polymerase, with fast extension times and extremely high fidelity.

The PCR reaction was performed as per manufacturer's directions. Briefly, for each 50 µL reaction, 25 µL Phusion Flash PCR Master Mix (2 x), 0.25 µM M13 (-40) forward primer, 0.25 µM M13 reverse primer (Section 2.1.2.), 10 ng bacmid template, was made up to 50 µL with dH20. Thermocycling consisted of a 5 sec denaturation step at 98 °C, 5 sec primer annealing step at 53 °C, and a primer extension step at 72 °C for 60 sec/Kb of template. Each PCR cycle was performed a total of 35 times.

2.2.1.4. Restriction digestion:

To perform restriction digestion analysis, 1 µg DNA vector was incubated with 10 units NheI-HF® (New England BioLabs® *Inc.*, # R3131S) in 3 µL CutSmart® Buffer (10 x), made up to 30 µL with dH_20. Reactions were incubated at 37 °C, 1 hr, followed by a heat inactivation step at 98 °C, 10 min.

2.2.1.5. Gel electrophoresis:

The size of DNA products were verified by running on a 0.5-1.5 % (w/v) agarose gel (UltraPure™ Agarose; Invitrogen™ #16500-500) containing SYBR® Safe DNA Gel Stain (1X) (Invitrogen™, #S33102). DNA gel loading dye (Thermo Scientific™, #R0611) was added to each DNA sample prior, and gels were run in TAE (Tris-acetate- EDTA) buffer (1X).

2.2.1.6. TOPO® cloning reaction:

The pENTR™ Directional TOPO® Cloning Kit (Invitrogen™, #K240020) uses a cloning strategy that directionally clones a blunt-end PCR product into a vector (pENTR™/D-TOPO®; Section 2.1.1.4.) and circumvents the need for restriction enzymes and ligase.

The TOPO® cloning reaction protocol was followed as per the manufacturer's instructions. Briefly, each 6 µL reaction contained: 1 µL Salt solution (1.2 M NaCl, 0.06 M $MgCl_2$), 1 µL TOPO® vector (15-20 ng/µL in: 50% glycerol, 50 mM Tris-HCl (pH 7.4 at 25°C), 1 mM EDTA, 2 mM DTT, 0.1% Triton X-100, 100 µg/mL BSA, 30 µM bromophenol blue), the desired amount (ng) of PCR fragment, made up to 6 µL with dH_2O. The reaction was mixed gently before incubation at room temperature (RT), 30 min. The reaction was returned to ice before transformation into One Shot® TOP10 Chemically Competent *E. coli* (Section 2.2.1.1.1).

2.2.1.7. LR cloning reaction:

The pENTR™/D-TOPO® vector is compatible for subsequent recombination with the Gateway® destination vector, BacMam pCMV-DEST (Section 2.1.1.5.), using the ViraPower™ BacMam Expression System kit (Invitrogen™, #A24227) and LR cloning.

The LR cloning reaction protocol was followed as per the manufacturer's instructions. Briefly, each reaction contained: 50-150 ng Entry clone, 250 ng BacMam pCMV-DEST vector, made up to 8 µL with TE Buffer (1X), pH 8.0. Only then is the LR Clonase® II Enzyme Mix (Invitrogen™, #11791100) removed from –20 °C and thawed on ice (2 min). To each sample, 2 µL of LR Clonase® II Enzyme Mix was added and mixed by pipetting, returning the enzyme to –20 °C immediately. The reaction was incubated at 25 °C, 1 hr. 1 µL Proteinase K solution was then added to each reaction and incubated at 37 °C, 10 min. The reaction was returned to ice, followed by transformation in One Shot® TOP10 Chemically Competent *E. coli* (Section 2.2.1.1.1).

2.2.1.8. Mutagenesis:

Deletion mutations were introduced into the amiloride-binding site of the GFP tagged ENaC α and δ1 subunit (WYRFHY at amino acid positions 251-256 or WYHFHY at amino acid positions 232-237, respectively) in the pCMV-DEST vectors. This was done using the Agilent QuikChange Lightning Site-Directed Mutagenesis Kit (Agilent Technologies, #210518). The mutagenic oligonucleotide primers (Section 2.1.2.) were designed individually according to the desired mutations, with both primers containing this mutation and able to anneal to the same sequence on opposite strands of the plasmid. Primers were designed to be between 25 and 45 bases in length with ~10–15 bases of correct sequence on both sides of the desired mutation. Additionally, the primers were required to have a melting temperature (T_m) of ≥78 °C, and a minimum GC content of 40%, terminating in one or more C or G bases.

The sample reaction was prepared as follows: 5 µl 10× reaction buffer, 50 ng dsDNA template, 125 ng each of the two oligonucleotide primers, 1 µl dNTP mix, 1.5 µl

QuikSolution reagent, and dH_2O to a final volume of 50 µl, before the final addition of 1 µl QuikChange Lightning Enzyme. The sample reactions were mixed by a brief centrifugation before thermocycling. This kit uses a proprietary *Pfu*-based polymerase blend together with an optimised *Dpn* I enzyme to allow for high fidelity but accelerated site-directed mutagenesis. Thermocycling consisted of an initial denaturation step of 95 °C for two minutes, followed by 18 cycles of a 20 sec denaturation step at 95 °C, a 10 sec primer annealing step at 60 °C, and a primer extension step at 68 °C for 30 sec/Kb of template. The PCR cycles were finally followed by a longer extension step for five minutes at 68 °C. *Dpn* I digestion of the parental methylated and hemimethylated supercoiled DNA were performed by addition of 2 µl *Dpn* I restriction enzyme (provided in the kit) directly to each amplification reaction. This was gently and thoroughly mixed by pipetting and briefly centrifuged before incubation at 37°C, five minutes. The reaction mix was then transformed in XL10-Gold Ultracompetent Cells (Section 2.2.1.1.4.).

2.2.2. Tissue culture:

2.2.2.1. HEK293 cell line:

HEK293 ENaC β*γ* cell lines (Section 2.1.3.2.) were maintained in DMEM/F-12 (1:1) (1X) medium supplemented with GlutaMAX™ (Invitrogen™, #31331093) and 10% fetal bovine serum, heat inactivated (Invitrogen™, #10500064), under constant selection of 0.5 mg/mL geneticin and 0.2 mg/mL hygromycin. Cultures were incubated in T175cm^2 flasks at 37 ^oC in a 95% humidified atmosphere of 5% (v/v) CO_2 /95% (v/v) air [standard cell culture conditions] and passaged every two days when the cells had reached ~70 % confluency. On passage, the flasks were washed with pre-warmed DPBS (1X, Gibco™,

#14190250) and dissociated with TryplE Express, no phenol red (Gibco™, #12604021) at 37 °C. Cell medium was used to gently lift the cell suspension, before cell counting. On determining number of cells, viability was checked by diluting the cells 1:2 with 20 µL of 0.4% (v/v) Trypan Blue solution. New flasks were seeded in T175cm^2 flasks for continuous culture at required seeding density (~4 x 10^6 cells/mL).

2.2.2.2. Sf9 cells:

Cells were cultured in the GDDC using Insect-Xpress™ Protein-free Insect Cell Medium, with L-Glutamine (Lonza, #12-730F), containing Penicillin (100 units/ mL) - Streptomycin (100 µg/ mL), and passaged every 3 days.

2.2.3. Transduction and transfection procedures:

2.2.3.1. Insect cell transfection for baculovirus generation:

Sf9 log-phase cells (Section 2.1.3.1.) with >95 % viability were used to perform a successful transfection. Cells were counted and viability determined, before seeding each well of a 6-well tissue culture plate (Corning° Costar®, #CLS3516-50EA) with 1 x 10^6 cells/well in 2 mL Insect-Xpress™ medium, free from antibiotics. Two wells were reserved as control wells, one containing just cells, and the other containing cells and treated with Cellfectin® II Reagent (Invitrogen™, #10362-010) but no virus. Cells were left at 27 °C, ≥1 hr for cells to attach. During this incubation, the transfection reagents were prepared. In separate 1.5 mL eppendorf tubes, 1 µg Bacmid DNA was added to 100 µL Insect-Xpress™ medium, and 8 µL Cellfectin® II Reagent was added to a separate 100 µL Insect-Xpress™ medium. The two solutions were then combined, mixed gently, and incubated at RT, 45 min.

After incubation, an additional 800 µL Insect-Xpress™ medium was added to the transfection solution. The medium was removed from each well of the cell plate, and cells were washed with Insect-Xpress™ medium before applying 2 mL transfection solution on top. Cells were incubated for 27 °C, 5 hr. The transfection solution was removed and replaced with 2 mL Insect-Xpress™ medium, containing antibiotics. Cells were incubated at 27 °C for a further 3-5 days in a humidified chamber whilst undergoing constant observation.

2.2.3.1.1. Preparation of P1 viral stock:

Budded virus should be released into the medium 72 hours after transfection, however transfection efficiency can vary and cells may not show all of the signs of viral infection until 4 or 5 days post-transfection. From 72 hours after transfection, cells were visually inspected for signs of infection (Table 5.). Once cells appeared infected (i.e. demonstrated characteristics typical of late to very late infection), the virus was harvested from the cell culture medium via centrifugation of the medium from each well at 1,500 × g, 5 min. The clarified supernatant was transferred to fresh 15 mL tubes and this was the P1 viral stock, which is typically 1–10 × 10^6 plaque forming units (pfu)/mL. P1 viral stocks were stored at 4 °C, protected from light, or used immediately to generate a P2 stock.

Sign of Infection	Phenotype
Early (first 24 hr)	Increased cell diameter
	Increased size of nuclei
Late (24-72 hr)	Cessation of cell growth
	Granular appearance
	Detachment
Very late (>72 hr)	Cell lysis

Table 5. Phenotypic changes in Sf9 insect cells post transfection with bacmid.

2.2.3.1.2. Generation of P2 and P3 viral stocks:

Assuming the P1 viral stock was 1–10 × 10^6 pfu/mL, 50 mL of Sf9 cells at a density of 2 x 10^6 cells/mL (log-phase, >95 % viability) were inoculated with 2 mL P1 virus (MOI ~ 0.1). Cells were shaken in a 1 L cell culture vessel at 27 °C, 3-5 days. The virus was harvested from the cell culture medium via centrifugation at 1,000 × g, 15 min. The clarified supernatant was transferred to fresh 50 mL tubes and became the P2 viral stock (1–10 × 10^7 pfu/mL), stored at 4 °C, protected from light. The process was repeated again to generate a further amplified P3 viral stock. The P2 stock is assumed to be 1–10 × 10^7 pfu/mL and 100 mL Sf9 cells at a density of 2 x 10^6 cells/mL (log-phase, >95 % viability) were inoculated with 100 µL P2 virus (MOI ~ 0.05). The harvested P3 viral stock was used for transduction in mammalian cells.

2.2.3.1.3. Plaque assay to determine P3 viral titre:

Sf9 cell suspension was prepared at 5 × 10^5 cells/mL in Insect-Xpress™ medium and 2mL of cell suspension was aliquoted into each well of a 6-well plate (one plate per virus). Cells were covered and incubated at 27 °C, 1 hr to allow for cells to settle to the

bottom. A 7-log serial dilution (10^{-1} to 10^{-7}) of the clarified baculoviral stock in Insect-Xpress™ medium was prepared by sequentially diluting 25 µL of the baculoviral stock, or previous dilution, in 225 µL of medium. Only dilutions of 10^{-5}, 10^{-6} and 10^{-7} were used in the assay.

Following the 1 hour incubation, the cell monolayers were observed using an inverted microscope, to check for cells were attached and at 50% confluence. The medium from each well was removed and immediately replaced with 200 µL of the appropriate virus dilution. As a negative control, the medium without virus was added to a well. Cells were incubated with virus at RT, 2 hr, on a plate shaker.

Plaquing medium consists of a mixture of culture medium and agarose, and was prepared immediately before use to immobilise the infected cells for the plaque assay. 2.5 % Agarose Gel was melted by heating the agarose in a waterbath. Once the agarose gel had liquefied, 4 mL of Insect-Xpress™ medium was combined with 2 mL of the melted 2.5 % Agarose Gel mixed gently. The medium containing virus was then removed from the wells and replaced with 2 mL of plaquing medium. This was performed quickly to prevent desiccation of the cell monolayer. The agarose overlay was allowed to harden at RT, 1 hr and an additional 1 mL Insect-Xpress™ medium was applied on top of the agarose to prevent it drying out. The plate was moved to 27 °C, 4-5 days, in a humidified incubator until plaques were visible and ready to count.

A 0.03% solution of neutral red (Sigma-Aldrich®, #N2889) was prepared in Dulbecco's phosphate-buffered saline, without calcium, magnesium or phenol red (DPBS; 1X, Gibco™, #14190144) and 1 mL added to each well before incubation at 37 °C, 2-3 hr. The stain was removed before inverting the plates to count the number of viral

plaques. Neutral red is taken up by healthy cells but not by dead cells, therefore plaques appear as clear circles against a red background. The following formula could be used to calculate the titre (plaque forming units (pfu)/mL) of the viral stock:

$$\text{Titre (pfu/mL)} = \text{no. of plaques} \times \frac{D}{V} \times 1$$

D = Dilution factor

V = Volume of diluted virus (mL) /well

2.2.3.2. HEK293 cell transduction with baculovirus:

Unless otherwise stated, HEK293 or HEK293-ENaC β*γ* cells (Section 2.1.3.2.), which had adhered to a flask or microtitre plate, were transduced with the BacMam virus in the presence of 50 µM amiloride hydrochloride (in dH_20) and 0.25 µM Trichostatin A ([TSA] in DMSO, 0.2 µm-filtered; Sigma Aldrich, #T1952).

2.2.3.3. Lipofectamine transfection:

On the day prior to assay, HEK293 ENaC β*γ* cells were plated onto 6-well tissue culture plates (Corning® Costar®, #CLS3516), which had been coated with pol-D-lysine, at a density of 1.6 x 10^5 cells/well in 1 mL of culture media (no selection). Cells were left to attach for 4-6 hr in standard cell culture conditions. Lipofectamine® 2000 reagent (Invitrogen™, #11668027) was diluted by 10-fold in Opti-MEM® Medium (150 µL total per well), and in a separate tube 14 µg DNA was mixed with 700 µl Opti-MEM® Medium. The diluted Lipofectamine® 2000 reagent and DNA were mixed at a ratio of 1:1 and incubated for 5 min, room temperature. To every well 250 µL of the DNA-lipid complexes were added to every well (~2.5 µg DNA). Cells were incubated for a further

16-24 hr in standard cell culture conditions. Before using the transfected cells, they were visualised with a Zeiss Axiovert fluorescence microscope (CO) with SimplePCI operating software, Infinity 3 multibeam confocal scanning head and Hamamatsu high sensitivity EMCCD camera. The presence of cells expressing GFP (excitation/emission λ 488/509 nm; green) indicated successful transfection and therefore functional ENaC expression.

2.2.4. Cell viability assay:

HEK293 ENaC β*γ* cells were plated onto 24-well tissue culture plates, at a density of 5 x 10^5 cells/well in 500 µL of culture media (no selection). Cells were left to attach for 4-6 hr in standard cell culture conditions. 500 µL selection-free culture media, containing treatment (e.g. BacMam virus, amiloride, TSA etc.) was added to each well on top of the existing media within the plates. Cells were incubated for a further 16-24 hr in standard cell culture conditions before harvesting. Cells were diluted 1:2 with Trypan Blue (0.4%) (Gibco™ #15250061) and cell viability determined using an automated cell counter.

2.2.5. IncuCyte® Live Cell Analysis assay:

2.2.5.1. Cell preparation:

HEK293 ENaC β*γ* cells were plated onto 24-well, clear, tissue culture plates (Corning™ Costar™, #3526) pre-coated with poly-D-lysine, at a density of 5 x 10^5 cells/well in 500 µL of culture media (no selection), unless otherwise stated. Cells were left to attach for 24 hr in standard cell culture conditions. The media was removed and 500 µL fresh selection-free culture media, containing treatment (e.g. BacMam virus containing GFP-tagged ENaC δ subunit, amiloride (in dH_2O), TSA etc.) was added to

each well on top of the existing media within the plates. All media added to the cells at this point contained 250 nM IncuCyte® Cytotox Red reagent (Essen Bioscience, #4632). Immediately following transduction, cells were loaded onto the system and whole-cell fluorescence (GFP: excitation/emission λ 480/540 nm; IncuCyte® Cytotox Red: excitation/emission λ 612/631 nm) was measured every 4 hr, over a 68 hr timeframe.

2.2.5.2. Data acquisition:

Data were captured on the IncuCyte® ZOOM Live Cell Analysis System. Images were displayed and quantification of data was performed using the IncuCyte® ZOOM 2016B Software. Graphs were drawn using GraphPad Prism version 7.0 for Windows (GraphPad Software, La Jolla California, USA) and data were represented as the mean ± SEM.

2.2.6. Whole-cell patch clamp:

2.2.6.1. Solutions and compound preparation:

Intracellular solution (in mM: 120 KCl, 4 NaCl, 10 HEPES, 31.25/10 KOH/EGTA, 4 ATP.Mg, 1.75 $MgCl_2$ and 5.374 $CaCl_2$, pH 7.2 with KOH, 285-300 mOsm with sucrose) and extracellular solution (in mM: 145 NaCl, 4 KCl, 2 $CaCl_2$, 1 MgCl2, 10 HEPES, 10 Glucose, pH 7.4 with NaOH, 305 mOsm with sucrose) were prepared and stored at 4˚C for up to two months. For cation permeability studies, 145 mM of the primary cation in the extracellular solution was exchanged between Na^+, Li^+ or K^+ in their chloride salt form. For proton sensing experiments, the ECS was prepared with equivalent MES (pK_a = 6.15) instead of HEPES (pK_a = 7.55) and adjusted to suitable pH with NaOH/HCl. All solutions were filtered with a 0.22 µm pore size on use. Prior to assay, amiloride

(positive) and ECS (vehicle) controls were freshly prepared using filtered ECS, with the DMSO concentration adjusted to match that of the test solutions or compounds.

Test compounds included those reordered from Life Chemicals Inc. (Section 2.1.5.2.) in their powdered forms, analogues ordered from Ambinter or synthesised in house (Section 2.1.5.4.), and reordered compounds from BioAscent (Section 2.1.5.3.). All compounds were prepared to 10 mM or 100 mM stock solutions in 100% (v/v) DMSO. For single-point screening and dose-response curves, compounds were prepared to the desired concentration in freshly filtered ECS, with DMSO concentrations adjusted to be equivalent across all compound solutions.

Prior to each run, 80 µL of solution (e.g. ECS, test compound) was loaded into the 16 wells of the Dynaflow® Resolve System (Cellectricon, Sweden) and secured onto the electrophysiology rig for assay (Figure 28.). The chip was thoroughly washed with ethanol and ddH_2O between experiments, and the channels were primed with filtered ECS prior to compound loading. This platform consisted of a microfluid-based perfusion system driven by a 2 mL syringe at a rate of 26 mL/min.

2.2.6.2. Cell preparation:

BacMam virus (MOI 100) was added to HEK293 ENaC β*γ* cells seeded on the previous day at 5 x 10^6 cells/T75 cm^2 flask in the presence of amiloride and TSA (Section 2.2.3.2.). Cells were incubated for a further 16-24 hr in standard cell culture conditions. Cells were harvested the following day using 1 mL TryplE Express and resuspended in serum free media (25 mL CHO-SFM (Invitrogen™, #31033), 25 mM HEPES, 0.04 mg/mL soy bean trypsin inhibitor, 100 units/mL Penicillin/Streptomycin) at a density of 3 x 10^6 cells/mL and kept in a stirred reservoir for up to 4 hr.

2.2.6.3. Recording protocol:

For standard whole-cell recording, patch pipettes were pulled from borosilicate glass capillaries (1.5 mm OD x 1.17 mm ID; Harvard Apparatus, #30-0068) using a P-97 Micropipette Puller (Sutter Instrument Co., CA, USA). This was done using the program in Table 6. Pipettes were fire polished with a glowing platinum glass coated wire to achieve a final resistance of 1.5 – 2.5 MΩ when filled with intracellular solution.

Line	Heat	Pull	Velocity	Time
1	285	10	55	195
2	265	-	55	195
3	275	30	55	195

Table 6. Program used on the P-97 Micropipette Puller for borosilicate glass patch pipettes suitable for whole-cell patch clamp.

Currents were measured by a 0.1 mm diameter silver wired that was chlorided at regular intervals (3-5 days) using 0.1 M HCl, in the region which would be in contact with ICS. The wire was connected via a polycarbonate microelectrode holder to the input headstage of an Axopatch 200B microelectrode amplifier (Axon Instruments, CA, USA) mounted of a micromanipulator (MärzHäuser Wetzlar, Germany).

Cells were applied to the ECS-filled cell bath of the Dynaflow® Resolve chip (Cellectricon, #DFP400105). High resistance electrical seals (Giga-seal) were obtained on contacting the cell membrane surface with the patch pipette whilst applying gentle negative pressure. After cancellation of the capacitance transients due to the patch pipette, whole-cell configuration was achieved by additional negative pressure applied to the patch pipette, through the suction module of the microelectrode holder. Cell

capacitance and series resistance were compensated using analog controls of the amplifier.

The Dynaflow® Resolve System fully integrated with standard patch clamp software, permitting the automated and rapid exchange between buffer/compound/ligand etc. Data were sampled at 5 kHz for a 1 s period and low pass filtered at 1 kHz. All experiments were performed at room temperature using the patch clamp technique (Neher & Sakmann, 1976).

2.2.6.4. Data acquisition:

Data were recorded and analysed using Axon™ pCLAMP® 9 Software (Molecular Devices, Sunnyvale, California USA), allowing the determination of current size (Peak - Antipeak amplitude (pA)). By convention, all inward flowing cations is designated as inward, negative current, and all voltages are recorded with respect to ground or bath. All data are reported as mean ± SEM (number).

For cation permeability studies, where reversal potentials were determined, junction potentials were calculated using Axon™ pCLAMP® 9 Software and corrected as described by Fenwick, Marty and Neher (Fenwick, et al., 1982). The maximal amiloride-sensitive current at each voltage increment was calculated by subtracting those measured in the presence of 30 µM amiloride from those exposed to just the ECS solution. Using GraphPad Prism v7.0, an I/V plot for each solution informed the E_{rev} for each cation. Ion permeabilities relative to Na^+ were calculated using the Goldman-Hodgkin-Katz equation (Hille, 1992):

$$E_{rev} = \frac{RT}{F} \ln \frac{[Na]_i + (P_x/P_{Na})[x]_i}{[Na]_o + (P_x/P_{Na})[x]_o}$$

Proton sensing experiments were normalised to the amiloride-sensitive inward current (pA) at -40 mV. pH-dependent activation was plotted on GraphPad Prism v7.0 and data were transformed onto a logarithmic scale, before performing a nonlinear regression (log(agonist) vs. response - variable slope (four parameters)) to plot dose-response curves. EC_{50} data were represented as the mean ± SEM (number).

For pharmacological interrogation with blockers in wild-type or mutant channels, current amplitudes were measured from the peak inward metrics (at -100 mV) and the amiloride-sensitive current was determined by subtracting the amount of current obtained after addition of 100 µM amiloride to the current measure pre-compound addition. Dose-response curves were normalised to I/I_{max}, with I_{max} representing maximal block of channel by amiloride. IC_{50} data were represented as the mean ± SEM (number).

2.2.7. Membrane potential assay:

2.2.7.1. Solutions and compound preparation:

All compounds for screening were obtained from Life Chemicals Inc. (Section 2.1.5.2.). Both single-point and dose response curves were prepared on the day of assay in 96-well polypropylene v-bottomed source plate (Sigma-Aldrich #M8185) using the FluidX xxp-721 automated liquid handling system.

Single-point compound plates (Plate layout 1.) were prepared to 4-times the final assay concentration in Tyrode's buffer (in mM: 136.9 NaCl, 2.7 KCl, 0.4 H_2NaO_4P, 1.1

$MgCl_2$, 1.8 $CaCl_2$, 5.6 D-glucose, 11.9 $NaHCO_3$, adjusted to pH 7.35 with NaOH). Controls included 150 µM amiloride (positive) and Tyrode's Buffer (vehicle) and were added to the plates at 4-times the final assay concentration and the DMSO concentration was adjusted to match that of the test compounds (0.1/0.5 %, dependent on the screening concentration).

Dose-response compound plates (Plate layout 2.) were prepared to 4-times the final assay concentration in Tyrode's buffer. Each compound was tested at a final top concentration of 30 µM and a 3-fold serial dilution of 5 concentrations was prepared in Tyrode's buffer, whilst ensuring the DMSO concentration was kept constant (0.3%). The controls used were the same as those in the single-point compound plates.

For screening, each experiment included addition from a second compound plate containing a uniform concentration of amiloride. The final assay concentration was 150 µM, and the source plate was prepared to 5-times this concentration in Tyrode's buffer.

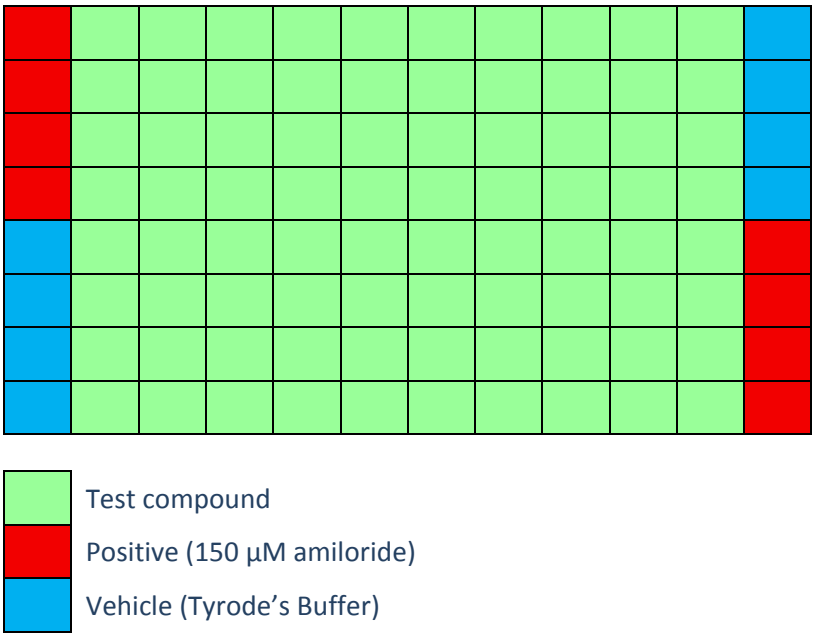

Plate layout 1. Layout of single-point compound plates for the membrane potential assay.

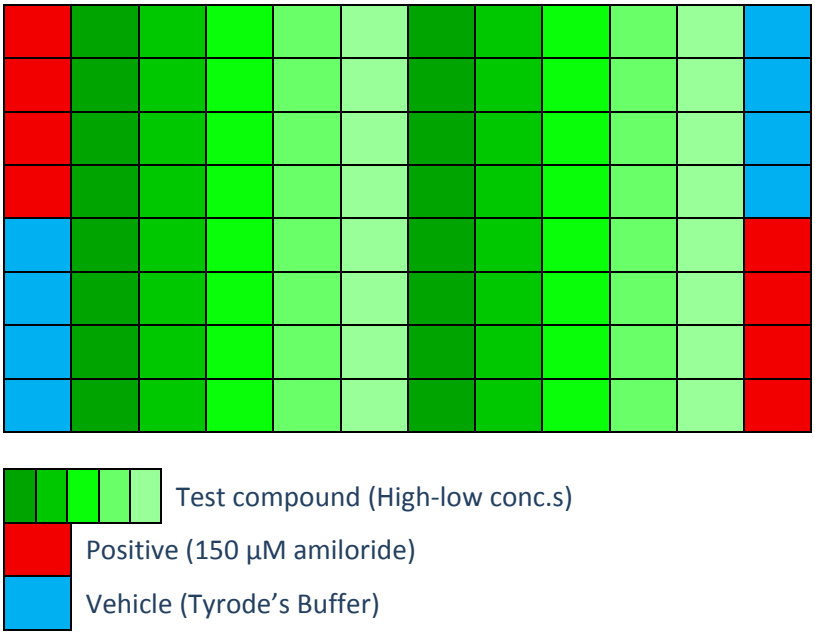

Plate layout 2. Layout of dose-response compound plates for the membrane potential assay.

2.2.7.2. Cell preparation:

Unless otherwise specified, 100 µL of culture media containing BacMam virus (MOI 2.5) was added on top of HEK293 ENaC β*γ* cells, seeded in 100 µL of culture media (no selection) one day previous in 96-well, black, clear-bottomed assay plates (Corning®, #3904), at a density of 7 x 10^4 cells/well. This was done in the presence of amiloride and TSA (Section 2.2.3.2.). Plates had been coated with pol-D-lysine 24 hr prior to cell plating. Cells were incubated for a further 16-24 hr in standard cell culture conditions.

FLIPR Membrane Potential Blue dye powder (Molecular Devices, #R8042) was suspended in 10 mL Tyrode's buffer + 0.05% (v/v) Pluronic F127 (Sigma-Aldrich, #P2443) and then further diluted 1:3 in Tyrode's buffer + 0.05% (v/v) Pluronic F127, unless otherwise specified. Cells were then washed once with DPBS (1X), before 120 µL membrane potential dye was added to the wells. The cell plate was incubated at 37 ^{o}C, 20 min. An initial background fluorescence read was taken before each run proceeded.

2.2.7.3. Recording protocol:

The fluorescence assay was transferred from the FlexStation® 3 Benchtop Multi-Mode Microplate Reader (Molecular Devices, Sunnyvale, California USA) to the FDSS/µCELL Functional Drug Screening System (Hamamatsu, Shizouka Japan), and despite basic parameters remaining similar, those used for the final assay were defined on the FDSS/µCELL. The FDSS/µCELL enabled a simultaneous addition of compound by the integrated dispensing head, and monitoring of whole-cell fluorescence (excitation/emission λ 531/565 nm) using a high-speed, high-sensitivity digital CCD

camera. The camera was programmed at an exposure time of 200 ms, and sensitivity of 2.

Briefly, a short baseline read of 15 samples, at a sampling interval time of 1.40 sec, was followed by the addition of 40 µL compound from the first compound plate into the cell plate at a speed of 40 µL/sec. During assay development the fluorescence was read over a 5 min interval using the SoftMax Pro® Software version 4.8 for Windows® (Molecular Devices, Sunnyvale, California USA) integrated with the FlexStation. The final assay included a second addition of 40 µL amiloride (150 µM, in-well control) to all wells of the plate, which was read over a further 5 min. The kinetic changes in fluorescence intensity following compound addition were recorded using the FDSS7000EX/µCELL Software (Hamamatsu Photonics, Shizouka, Japan).

2.2.7.4. Data acquisition:

Data from the assay development on the FlexStation, were exported from SoftMax Pro® Software after the reduction parameter of *maximum fluorescence – minimum fluorescence* had been applied across the full spectra of raw signal values for each well of the microplate. Data were plotted using GraphPad Prism v7.0. Data were transformed onto a logarithmic scale, before performing a nonlinear regression (log(agonist) vs. response - variable slope (four parameters)) to plot dose-response curves. IC_{50} data were represented as the mean $\pm$ SEM (number).

Screening data were exported from FDSS7000EX/µCELL Software over three separate time intervals per recording (*Interval 1*: samples 0-15; *Interval 2*: samples 50-214; *Interval 3*: samples 250-431). Data were a function of *average fluorescence* over these time periods. Data were then analysed in Microsoft Excel, whereby the change in

fluorescence between the baseline (*Interval 1*) and first compound addition (*Interval 2*) was normalised to the change in fluorescence between the baseline and addition of a high concentration of amiloride (*Interval 3*), using the following formula:

$$\textbf{Normalised Fluorescence} = \frac{Interval\ 1_{average} - Interval\ 2_{average}}{Interval\ 1_{average} - Interval\ 3_{average}}$$

To avoid the reporting of compounds that caused an increase in fluorescence or inclusion of data from a well that did not have the expected response to the amiloride in-well control, two rules were formed which were used to exclude samples from the data collection:

1. $Interval\ 2_{average}$ **must not be ≥ 1.2 *** $Interval\ 1_{average}$
2. $Interval\ 3_{average}$ **must be <** $Interval\ 1_{average}$

Data were then uploaded to the Dotmatics database (Hertfordshire, UK) and exported to Vortex v2015.11.46033 [© Dotmatics Ltd. 2007-2015]. Sample distribution graphs and Z primes were analysed within and across compound plates.

2.2.8. IonWorks Quattro™ assay:

2.2.8.1. Solutions and compound preparation:

Intracellular solution (in mM: 120 K Gluconate, 20 KCl, 10 HEPES, 5 NaCl, 1 $MgCl_2$ and 1 $CaCl_2$, pH 7.4 with KOH, 285-300 mOsm with sucrose) and extracellular solution (in mM: 120 Na Gluconate, 20 NaCl, 10 HEPES, 5 KCl, 1 $MgCl_2$, 2 $CaCl_2$, 10 Glucose, pH 7.4 with NaOH, 305 mOsm with sucrose) were prepared, filtered at 0.22 µm and stored at 4˚C. DPBS, with calcium and magnesium, no phenol red (1X, Gibco™, #14040133) was used for E-Head and F-Head solutions. ECS was used to prepare all compounds, the cells and in the buffer boat for assay. Cell membranes were permeabilised with 100

µg/mL Amphotericin B (Sigma-Aldrich, #A4888) in ICS (Access buffer). Prior to use 20 mg of Amphotericin B was dissolved in 670 µL DMSO, sonicated for 5 min, and then transferred into 200 mL ICS. All solutions were used at room temperature.

Controls included 100 µM amiloride (positive; 100 % channel block), 3 µM amiloride (positive; 50 % channel block), ECS (v/v) 0.5 % DMSO (vehicle), and an 8-point amiloride concentration-response curve (300 µM top concentration, 1 in 3 dilution per concentration). The Diverse 12K compound set from BioAscent (Section 2.1.5.2.) was delivered pre-plated in 384-well v-bottomed plates (2 µL at 2 mM) and the CUTE Ion Channel library from Life Chemicals Inc. (Section 2.1.5.3.) was prepared in 96-well polypropylene v-bottomed plates (1 µL at 10 mM; Sigma-Aldrich, #M8185). All compounds were stored at -80 °C before use.

Both 384-well and 96-well compound plates were prepared immediately prior to assay. Two compound plates were prepared per experiment. The first contained the test compounds, which were tested at a final concentration of 40 µM. ECS was added directly onto the test compound wells and the empty wells were filled with the controls were, all at 3-times the final assay concentration (Plate layout 3.). The DMSO concentration was adjusted to be the same across every plate. The second compound plates (96-well and 384-well) were prepared at the start of each day and used repetitively. These contained of a uniform concentration of amiloride (100 % channel block) prepared to 4-times the final assay concentration of 100 µM.

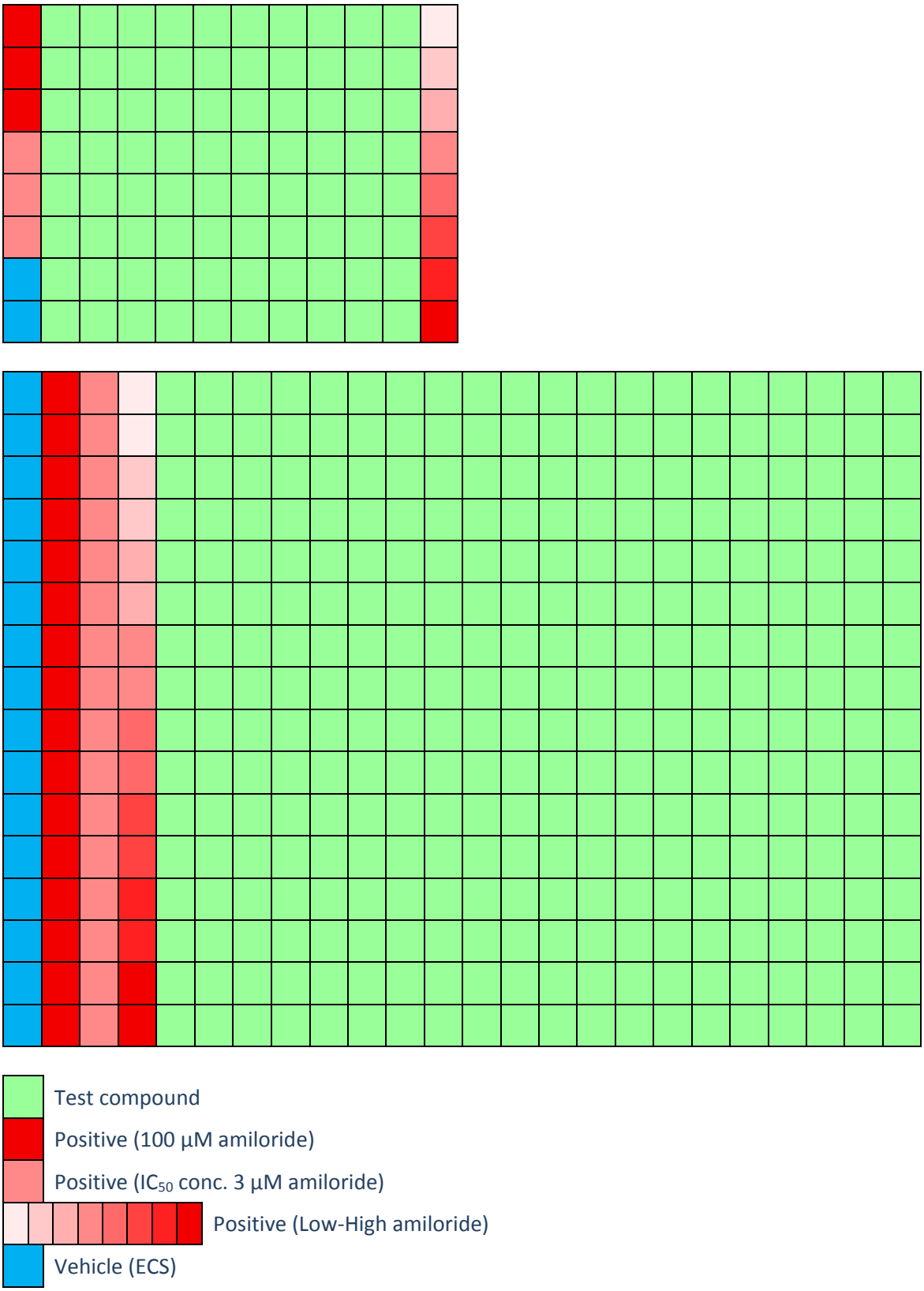

Plate layout 3. Layout of single-point compound plates in 96-well (top) and 384-well (bottom) format for the IonWorks Quattro™ assay.

2.2.8.2. Cell preparation:

BacMam virus (MOI 10), in the presence of amiloride and TSA (Section 2.2.3.2.), was added to HEK293 ENaC β*γ* cells seeded the previous day at 6 x 10^6 cells/T175 cm^2 flask (Corning #431080). Cells were incubated for a further 16-24 hr in standard cell culture conditions. Cells were harvested the following day using 1 mL TryplE Express, centrifuged for 2 min at 800 x g, and resuspended in 3-4 mL ECS (~2 x 10^6 cells/mL) before loading into the cell boat immediately prior to assay.

2.2.8.3. Recording protocol:

The assay was run using PatchPlates™ with Population Patch Clamp™ (PPC) Technology (Molecular Devices, #9000-0902), in singlicate with an 'all-at-once' scan. The parameters of the assay are defined in the assay protocol, which is split into a series of events.

Briefly, the first sequence of events concerned the priming and sealing steps. For priming, 2.5 µL ECS was added from the buffer boat to each well of the Population Patch Clamp™ (PPC) PatchPlate™. A hole test was performed with a 100 ms square pulse stepped from 0 mV to -10 mV. The resistance for each hole was measured and was expected to be between 2-4 MΩ. For sealing, 2.5 µL cell suspension was added from the cell boat to every well. After 240 s the seal was recorded by running a 160 ms square pulse stepped from 30 mV to 25 mV.

The second step involves cell perforation to obtain electrical access. After a 120 s pause, 50 mL of access solution was added to the intracellular side for 70 s and circulated for 240 s, followed by a second 300 s pause.

Currents could then be recorded using the voltage protocol, which consisted of a 100 ms ramp between -100 mV and +30 mV. This voltage ramp was applied pre-compound, post-compound addition 1, and post-compound addition 2, whilst the E-Head was submerged into the extracellular side of the plate. Between these recording periods, the cells were not voltage clamped. After the pre-compound read, 2.5 µL of the first compound was added to the corresponding wells of the PatchPlate™ in singlicate and incubated for 223 s before the post-compound addition 1 current measurement. The second compound addition then follows and 2.5 µL of the second compound (amiloride) was added and incubated for 223 s before the post-compound addition 2 current measurement.

2.2.8.4. Data acquisition:

Current amplitudes were measured from the peak inward metrics (at -100 mV). The amiloride-sensitive current was determined by subtracting the amount of current obtained after addition of 100 µM amiloride from the current measured pre-compound addition after electrical access was obtained through addition of amphotericin B. This was used to normalise the current of each well after the addition of the test compound (post-compound addition 1). The percentage of ENaC inhibition was then determined for each compound. Data were expressed as the mean ± standard error of the mean (SEM). A minimum seal resistance of 20 MΩ at post compound addition 2 (amiloride) and a minimum amiloride-sensitive current value of 1 nA were used as thresholds to filter out wells which were deemed to not be able to ensure accuracy of the voltage clamp and to minimise variability during normalisation.

Data were then uploaded to the Dotmatics database (Hertfordshire, UK) and exported to Vortex v2015.11.46033 [© Dotmatics Ltd. 2007-2015]. Sample distribution graphs, plotting the number of samples against each percentage inhibition after normalisation, and Z primes, calculated as a measure of assay quality, showing the separation between the distributions of the positive and negative controls, were analysed within and across compound plates.

2.2.9. QPatch HTX assay:

2.2.9.1. Solutions and compound preparation:

Intracellular solution (in mM: 120 KF, 20 KCl, 10 HEPES, 10 EGTA, pH 7.4 with KOH, 285-300 mOsm with sucrose) and extracellular solution (in mM: 140 NaCl, 10 HEPES, 4 KCl, 2 $CaCl_2$, 10 Glucose, pH 7.4 with NaOH, 305 mOsm with sucrose) were prepared, filtered at 0.22 µm and stored at 4˚C. All solutions were used at room temperature.

Into the on-board reservoir, sufficient volumes of ECS, ICS and Reference (100 µM amiloride in ECS) were loaded, with the ECS and Reference solutions in opposite positions to that specified by Sophion Biosciences for general assay set up. This was to allow for the cell sealing and whole-cell protocol step of the assay to take place in the presence of amiloride, ensuring closed ENaC channels and therefore an increased likelihood of high resistance seal formation.

Controls included 100 µM amiloride (positive; 100 % channel block) in the reservoir, to be seen by all cells at the end of the application protocol, and a 4-point concentration response curve of amiloride in glass inserts A1-4 of the compound plate. Insert A1 contained ECS (v/v) 0.3 % DMSO (vehicle), and A4 contained the highest concentration of amiloride (30 µM), which was diluted 10-fold, sequentially, in A3 and then A2 (Plate

layout 4.). The reordered hits for validation, from the original Diverse 12K compound set (BioAscent), were delivered at 10 mM (v/v) 100 % DMSO, in a total volume of 5.5 µL. All compounds were tested in duplicate, at 3 concentrations (0.3 µM, 3 µM, 30 µM; Plate layout 4.), and were prepared in ECS 0.3 % (v/v) DMSO.

The waste reservoir was emptied and wash station refilled with ddH_20 and the beginning of each day.

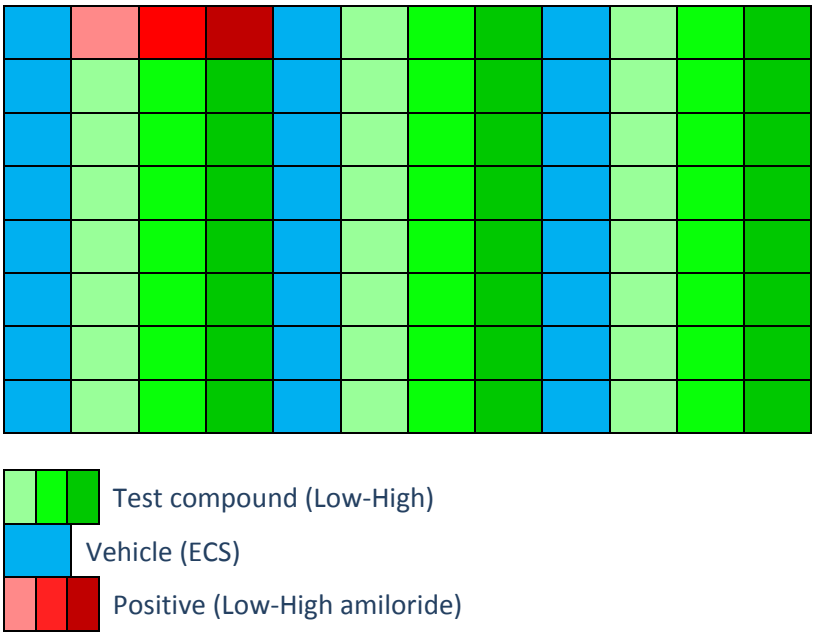

Plate layout 4. Layout of dose-response compound plates for the QPatch HTX assay.

2.2.9.2. Cell preparation:

Cell preparation was the same as that of the IonWorks Quattro™ assay (Section 2.2.8.2.), but on harvesting, cells were resuspended in serum free media (25 mL CHO-SFM (Invitrogen™, #31033), 25 mM HEPES, 0.04 mg/mL soy bean trypsin inhibitor, 100 units/mL Penicillin/Streptomycin) in the presence of 100 µM amiloride (in dH_2O), at a

density of 3 x 10^6 cells/mL, left to recover for at least 30 min, and kept in a stirred reservoir for up to 2 hr.

2.2.9.3. Recording protocol:

Whole-cell patch clamp experiments were carried out on both the QPatch 16 and QPatch HTX automated electrophysiology platforms (Sophion Biosciences) using disposable 16-channel or 48-channel planar patch chip plates (QPlates), respectively. Despite differences in the throughput of the platforms, no changes were made to the assay on transfer between the two. Data were recorded using the QPatch Assay Software version 5.6.4 (Sophion Biosciences).

Cell positioning and sealing parameters were set as follows: positioning pressure −70 mbar, resistance increase for success 750 %, minimum seal resistance 0.1 GΩ, holding potential −90 mV, holding pressure −20 mbar. Access was obtained with the following sequence: (1) suction pulses in 50 mbar increments from −250 mbar to −400 mbar; (2) a suction ramp of an amplitude of −450 mbar at 100 ms/mbar; (3) −400 mV voltage zaps of 1 ms duration (x 10). To avoid rejection of cells with large ENaC currents, the minimum seal resistance for whole-cell requirement was lowered to 0 GΩ. Following establishment of the whole-cell configuration, cells were held at −40 mV and ENaC currents elicited by a voltage protocol that ramped from −100 to +30 mV in 500 ms, and then stepped back to −40 mV for 100 ms. This pulse protocol was applied every 10 s.

2.2.9.4. Data acquisition:

Current amplitudes were measured from the peak inward metrics (at -100 mV) using the QPatch Assay Software v5.6.4. Repeated additions of ECS were performed initially

to wash out the amiloride that had been present during cell sealing and obtaining whole-cell configuration. The amiloride-sensitive current was calculated by subtracting the current size after addition of 100 μM amiloride from the current measured pre-compound addition. The inhibition by the test compound was then calculated as a percentage of the amiloride-sensitive current. Dose-response curves were plotted using GraphPad Prism v7.0 and IC_{50} data were represented as the mean ± SEM (number).

3

RESULTS: CELL LINE GENERATION AND CHARACTERISTION

Chapter 3

3.1. Background:

3.1.1. Heterologous expression systems using BacMam technology:

Heterologous expression is the introduction of either complementary DNA (cDNA) or RNA (cRNA) encoding for a protein of interest from one species into the cell of another species (reviewed in Gomes et al. (2016)). This is used successfully in both research and therapeutic settings. For example, it enables the investigation of a particular protein's function whilst circumventing technical difficulties associated with purifying the protein from biological material. It also facilitates the production of large quantities of protein, which is essential in the practical and therapeutic application of producing antibodies for vaccines (Balamurugan, et al., 2006). In the case of studying ion channels, heterologous expression enables the functional characterisation of the target protein in isolation. It permits high levels of expression, which is required for high quality voltage clamp experiments, whereby whole cell currents in the range of 0.1-2.5 nA are required. With regards to structure-function investigations, engineering the coding sequence of the cloned gene allows the examination of the contribution of specific regions of the protein, and even single amino acids, to channel function (Jan & Jan, 1992). Finally, as ion channels tend to comprise multiple subunits, coexpressing different combinations of subunits for channel reconstitution allows the exploration of the subunit coassembly process (Ruppersberg, et al., 1990).

The host system is usually a cultured immortalised cell, and may be of bacterial (Beneyx, 1999), mammalian (Kost & Condreay, 1999), insect (Altmann, et al., 1999), yeast (Malys, et al., 2011) or plant (Vyacheslavova, et al., 2012) origin. Each type of

system has its advantages and limitations, but in general, biological and biochemical properties of the protein of interest dictate the type of expression system that can be used successfully (Geisse, et al., 1996). Although the DNA template for protein expression is simple to construct synthetically, aspects such as codon usage of the DNA must be compatible with the corresponding tRNA population available in the host cell (Brown, 2006). In addition to this, the host then must be able to provide the conditions required for correct post-translational processing, essential for a functionally active protein (Khan, 2013). Useful additions to the synthetic DNA could include reporter or affinity tag sequences, which permit downstream detection or purification methods (Waugh, 2005). Key considerations for industrial production of proteins such as antibodies, include the cost of reagents and a high economic yield, but also the quality of human pharmaceuticals governed by strict safety guidelines (Gellissen, 2005).

Exploiting mammalian cells for recombinant proteins has a number of benefits, particularly when considering more complex protein structures like ion channels. Mammalian cell hosts can be difficult and expensive to work with, however they are able to introduce the proper protein folding, post-translational modifications and product assembly key for complete biological activity (Khan, 2013). Such expression of a foreign protein by mammalian cellular machinery can be either transient (24-72 hr) or stable/permanent. This is determined by whether foreign DNA is integrated into the host genome. While stable cell lines can be used over several experiments, transient production can generate large amounts of protein over a shorter time period (Khan, 2013). A number of mammalian cell lines are used for protein expression but

the most common are HEK 293 (Human embryonic kidney) and CHO (Chinese hamster ovary).

The DNA templates encoding the protein of interest are carried on autonomously replicating DNA molecules called vectors (Khan, 2013). For mammalian cell expression, the vector is often derived from mammalian viruses, such as Simian Viruses 40 (SV40), polyomavirus, herpesvirus and papovirus, and includes an efficient promoter and selection marker. A further type of viral vector used as a vehicle to efficiently deliver and express genes in mammalian cells is a BacMam baculovirus (Hüser & Hofmann, 2003; Fornwald, et al., 2007). This system uses a modified, double-stranded DNA insect cell virus (baculovirus) with a mammalian expression cassette upstream of the gene of interest (GOI). The BacMam baculovirus is harvested from insect cell cultures, which are previously transfected with a bacmid containing the GOI (Figure 15.a). The GOI is introduced into the host via endocytosis of BacMam particles. On migration of the gene into the nucleus, expression can be seen as little as 4-6 hr post transduction and can remain detectable for up to 14 days, dependent on cell type and division rate (Fornwald, et al., 2007).

BacMam technology offers a number of advantages over other viral gene delivery vectors: they have a high transduction efficiency across a broad range of cell types, including primary and stem cells (Mansouri, et al., 2016); they are capable of expressing large gene inserts in mammalian systems with minimal cytopathic effects; the level of expression is highly reproducible and titratable; it can be used for simultaneous delivery of multiple genes; and finally, they are relatively easy to generate.

3.1.2. Heterologous expression of the ENaC channel for drug discovery:

BacMam baculoviral technology has been successfully implemented and reviewed for a number of cell-based assays, including those for the human ENaC αβγ channel (Chen, et al., 2015). Although this ENaC channel subtype is directly associated with human diseases (Grunder, et al., 1998; Hanukoglu & Hanukoglu, 2016), identification of novel channel modulators has proven arduous, in part due to two reasons.

Firstly, technological limitations have meant a reliance on conventional patch clamp electrophysiology and short-circuit measurements in Ussing chambers to perform studies. Although these convey detailed functional information, they are very low throughput (Chen, et al., 2015). The ability to screen large compound libraries relies on established higher-throughput assays, which are now possible through enabling platforms. Examples include fluorescent plate readers, or automated patch clamp electrophysiology systems.

Secondly, difficulties exist in generating a heterologous expression system for the ENaC channel. Due to its constitutive activity, the ENaC channel's expression at the cell membrane in a physiological setting is highly regulated through rapid turnover, with a half-life of under an hour (Hanwell, et al., 2002; Lu, et al., 2007). Additionally, overexpression of the channel leads to cytotoxicity. Chen and colleagues (2015) managed to overcome problems regarding the subunits' rapid turnover by introducing mutations in the C-terminus PY motif of the ENaC β and γ subunits. These mutations were representative of Liddle's syndrome (Abriel, et al., 1999), preventing ubiquitination and subsequent degradation of the subunits. This was then used

alongside a BacMam baculoviral transduction to transiently express the final ENaC subunit to reconstitute channel function. Circumventing stable expression of the channel overcomes toxicity associated with long-term expression. This strategy can also be applicable to the study and identification of novel channel modulators of the ENaC δβγ channel subtype.

3.1.3. Whole-cell patch clamp technique:

The patch clamp technique (Neher & Sakmann, 1976) remains the gold standard for studying ion channel function and involves bringing a fine glass pipette in close contact with the cell membrane under the control of a skilled operator using a microscope and fine micromanipulator. A high resistance seal can then be formed between the end of the pipette and the cell membrane in the range of GΩ. The patch of membrane across the end of the pipette is then ruptured in order to gain electrical access to the interior of the cell. A continuous electrical circuit is established between the intracellular milieu of the cell, and the intracellular solution (ICS) and electrode contained within the patch clamp pipette.

This configuration is called the whole cell patch clamp technique and permits the monitoring of a macroscopic electrical current relating to ion channel openings and closings over the entire cell membrane. Electrical interference is reduced by containing the conventional patch clamp rig within a Faraday cage, on top of a vibration isolation table. The experimenter can then measure changes in ion channel activity in response to external stimuli e.g. a ligand or a drug. Although this technique is low-throughput and requires a highly skilled experimenter, the data yielded is information rich. This technique provides functional information which can be used to

identify the presence of a specific ion channel based on known biophysical and pharmacological properties.

3.2. Methods:

3.2.1. BacMam expression vector generation:

The desiccated DNA construct containing the *SCNN1D* gene (Section 2.1.1.1.) was dissolved into solution with deionised water (dH_2O) and chemically transformed in One Shot® TOP10 Chemically Competent *E. coli* (Section 2.2.1.1.1.). Preparation of DNA constructs for subsequent cloning was performed using the QIAGEN Plasmid Maxi Kit following manufacturers' instructions (Section 2.2.1.2.1.).

Initially the ENaC δ1 gene was PCR amplified from pUC57, using Platinum® Pfx DNA Polymerase to produce blunt-end PCR products (Section 2.2.1.3.1.). Primers were designed using specific criteria to ensure maximal specificity and efficiency for use with the pENTR™/D-TOPO®cloning kit**.** This included a 4 base pair sequence (CACC) on the 5' end of the forward primer, necessary for directional cloning, followed by a sequence specific to target gene of ~18-25 bp in length (Table 4.; Section 2.1.2.). Both forward and reverse primer had a CG-content of ~40-60% and a Tm of ~60 ˚C, with ≤ 4 ˚C difference.

The pENTR™ Directional TOPO® Cloning Kit uses a cloning strategy that directionally clones a blunt-end PCR product into a vector and circumvents the need for restriction enzymes and ligase (Figure 11.a). This vector is compatible for subsequent recombination with the Gateway® destination vector, BacMam pCMV-DEST, using the ViraPower™ BacMam Expression System kit.

The TOPO® cloning reaction protocol was followed as per the manufacturer's instructions (Section 2.2.1.6.) using a 2:1 molar ratio of PCR product to TOPO® vector, resulting in a pENTR™/D-TOPO® vector (Section 2.1.1.4.) encoding the *SCNN1D* gene. A second pENTR™/D-TOPO® vector containing the *SCNN1A* gene (Section 2.1.1.2.), encoding the ENaC α subunit (Entry P37088, www.uniprot.org), was kindly donated by GlaxoSmith Kline (GSK, Stevenage, UK). TOPO® clones were transformed into One Shot® TOP10 Chemically Competent *E. coli* (Section 2.2.1.1.1.) and DNA prepared using the QIAGEN Plasmid Miniprep Kit (Section 2.2.1.2.1.).

Colony PCR was performed using Maxima Hot start Taq DNA polymerase (Section 2.2.1.3.2.) to check for the presence of the gene insert flanked by two M13 cloning sites (Table 4.; Section 2.1.2.). Simultaneously, restriction digestion analysis was performed by using a unique 6+ cutter of this vector, NheI-HF®, to linearise and determine the size of the vector (Section 2.2.1.4.). Products from colony PCR and restriction enzyme analysis were observed using gel electrophoresis (Section 2.2.1.5.).

The ViraPower™ BacMam Expression System Kit allows you to construct an engineered viral genome, called a bacmid, using Gateway® technology (Figure 12.a). This universal cloning method takes advantage of the site-specific recombination properties of bacteriophage λ (Landy, 1989). By using the *att*L-containing entry clone (pENTR™/D-TOPO®) containing the gene of interest, with the *att*R-containing BacMam pCMV destination vector (BacMam pCMV-DEST), the gene of interest can be moved between the two to create an expression clone.

Prior to Gateway® cloning, the pCMV-DEST vector was transformed in One Shot® *ccdB* Survival™ T1^{R} Competent Cells (Section 2.2.1.1.2.) due to the presence of the *ccdB*

gene in the vector which prevents propagation in non-resistant *E. coli* strains. DNA was prepared the QIAGEN Plasmid Miniprep kit (Section 2.2.1.2.1.). The LR cloning reaction (Section 2.2.1.7.) was performed using 100 ng Entry clone to 250 ng BacMam pCMV-DEST vector. The reaction mix was transformed in One Shot® TOP10 Chemically Competent *E. coli* (Section 2.2.1.1.1.). All clones were sequenced via the Eurofins Genomics' Value Read sequencing (https://www.eurofinsgenomics.eu/en/custom-dna-sequencing/tube-sequencing-service/value-read.aspx) service, using a T7 primer.

3.2.2. Bacmid generation:

BacMam expression constructs were either stored at -20 °C or transformed into MAX Efficiency® DH10Bac™ Competent Cells (Section 2.2.1.1.3.) for transposition into a bacmid (Figure 12.b). Antibiotic and blue/white selection identified colonies containing the recombinant bacmid. White colonies on antibiotic plates (50 µg/ml kanamycin, 7 µg/ml gentamicin, 10 µg/ml tetracycline, 100 µg/ml Bluo-gal and 40 µg/ml IPTG; Section 2.1.4.) indicated the likelihood of successful recombination of the bacmid. The largest, most isolated white colonies were selected for restreaking onto fresh plates to determine true positive clones.

A single colony, confirmed as having a white phenotype after restreaking, was inoculated in LB medium and the bacmid was isolated (Section 2.2.1.2.2.). The bacmid contained M13 Forward (-40) and M13 Reverse priming sites (Table 4.; Section 2.1.2.) flanking the mini-attTn7 site within the lacZα-complementation region therefore PCR analysis was performed on isolated bacmids, using Phusion Flash High-Fidelity PCR Master Mix (Section 2.2.1.3.3.). An indication of successfully transposed gene insert

was a band of ~5000 bp more than the size of the gene insert, observed using gel electrophoresis (Section 2.2.1.5.).

3.2.3. BacMam baculovirus generation in insect cells:

Sf9 log-phase cells (Section 2.1.3.1.) with >95 % viability were used to perform a successful transfections (Section 2.2.3.1.). The P1 viral stocks (typically 1–10 × 10^6 plaque forming units (pfu)/ml) were harvested between 3-5 days post transfection, when cells displayed 'late'-'very late' signs of infection (Table 5.; Section 2.2.3.1.1.)

To generate a viral stock at a high enough titre for mammalian cell transduction, the virus underwent two subsequent rounds of amplification (P2, then P3 viral stocks), using the previous viral stock as the inoculating agent for the next (Section 2.2.3.1.2.). A viral plaque assay (Section 2.2.3.1.3.) was performed to determine the titre of the harvested P3 stocks, which could then be used for transduction in mammalian cells.

3.2.4. Viral transduction of mammalian cells:

HEK 293 ENaC β*γ* cells were transduced with the baculovirus encoding either ENaC α or ENaC δ subunits, in the presence of 50 µM amiloride (in dH_2O) and 0.25 µM TSA, 16-24 hr prior to the start of an experiment (Section 2.2.3.2.), unless otherwise specified.

3.2.5. Visualisation of ENaC δ subunit transduction:

Visualising successful transduction of the ENaC δ subunit was performed on the IncuCyte® Live Cell Analysis System (Section 2.2.5.) using a baculovirus encoding a GFP-tagged ENaC subunit (Section 2.1.1.3.). Cells were plated in 24-well, clear tissue culture treated plates 24 hr prior to transduction (Section 2.2.5.1.). In parallel to baculoviral transduction, cells were treated with IncuCyte® Cytotox Red reagent

(Section 2.2.5.1.) as per manufacturer's instructions. Immediately following transduction, cells were loaded onto the system and whole-cell fluorescence was measured every 4 hr, over a 68 hr period.

3.2.6. Measuring functional ENaC activity:

Whole-cell configuration of the patch clamp technique (Section 2.2.6.), using buffers detailed in Section 2.2.6.1., was used to measure amiloride-sensitive currents from HEK293 cells expressing either ENaC δβ*γ*, ENaC β*γ* or no ENaC subunits. Where specified, cells were transduced with the ENaC α/δ subunit at MOI 100.

For cation permeability studies, transduced cells were perfused with a bathing solution containing 145 mM of the primary cation (Na^+, Li^+ or K^+), pH7.2. Cells were stepped from a holding potential of 0 mV to voltages between -120 mV and +100 mV, in 20 mV increments, for 500 ms. This was done in the presence and absence of 30 µM amiloride to determine the properties of the amiloride-sensitive current carrying each cation.

For pH sensitivity experiments, cells were perfused with a bathing solution at pH7.4, and held at a continuous holding potential of -40 mV. Cells were then subject to a 5 sec exposure to the same bathing solution of a more acidic pH (pH5, pH5.5, pH6, pH6.5 or pH7). At the start of each recording cells were exposed to 30 µM amiloride, to verify the presence of constitutive amiloride-sensitive ENaC currents.

For experiments testing known ENaC blockers, cells were exposed to increasing concentrations of drug, and currents measured by holding the cells at -40 mV, followed by a voltage ramp from -100 mV to +100 mV over 1 s.

Data were analysed using Axon™ pCLAMP® 9 Software and graphs were plotted using GraphPad Prism v7.0 (Section 2.2.6.4.). All data are reported as mean ± SEM (number).

3.3. Results:

3.3.1. BacMam vector encoding the ENaC subunits:

To ensure the gene encoding the ENaC δ subunit was successfully passed between each vector, the presence of *SCNN1D* was confirmed at each stage before continuing with subsequent cloning steps. Initially the *SCNN1D* gene (1917 base pairs) was amplified out of the pUC57 vector with a proofreading DNA polymerase to generate a blunt-ended PCR product for TOPO® cloning (Figure 10.a). Successful PCR was confirmed by gel electrophoresis (Figure 10.b) on observation that the size of the PCR product corresponded to the size of *SCNN1D.*

Successful TOPO® cloning (Figure 11.a) was confirmed by both PCR analysis of the inserted DNA (Figure 11.b) and restriction digestion analysis of the cloned entry vector (Figure 11.c). The entry vector containing the *SCNN1A* gene, obtained from GSK, was also linearised in the same way. PCR products and the linearised vectors were confirmed to be the correct number of base pairs by gel electrophoresis (Figure 11.c).

LR Clonase® II enzyme mix was used in Gateway® cloning (Figure 11.a) to catalyse the *in vitro* recombination between an entry clone (containing a gene of interest flanked by *att*L sites) and a destination vector (containing *att*R sites). It was important that equal quantities (50-150 ng) of entry vector and destination vector were: too much vector could result in colonies containing multiple DNA molecules; and too little entry clone significantly reduced the number of colonies seen. The process was highly

efficient, using only a 10 µl reaction volume and 1 hr incubation time, before transformation in *E. coli*. Restriction digestion analysis of the cloned destination vector was not appropriate in this case as the cloned vector was large (~10 kB base pairs). Instead, the vector DNA was sequenced with a T7 primer before proceeding any further. Sequencing results confirmed both ENaC subunits had been cloned into their three respective BacMam destination vectors in the correct orientation.

3.3.2. Bacmid encoding the ENaC subunits:

The purified plasmid DNA was transformed into DH10Bac™ *E. coli* for transposition into the bacmid (Figure 12.b). Insertions of the mini-Tn7 into the mini-attTn7 attachment site on the bacmid disrupted the expression of the LacZα peptide, allowing for identification of recombinant bacmid through blue/white selection. Many more blue colonies were seen than white ones (positive clones). Since bacmid DNA is >135 kb in size, those that were still white on restreaking were analysed by PCR to verify the presence of the gene of interest. The size of the PCR product was checked using gel electrophoresis (Figure 12.c). PCR products from the bacmid (lanes 5 and 6) were run against those from PCR analysis of the entry vectors (lanes 2 and 3) to confirm the size of the inserts had increased by~5000 bp during the transfer between vectors. Non-recombinant bacmid was ran as a control (lane 4).

3.3.3. Baculovirus encoding the ENaC subunits:

Transfection of Sf9 cells (Figure 13.a) with bacmid, or subsequent viral stocks, caused the cells to die and virus to bud from the cells. The virus was then harvested. Time of harvest post transfection was dictated by a series of observable phenotypic changes in the cells, with the ultimate being cell lysis. This was observed in the transfected

population by Day 5, but not in the control populations (Figure 13.b). The viral titres of the P3 stocks were determined by a cell plaque assay and were found to be towards the upper range of what was expected (Figure 13.c). These were therefore suitable to use for mammalian transduction.

3.3.4. Mammalian cell transduction to reconstitute ENaC channel activity:

Fluorescence microscopy was used to visualise delivery of GFP-tagged ENaC subunits (ENaC δ-GFP) into the mammalian cells (HEK293 and HEK293-ENaCβ*γ*) (Figure 14.a-d), and amiloride sensitivity was used as a functional assessment of channel formation using manual patch clamp (Figure 15.b-c).

Whole-cell fluorescence was monitored in HEK293 and HEK293-ENaC β*γ* cells transduced with ENaC δ-GFP (Figure 14.a-d). Cells were first seeded in the tissue culture plate and left for 24 hr to attach prior to transduction. At the point of transduction cells were simultaneously treated with IncuCyte® Cytotox Red reagent to monitor real-time cell death. Despite all wells initially being seeded at the same density, the confluency of the two populations of cells prior to transduction was vastly different. Those stably expressing the ENaC β*γ* subunits were much less confluent (22.15 ± 2.19 % (n=4)) compared with the HEK293 cells expressing no ENaC subunits (87.55 ± 1.33 % (n=4)). Images were taken from time of transduction, every 4 hr, over a total of 68 hr. One day post-transduction, cells that had been treated with virus saw no increase in confluency (Figure 14.b); had a high proportion of cells expressing the ENaC δ-GFP subunit (Figure 14.c); and had a higher proportion of cells labelled with the Cytotox Red reagent (Figure 14.d), representative of the loss of cell membrane

integrity i.e. greater cell death. Cells that had not been treated with virus did not express any GFP, confirming the signal observed in the treated population was specific. Furthermore, they increased in confluency, with minimal cell death.

To validate that this expression was reflective of functional ENaC channel, whole-cell currents were measured using patch clamp, 16 hr post transduction with virus (Figure 15.b-c). Cells were held at a holding potential of -40 mV and then ramped between -100 mV and +100 mV over 1 s. Inward and outward currents were observed which reversed at ~+80 mV (Figure 15.c). The reversal potential calculated by the Nernst equation is 91.0 mV, suggesting the currents were ENaC. A leak current would reverse at 0 mV. In the presence of 30 µM amiloride the currents were abolished (red), confirming the presence of amiloride-sensitive ENaC channels. The observation of an inward current whilst holding the cells at -40 mV reflected the constitutive activity of the ENaC channel. This was not present when recording from HEK293 cells expressing either ENaC δ alone, or just ENaC β*γ* subunits, nor was any sensitivity to amiloride (Figure 15.b). This demonstrates that all three subunits are required for functional activity of the channel.

3.3.5. Cation permeability of the two ENaC channel isoforms:

The cation selectivity of each ENaC channel was examined by applying a voltage stepped stimulus of 20 mV increments, between -100 mV and +100 mV for 500 ms, to determine the current reversal potentials in extracellular solutions in which sodium chloride (NaCl) was replaced by equivalent molar concentrations of either lithium or potassium chloride. From the amiloride-sensitive current-voltage curves, which were obtained by subtracting the current measured in the presence of amiloride from those

without, the reversal potentials (E_{rev}) were evaluated. Ion permeabilities relative to Na^+ were calculated using the Goldman-Hodkin-Katz equation (Hille, 2001), under the assumption that currents were carried by cations alone (Table 7.).

	ENaC δβγ		ENaC αβγ	
Cation	**E_{rev}**	**P_x/P_{Na}**	**E_{rev}**	**P_x/P_{Na}**
Na^+	+64.86	1	+34.11	1
Li^+	+47.60	0.44	+36.87	1.12
K^+	-29.89	0.02	-27.95	0.08

Table 7. Ion permeability ratios of the ENaC α and δ channels. Values were adjusted for calculated liquid junction potentials.

Increased permeability of Na^+ over Li^+ ions (I_{Li}/I_{Na} = 0.44) through δβγ channels was observed (Figure 16.a), which was the converse to that of the αβγ channels (I_{Li}/I_{Na} = 1.12; Table 7.). Both channels showed little or no permeability to K^+ ions. We report the reversal potential calculated experimentally for Na^+ at the ENaC δβ*γ* channel as being +64.86 mV.

3.3.6. pH sensitivity of the ENaC δβγ channel:

Sensitivity to an increase in extracellular proton concentration (drop in pH) was assessed in HEK293-ENaC β*γ* cells that were either untransduced (negative control) or expressing α or δ ENaC channels, and in HEK293 cells expressing ASIC 1a channels (positive control), which are known to be activated by an increase in extracellular proton levels. The sensitivity of each channel was demonstrated at a holding potential of 0 mV, to ensure the inward current was submaximal. Cells were first perfused with extracellular solution at pH 7.4 for 5 s. This was followed by a brief

exposure to 30 µM amiloride for 5 s, followed by a washout step of 5 s. In both ENaC channel recordings, this illustrated the presence of constitutively active, amiloride-sensitive currents (Figure 17.a). This was not seen in untransduced cells expressing just two subunits due to the absence of functionally active channel; nor was it seen in ASIC 1 channels, which do not exhibit constitutive activity. Cells then proceeded to be subject to extracellular solution at pH 5.0 for 5 s, followed by a second washout step at pH 7.4. This reported a rapid activation, then deactivation of the ASIC 1 channel (690 ± 70 ms (n=6)), and an increase in current amplitude in the ENaC δβγ channel of 386 ± 96 %, which inactivated much more slowly (> 5 s (n=5)). No change in channel recording was observed in the control cells or ENaC αβγ channel as a result of increased acidity.

To ensure this response in both ENaC δβγ and ASIC 1a channels was mediated through these two channels, extracellular solution at pH 5.0 was applied, followed by the same solution with 100 µM amiloride. In both cell lines the observed currents seen at pH 5.0 were abolished in the presence of the blocker.

Both channels exhibited pH-dependent activation (Figure 17.b-c) and, on exposure to solutions that ranged from a pH 7.0 to pH 5.5, their EC_{50} values for pH activation could be determined. These were found to be similar (ENaC δβγ: pH EC_{50} = 5.96 ± 0.05 µM (n=6); Figure 17.b; ASIC 1a: pH EC_{50} = 6.04 ± 0.03 µM (n=8); Figure 17.c). Interestingly, more acidic values than pH 5.5, gave gradually smaller responses, as current sizes decreased in amplitude for both channels.

3.3.7. Sensitivity to ENaC channel blockers:

The effects of the ENaC channel blockers, amiloride and benzamil, on the ENaC currents were tested on both isoforms. Both drugs suppressed the currents in each

channel rapidly and in a concentration-dependent manner (Figure 18.). This blockade was observed for both inward and outward current, suggesting a lack of voltage-dependence of block. For amiloride, the half-maximal inhibitory concentration (IC_{50}) for the inward current at -50 mV was 0.52 ± 0.05 µM (n=5) for ENaC αβγ (Figure 18.a) and 1.55 ± 0.12 µM (n=3) for ENaC δβγ (Figure 18.b). For benzamil the IC_{50} for the inward current at -50 mV was 0.04 ± 0.003 µM (n=11) for ENaC αβγ (Figure 18.a) and 0.15 ± 0.01 µM (n=5) for ENaC δβγ (Figure 18.b). Benzamil was more potent than amiloride at both channels, and both drugs were more potent at the ENaC αβγ channel.

3.4. Discussion:

To screen for novel inhibitors of the ENaC δβγ channel requires the use of high-throughput assay, for example a fluorescence-based membrane potential assay and/or an automated patch clamp assay. The platforms used to perform such assays require a high level and uniform expression of the protein (Clare, et al., 2009), which, in the case of the ENaC channel, would not be fulfilled by use of a native cell line. By employing a HEK293 cell line that stably expresses the ENaC β and γ subunits that harbour Liddle's Syndrome mutations, a higher level of expression of ENaC at the cell surface is achieved by prevention of internalisation and degradation of the subunits (Lu, et al., 2007). Chen et al. (2015) demonstrated that when using a cell line expressing the wildtype β and γ subunits, whereby the proteins are rapidly internalised and degraded, there was only a slight increase in the amiloride response on introduction of the α subunit. Use of the mutated subunits increased this response by over 2-fold, which is important for measuring functional block of ENaC-mediated currents.

This cell line is then compatible with the BacMam baculoviral expression system, as shown by Chen, et al. (2015). The virus transiently delivers the third subunit (ENaC α or δ) at easily titratable levels into the cell, whilst negating problems of cytotoxicity associated with long term overexpression of a functionally active ENaC channel. The flexibility of studying either ENaC channel is useful for comparative studies, and the ability to introduce mutated ENaC α or δ subunits, enables the functions of specific regions of the channel to be investigated. For example, by mutating the documented amiloride binding site, confirmed blockers can be examined for their ability to inhibit the mutant channel compared to the wild-type. This can be used to deduce if lead compounds share the same binding site as amiloride and its analogues.

These results show the successful cloning of the human ENaC δ and α subunit genes, *SCNN1D* and *SCNN1A* respectively, into the BacMam baculoviral expression system for subsequent mammalian cell transduction. The genes' presence was verified using a combination of PCR, restriction digestion and DNA sequencing analytical techniques. These techniques monitored the transfer of the gene between the pUC57 vector, the pENTR™/D-TOPO® vector, and lastly the BacMam pCMV-DEST destination vector.

Overall, the process up to generation of the BacMam expression vector was relatively efficient, with only a little optimisation required for the TOPO® cloning step. The pENTR™/D-TOPO® vector contains a number of key elements which aided this cloning step. Firstly the TOPO® Cloning site exploited the activity of the Topoisomerase I enzyme from *Vaccinia* virus. This enzyme binds to specific sites on duplex DNA (CCCTT) and is able to convert energy from the cleavage of the phosphodiester bond of the DNA backbone, to the formation of a covalent bond between the 3' phosphate of

the cleaved strand and its own tyrosyl residue (Tyr-274). This bond is then attacked by 5'hydroxyl groups of the original strand of DNA, which enabled cloning of the PCR products into these sites. Additionally, the incorporation of a 3' single-strand overhang (CACC) to the incoming DNA, which anneals to the overhang in the cloning vector, ensured the PCR product is cloned in the correct orientation (Cheng & Shuman, 2000).

Secondly, the M13 forward (-20) and reverse priming sites fall either side of the inserted DNA. These provided a useful means of verifying that the size of the DNA insert was the same as that of the PCR product, before continuing with subsequent cloning steps. Furthermore the existence of a number of unique 6+ cutting sites for restriction enzyme digestion provided a quick and easy way to assess the overall size of the vector.

Finally, the *att*L1 and *att*L2 sites for site-specific recombination of the entry clone with a Gateway® destination vector, allows the GOI to be shuttled to the pCMV-DEST vector, circumventing traditional restriction enzyme based cloning limitations. This was a very fast and efficient step that was easily verified through sequencing using the T7 primer, again ensuring the GOI was inserted before continuing with subsequent cloning steps.

The TOPO® cloning step was unsuccessful when following the manufacturer's generic protocol. Initially no colonies were observed indicating no DNA had been inserted into the vector. As no colonies were seen using PCR product that had been extracted out from the agarose gel, the cloning was carried out with unpurified PCR product (before gel electrophoresis). This eliminated the possibility that the gel extraction step

introduced residual salts from the wash buffers that inhibited ligation. Removing this step did yield colonies, but many contained non-specific DNA inserts. It was recommended that the incubation of PCR product and vector could be extended if working with large (> 1 kb), or a pool of, PCR products. The incubation time for the reaction was increased accordingly, from the proposed 5 min to 30 min. This increased the number of colonies, and therefore the likelihood that at least one was a positive clone.

Transfer of the genes into the pCMV-DEST vector put the gene under the control of a Cytomegalovirus (CMV) promoter for efficient and high levels of recombinant protein expression in mammalian cells (Boshart, et al., 1985). The vector also contains key elements such as VSV-G (Vesicular stomatitis virus G protein) to enable viral delivery to mammalian cells, and WPRE (Woodchuck Hepatitis Virus Posttranscriptional Regulatory Element) for increased duration of gene expression.

For the transposition of the GOI, with these additional elements, into a bacmid, a specific strain of *E.coli* were used, which contained the Bacmid and a plasmid encoding a transposase enzyme. Successful transformation into these DH10Bac™ competent cells was selected for via antibiotics and blue/white screening, however required multiple attempts under different conditions to yield positive clones. Fortunately, colonies could be analysed by PCR as the insert site was flanked by M13 Forward (-40) ad Reverse priming sites. As soon as two bacmids, containing either the *SCNN1A* or *SCNN1D* genes, were identified and isolated, viral stocks could be made via insect cell transfection.

Visible signs of infection with the bacmid were observed in Sf9 cells. These could not be observed in untransfected cells or cells treated with just the Cellfectin® reagent, which gave confidence that the transfection had been successful. The P2 viral stock could be stored long-term in the dark, at 4°C. This was useful for when the P3 stocks was used up as only 100 µl of the P2 was required to make a new batch of P3 stock. This meant it was never necessary to go back to any of the previous cloning steps.

In order to observe expression of the ENaC subunit encoded by the baculovirus, cells were transduced with the *SCNN1D* gene tagged to the *egfp* gene, encoding enhanced green fluorescent protein (GFP). This enabled the whole-cell fluorescence to be monitored from the point of cell transduction, and then quantify the level of GFP expression as a read-out of ENaC δ subunit expression. This was performed across two different cell lines: one expressing the ENaC β*γ* subunits, and the other not. This examined both the baculoviral transduction efficiencies, and the possibility of previously reported homotrimeric ENaC δ channels (Waldmann, et al., 1995; Giraldez, et al., 2007), which has not be seen with ENaC α subunits.

Interestingly ENaC δ subunit expression was observed in both cell lines 16 hr post transduction with the virus (MOI 100), suggesting protein expression is independent from the presence of the two other ENaC subunits (β and γ). The untransduced cells shown no GFP expression, confirming that this is not an artefact. On first glance it appears the level of ENaC δ expression is much higher in the HEK293 cell line without the other two subunits, however this is reflective of the higher number of cells in the well at time of transduction. Despite cells being seeded at the same density 24 hr prior to transduction, the HEK293-ENaCβ*γ* cells are subject to selection by antibiotics,

which may affect their growth rate and therefore confluency. Levels of GFP and Cytotox Red were normalised to the confluency of the wells for a fairer comparison.

After transduction, both cell lines did not increase any further in confluency, suggesting a cessation in cell growth. In fact, the confluency of both slightly decreased. This may be representative of the increase in cell death, meaning cells detach from the bottom of the well and are not in the same plane as the camera. The only cells which do increase in confluency are those cells that are untransduced.

The increase in cytotoxic cells in both transduced cell lines correlates with the increase in GFP, and therefore ENaC δ expression. Whereas the peak ENaC δ expression in HEK293- ENaCβ*γ* cells is at 16-20 hr, the peak expression in HEK293 cells is between 28-36 hr. The time lag between these two cell lines is paralleled with a similar time lag in the levels of cytotoxic cells, suggesting that this cytotoxicity is likely directly linked to ENaC δ overexpression (Schild, 2010; Chen, et al., 2015). The difference in time taken to reach peak expression of the ENaC δ subunit may be linked to the confluency of the cells. The optimal cell density for transduction varies for different cell types, but as a general rule cells that are actively dividing have a higher chance of taking up foreign nucleic acid than those that are too confluent and therefore in a stationary phase. This is therefore an important factor to consider in future assay development and optimisation.

Functional studies in patch-clamp shows no amiloride-sensitive currents present in either wild type HEK293 cells transduced with ENaC δ alone or HEK293- ENaCβ*γ* which hadn't been transduced. This contradicts previous work by Waldmann et al. (1995) that showed a small, but reproducible, amiloride-sensitive current in

homomeric ENaC δ channels, and suggests the requirement of all three subunits to be present for biological activity.

On further inspection of the channel, ENaC δβ*γ* was shown to have a cation permeability sequence of $Na^+>Li^+>>>K^+$ (1/0.44/0.02) and ENaC αβ*γ* $Li^+>Na^+>>>K^+$ (1.12/1/0.08), which is concurrent with prior literature (Waldmann, et al., 1995; Ji, et al., 2004; Ji, et al., 2006). The reversal potential of ENaC δβ*γ*, as predicted by the Nernst equation, is +91.0 mV. We report the reversal potential calculated experimentally for Na^+ at the ENaC δβ*γ* channel as being +64.86 mV, indicative of a slight leak current, or contribution of another ionic species.

The ENaC δβ*γ* channels displays pH sensitivity (Ji & Benos, 2004; Yamamura, et al., 2004), which is absent in the ENaC αβ*γ* channel, but present in ASIC channels. As the ENaC δ channel is constitutively active, a decrease in extracellular pH caused an increase in the amplitude of an existing inward current, whereas the ASIC1a channel is opened by extracellular protons from a closed, nonconducting state. Both channel's responses to pH have been linked to the conserved degenerin site (Ji & Benos, 2004; Li, et al., 2011).

The kinetics of the pH-induced current in these two channels also differ. The ASIC 1a channel has much faster activation/deactivation compared to the ENaC δ channel. Given that both of these channels are expressed in the CNS, and ASIC 1a has already been implemented in the neurodegeneration, this could support a role for the ENaC δ channel in the ischaemia-related signalling, which happens over longer timeframes than milliseconds. Blockade of this response by amiloride confirmed that it is mediated via an amiloride-sensitive channel e.g. ENaC. Both EC_{50} values for pH-

activation for ASIC 1a and ENaC δ are at physiologically relevant values, and deactivation in ASIC channels has been linked to residues near the degenerin site (Li, et al., 2011), which is conserved in the ENaC δ channel.

Finally, the differential pharmacology of the two ENaC channels was shown using two known ENaC channel blockers. The ENaC α channel is more sensitive to both amiloride and benzamil, at concentrations that are consistent with the published literature (Kleyman & Cragoe, 1988; Waldmann, et al., 1995; Ji, et al., 2006), and demonstrate the need to identify a novel pharmacological tool of the ENaC δ channel in order to investigate its function.

3.5. Conclusion:

The BacMam baculoviral system provides an efficient and reproducible method to transiently reconstitute ENaC channel activity, of either isoform, in a HEK293 cell line. This cell line stably expresses ENaC β and γ subunit, harbouring Liddle's Syndrome mutations, to increase functional channel activity at the cell surface on transduction of the third subunit. Transduction efficiency can be both visualised and quantified via fluorescent microscopy, and can be validated through functional studies via patch clamp. Patch clamp studies suggest all three subunit of the ENaC δ channel must be present for complete biological activity, despite observation that the ENaC δ may be expressed alone. Here I have shown that the ENaC δ channel differs to the ENaC α channel in its cation permeability, pH sensitivity, and pharmacological profile. Given its additional differential tissue expression profile to the ENaC α channel, these findings suggest a distinct physiological relevance of the ENaC δ channel.

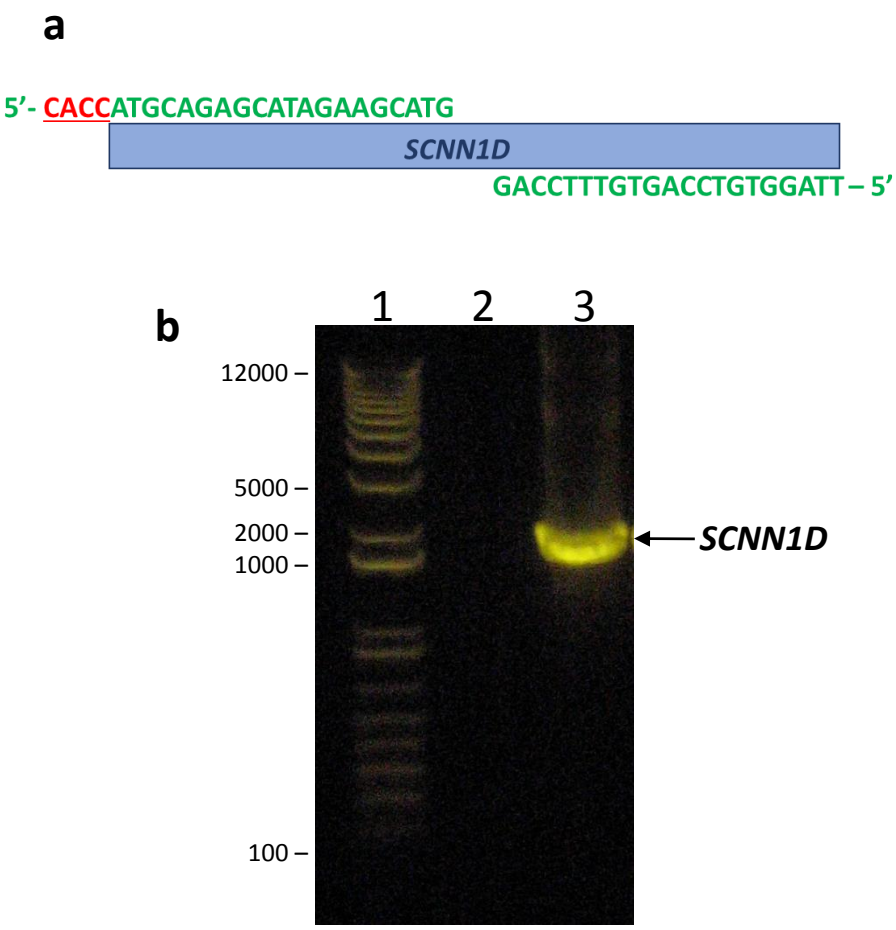

Figure 10. Blunt-ended PCR of ENaC δ gene from pUC57 vector. a Diagram to show primer designed to specifically amplify *SCNN1D,* adding the 4 bases CACC to the 5' end of the gene . This is important for sequence-specific recognition by the enzyme Topoisomerase, to ensure directional cloning into the TOPO® Entry vector. **b** PCR of *SCNN1D* with (lane 3) and without (lane 2, negative control) enzyme added to the reaction. Run with 1kB DNA plus ladder (lane 1).

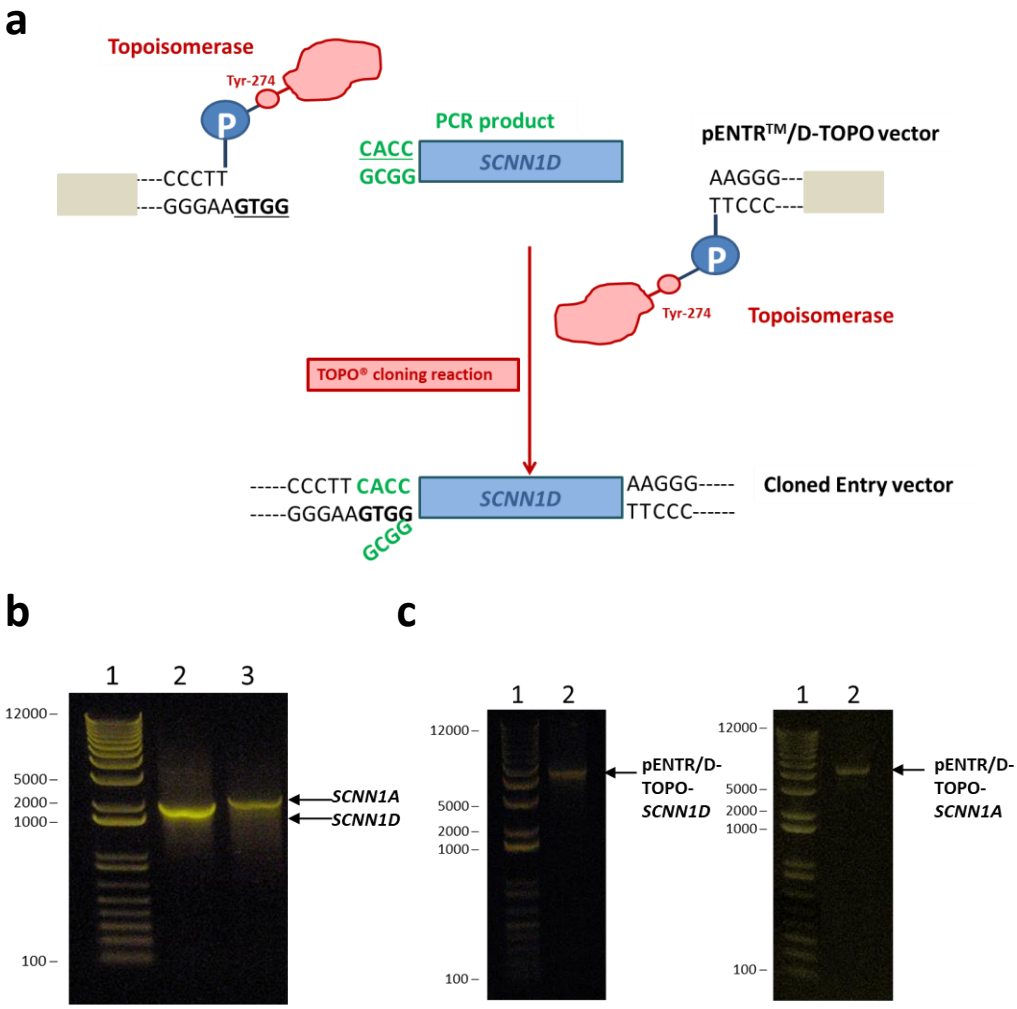

Figure 11. pENTR™ Directional TOPO® cloning. a The enzyme, Topoisomerase, recognises sequence-specific sites (CCCTT) on the linearised entry vector, and is bound via a phospho-tyrosyl bond between the DNA and enzyme. A PCR product with a 5' CACC sequence, binds to the 3' overhang (GTGG) on one end of the vector DNA. Topoisomerase is released on insertion of the PCR product between the two end of the vector. **b** Colony PCR products using M13 primers to observe size of DNA insert in recombinant entry vectors. *SCNN1D* (lane 2) and *SCNN1A* (lane 3) run with 1kB DNA plus ladder (lane 1). **c** Recombinant entry vectors linearised with NheI containing *SCNN1D* (left, lane 2) and *SCNN1A* (right, lane 2) run with 1kB DNA plus ladder (lanes 1).

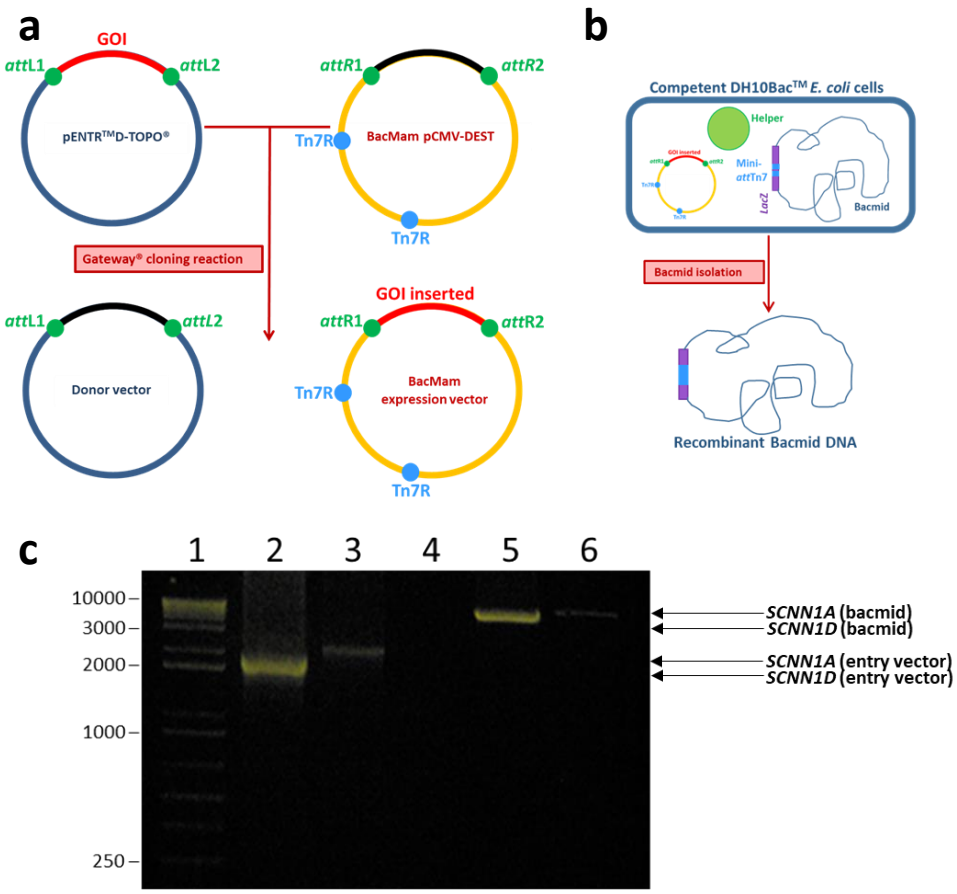

Figure 12. Transfer of Gene of Interest (GOI) pENTR™ - D/TOPO® vector to a bacmid via Gateway® cloning and transposition. **a** The Gateway® cloning method, whereby DNA between the *att*L sites on the entry clone is exchanged with DNA between the *att*R sites on the BacMam pCMV destination vector, forming an expression clone containing the GOI. **b** Site-specific transposition of the GOI occurs from the miniTn7 element of the pCMV-DEST vector to the mini-attTn7 attachment site on the bacmid, inserted within the LacZα gene. The recombinant bacmid is then isolated from the *E.Coli*. **c** Recombinant bacmids were analysed by PCR using M13 primers. Observed bands are the size of the GOI plus an additional ~500 base pairs also contained within the miniTN7 elements of the pCMV-DEST vectors. PCR analysis of gene in recombinant entry vectors (*SCNN1D,* lane 2; *SCNN1A,* lane 3) demonstrates the size of the GOI, and PCR analysis of the recombinant bacmids (*SCNN1D,* lane 5; *SCNN1A,* lane 6) confirms the GOI is the size of the GOI plus ~500 base pairs. Non-recombinant bacmid was run as a control (lane 4). All products were run with 1kB DNA ladder (lane 1).

a

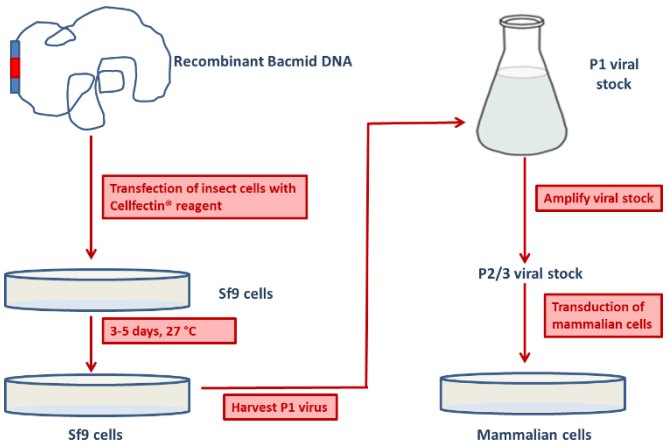

b

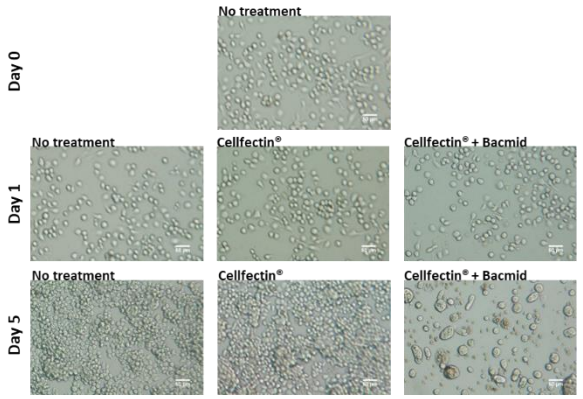

c

	Virus titre (pfu/ml)	
Dilution	**ENaC α**	**ENaC δ**
10^{-7}	15 plaques, Titre= 7.5×10^8	4 plaques, Titre= 2×10^8
10^{-6}	121 plaques, Titre= 6.1×10^8	56 plaques, Titre= 2.9×10^8
10^{-5}	Many	Many

Figure 13. Generation of viral stocks in Sf9 insect cells. a Sf9 insect cell monolayers are transfected with the Bacmid and Cellfectin® reagent. After phenotypic changes in the cells resulting in cell lysis is observed the P1 stock of virus is harvested via centrifugation. P2 and P3 stocks are amplified viral stocks generated via transfection of insect cell monolayers with P1 or P2 stocks, respectively. **b** Representative images of Sf9 insect cells through a bright field microscope (10X objective) at 3 stages during transfection with bacmid. Two control were set up simultaneously for comparison (no treatment and Cellfectin® treatment without bacmid). At each stage, transfected cells display characteristic phenotypes. **c** Calculated viral titres (plaque forming units per mL) of baculovirus encoding ENaC α and ENaC δ subunits obtained by viral plaque assay.

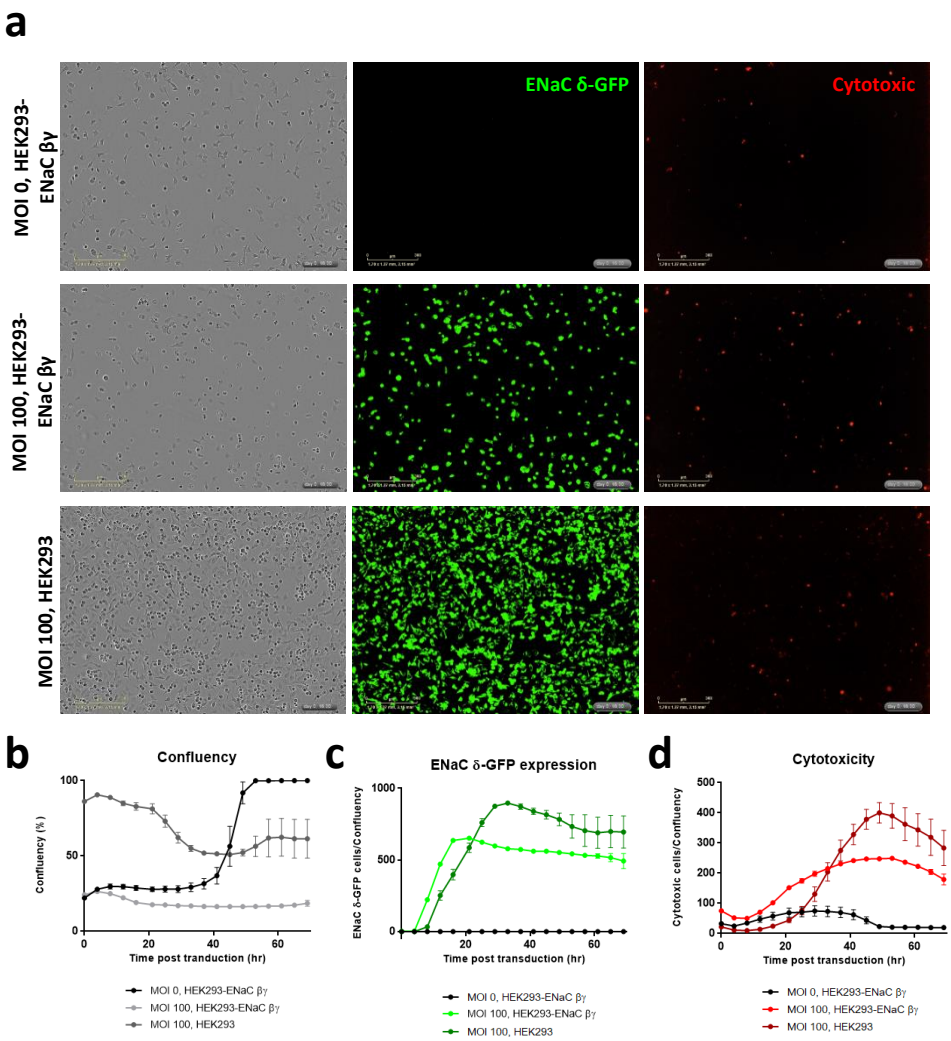

Figure 14. Time course of transduction of HEK293 and HEK293-ENaCβ*γ* cells with BacMam baculovirus encoding the GFP-tagged ENaC δ subunit. a Images taken by the IncuCyte® S3 Live Cell Analysis System 16 hr post transduction with a baculovirus containing a GFP-tagged ENaC δ gene. HEK293-ENaCβ*γ* cell were transduced at MOI 0 (no virus; top) and at MOI 100 (middle), and HEK293 cell not expressing any ENaC subunit were transduced at MOI 100 (bottom). In parallel to viral transduction, cells were loaded with IncuCyte® Cytotox Red reagent to detect cell death. **b-d** Time-course of cell confluency, ENaC δ-GFP expression , and extent of cytotoxicity in untransduced HEK293-ENaCβ*γ* cells (MOI 0) and HEK293-ENaCβ*γ* and HEK293 cells transduced with the baculovirus (MOI 100), in the presence of 50 µM amiloride and 0.5 µM TSA. Data were quantified using the IncuCyte® ZOOM 2016B analysis software.

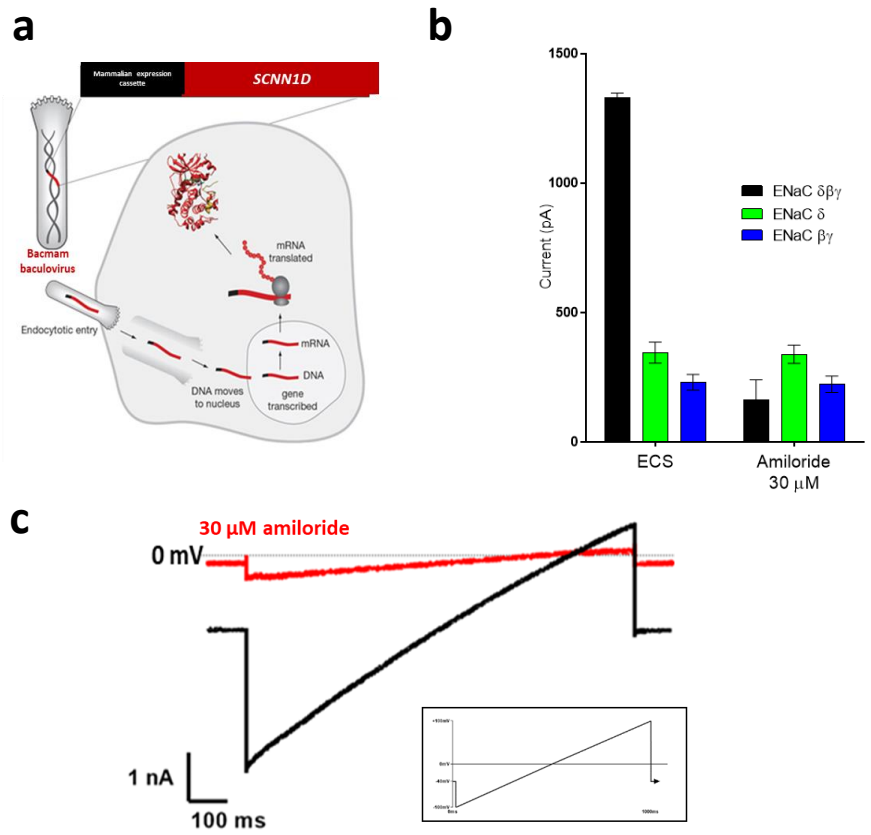

Figure 15. Transduction of HEK293-ENaCβ*γ* cells with BacMam baculovirus encoding the ENaC δ subunit. **a** BacMam-mediated gene delivery of the SCNN1D gene into a mammalian cell, HEK293-ENaC β*γ*. BacMam particles are taken up by endocytosis and released for transcription and expression following migration to the nucleus. Adapted from www.thermofisher.com (Accessed Jan 2016). **b** Current amplitudes measured in cells expressing all three ENaC subunits (δ, β and γ), just the ENaC δ subunit, or just ENaC β and γ subunits, before and after the addition of 30 μM amiloride. Data are expressed as mean ± SEM. **c** Whole-cell amiloride-sensitive currents measured in HEK293-ENaCβ*γ* cells 24 hr after transduction with the baculovirus containing the ENaC δ gene. Cells were held at -40 mV and then ramped between -100 mV to +100 mV over 1 s. Currents were recorded both in the presence (red) and absence (black) of 30 μM amiloride.

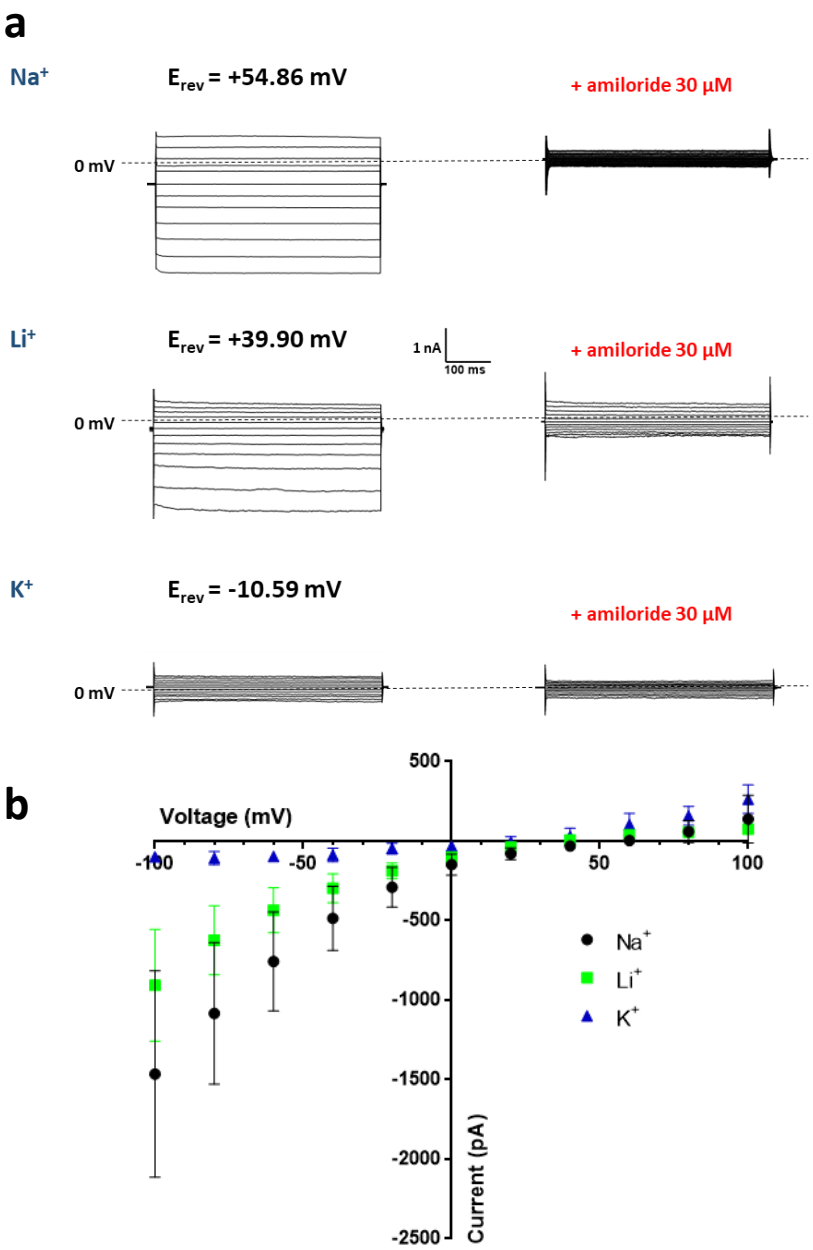

Figure 16. Cation permeability of the ENaC δ channel expressed in HEK293 cells. a Whole-cell current traces of the ENaC δ channel in extracellular solution containing 145 mM of the primary cation, Na^+, Li^+ or K^+. Currents were elicited by 500 ms voltage steps between 100 mV and +100 mV in 20 mV increments from a holding potential of 0 mV. Currents were measured in the absence and presence of 30 µM amiloride. **b** Current-voltage relationship of amiloride-sensitive Na^+, Li^+ or K^+ currents. Currents measured in the presence of 30 µM amiloride were subtracted from those measured in the absence of amiloride.

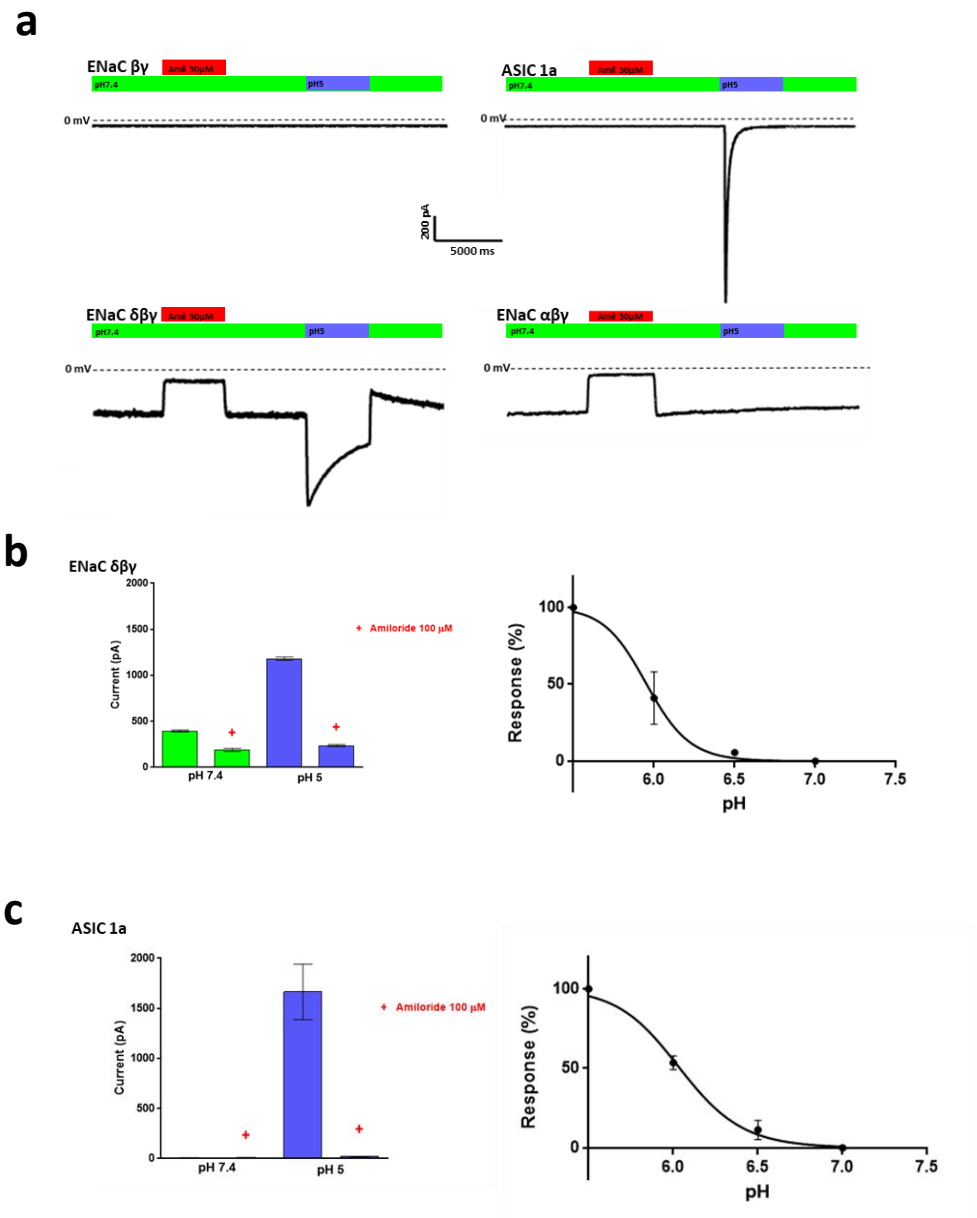

Figure 17. Proton-sensing capacity of the ENaC and ASIC 1a channels. a Whole cell current traces of cells over-expressing either ENaC β and γ subunits, the ASIC 1a channel, the ENaC αβγ channel or the ENaC δβγ channel, held at a patch potential of –40 mV and exposed to 30 μM amiloride or pH 5 extracellular solution for 5 s. **b** Normalised pH-induced currents of the ENaC δβγ channel (right; pH EC_{50} = 5.96 ± 0.05 μM (n=6)), which can be blocked in the presence of 30 μM amiloride (left). **c** Normalised pH-induced currents of the ASIC 1a channel (right; pH EC_{50} = 6.04 ± 0.03 μM (n=8)), which can be blocked in the presence of 30 μM amiloride (left).

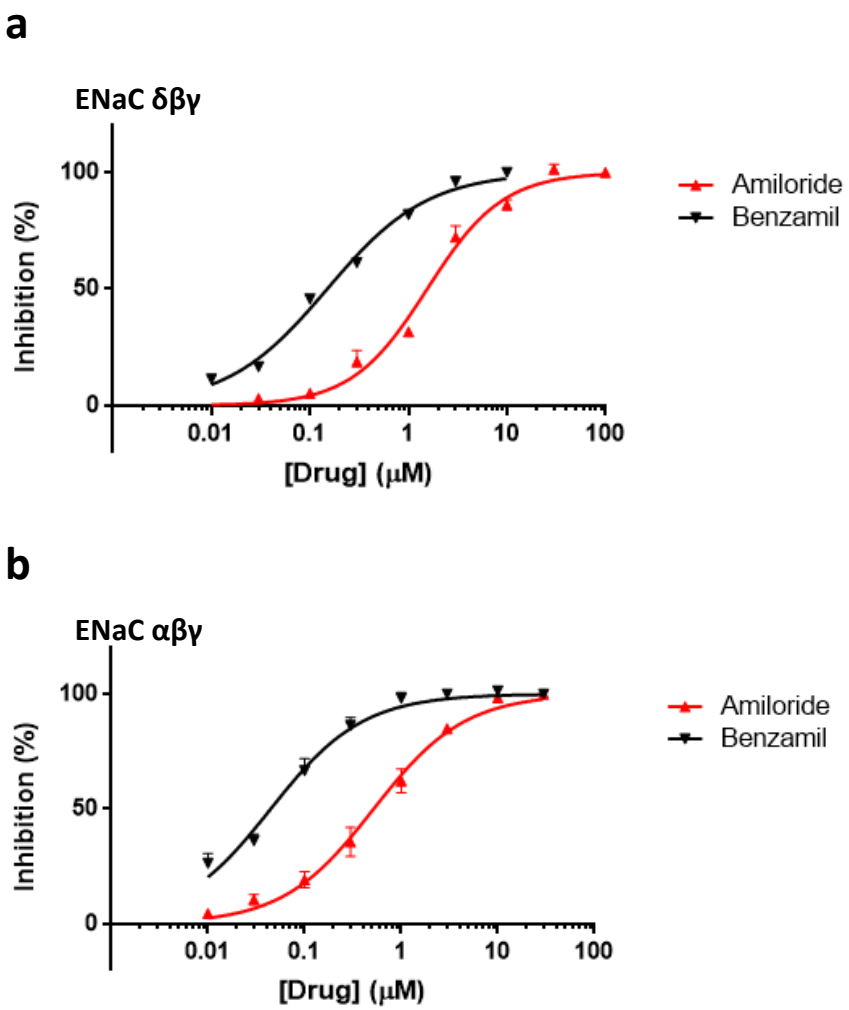

Figure 18. Differential pharmacology of known ENaC blockers at both ENaC channel isoforms. a Dose-response curves of Amiloride (IC_{50}= 1.55 ± 0.12 μM (n=3)) and Benzamil (IC_{50}= 0.15 ± 0.01 μM (n=5)) at the ENaC δβγ channel. **b** Dose-response curves of Amiloride (IC_{50}= 0.52 ± 0.05 μM (n=5)) and Benzamil (IC_{50}= 0.04 ± 0.003 μM (n=11)) at the ENaC αβγ channel.

4

RESULTS: MEMBRANE POTENTIAL ASSAY DEVELOPMENT

Chapter 4

4.1. Background:

Ion channels represent a class of attractive drug targets (Gonzalez, et al., 1991; Lachnit, et al., 2001) but the gold standard for ion channel studies, patch clamp electrophysiology, is labour-intensive, low throughput and requires highly skilled experimenters. In recent year, there has been progress in the development of instrumentation, and therefore functional assays, which enable higher-throughput studies on an increasing number of channel types. This has benefitted both industrial and academic endeavours in the ion channel field, and includes techniques that are both non-electrophysiological and electrophysiological, each with their own advantages and limitations. Initially, due to the high throughput capability, low cost per data point, and relative ease to develop, a non-electrophysiological fluorescence-based primary screening assay was pursued.

4.1.1. Non-electrophysiological fluorescence-based assays:

Fluorescence-based assays provide a measurement of ion channel function and modulation by employing either voltage-sensitive dyes or ion-specific probes to detect real-time changes in ionic flux across a membrane.

Fluorescent voltage-sensitive dyes detect voltage changes across the cell plasma membrane using either the potential-dependent accumulation and redistribution (Waggoner, 1976) or the fluorescence resonance energy transfer (FRET) mechanism. The lipophilic and anionic FMP (Fluorometric imaging plate reader (FLIPR) membrane potential) dyes exploited by the FLIPR Membrane Potential Assay kit (Molecular Devices, USA) are an example of the former. These dye molecules are redistributed across the plasma membrane upon changes in membrane potential. They have low

fluorescence in aqueous environments but display an increased quantum yield upon binding to hydrophobic intracellular molecules. This specific assay kit uses an extracellular quenching molecule, which binds to the fluorescent molecule on the aqueous, extracellular side of the cell to further reduce background fluorescence and improve the signal-to-noise ratio. Upon membrane depolarisation, the fluorescent signal increases in intensity as the negatively charged dye follows the positively charged ions into the cell. During membrane hyperpolarisation, there is a redistribution of charges across the membrane, causing the interior of the cell to become negatively charged. The negatively charged dye therefore moves out of the cell and the fluorescent signal decreases.

Whereas traditional oxonol dyes, such as bis-(1,3-dibutylbarbituric acid) trimethine oxonol (DiBAC4) (Gonzalez, et al., 1991), are only able to detect changes in membrane potential in the order of minutes, these FMP dyes are able to detect changes within the tens of seconds range which permits the measurement of kinetic signal changes, albeit relatively slow. These measurements can be carried out in 384 well microplate improving both throughput and cost per data point (Cronk, 2001).

Unfortunately, in high-throughput screening (HTS), compound fluorescence and compound–dye interactions are major sources of artefacts that result in high false-positive rates. Furthermore, the lipophilic nature of the dye prevents a response that is selective to the plasma membrane. The dye may respond to a change in membrane potential at both the plasma membrane, and at intracellular membranes. FRET-based assays may be used to eliminate this non-selective response. They use negatively charged, membrane-soluble oxonol dyes as FRET acceptors, and coumarin-tagged

phospholipids as FRET donors. These donors are integrated into the outer leaflet of the membrane when loaded into the cells. In this instance, the phospholipid-anchored FRET donor restricts the location of FRET in the plasma membrane. The result is a fast, ratiometric response, specific to a voltage change across the plasma membrane rather than in other subcellular compartments such as the mitochondria.

In addition to voltage-sensitive dyes are ion-specific fluorescent probes. These have been developed to measure intracellular ionic concentrations, for example calcium (Fura-2, Fluo-3, Fluo-4 (Minta, et al., 1989)), potassium (FluxOR (Beacham, et al., 2010) and PBFI (Meuwis, et al., 1995)) or sodium (SBFI (Minta & Tsien, 1989)), to achieve high-throughput and low-noise detection of absolute levels of a specific ion. A major limitation to these assays, however, is the availability of robust ion-specific indicators. Even so, calcium indicators are one example that is used extensively and successfully. Indicator dyes of various affinities for calcium and excitation and emission spectra, can be employed dependent on the application. For example, the kinetics and size of the expected calcium currents would be factors in deciding which indicator to use. Na^+-specific indicators have been less effectively pursued, with few Na^+ indicator dyes, such as SBFI, CoroNa, and ANG-2, commercially available. One factor has been the relatively small changes in Na^+ concentrations that occur across the cell, when compared with the large Ca^{2+} fluxes which occur during cellular signalling. When considering the constitutively active ENaC channel, small Na^+ flux would make it difficult to decipher a signal above background levels and would therefore be unsuitable in an HTS setting.

4.1.2. Comparison of fluorescence-based assay plate readers:

The FlexStation® 3 Multi-Mode Microplate Reader (Molecular Devices, Sunnyvale, California, USA) and the FDSS/µCELL Functional Drug Screening System (Hamamatsu Photonics, Shizouka, Japan) are both suitable platforms to detect whole-cell fluorescence during a membrane potential assay. Each has a number of advantages and limitations over the other, which should be considered when designing the assay parameters. The development of the primary screening assay for investigation of inhibitors of the ENaC δ channel was compared across both of these platforms.

Firstly, both instruments are comprised of two modules - a fluidics module and a detection module. The detection module of the FlexStation® comprises a Xenon flashlamp and monochromators for both excitation and emission light, and a photomultiplier tube (PMT) detector to monitor changes in whole-cell fluorescence. The FDSS/µCELL, however, has an LED excitation source that can output just two wavelengths (Blue, 480 nm; Green, 530 nm), and detects whole-cell fluorescence with a charge-coupled device (CCD) camera.

In terms of the excitation source, monochromators allow the use of a wide range of fluorescent indicators, whereas the LED excitation source is limited to the wavelength it can use. Nevertheless, for applications using the Molecular Devices' FMP dyes either platforms are suitable (excitation/emission λ 531/565 nm). With respect to the PMT and CCD detection technologies, both give spectra but there are some important differences. The PMT converts photons to an electrical signal and uses a small slit in the front of it to limit the bandwidth of the light being detected. This increases the resolution of the instrument, and with a high internal gain they are sensitive detectors

for low intensity applications. This makes them the detector of choice in spectroscopic applications. However, as only a single point in the spectrum can be measured at a time, it requires the scanning of the monochromator to collect all the spectra. This greatly increases the time it would take to measure the fluorescence in all wells of a microtitre plate, for example. The CCD camera captures the complete spectrum at the same time, allowing a snap shot of every well of the entire plate at once. This greatly reduces the run time of each plate, but compromises its sensitivity and dynamic range.

The fluidics module on both instruments incorporates a fluid transfer system for addition of test compounds from a source plate to the cell plate during data acquisition. Plates are contained within a temperature-controlled unit that can be controlled accurately between room temperature and 45°C. Both instruments can be configured to read a range of plate sizes.

The fluidics module of the FlexStation® contains an 8-channel pipette that delivers solutions from the source plate to the 96-well cell plate. This is done in columns of wells across a microtitre plate to correspond with the scanning of the monochromator between wells. Although the fluids module may be changed to a 384 pipetting system with 16-channels, the time taken to read one plate is significantly increased due to the requirement for scanning across the spectra. On the other hand, the dispensing head of the FDSS/µCELL contains either 96 or 384 individual channels. This means the addition of compound to every well at once can be synchronised with the monitoring of whole-cell fluorescence across the entire plate. The high-speed CCD camera keeps the overall time to read each plate to an absolute minimum.

Finally, the FDSS/µCELL allows for two source plates to be loaded into the system for multiple additions into each well of the cell plate. An example of when this would be advantageous is the study of inhibitors/agonists of ligand-gated channels, whereby the test compound and ligand must both be applied to the same cells. This platform includes a wash station so the same tips can be reused both within and across the experiments.

4.2. Methods:

4.2.1. Analysis of protein expression and cytotoxicity:

Levels of protein expression and cytotoxicity were monitored using the IncuCyte® Live Cell Analysis System (Section 2.2.5.). HEK293 ENaC β*γ* cells were harvested and plated in poly-D-lysine- coated 24-well, clear, tissue culture plates, and once adherent (24 hr) to the plate, were treated with combinations of virus MOI, amiloride and TSA concentrations. The BacMam baculovirus used contained a GFP-tagged ENaC δ subunit (Section 2.1.1.3.) to enable detection of protein levels, and cells were simultaneously loaded with IncuCyte® Cytotox Red reagent to detect cell death (Section 2.2.5.1.). Cell viability was also analysed using the trypan blue method (Section 2.2.4.).

Whole-cell fluorescence (GFP: excitation/emission λ 480/540 nm; IncuCyte® Cytotox Red: excitation/emission λ 612/631 nm) was monitored immediately following treatment every 4 hr, over a 100 hr period. Data were analysed and images obtained using the IncuCyte® ZOOM 2016B Software (Section 2.2.5.2.). Graphs were drawn using GraphPad Prism version 7.0 for Windows®.

4.2.2. Membrane potential assay:

HEK293 ENaC β*γ* cells were harvested and plated in 96-well, black, clear-bottomed assay plates (Section 2.2.7.2.). Once attached (4-6 hr) cell were transduced overnight with the BacMam baculovirus (Section 2.2.3.2.). Prior to assay, a 96-well source plate containing test compounds, amiloride or benzamil during assay development, were prepared from their stock solutions in Tyrode's Buffer at 4-times higher than the final test concentration (Section 2.2.7.1.). In experiments using the double-addition protocol the second 96-well source plate contained uniform amiloride at 5-times higher than the final test concentration (Section 2.2.7.1.). The DMSO concentration across the plate was consistent and ≤ 0.5 %, unless otherwise specified.

On assay, cells were loaded with FLIPR Membrane Potential Blue dye (Section 2.2.7.2.) and whole-cell fluorescence (excitation/emission λ 531/565 nm) was monitored before and during the addition of compounds from the source plates (Section 2.2.7.3.). The majority of the assay development was performed on the FlexStation®. Data were exported from SoftMax Pro® Software v4.8 and graphs were plotted using GraphPad Prism v7.0 (Section 2.2.7.4.). After transfer of the assay onto the FDSS/µCELL Functional Drug Screening System, screening data were exported from FDSS7000EX/µCELL software, uploaded onto the Dotmatics database and analysed using Vortex v2015.11.46033 (Section 2.2.7.4.).

4.3. Results:

4.3.1. BacMam baculovirus transduction optimisation:

The aim of the BacMam baculovirus transduction is to reconstitute an optimal level of functional ENaC expression in the HEK293 cells with regards to functional activity, pharmacological sensitivity, and cell health. Signal size and window, amiloride pharmacology, and cell viability, were accessed for a number of transduction and assay conditions. Although BacMam technology is seen to have minimal cytopathic effects on a cell, overexpression of the constitutively active ENaC channel causes toxicity by Na^+ loading (Chen, 2015). Therefore simultaneously monitoring functional activity and cell health was important to optimise assay performance.

4.3.1.1. Amiloride rescue from cell cytotoxicity:

Transient, rather than stable, expression by viral transduction limits the cytotoxic effect of constitutive ENaC activity. To further counteract this, it was proposed that transduction of the third ENaC subunit in the presence of a channel blocker could be protective to these cells. The prototypical blocker, amiloride, was therefore assessed for its ability to enhance cell viability following transduction.

Initially, cell viability studies were performed for a range of amiloride concentrations (0 – 100 µM) in the absence of virus to ensure the channel blocker itself did not cause toxicity (Figure 19., red). It was observed that cell death increased considerably with treatment of over 50 µM amiloride for the 16 hr period. Subsequently, to be confident of complete channel block, 50 µM amiloride was used for all transductions to 'rescue' the cells as this was the highest concentration tested which did not cause any notable toxicity itself.

To monitor ENaC expression and cytotoxicity in parallel, cells were incubated with a baculovirus encoding a GFP-tagged ENaC δ subunit and IncuCyte® Cytotox Red reagent

over the course of 68 hr (Figure 20.). Fluorescence signal was then monitored in the IncuCyte® Live Cell Analysis System. In cells transduced with the baculovirus (MOI 2.5) in the absence of amiloride, GFP was detected within 4 hr of transduction, peaking at between 48 hr and 52 hr post transduction (Figure 20.a and c). Levels of cytotoxic cells began increasing from 8 hr post transduction, which is approximately 4 hr post the first observed ENaC δ-GFP expression (Figure 20.a and d). No GFP expression or cytotoxicity was detected in untransduced cells. GFP expression was higher in cells transduced in the presence of 50 µM amiloride and 0.25 µM trichostatin A (TSA). Under these conditions there was a simultaneous reduction in cytotoxicity, with no considerable increase in cytotoxicity within the first 24 hr post transduction. This 24 hr window represents the timeframe that the cells would be used for assay. Over the 68 hr, transduced cells did not grow, however untreated cells grew exponentially (Figure 20.a and b).

4.3.1.2. MOI of virus:

In an attempt to address the underestimation in amiloride's ENaC-blocking activity, the nonlinearity of channel block with change in membrane potential was explored. Virus MOI refers to the number of plaque forming units (pfu) of virus used for infection per cell. Increasing the virus MOI affected a number of parameters including the sensitivity of the membrane potential assay to amiloride (Figure 21.a), the signal size and window (Figure 21.b), and the levels of GFP expression (Figure 21.c) and cell cytotoxicity (Figure 19 and 21.d).

As the quenching of fluorescence is a nonlinear readout of ion channel activity, the levels of functional ENaC activity expressed at the cell surface affects assay sensitivity.

This was reflected in functional studies, whereby amiloride potency decreased at an MOI above 2.5. Titrating the MOI lower in order to improve sensitivity still reported amiloride to be less potent (MOI 1: IC_{50} = 19.4 ± 2.3 µM (n=6)) than literature values (Yamamura, et al., 2006), and also decreased the signal size and window.

Increasing MOI also decreased the signal size and window despite an increase in ENaC δ-GFP expression and a shorter time period between transduction and peak GFP expression. This may be due to the correlation of virus MOI and cytotoxicity. Higher numbers of cytotoxic cells was associated of higher virus MOI. As the MOI was lowered, GFP expression decreased and the time to reach peak expression increased. Even at low MOIs, there was significant cell death compared to untreated cells. However, both IncuCyte® Cytotox assay and the trypan blue cell viability assay (Figure 19.) demonstrated that amiloride's presence during transduction can rescue the cells across a range of MOIs. This confirmed that cell toxicity was caused by an amiloride-sensitive current.

4.3.1.3. Effect of Trichostatin A (TSA) on protein expression:

In addition to titrating the MOI, changes in expression levels were examined in cells transduced in combination with TSA or pluronic acid. TSA is a histone deacetylase (HDAC) inhibitor and pluronic is a surfactant. Both are commonly used in a laboratory setting to facilitate the uptake or incorporation of a gene into the host's genome.

Although pluronic acid did increase the signal size very slightly, the signal window was unaffected (Figure 22.a) and therefore not pursued further. Conversely, signal size and window was increased in the presence of up to 0.25 µM TSA compared to no TSA (Figure 22.b). This was supported by experiments on the IncuCyte® using 0.25 µM TSA

which increased peak expression of the GFP-tagged ENaC δ subunit by approximately 8-fold (Figure 22.c).

These two measures of assay quality parameters, signal size and window, did however decline at concentrations over 0.25 µM TSA. Cell cytotoxicity studies revealed that there was no real difference in toxicity up to 1 µM TSA compared to cell treated with virus in the absence of TSA (Figure 22.d). As such in all subsequent experiments TSA was used at 0.25 µM.

4.3.1.4. Cell seeding density:

Different seeding cell densities were examined for an effect on the transduction efficiency of the baculovirus. For experiment using the IncuCyte®, cells were plated at different densities (5 – 9 x 10^6 cells/well) in a 24-well cell plate, 24 hr before treatment. Images were taken immediately prior to transduction to observe confluency (Figure 23.a). At this time point wells ranged between ~40 % and 95 % confluent. All wells showed an apparent decrease in confluency over time, beginning between 10-20 hr post transduction, which correlates with the increase in cytotoxicity at a similar time point (Figure 23.b, right). Regardless of confluency, all cells were transduced with the virus at MOI 2.5, in the presence of 50 µM amiloride and 0.25 µM TSA. ENaC δ-GFP expression was greatest in those wells seeded at 5 x 10^6 cells/well, and least confluent on transduction (Figure 23.b, left). Within the ideal timeframe of assay (14-24 hr post transduction), this seeding density results in both the highest level of ENaC expression and cytotoxicity.

To assess the functional consequence of this, cells were seeded at densities between 4 and 8 x 10^4 cells/well in a 96-well cell plate, 6 hr before transduction. These cell

seeding densities tried to replicate the same confluency levels observed on the IncuCyte®. The surface area of the 96-well plates was approximately 6 times smaller, and therefore the highest seeding density of 8 x 10^4 cells/well is equivalent to the wells seeded at 5 x 10^5 cells/well in the 24-well cell plates. Cell densities of this and below were investigated. With consideration of the parameters of signal size and assay window (Figure 23.c), and pharmacology (Figure 23.d), cells were seeded at a density of 7 x 10^4 cells/ well for all experiments.

4.3.1.5. Time window for screening:

For convenience, using the cell plates the day post transduction during screening was preferable. Outlining the time window at which ENaC expression is optimal post transduction, and at what time the cells are no longer usable, was therefore important. It was seen that assay performance, with respect to signal size, assay window and pharmacology, declined between 16 and 24 hr (Figure 24.). The assay window had always been low, but by 24 hr post transduction was below 2-fold. This may be reflective of the increase in cell death between 20 and 24 hr (Figure 20.d). This confirmed that cells must be used before 20 hr post transduction.

4.3.1.6. Transfer from the FlexStation® to the FDSS/µCELL platform:

During development of the primary screening assay, the choice was made to transfer it from the FlexStation® 3 Multi-Mode Microplate Reader (Molecular Devices) to the FDSS/µCELL Functional Drug Screening System (Hamamatsu Photonics), which was kindly loaned on a short-term basis to the Sussex Drug Discovery Centre, Sussex University. This transfer was informed by the ability of the FDSS/µCELL to save money

on reagents, and save time for each run and therefore reduce the overall time to complete the entire screen.

4.3.1.6.1. Membrane potential dye formula and concentration:

Molecular Devices provides dye in two formulations which give either a blue or a red fluorescence. Information on specific differences between the two formulas, however, is undisclosed. Each utilises a proprietary indicator dye and quencher combination that is designed to be temperature stable and quick to respond to any change in membrane potential. Due to variability between ion channels' activity and sensitivity to pharmacological agents, the manufacturer recommends that the dye colour and concentration must be optimised for every new cell line used.

In initial experiments on the FlexStation®, both dyes showed some level of dose-dependent response to amiloride (Figure 25.a), but studies using the blue dye gave a greater signal window compared to the red dye (Figure 25.b). The sensitivity of the assay to amiloride whilst using the red dye was much lower (ENaCδβ*γ*: red dye, IC_{50} > 100 µM (n=3); blue dye, IC_{50}= 36.91 ± 3.41 µM (n=3)). For these reasons, blue dye was used hereinafter.

The FLIPR Membrane Potential dye is the major expense of this assay. As such, the dye was tested at more dilute concentrations. On the FlexStation® it was observed that any dilution of the dye resulted in a substantial reduction the assay window (Figure 25.c, left), and was therefore required to be used neat for optimal assay performance. This meant that the cost per plate amounted to the cost of one bottle of dye, which was approximately £100. Once the assay was transferred onto the FDSS/µCELL, this experiment was repeated. The assay window using neat dye was much larger than

that on the FlexStation® (Figure 25.c, right). In addition, when diluted by 3 times in assay buffer, the assay performance parameters remained above acceptable levels, and were better than they had been using neat dye on the FlexStation®. There was no adverse effect on pharmacology (Figure 25.d). This enabled one bottle of dye to serve 3 assay plates, significantly reducing the cost of this reagent for screening.

4.3.1.6.2. Compound incubation time and double-addition protocol:

In order to capture the activity of a compound, whilst minimising the run time per plate, the effect of three read times were tested (1.5 min, 5 min, 10 min).

The calculated amiloride potency for the three different read times reported a lower potency at the shortest read time (1.5 min), but no difference seen between a 5 and 10 minute read (Figure 26.a). Longer reads were able to capture the complete effect of amiloride block, evidenced by the fluorescence decreasing and reaching a plateau. The size of the assay window was also increased in the longer read times (Figure 26.b). A 5 min read was used in the final assay.

Although the FlexStation® allows for multiple additions per well, the system is only capable of adding compound to and read fluorescence from two columns at a time. This meant that in 96-well format with a 5 minute read time each run took over half an hour. The FDSS/µCELL platform allows for the synchronised addition of compound by an integrated dispensing head, and monitoring of whole-cell fluorescence from every well in the plate at the same time. This kept the run time per plate to a minimum (5 minutes).

Furthermore, plate uniformity on the FDSS/ µCELL was assessed prior to reading each plate via a background fluorescence read. An 'edge effect' was observed across all plates, which consistently gave lower and variable data for the outer wells of the plate. Due to the plate layout, these outer wells included the top concentrations of compounds tested and therefore impacted on the consistency of IC_{50} curves generated.

A double-addition protocol was introduced, which implemented an in-well control in the form of a second addition of a high concentration of amiloride (150 µM). Figure 26.c shows a typical trace for the two additions. For each well, the minimum fluorescence after compound addition was subtracted from the baseline fluorescence, and then normalised to the response of each well to maximum block by amiloride. In this way the well-to-well variability was accounted for. A series of plates containing columns of vehicle (Buffer (0.5 % DMSO)) and maximum (150 µM Amiloride (0.5 % DMSO)) control were used to assess Z' values across three separate days comparing the single- and double-addition assay setup. The double-addition improved Z' values (Figure 26.d) to consistently > 0.5, which is considered the threshold measure of good assay performance.

4.3.1.7. DMSO tolerance and pharmacological validation:

DMSO tolerance was initially performed on the FlexStation®, before transfer of the assay onto the FDSS/µCELL. Pharmacological validation was performed after assay transfer as the final step prior to screening.

DMSO tolerance experiments are important as compound libraries are typically dissolved in DMSO. These studies therefore indicate the highest concentration at

which the compounds can be tested, so as to ensure that DMSO itself is not influencing data. Whereas whole cell assays normally tolerate no more than 1% DMSO, biochemical assays can withstand higher DMSO concentrations. This assay was seen to be sensitive to DMSO. The background fluorescence, on complete blockade of ENaC by amiloride, was increased in the presence of 0.5 % DMSO, meaning a slight decrease in the size of the assay window compared with no DMSO (Figure 27.a). Both signal size and the assay window were dramatically reduced at a DMSO concentration of 1 %. This indicated that using concentrations closer to 0 % was more desirable.

Three known ENaC blockers, amiloride, benzamil, and 5-(N-Ethyl-N-isopropyl) amiloride (EIPA), were tested in the assay against the ENaC δβγ channel (Figure 27.b) as a final step before screening. This was to ensure the assay could make pharmacological distinctions between compounds of known differential potencies. Benzamil and EIPA were tested from a stock of 100 mM in 100% (v/v) DMSO, to a maximum concentration of 150 µM (0.15% DMSO). Amiloride was tested from a stock of 10 mM dissolved in dH_20. DMSO was added in to ensure uniformity in its concentration across each compound tested. The order of potency at this ENaC channel was benzamil>amiloride>>>EIPA. However the difference in potency between benzamil and amiloride was much lower than reported in the literature (Kleyman & Cragoe, 1988), and EIPA was shown to have no activity in this assay (amiloride, IC_{50} = 29.4 ± 3.7 µM (n=3); benzamil, IC_{50}= 21.8 ± 3.3 µM (n=3); EIPA, IC_{50} > 150 µM (n=3)).

4.4. Discussion:

A robust and reproducible primary screening assay was made possible, firstly, by use of a HEK293 cell line expressing mutant ENaC β and γ subunits (βP618AY620L,

γP624Stop). These mutations in the β and γ subunits, which mimic those found in Liddle's syndrome, prevent fast internalisation and degradation of the channel, in addition to increasing the open probability (P_o) of the channel (Knight, et al., 2006). Chen et al. (2015) had previously demonstrated that use of a cell line stably expressing these mutant subunits, as opposed to wild type, increased their cell surface expression, without affecting the potency of compounds at the ENaC channel. These mutations alter a peripheral region of the channel involved in channel trafficking, which is not in close proximity to the channel pore (Stockand, et al., 2008).

Secondly, using BacMam technology to reconstitute functional ENaC channel circumvents long-term functional overexpression, which has been associated with cell toxicity due to excessive Na^+ influx (Chen, et al., 2015). It also allowed for a choice between the ENaC channel subtypes to express (α or δ), which would become important for subsequent selectivity studies. However, transient expression of recombinant protein is often met with low reproducibility, heterogeneity and high variability (Hopkins, et al., 2012). Therefore optimisation of the viral transduction, with respect to the fluorescence-based membrane potential assay, was a compromise between functional expression and cell toxicity.

Key considerations to maximise functional expression included the MOI of the virus, the use of TSA during transduction, the cell seeding density and the incubation time for cells and virus before assay. The most important factors in minimising cell toxicity were the use of amiloride during transduction, and the use of the cells before a certain time point post transduction.

An interesting observation was the effect of viral load on the pharmacological profile of the cells. The reported potency of compounds were found to decrease as viral load (i.e. MOI) was increased. Increased MOI was also reflected by an increase in the levels of functional ENaC at the cell surface, and an increase in cytotoxicity. The potency value of amiloride was about 1 log unit lower than obtained with conventional patch clamp (Chapter 3). This level of potency shift is often true for membrane potential FLIPR assays (Chen, et al., 2015). As membrane potential represents an indirect means of assessing channel activity, in many cases, inhibition of a significant number of channels is required to obtain a membrane potential readout. The assay can therefore be affected by channel expression number and IC_{50} values determined can be significantly shifted to lower potency from those determined by direct measurements of channel activity. A cell system with high expression levels of ENaC is less sensitive to amiloride when determined by membrane potential. A compromise must be made between the size of the signal and assay window, and the sensitivity of the assay. Although electrophysiology studies report amiloride, benzamil and EIPA to be more potent than the data obtained with this assay, literature values obtained using the membrane potential assay are consistent with our findings (Chen, et al., 2015).

Pluronic acid has applications in gene delivery through the incorporation of DNA into the core of the micelles formed by the surfactant. This increases solubility of the DNA and has been shown to improve transduction efficiency with lentiviral vectors (Strappe, 2005). Despite a small increase in the maximum assay signal, the background fluorescence was also increased and therefore there was no improvement in the size of the assay window. This could be due to increased membrane solubility

allowing dye molecules to cross the membrane too freely, where they would then fluoresce.

TSA, however, was a beneficial addition to transduction media. TSA has the ability to stop the deacetylation of α-acetyl lysine that resides within the NH_2-terminal tail of core histones in the host's DNA. In a physiological setting, this regulates the balance between silent and transcriptionally active chromatin as normally HDACs remove the acetyl group to inhibit gene expression by causing chromatin compaction. By relieving this inhibition and facilitating the incorporation of the gene into the host's genome during baculoviral transduction, it was shown that with 0.25 µM TSA a lower MOI could still be capable of achieving high levels of ENaC expression. Caution must be taken, however, as high levels of TSA, demonstrated here at 5 µM, have been seen to been toxic to cells, with applications in inducing apoptosis in cancer cells (Olaharski, et al., 2006).

Cell seeding density experiments showed that cell confluency at the time of transduction had an effect on gene expression, cytotoxicity and therefore assay performance. It is well documented that cell culture conditions and cell health can be a big cause of variability in cell-based screening assays (Zhanga, et al., 2012). For example, cells must be passaged regularly so as to establish their normal growth rate and not be allowed to become over confluent, and they must be > 90 % viable. Therefore, it is unsurprising that the confluency of the cells upon transduction would affect its efficiency and performance of the cells in the assay. Although it is recommended that cells are between 70-90 % confluent on transduction, cell seeding densities which put the cells between 40-90 % confluent were investigated. There was

very little difference in absolute gene expression and cytotoxicity shown by the IncuCyte® data. However, as a proportion of the total number of cells, the wells seeded at the lowest density had the highest ENaC δ-expressing and cytotoxic populations. This is important when considering the functional readout on the assay. The equivalent cell density i.e. the lowest in the 96-well assay plate did not perform as well, with respect to signal size, assay window, and pharmacological sensitivity to amiloride, compared to cells seeded at a slightly higher density.

All of these factors discussed so far, which affect the level of gene expression and cell health, contribute to slight differences in assay performance over time. As the assay would ideally be performed the day after transduction between a window of 8 hrs, or one working day, it was important to determine if the data would change over this time period. There was a very slight deterioration in signal size and assay window 24 hr post transduction when compared to 16 hr. On the other hand the assay appeared to increase in sensitivity by 24 hr, and therefore suggested that it was necessary to transduce the cells earlier the day before to allow for a longer incubation time for the cells with the baculovirus.

Once the basic parameters of the transduction were established, the focus then fell on the setup of the assay for screening, such as dye formulation, the addition protocol and DMSO tolerance. A number of potential problems had been identified on the FlexStation®. The first of which was the assay window and cost of the dye reagent. It was clear on comparison of the red and blue dye formulations from Molecular Devices that the blue dye would be used going forward, however the cost of each bottle was over £100 and was sufficient for just one plate. Commonly, the experimenter would

dilute the dye to reduce the cost per plate. However, with such a small assay window using the dye neat (~2-fold), a dilution of the dye only contributed to a vast reduction in the window, beyond reasonable levels. Fortunately, access to an alternative detector, the FDSS/µCELL, both increased the assay window size using the dye neat but also enabled the dye to be diluted up to three times without a substantial loss in assay window or change in pharmacology of amiloride. It is unclear if this improvement in the assay window is due to a reduction in background fluorescence i.e. the level of fluorescence when there is complete block of ENaC channels by amiloride, or if it is due to an increase in the maximum fluorescence, due to an increased fluorescence intensity when all ENaC channels are constitutively active at basal levels. As the same conditions were used for both plates, the cells were likely to have very similar levels of ENaC expression, and therefore it is likely that the camera on each machine is contributing to these differences.

Another problem which was observed in this assay on the FlexStation®, was the variability of the minimum and maximum fluorescence across a plate, namely an 'edge effect' seen in the outer wells, whereby the fluorescent intensity was generally much lower. Edge effects in cell-based assays occur when the environment is not homogenous. The pair of related problems associated with a heterogeneous cell culture environment include a differential temperature distribution across the microtitre plate, and differential evaporation between wells (Syberg, 2016), which become more exacerbated in application requiring long incubation periods. For example, temperature gradients can cause uneven cell seeding, and evaporation of media can lead to reduced cell viability due to changes in pH and osmolarity (Syberg,

2016). More specifically, in this application, the observed edge effect may have been caused during cell plating, cell transduction, dye loading, or any of the incubation periods throughout setting up the cell plate.

In a 96 well plate, an edge effect can leave 36 wells unusable, decreasing the throughput of each plate, and therefore the entire screen, by 37.5%. Excluding these wells would also require reformatting the entire compound library from its 96 well format. Various steps were therefore taken to try and eliminate this problem. These included: transducing the cells in a flask before plating; keeping plates in a humidified box during incubations; and using a gas-permeable sealing film on the cell plates.

Unfortunately there was no improvement in the edge effect with any of these attempts, which impacted on plate statistics, including Z prime values, making the assay below the accepted standard to proceed with a screen (Z' < 0.5). A key advantage to the FDSS/µCELL is its ability to read from and dispense into every well of the plate at the same time. This reduction in read time for a single addition per plate, from over 30 min to just 5 min, in combination with the ability to load and add from multiple compound/source plates, meant that a double-addition protocol could be implemented. Two additions per plate only increased the overall run time to 10 min, which would still allow for a large number of plates to be run across one day. Furthermore it allowed each well to have an in-well control (maximum concentration of amiloride) added from a second source plate, after the addition of the test compound from the first source plate. This could normalise the response of each well to the test compound to its response upon complete amiloride block of ENaC.

Finally, this assay was able to report differential pharmacology and selectivity of known ENaC blockers, amiloride, benzamil, and EIPA, across the ENaC α and δ channels. Although these data were consistent with published values using this platform (Chen, et al., 2015), the sensitivity of this assay is not comparable to that of the gold standard patch clamp. This was therefore taken into consideration when deciding on the concentration of the compound library to complete the primary screen.

4.5. Conclusion:

The HEK293-ENaC β*γ* cell line and BacMam technology can be used successfully in the development of a fluorescent-based membrane potential primary screening assay against the ENaC δ ion channel. Here I have outlined optimal transduction conditions and setup of the assay in order for it to be able to differentiate between different potencies of ENaC blocker, whilst meeting acceptable screening criteria (assay window, Z primes). I have also detailed the main advantageous of the FDSS/µCELL platform over the FlexStation®, and how these facilitated the development of the screen, and increased the efficiency of the screen and limited the cost.

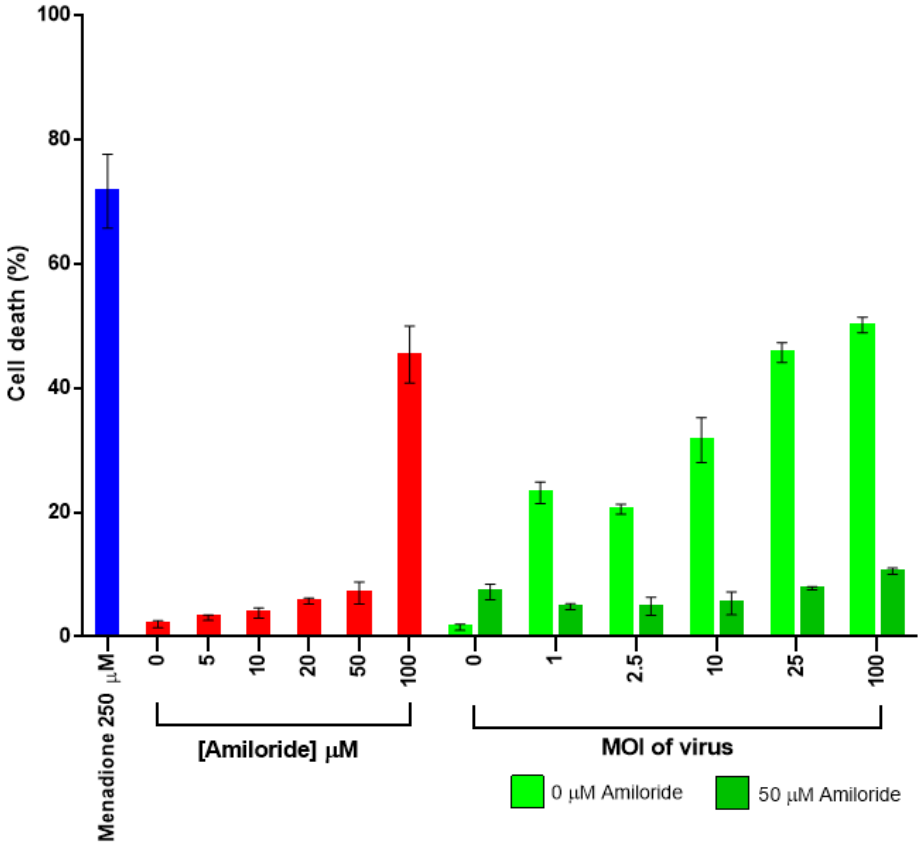

Figure 19. . Investigating amiloride's ability to rescue cells from toxicity induced by ENaC overexpression. Viability of cells measured with Trypan Blue after overnight treatment with either increasing amiloride concentrations, increasing virus MOI, or the same virus MOI in the presence of 50 µM amiloride. Positive control = 250 µM Menadione, Vehicle = Culture media (0 µM amiloride and MOI 0).

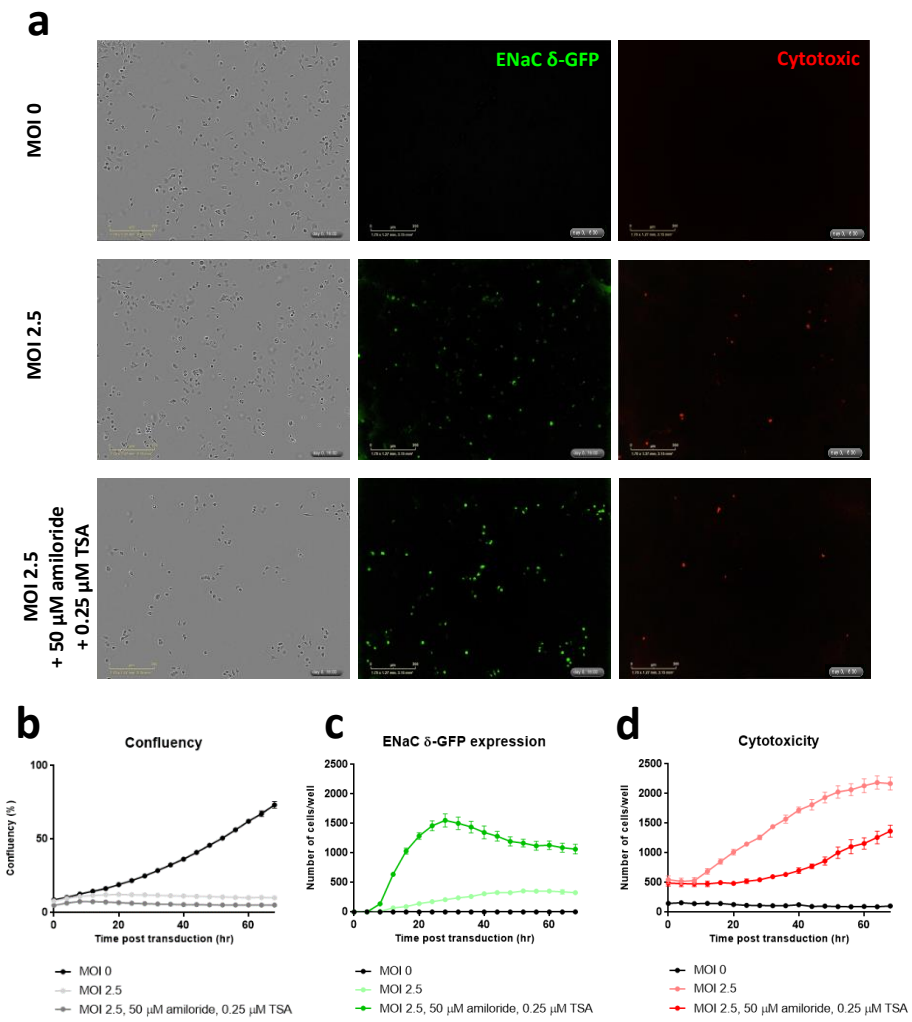

Figure 20. Time course of transduction of HEK293-ENaCβ*γ* cells with BacMam baculovirus encoding the GFP-tagged ENaC δ subunit. a Images taken by the IncuCyte® S3 Live Cell Analysis System 16 hr post transduction with a baculovirus containing a GFP-tagged ENaC δ gene. HEK293-ENaCβ*γ* cell were transduced at MOI 0 (no virus; top) and at MOI 2.5 in the absence (middle) and the presence of 50 µM amiloride and 0.25 µM TSA (bottom). In parallel to viral transduction, cells were loaded with IncuCyte® Cytotox Red reagent to detect cell death. **b-d** Time-course of cell confluency, ENaC δ-GFP expression , and extent of cytotoxicity in untransduced HEK293-ENaCβ*γ* cells (MOI 0) and HEK293-ENaCβ*γ* cells transduced with the baculovirus (MOI 100), in the absence/presence of 50 µM amiloride and 0.25 µM TSA. Data were quantified using the IncuCyte® ZOOM 2016B analysis software.

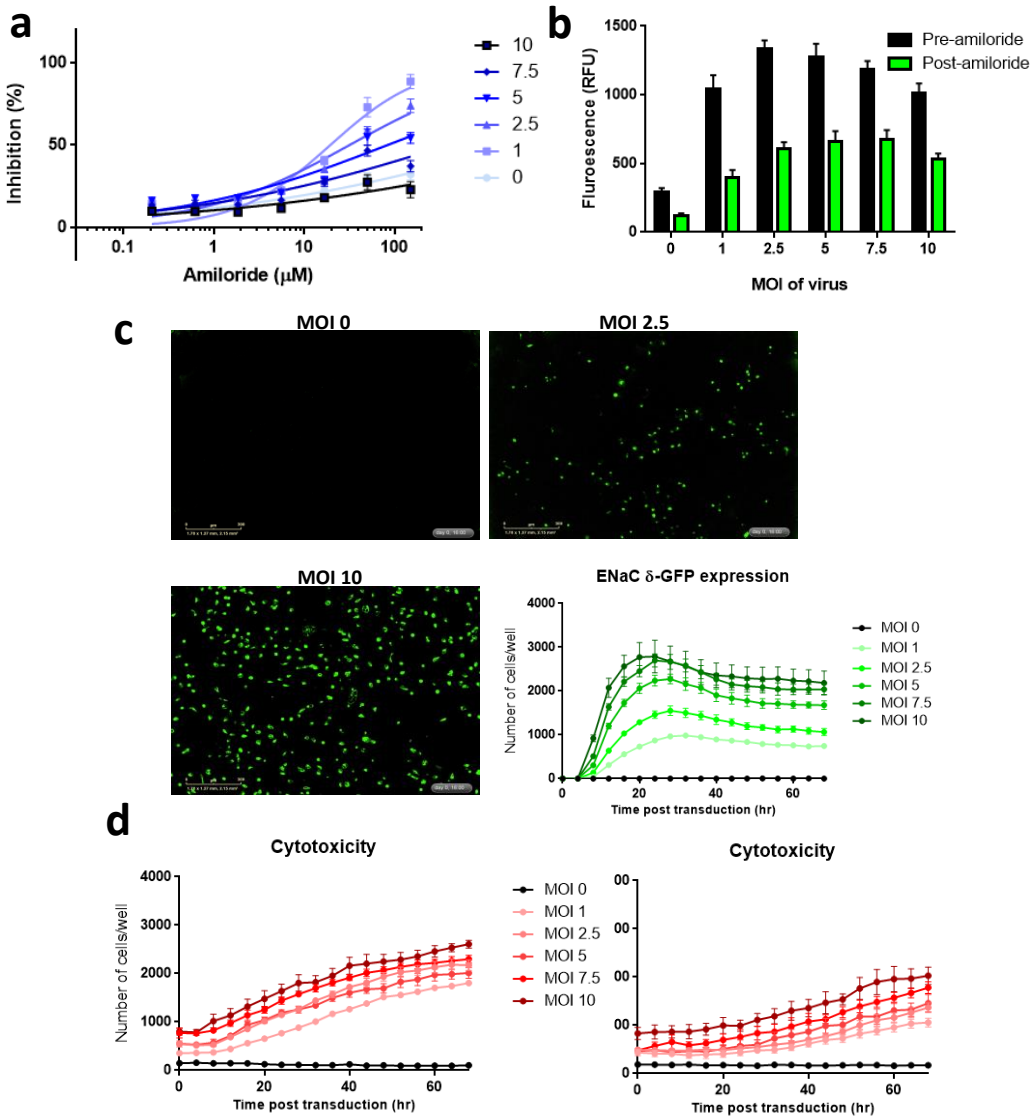

Figure 21. Determination of optimal virus MOI. a Amiloride dose-response curve (n=3) in ENaCαβ*γ* cells transduced with virus MOI 2.5 with 50 µM amiloride at different seeding cell densities. **b** Mean fluorescence (n=3) before and after amiloride addition in ENaCαβ*γ* cells transduced with virus MOI 2.5 with 50 µM amiloride at different seeding cell densities. **c** Representative images taken by the IncuCyte® S3 Live Cell Analysis System 16 hr post transduction of HEK293-ENaCβ*γ* cells with a baculovirus containing a GFP-tagged ENaC δ gene at three different virus MOIs. The time-course of ENaC δ-GFP expression in cells treated with increasing virus MOI is shown (bottom right). **d** Time-course of cytotoxicity of cells treated with increasing virus MOI in the absence (left) and presence (right) of 50 µM amiloride. Data were quantified using the IncuCyte® ZOOM 2016B analysis software.

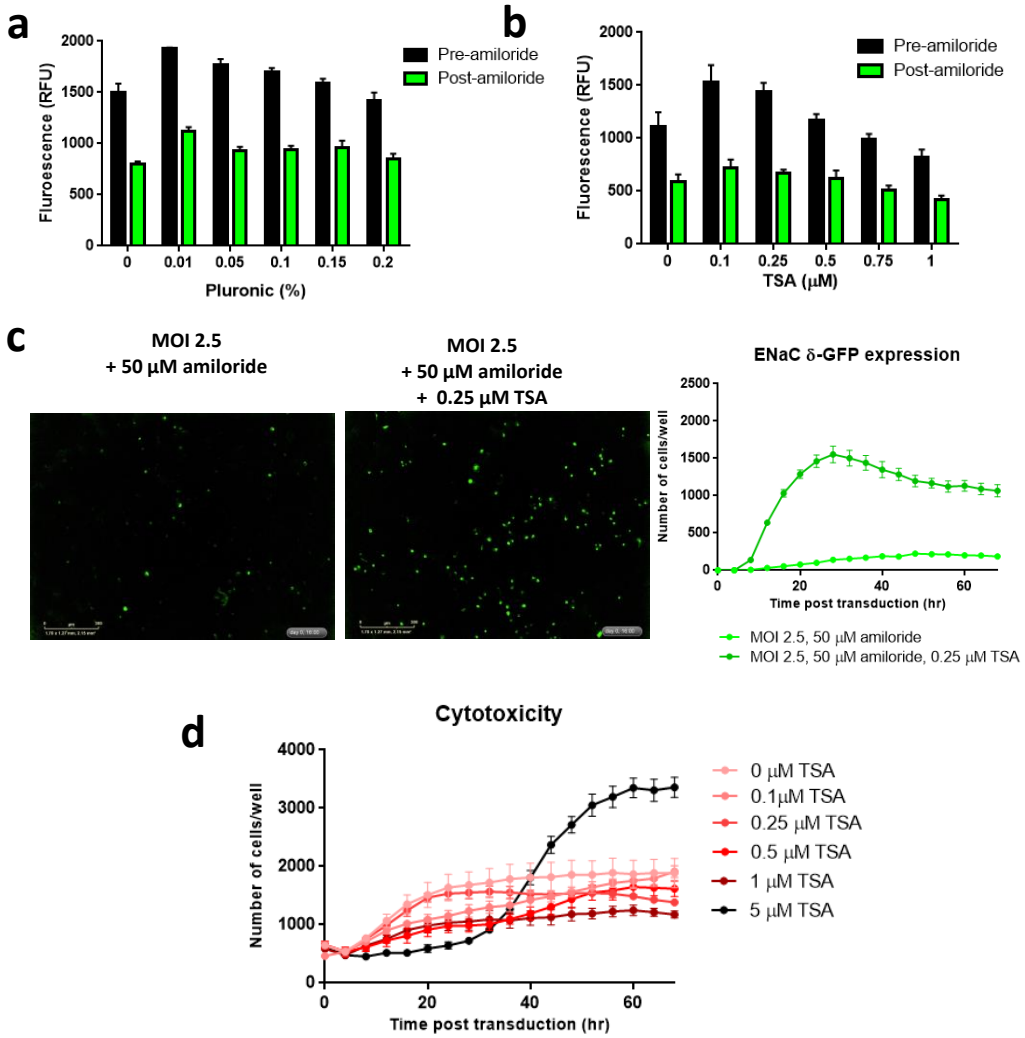

Figure 22. Determination of optimal TSA and Pluronic concentrations. **a** Mean fluorescence (n=3) before and after amiloride addition in ENaCδβ*γ* cells transduced with virus MOI 2.5 with 50 µM amiloride and increasing concentrations of Pluronic. **b** Mean fluorescence (n=3) before and after amiloride addition in ENaCδβ*γ* cells transduced with virus MOI 2.5 with 50 µM amiloride and increasing concentrations of TSA. **c** Representative images taken by the IncuCyte® S3 Live Cell Analysis System 16 hr post transduction with a baculovirus containing a GFP-tagged ENaC δ gene at MOI 2.5 with 50 µM amiloride and in the absence (left) and presence (middle) of 0.25 µM TSA. The time-course of ENaC δ-GFP expression in cells treated with and without TSA is shown (right). **d** Time-course of cytotoxicity of cells transduced with increasing TSA concentrations. Data were quantified using the IncuCyte® ZOOM 2016B analysis software.

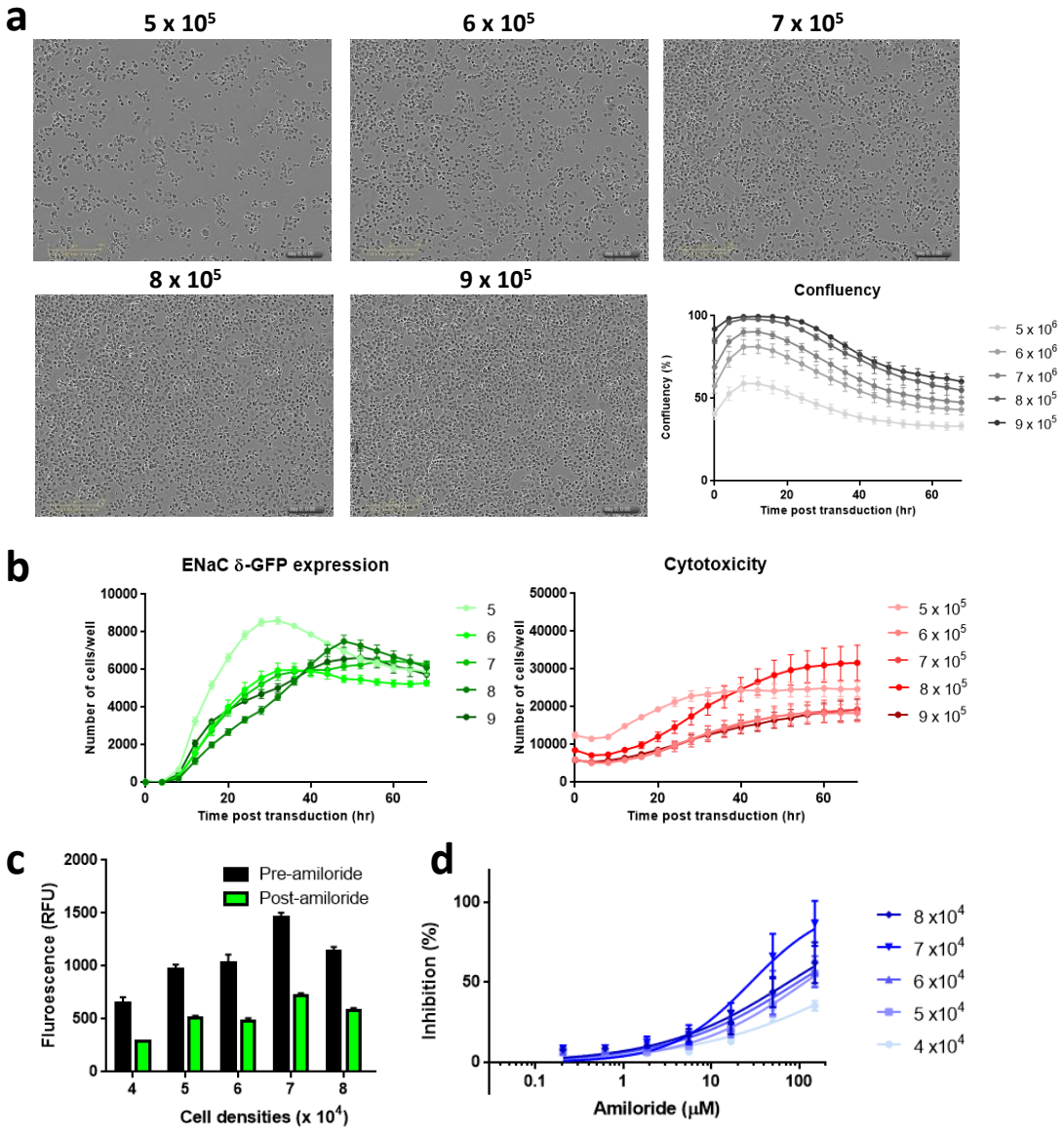

Figure 23. Determination of optimal cell seeding density. a Representative images taken by the IncuCyte® S3 Live Cell Analysis System immediately following transduction at 5 different cell confluency's. The time-course of cell confluency is shown (bottom right). **b** . The time-course of ENaC δ-GFP expression (left) and cytotoxicity (right) in cells seeded at different densities and transduced with the BacMam baculovirus. Data were quantified using the IncuCyte® ZOOM 2016B analysis software. **c** Mean fluorescence (n=3) before and after amiloride addition in ENaCαβ*γ* cells transduced with virus MOI 2.5 at different seeding cell densities, using blue dye (1 x). **d** Amiloride dose-response curve (n=3) in ENaCαβ*γ* cells transduced with virus MOI 2.5 at different seeding cell densities, using blue dye (1 x).

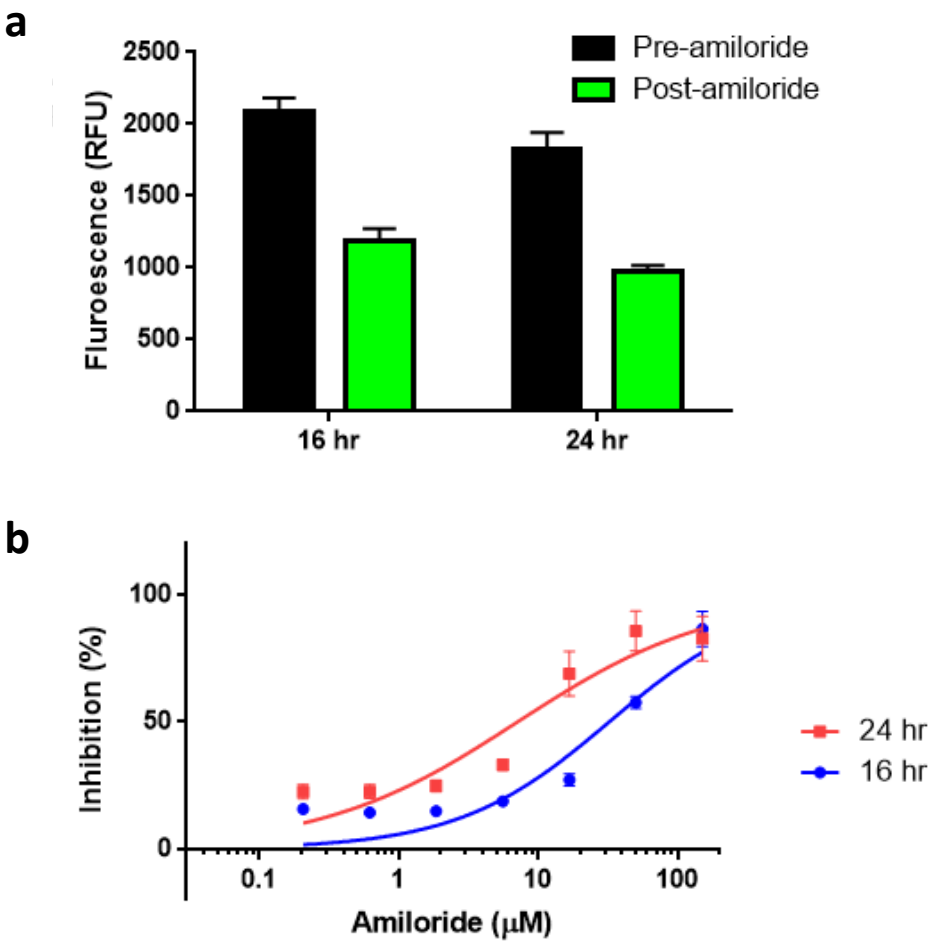

Figure 24. Determination of optimal assay window time post transduction. a Mean fluorescence (n=1) before and after amiloride addition in ENaCδβ*γ* cells transduced with virus MOI 2.5 with 50 µM amiloride and 0.25 µM TSA at t= 16 hr and t=24 hr post transduction, using blue dye (1 x) **b** Amiloride dose-response curve (n=1) in ENaCδβ*γ* cells transduced with virus MOI 2.5 with 50 µM amiloride and 0.25 µM TSA at t= 16 hr and t=24 hr post transduction, using blue dye (1 x).

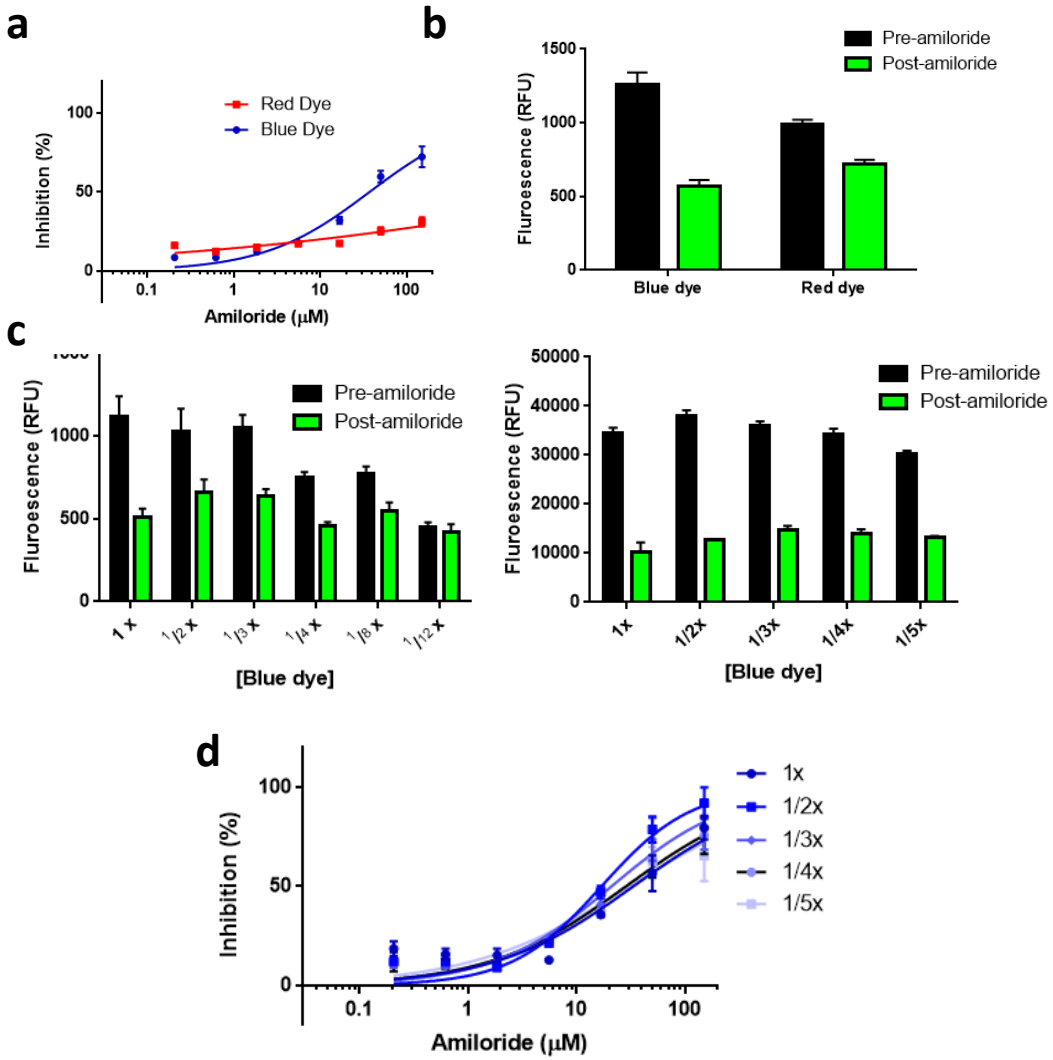

Figure 25. Determination of optimal dye formulation (colour) and concentration across two different platforms. **a** Amiloride dose-response curve in ENaCαβ*γ* cells (n=3) using blue and red dye (1 x)**. d** Mean fluorescence (n=3) before and after amiloride addition using red or blue (1 x) dye in ENaCαβ*γ* cells. **b** Mean fluorescence (n=3) before and after amiloride addition using different concentrations of blue dye in ENaCδβ*γ* cells. Measured on the FlexStation. **c** Mean fluorescence (n=3) before and after amiloride addition using different concentrations of blue dye in ENaCδβ*γ* cells. Measured on the FlexStation (left) and the FDSS/µCELL (right). **d** Amiloride dose-response curve (n=3) using different concentrations of blue dye in ENaCδβ*γ*, measured on the FDSS/µCELL.

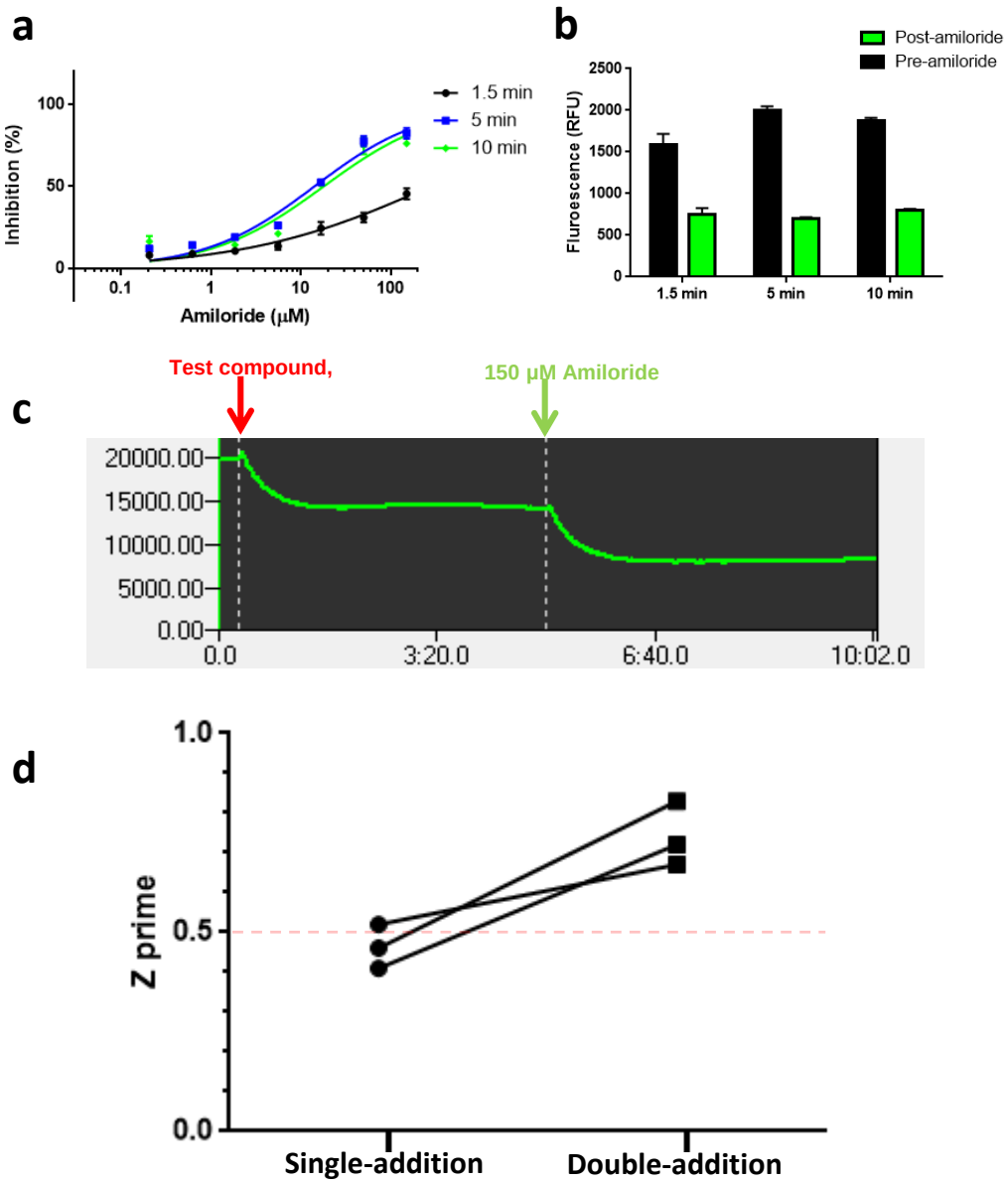

Figure 26. Determination of optimal read time and implementation of a double-addition protocol. a Amiloride dose-response curve (n=2) in ENaCδβ*γ* cells transduced with virus MOI 2.5 with 50 µM amiloride and 0.25 µM TSA read for 90 sec, 5 min or 10 min, using blue dye (1 x). **b** Mean fluorescence (n=2) in ENaCδβ*γ* cells transduced with virus MOI 2.5 with 50 µM amiloride and 0.25 µM TSA read for 90 sec, 5 min or 10 min, using blue dye (1 x). **c** Diagram of the double-addition protocol implemented to normalise for this variability. **d** Z' values obtained over three days with either the single- or double-addition protocol, using min/max plates.

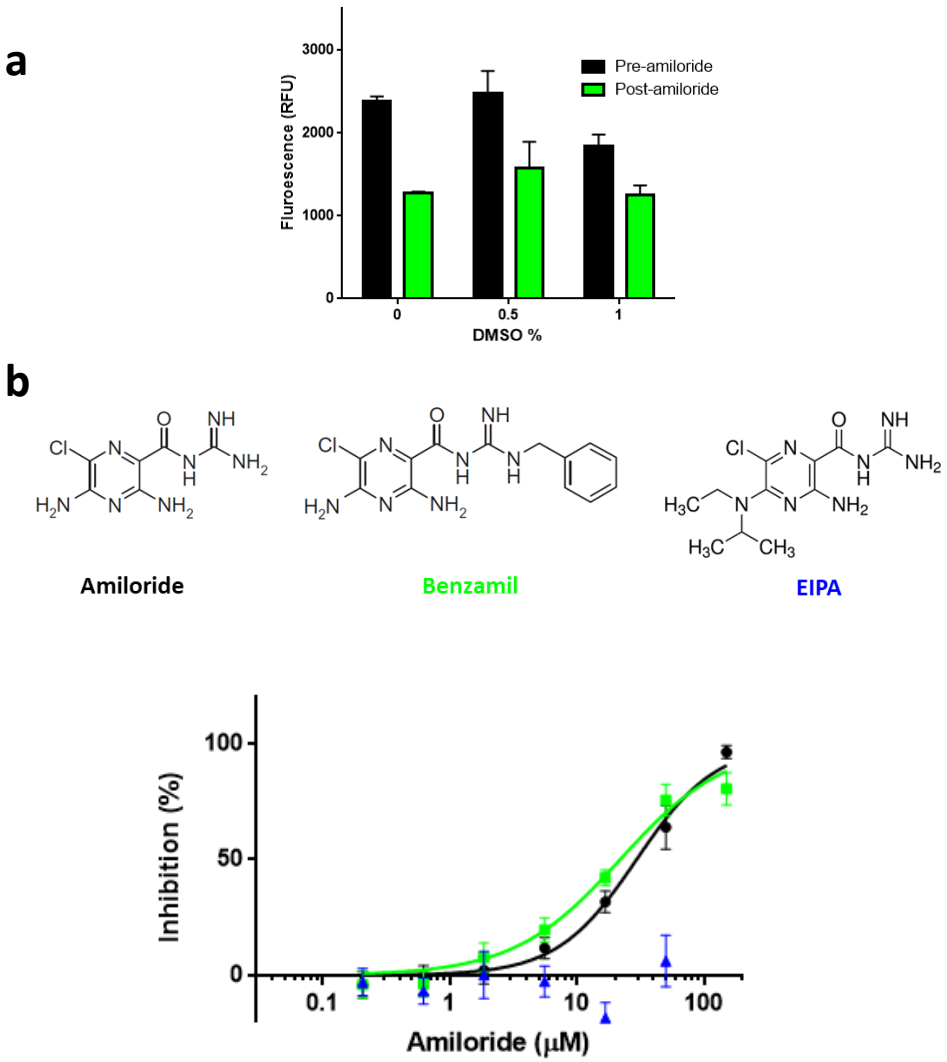

Figure 27. DMSO tolerance and pharmacological validation. a Mean fluorescence (n=3) before and after amiloride addition in ENaCδβ*γ* cells transduced with virus MOI 2.5 with 50 µM amiloride and 0.25 µM TSA after treatment with increasing DMSO concentrations for 5 min **b** Amiloride, benzamil and EIPA dose-response curve (n=3) in ENaCαβ*γ* cells transduced with virus MOI 2.5 with 50 µM amiloride and 0.25 µM TSA, using blue dye (1/3 x), the double- addition protocol on the FDSS/µCELL (amiloride, IC_{50} = 29.4 ± 3.7 µM (n=3); benzamil, IC_{50}= 21.8 ± 3.3 µM (n=3); EIPA, IC_{50} > 150 µM (n=3)).

5

RESULTS: MEMBRANE POTENTIAL SCREEN

Chapter 5

5.1. Background:

5.1.1. High-throughput primary screening assays:

Drug discovery largely depends on high-throughput screening (HTS) as one of the major sources of drug leads, driven by advances in automation technology and combinatorial chemistry. This is reflected in the establishment of screening centres and the increase in commercially available screening libraries. Remarkably, there has been a concurrent decrease in the number of new chemical entities (NCEs) that have reached the market (David, et al., 2009), with over half of clinical trial failures attributed to those lead compounds identified from HTS (Macarron, et al., 2011). Therefore there is an ongoing emphasis on improving the quality of leads which arise from HTS to increase the NCEs progressing in the drug discovery process.

In general, the use of cell-based assays earlier on in the drug discovery process is now being implemented, and accounts for an increasing proportion of HTS efforts (Zhang, et al., 2012). These may provide information on not only the potencies of compounds, but also other predictors which can determine success of a compound in later stages. These may include compound cytotoxicity and permeability. An HTS program, which encompasses the search for ENaC δ inhibitors, consists of target identification (discussed in Chapter 1), reagent preparation (Chapter 3), assay development (Chapter 4), compound management and high-throughput screening (Landro, et al., 2000).

In terms of compound management, it can be assumed that more hits would be generated when screening larger compound sets. This is usually limited by the cost of the compounds and screening reagents. Therefore, this project started with screening a small- to medium-sized library. Additional considerations include the likelihood of

the compound to generate artefacts in the chosen assay, the solubility of the compounds in the buffers used in the assay, and the novelty and structural diversity of the compounds to ensure adequate chemical space is accounted for (Valler & Green, 2000). Nonetheless, screening well-characterised chemical space is beneficial as it increases the number of hits found as compounds have already been confirmed to have biological activity. The CUTE Ion Channel library (Life Chemicals Inc., Niagara-on-the-Lake, Canada) used in this screen was known to be biologically active at similar targets i.e. membrane bound proteins such as ion channels. Due to a lack of any screening data associated with the ENaC δ channel, and previous unsuccessful attempts at identifying ENaC α channel inhibitors that are not based on amiloride, initially the focus was to successfully identify a reasonable number of hits.

After screening, analysing vast quantities of data requires an approach to data processing, quality control and hit identification that gives confidence in compounds taken further in the drug discovery process. These compounds must meet appropriate criteria that decrease the probability of them being due to systematic error, being false positive/negative samples, or not possessing drug-like properties, outlined by Lipinski's 'rule of 5' (Lipinski, et al., 2001). The thresholds for hit identification may vary depending on the target. Reducing the threshold will increase the number of hits, but also the number of false positives, and vice versa.

Identified hits must then be validated either through repetition in the same assay, and/or a second method. In the case of ENaC δ, this was the gold stand patch clamp technique (Hodgkin & Huxley, 1939), which can directly measure the functional activity of the compound at its target. At this step it is common for many of the primary hits

to not be confirmed either on repeat of the primary assay or on functional assessment. This highlights the importance of identifying a reasonable number of hits from the primary screen.

5.1.2. SAR-based drug discovery:

Structure-activity relationships (SAR) are an important concept in drug discovery, applicable through primary screening to lead optimisation. It is an enabling tool, which explores the relationship between a molecule's biological activity and the three dimensional structure of the molecule (Guha, 2013). By helping to identify the existence of specific functional groups within a collection of molecules and clarifying the contribution of these groups to the activity of the molecule, it can ultimately lead to the optimisation of specific physicochemical and biological properties of that molecule. These may include its solubility, permeability, toxicity, pharmacokinetics, selectivity and potency. Usually the aim of SAR would be to simultaneously improve more than one of these (Nicolotti, et al., 2009), for example during lead optimisation, whereby there may be an emphasis on improving potency at its target whilst reducing toxicity through off-target interactions.

When there are a large number of molecules to interrogate, SAR data can be generated and interpreted via high throughput experimental techniques combined with *in silico* methods (Guha, 2013). These *in silico* methods can be used if the target structure is known. They involve using computational chemistry and molecular models to capture SARs and then predict the activity of new molecules (Dudek, et al., 2006). This helps to prioritise specific series of molecules and strategise the synthesis of new

molecules. Although modelling SAR cannot replace medicinal chemistry, an inability for *in silico* modelling increases the reliance on medicinal chemistry, which is much less focussed and therefore less efficient.

When structural information of the molecule's target is lacking, as is the case with the ENaC channel, these *in silico* techniques do become harder to implement. Non-computational methods to probe SAR must then be employed. These include synthesising and testing several structural analogues of the lead compound. The impact of removing or modifying different functional groups on the molecule can help to better understand which are important for biological activity, and to describe the pharmacophore (Yang, 2010). The pharmacophore outlines the main molecular features in their relative positions in space that are necessary for biological activity. Medicinal chemists can then introduce structural changes to a compound, which can include, but are not limited to: modifying the steric bulk or chain length of alkyl substituents; simplification of complex chemical structures like natural sources; rigidification of unhindered single bonds to prevent free rotation and keep it in its bioactive conformation; and finally, the use of conformational blockers, such as a methyl group, to similarly prevent free rotation about a single bond (PharmaFactz, 2018).

5.1.3. Site-directed mutagenesis studies of drug binding:

Site-directed mutagenesis is a PCR-based technique to mutate specified nucleotides of a sequence within a plasmid vector (Carter, 1986). It can be an invaluable tool to modify genes and study the structural and functional properties of a protein and the relative importance of specific amino acid residues. Commonly the method uses

oligonucleotides complementary to part of a DNA template containing an internal mismatch to direct the mutation. These mutations can be designed to probe protein-protein interactions, protein-ligand binding, or silence enzymatic activity of the protein, for example. In addition to directing a single-point mutation, site-directed mutagenesis can incorporation multiple mutations, insertion or completes deletion of amino acid motifs.

In terms of aiding drug discovery, this method becomes essential to probe the binding site of a target that lacks a resolved structure. It can assess the role of specific amino acids in determining the interaction with a known molecule. This method makes it possible to evaluate several mutations of a key amino acid for binding and to determine the relationship between protein structure and molecule interaction. Complementary to SAR-based studies, understanding specific amino acid interactions can help guide the optimisation of a lead molecule. This has been a useful approach to determine the interaction between amiloride and the ENaC subunits (Ismailov, et al., 1996; Schild, et al., 1997), which leads to the functional block in Na^+ permeation.

5.2. Methods:

5.2.1. Membrane potential assay:

HEK293 ENaC β*γ* cells were harvested and plated in 96-well, black, clear-bottomed assay plates (Section 2.2.7.2.). Once attached (4-6 hr), cells were transduced overnight with the BacMam baculovirus (Section 2.2.7.2.).

Prior to assay, all test compounds from Life Chemicals Inc. (Section 2.1.5.2.) were prepared from their stock solutions in Tyrode's Buffer into a 96-well source plate at 4-

times higher than the test concentration (Section 2.2.7.1.). This was done in either single-point or dose-response format (Section 2.2.7.1.), and control wells (amiloride (100% channel block); Tyrode's Buffer inc. DMSO (vehicle)) were added to every plate (see plate layouts; Section 2.2.7.1.). DMSO concentration was kept uniform across the plate. The second source plate contained the same concentration of amiloride in every well, prepared at 5 times higher than the final test concentration of 150 µM.

On assay, cells were loaded with FLIPR Membrane Potential Blue dye (Section 2.2.7.2.) at 37 ^{o}C, 20 min, before loading onto the platform, with the source plates and dispensing tips. Whole-cell fluorescence (excitation/emission λ 531/565 nm) was monitored every 1.40 sec, before and during the addition of both test compound and amiloride control (Section 2.2.7.3.). The kinetic changes in fluorescence intensity following compound addition were recorded using the FDSS7000EX/µCELL Software.

Screening data were exported from FDSS7000EX/µCELL software, uploaded onto the Dotmatics database (Hertfordshire, UK) and analysed using Vortex v2015.11.46033 [© Dotmatics Ltd. 2007-2015] (Section 2.2.7.4.).

5.2.2. Hit validation using conventional patch clamp:

Follow-up studies of compounds that show dose-dependent activity at the ENaC δ channel were performed using the patch-clamp technique (Section 2.2.6.). Cells were transduced 24 hr prior to patching and were harvested in serum free media (Section 2.2.6.2.). Cells were kept for up to 4 hr in a reservoir under constant agitation. Standard solutions were used (Section 2.2.6.1.), and reordered test compounds from Life Chemical Inc. (Section 2.1.5.2.), and analogues synthesised in-house or bought from Ambinter (Section 2.1.5.4.), were prepared from stock (100 mM in 100 % (v/v)

DMSO) immediately prior to assay in fresh ECS buffer. To each well of the Dynaflow® Resolve System (Figure 28.) 80 µl of ECS, vehicle control (ECS with standardised DMSO), positive control (30 µM amiloride) or test compound were loaded. As a rule, the DMSO concentration was kept lower than 0.5 %, and was equivalent across every addition regardless of compound concentration.

Whole-cell recording was performed using the Axon™ pCLAMP® 9 Software. Cells were clamped at -40 mV between recording periods, which then included a ramp voltage protocol from -100 mV to + 100 mV over a 1 s period. Every cell was exposed to the vehicle and the positive control before testing any compound. Currents were recorded over a 10 s application period. For single-concentration experiments, cells were washed out with ECS for 1 min in between each test compound. For dose-response experiments, the cell was exposed to increasing concentrations of the test compound without any washout period between.

Data were analysed using Axon™ pCLAMP® 9 Software (Section 2.2.6.4.). Dose-response curves were normalised to I/I_{max} and plotted using GraphPad Prism v7.0. All data are reported as mean ± SEM (number) (Section 2.2.6.4.).

5.2.3. Mutant generation:

Mutations that are documented in the literature for playing a role in amiloride binding at the ENaC α channel (Ismailov, et al., 1996; Schild, et al., 1997) were introduced to the GFP-tagged *SCNN1A* encoded within a pCMV-DEST vector (Section 2.1.1.3.). Homologous mutations were introduced into the GFP-tagged *SCNN1D* gene within a pCMV-DEST vector, encoding the ENaC δ subunit. The ENaC α and δ deletion mutations of the WYRFHY/WYHFHY motif were introduced (Table 4.; Section 2.1.2.)

using the Agilent QuikChange Lightning Site-Directed Mutagenesis Kit (Section 2.2.1.8.), whereas the single-point mutations of the serine residues 556/533 were generated from Genscript® via the Site-Directed Mutagenesis Service (Section 2.1.1.6.).

These mutant plasmids were transfected into HEK293-ENaC β*γ* cells using Lipofectamine® 2000 (Section 2.2.3.3.) and cells were harvested for patch clamp investigation 16-24 hr later. Prior to harvesting, cells were observed under a fluorescent lamp (excitation/emission λ 475/509 nm) to verify expression of the GFP-tagged ENaC subunit. Whole-cell current measurements using the voltage ramp protocol (Section 2.2.6.) were made whilst cells were first exposed to the vehicle and positive control before the test compound (amiloride, benzamil or UoS-00017907). The positive control (300 µM amiloride) was higher in concentration to account for the predicted loss of sensitivity to this drug.

5.3. Results:

5.3.1. Identification of potential ENaC δ inhibitors using a membrane potential assay:

Initially 1491 compounds from the CUTE ion channel library (Life Chemicals, Canada) were screened against the ENaC δ channel at 50 µM (0.5 % DMSO). The screen was repeated later with compounds at 10 µM (0.1 % DMSO). Assay quality parameters (Z' values) were assessed for each plate, and the sample distribution plotted as sample number over percentage inhibition.

The screen was first completed with compounds at 50 µM (0.5% DMSO), despite this pushing the upper limits of DMSO tolerance. Given the insensitivity of the assay and

underestimation of amiloride's potency, this was the highest concentration that still kept the DMSO concentration within reasonable limits. Assay quality remained high across all 19 plates (all Z' values > 0.5; Figure 29.b) but the distribution of sample data was wide (Sample standard deviation ($SD_{samples}$) = 46.26 (n = 1328); Figure 29.a). The median of the data was 21.25%, reporting a bias towards positive inhibition. Specifically there was an enrichment of compounds at ~30 % inhibition and ~100 % inhibition.

As there was a high number of 'hits' (Table 8.), and a large number of compounds which were observed to not be in solution at 50 µM, the entire library was screened at the lower concentration of 10 µM (0.1 % DMSO). Compound solubility was improved, and the DMSO concentration was now well within acceptable limits. Assay quality remained high across all 19 plates (all Z' values > 0.5; Figure 30.b) and the distribution of sample data was tighter ($SD_{samples}$ = 26.96 (n = 1456); Figure 30.a). The median of the data was closer to 0 % inhibition (median = 9.04 %) and displayed a normalised distribution, with a reduced bias towards positive inhibition.

	Number of Compounds	
Inhibition (%)	**10 µM**	**50 µM**
≥ 0	1076	892
≥ 50	100	313
≥ 80	55	173

Table 8. Number of compounds reported to inhibit the ENaC δ channel above a specified percentage. Inhibition (%) of each compound is calculated relative to the inhibition by 150 µM amiloride.

There was a weak positive correlation between compound activity reported by the two screens of different compound concentrations (R^2 = 0.23, 95% CI 0.44 to 0.52; Figure 31.). The data is skewed to the left due to a number of compounds that were reported as giving a much higher percentage inhibition at 50 µM. Interestingly there is some good correlation between some compounds showing ~100% inhibition at both screening concentrations.

'Hits' were considered as any compound reported as giving a positive inhibition of greater than 3 times the standard deviation of the samples (= 80.88 %). From the screen performed at 10 µM there were 55 compounds that showed > 80.88 % inhibition, relative to inhibition by 150 µM amiloride. These compounds were tested at five concentrations to assess dose-dependence of inhibition and therefore potency (Figure 32.a). All compounds were tested in duplicate, and there was good reproducibility between n=1 and n=2 values (R^2 = 0.71, 95% CI 0.75 to 0.90; Figure 32.b).

From the 55 compounds, 10 compounds exhibited IC_{50} values of > 30 µM (grey; Figure 32.a) and were excluded from further studies. In addition, compounds were examined for both structure-activity relationship (SAR) similarities and inherent liabilities of their functional groups. A further 22 were excluded as their structures included unstable moieties (orange). The remaining 23 compounds (blue) were compared for any structural similarities (Figure 33.). It was observed that there were consistent moieties across a number of the compound, for example an aminopropanediol group (blue), an acetamide group (red) and a methanesulfonamide group (green). They were reordered from Life Chemicals as solid powders. These powders were checked against

the original library of liquid stocks using liquid chromatography–mass spectrometry (LC-MS) to identify any differences in compound stability and purity between stocks. All reordered compounds were identical to their respective original liquid stock used for screening.

5.3.2. Hit confirmation using patch clamp:

Patch clamp was used to confirm any compound considered a 'hit' from the membrane potential screen. The 23 reordered compounds were prepared to 10 mM in 100% (v/v) DMSO, and initially screened at a single concentration of 30 µM (0.3% DMSO).

Whole-cell currents were measured using patch clamp, which held the cells at a -40 mV and then ramped them between -100 mV and +100 mV over 1 s. This ramp voltage protocol was performed in the presence of ECS, vehicle control (ECS (0.3% DMSO)), and the positive control (30µM amiloride) to first check for DMSO tolerance and presence of an amiloride-sensitive current prior to exposure to each test compound.

One of the 23 compounds (UoS-00017907; Figure 34.a) tested showed inhibition of the ENaC current when tested at 30 µM. All other test compounds had no effect on the inward or outward amiloride-sensitive current. UoS-00017907 was prepared to 100 mM stock in 100 % (v/v) DMSO and solubility was good. Figure 34.b shows the raw current trace of the ENaC current when exposed to ECS (black), 30 µM amiloride (red), and 4 increasing concentrations of UoS-00017907 (blue).

The potency and selectivity of UoS-00017907 was determined at the ENaC δβγ and αβγ channels (ENaC δβγ, IC_{50} = 149.2 ± 5.01 µM (n=8), Figure 34.c; ENaC αβγ, IC_{50}= 134.4 ±

6.5 µM (n=4)), with the highest test concentration of 1 mM (1 % DMSO). This compound showed no selectivity between the two ENaC channels (Figure 34.d).

5.3.3. Structure-activity relationship (SAR) - based electrophysiological study:

To understand the relationship between the structure of the lead compound and its ability to modulate the ENaC current, a search for commercially available analogues, alongside in-house medicinal chemistry support, was pursued. SAR studies are widely used to optimise the activity of a lead compound toward a specific target through generation of structural analogues. In this way, the combination of functional groups necessary for optimal drug activity is ascertained. For this purpose, patch clamp was used to measure the outcome of each change in the molecule.

In total, 9 analogues of UoS-00017907 were tested (Figure 35.), 6 of which were ordered from Ambinter (Orléans, France), and 3 of which were synthesised in-house (R.Huckvale, SDDC). Compounds were made up to 100mM stocks in 100% (v/v) DMSO and first tested at 100 µM (0.1% DMSO), using the voltage ramp protocol (Section 2.2.6.4.). Compounds which showed activity were followed up with concentration-response studies (0 – 1mM) to determine their potencies.

The compound UoS-00017907 had a benzimidazole core, with a phenyl moiety and an aliphatic amine linked to a furan moiety (Figure 35.). Broadly, analogues were categorised by changes made to the phenyl moiety (blue), and to the furan moiety (orange). 5 compounds fulfilled both groups' requirements. Interestingly, all 6 compounds, which had altered the phenyl functional group, lost all activity against the

ENaC δβγ channel. Changes to the furan moiety alone did not appear to significantly affect the potency of any molecule (Figure 36.a-c), but there was no improvement in potency compared to UoS-00017907.

5.3.4. Binding site of amiloride, its analogues and the lead compound, UoS-00017907:

Two characterised amiloride-binding domains (ABD) of the ENaC αβγ channel were mutated in both channel isoforms to determine the likelihood of the lead compound binding at the same site, despite having a novel chemical structure. Deletion mutations were introduced into the first of these sites in the ENaC α and δ subunit (WYRFHY at amino acid positions 251-256 or WYHFHY at amino acid positions 232-237, respectively; Figure 37.). Initially, this mutation was validated by measuring whole-cell currents in the ENaC α wild-type (wt) and ENaC α mutant (Δ251-256) channel on exposure to amiloride during a voltage-ramp protocol (Section 2.2.6.4.). This deletion mutation caused ~750-fold reduction in the potency of amiloride at the ENaC α channel (IC_{50} = 382.1 ± 56.8 μM (n=2); Figure 37.a). The introduction of the homologous mutation to the ENaC δ wild-type (wt) channel (Figure 37.b) also a large decrease in amiloride and benzamil's potencies at this channel (amiloride: IC_{50} > 1000 μM (n=8); benzamil: IC_{50} = 139.4 ± 49.1 μM (n=3); Figure 37.c), and the removal of any inhibition measured from application of UoS-00017907.

On a single-point mutation of the second ABD, from a serine (S) at position 556 of the ENaC α subunit (Figure 38.a) to a tyrosine (Y), amiloride potency is decreased by over 100-fold (IC_{50} = 60.0 ± 8.4 μM (n=1)). However, if the serine is mutated to leucine, there is no real difference in the ability of amiloride to block the channel (IC_{50} = 0.47 ±

0.1 µM (n=3)). At the ENaC δ channel, mutating the equivalent serine at position 533 (Figure 38.b), the same pattern is observed (Figure 38.c). Mutation of this residue to a tyrosine reduces the ability of amiloride to block the channel by 100-fold and UoS-00017907 completely, respectively. Mutation to a leucine residue has no effect on inhibition of the ENaC δ channel by these two compounds compared to wt.

5.4. Discussion:

The fluorescence-based membrane potential assay performed on the FDSS/µCELL platform with HEK293-ENaCβ*γ*, was robust and reproducible, identifying 55 compounds which showed a significant inhibition of the ENaC δ channel. The assay lacked the sensitivity to known inhibitors of the gold-standard patch clamp, as discussed in Chapter 4, and therefore test compounds were first screened at 50 µM (0.5 % DMSO). The compound library selected for screening was also biased as all of the compounds in the collection were known to exhibit activity to ion channel targets. As this target has limited pharmacological data documented in the literature (Giraldez, et al., 2012), and the ENaC α channel blockers occupy a narrow chemical space, the main emphasis of the primary screen was to identify enough hits to proceed with validation steps that would result in more than one lead series of compound. Both the high screening concentration and the bias of the compound set increased this likelihood.

Other factors that could negatively influence the sample data include those that increase the frequency of false positive and false negative results, the former of which is characteristic of membrane potential assays. Reasons for this can be due to, but not exclusive to, the pharmacology of the compound for the quenching molecule

contained in the dye formula, intrinsic fluorescence of the compound itself, the pharmacology of the compound for an endogenous ion channel which is not the target, and toxicology of the compound which may compromise the membrane integrity of the cells. As membrane potential cannot discriminate between ionic species, and only changes in membrane potential, buffers were carefully selected to minimise contribution of other endogenous ion channels. However using a biased library of ion-channel specific compounds increased the probability of an off-target interaction.

As a result of the high screening concentration, the spread of the sample data was too wide to find compounds that gave a statistically significant level of inhibition. Compounds were therefore rescreened at 10 µM and the hit rate was 3.6 % (55 compounds), of which 23 were reordered for validation studies. Although a small number of compounds could not be reordered as they were not commercially available, the 55 hits were scrutinised by a medicinal chemist before validation. This could eliminate the compounds that were known to be fluorescent, or that were deemed no to be 'drug-like' due to unstable moieties or solubility problems, which would prevent the ability to work with them further. In hind-sight, if more time had been available to use the demo FDSS/µCELL platform, counter screens using the membrane potential assay would have been useful to eliminate those compounds which were either inherently fluorescent, toxic to the cells, or acting at endogenous channels. Such counter screens would have involved screening the compound alone, without cells, to assess their own fluorescence, and screening the compounds with HEK293 cells containing no ENaC, to access if a compound was toxic and therefore

compromising the membrane integrity of the cells, or if it was acting at an endogenous channel and not ENaC.

Without a time extension available with the platform, validation of compound activity was performed using patch clamp instead. As is common, the attrition rate from primary hits to confirmed hits after validation was high (95.7 %) (Hughes, et al., 2011). Just one compound, and therefore one compound series, could be further investigated. The lack of a resolved structure for this channel limited the extent of *in silico* modelling to predict protein-compound interactions and therefore a functional approach to SAR, using patch clamp, had to be pursued. Although this is the gold standard technique in the study of ion channels, it required high level of technicality from the experimenter and is laborious, rendering this SAR-based approach fairly inefficient. This was primarily supported by in-house medicinal chemistry capabilities as commercially available analogues were associated with a high cost. However, due to the low potency of the lead compound, the SAR studies were hard to decipher: the compounds needed to be soluble at 100 mM (100% DMSO) to be able to test the range of concentrations required and any small decreases in potency were quite often missed as the compound's activity was beyond measurable limits.

Although this SAR effort was unsuccessful in improving the potency of the compound, it did indicate how regions of UoS-00017907 may interact within the binding site of the ENaC α/δ subunits. Although changes to the furan moiety thus far, seen in UoS-00032822 (furan to tetrahydrofuran) and UoS-00032883 (furan to oxetane), saw no significant impact on potency, these compounds maintained activity. This would suggest that this region is not fundamental to ligand-protein interaction. On the other

hand, a change in the phenyl moiety resulted in no inhibition of the ENaC current. This would infer that the compounds interaction with the channel had been sufficiently disrupted to prevent channel block. Phenyl groups are involved in π-stacking interactions, which are one of the most frequently observed ligand-protein interactions, widely used in ligand design (Mohamed, et al., 2015). A change in the electronic nature of this group, for example by the addition of a methoxy and CF_3 substituents to the phenyl group UoS-00032870, has rendered this compound inactive.

Almost 50% of all π-stacking interactions are observed between the aromatic ring of phenylalanine (F) and an aromatic ring in the ligand, followed by tyrosine (Y) (36.8%), tryptophan (W) (8.7%) and histidine (H) (5.1%) (Ferreira de Freitas & Schapira, 2017). Interestingly, the reported amiloride binding site, WYHFHY (Ismailov, et al., 1996), is made up of these four amino acids. The data suggests that alterations either to the phenyl group of UoS-00017907, or the amino acid motif, WYHFHY, removes the ability of the compound to interact and inhibit the ENaC current, inferring interactions here may be key to the compound activity.

Mutagenic analysis of compound binding was investigated by mutating two distinct amiloride binding sites (Ismailov, et al., 1996; Schild, et al., 1997). The aim of this was to indicate the possibility of the novel compound, which occupies a distinct chemical space to amiloride and its analogues, interacting with the channel at the same site. The first of the mutations tested was a deletion mutation, which completely removed the WYHFHY motif located in the extracellular domain (Ismailov, et al., 1996). In the ENaC α channel, deletion of the homologous motif had been shown with electrophysiology to decrease amiloride's potency by ~ 1000-fold (Kelly, et al., 2003).

Our findings were able to replicate this, and the same outcome was seen to the ENaC δ channel. Furthermore the loss of inhibition by UoS-00017907 in the mutant ENaC δ channel indicated a similar mechanism of block by this novel lead compound.

The second site, documented to contribute to amiloride block in the ENaC α channel, was the serine residue at position 556 in the human subunit (583 in mouse) (Schild, et al., 1997). Previous studies had shown that if a single-point mutation change of the serine residue to a tyrosine residue, amiloride potency was 100-fold lower, however mutating the serine to leucine had no effect of amiloride block. Again, this was replicated in the ENaC α channel, and with equivalent mutations in the ENaC δ channel. The same pattern was observed with UoS-00017907.

A serine residue is polar amino acid, containing a protonated $–NH_3^+$ and deprotonated $–COO^-$ group under physiological conditions, with a hydroxyl side chain. In a biological setting they play important structural roles, with their side chains associated with hydrogen bond formation, O-linked glycosylation, and phosphorylation (PubChem, 2018). Although leucine is non-polar due to its isobutyl side group, it also contains a protonated $–NH_3^+$ and deprotonated $–COO^-$ group, under physiological conditions (PubChem, 2018). Furthermore the size of serine and leucine is very similar, and therefore exchanging one for the other may not cause any disruption in the structure of the binding site. On the other hand, although its side chain is also involved in phosphorylation, a tyrosine residue is a much bulkier aromatic and partly hydrophobic amino acid. Therefore with regard to the structure of the binding site for amiloride, tyrosine is likely to cause a greater change than leucine, which may be reflective of the differences in the ability of the drug to block the channel.

Although initial findings with these mutants suggested a shared binding site for both amiloride and UoS-00017907, limited medicinal chemistry support, with limited success with preliminary SAR efforts meant that this lead compound was no longer pursued. The requirement for a second series of compound became the priority, and therefore a collaboration with ApconiX Ltd., Alderley Park was set up, funded by a MRC Confidence in Concept Grant to establish a higher throughput screening assay using the automated electrophysiology platform, the IonWorks® Quattro.

5.5. Conclusion:

Fluorescence-based technologies including ion sensitive and potentiometric dyes have been the mainstay of ion channel medium/high throughput screening. Although enabling with respect to being able to interrogate large compound libraries, these formats suffer from high false positive and negative rates due to assay interference. The preliminary membrane potential screening campaign run against ENaC δ had a primary hit rate approaching 5%, of which only a single (non-selective) compound was confirmed as active in the patch clamp electrophysiology assay. After an SAR-based electrophysiological approach did not yield any improvements in potency or selectivity of the lead compound, an academic-industrial collaboration (SDDC & ApconiX Limited) was established to utilise the benchmark technique for ion channel screening, electrophysiology.

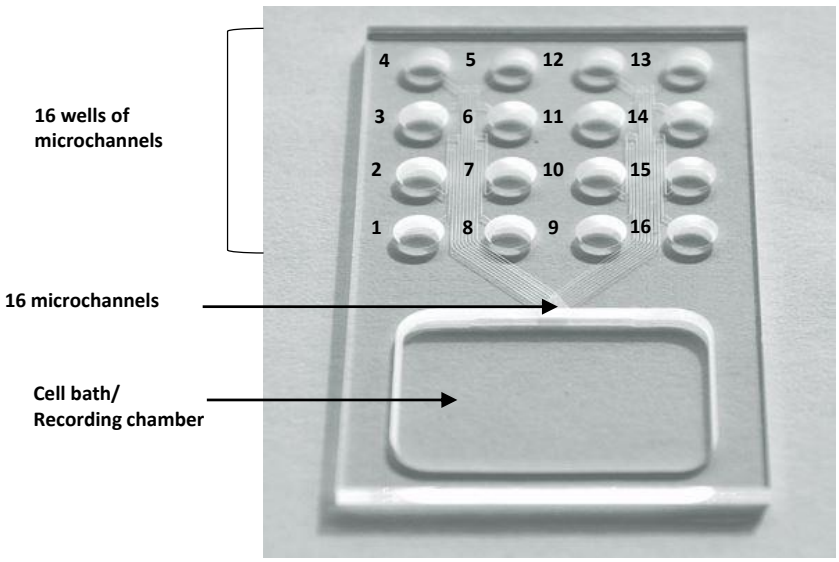

Dynaflow® Resolve Chip

1. ECS
2. DMSO control
3. ECS
4. 30 µM Amiloride
5. ECS

6. – 16. Test compounds (max. 6)
Single concentration, separated by ECS washout

6. – 16. Test compound (max. 1)
Concentration response curve, no ECS washout

Figure 28. Diagram of the Dynaflow Resolve® Chip. The chip contains 16 microfluidic channels, which can hold 80 µL solution in its corresponding well (labelled 1-16) and flows out into the cell bath/recording chamber. Wells 1-5 remained constant in every recording using this system, but wells 6-16 contained test compounds at either a single concentration, separated by an ECS washout, or increasing concentrations of compound to generate a cumulative concentration response curve.

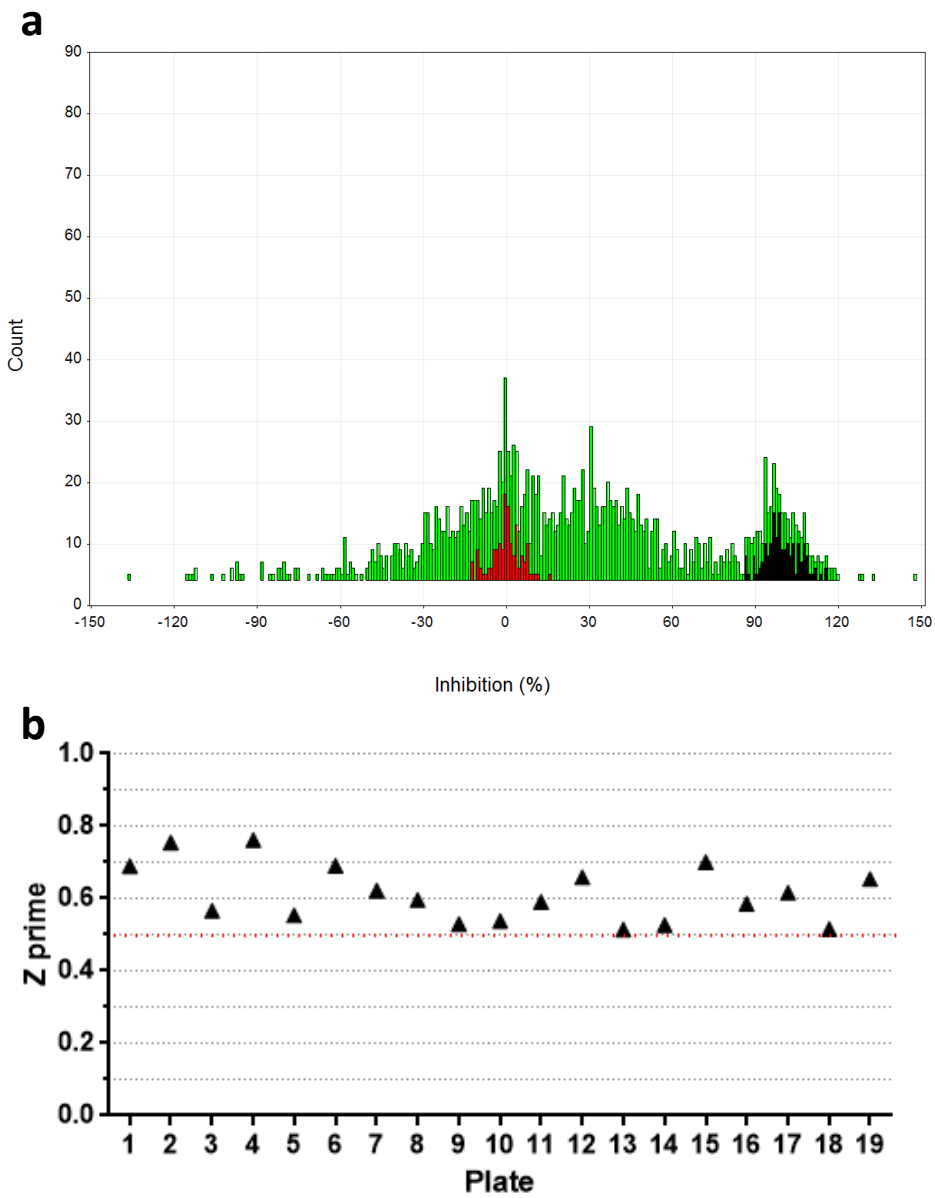

Figure 29. Data from membrane potential primary screen of compounds at 50 µM (0.5 % DMSO) against the ENaC δβ*γ* channel. **a** Distribution of inhibition (%) measured from CUTE ion channel library screened at 50 µM (n=1) in ENaC δβ*γ* cells. Inhibition is normalised to the change in fluorescence upon complete channel block by 150 µM amiloride. Red=vehicle (buffer(0.5 % DMSO), black= maximum control (150 µM amiloride (0.5% DMSO), green= samples. **b** Z' values for all 19 assay plates. Red dotted line represents a Z' value of 0.5, which is the threshold value which signifies acceptable assay performance.

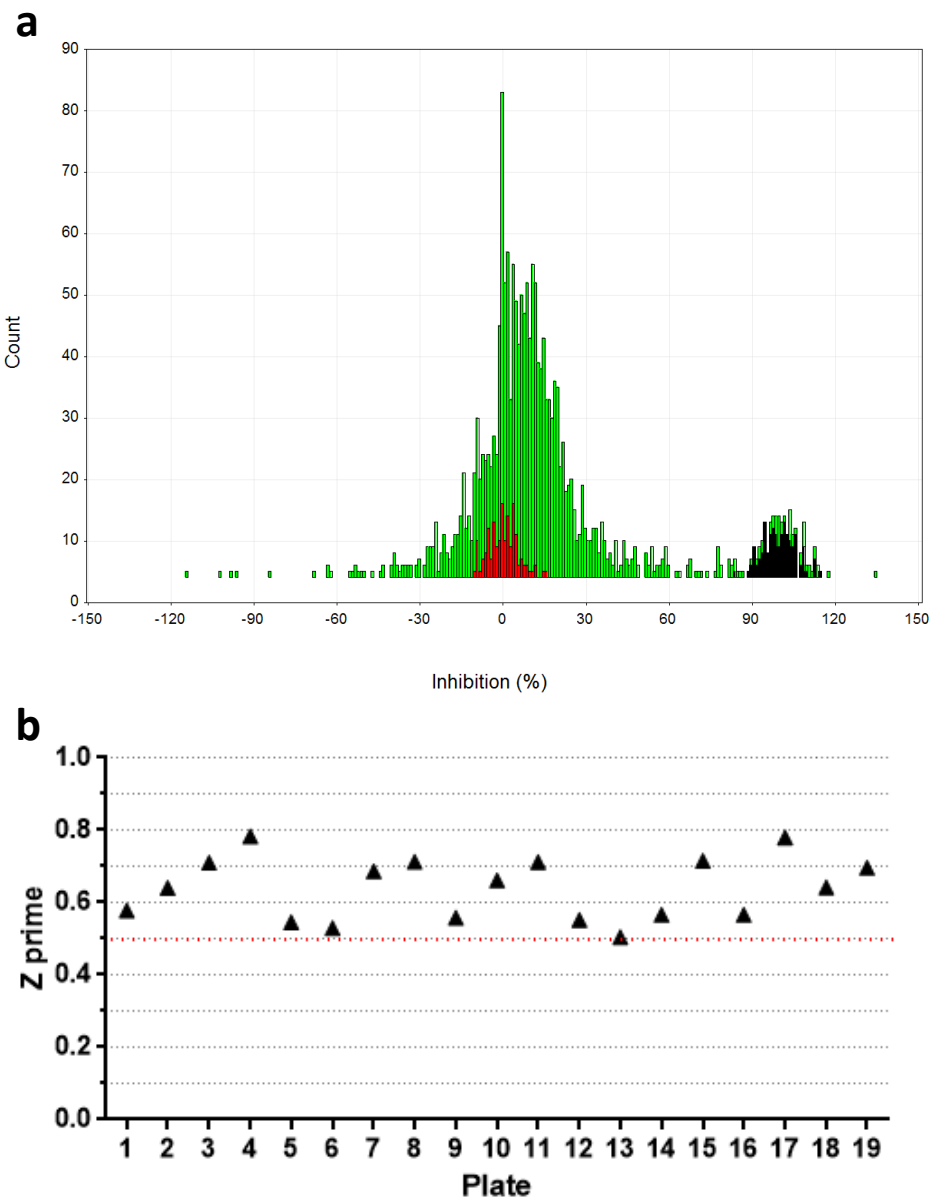

Figure 30. Data from membrane potential primary screen of compounds at 10 µM (0.1 % DMSO) against the ENaC δβ*γ* channel. **a** Distribution of inhibition (%) measured from CUTE ion channel library screened at 10 µM (n=1) in ENaC δβ*γ* cells. Inhibition is normalised to the change in fluorescence upon complete channel block by 150 µM amiloride. Red = vehicle (buffer(0.5 % DMSO), black = maximum control (150 µM amiloride (0.5% DMSO), green = samples. **b** Z' values for all 19 assay plates. Red dotted line represents a Z' value of 0.5, which is the threshold value which signifies acceptable assay performance.

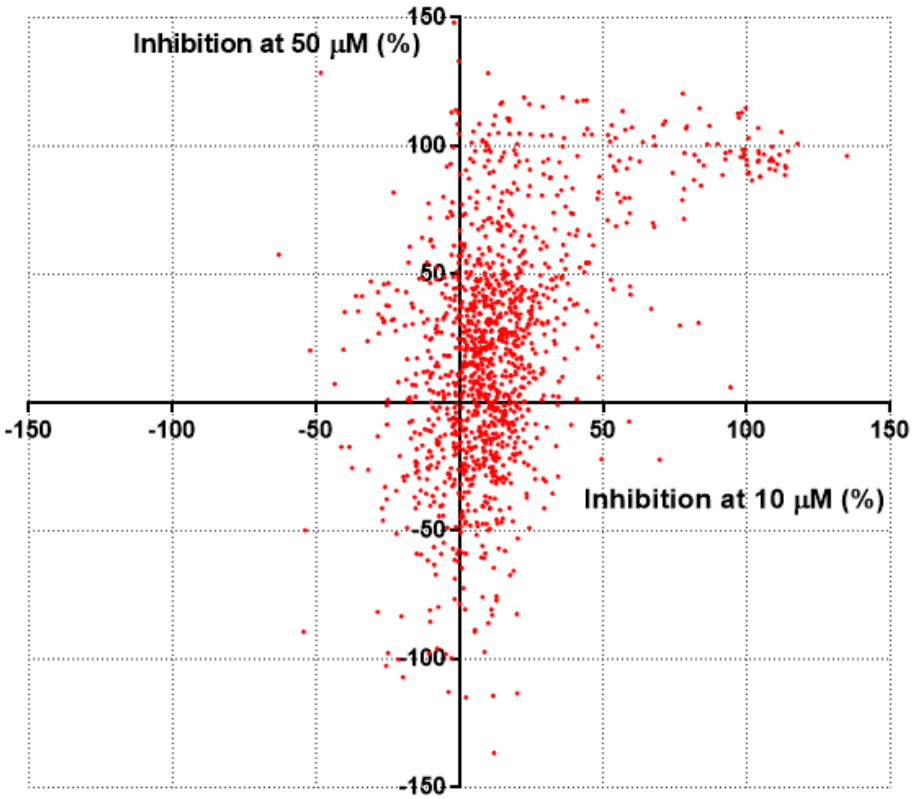

Figure 31. Correlation of inhibition (%) for each compounds screened at 50 µM and 10 µM. Weak positive correlation is observed (R^2 = 0.23, 95% CI 0.44 to 0.52).

a

Compound	n = 1	n = 2
UOS-00016616-001	2.95	2.64
UOS-00016782-001	6.27	5.07
UOS-00016783-001	7.51	11.84
UOS-00016804-001	5.33	10.03
UOS-00016817-001	4.99	4.47
UOS-00016819-001	1.04	2.66
UOS-00016820-001	1.4	3.03
UOS-00016844-001	3.82	7
UOS-00016859-001	15.67	>30
UOS-00016870-001	10.06	15.89
UOS-00016893-001	18.24	12.83
UOS-00016899-001	14.07	6.25
UOS-00016975-001	9.74	3.8
UOS-00017071-001	4.14	6.8
UOS-00017082-001	>30	>30
UOS-00017320-001	3.05	5.5
UOS-00017378-001	3.01	1.76
UOS-00017430-001	>30	>30
UOS-00017498-001	13.49	7.76
UOS-00017502-001	5.05	5.21
UOS-00017503-001	9.67	5.58
UOS-00017507-001	5.48	3.58
UOS-00017530-001	3.44	4.6
UOS-00017531-001	9.36	11.1
UOS-00017544-001	9.17	7.77
UOS-00017557-001	10.24	5.26
UOS-00017576-001	4.18	4.75
UOS-00017716-001	12.59	>30
UOS-00017718-001	4.21	2.87
UOS-00017721-001	>30	>30
UOS-00017724-001	3.01	7.99
UOS-00017727-001	3.96	2.11

Compound	n = 1	n = 2
UOS-00017766-001	17.43	19.83
UOS-00017767-001	10.14	10.53
UOS-00017768-001	2.62	3.84
UOS-00017770-001	10.9	8.71
UOS-00017771-001	18.77	13.21
UOS-00017772-001	>30	>30
UOS-00017773-001	15.59	13.1
UOS-00017774-001	>30	>30
UOS-00017785-001	16.65	15.91
UOS-00017787-001	>30	17.79
UOS-00017788-001	>30	18.67
UOS-00017790-001	15.46	16.39
UOS-00017791-001	>30	>30
UOS-00017792-001	16.2	14.04
UOS-00017793-001	13.29	13.73
UOS-00017795-001	14.91	14.24
UOS-00017798-001	8.89	16.14
UOS-00017799-001	2.96	2.98
UOS-00017800-001	9.5	9.82
UOS-00017808-001	7.07	15.73
UOS-00017846-001	7.25	8.94
UOS-00017851-001	5	7.63
UOS-00017907-001	14.94	13

b

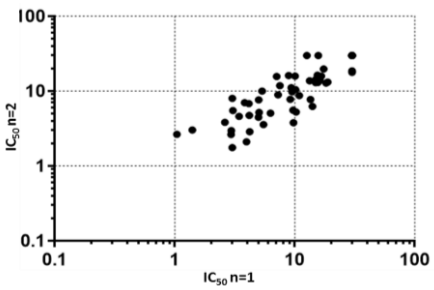

Figure 32. Potency of 'hits' from the 10 µM screen determined using the membrane potential assay. **a** Table of compound IC_{50} values calculated from a 5-point concentration-response curve. Each compound was run in duplicate. Grey = excluded, IC_{50} values of > 30 µM, orange = excluded, unstable moieties, blue = reordered compounds for follow-up studies. **b** Strong positive correlation of n=1 and n=2 compound IC_{50} values (R^2 = 0.71, 95% CI 0.75 to 0.90).

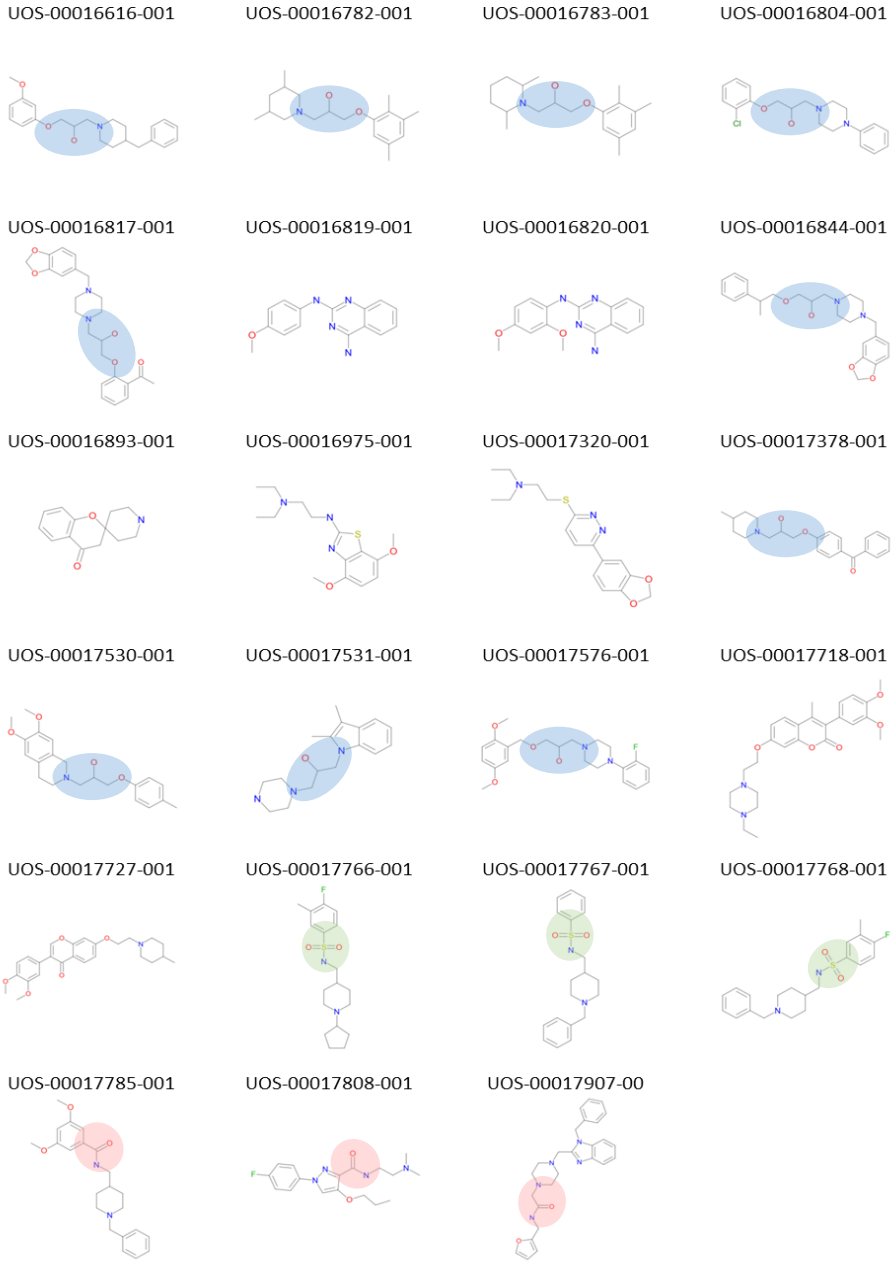

Figure 33. Chemical structures of 'hits' reordered for follow-up studies. Of the 55 'hits', compounds were excluded if they did not exhibit an IC_{50} values of > 30 µM using the MP assay, or if they possessed any unstable moieties. For the remaining 23 compounds which were reordered, structural similarities were observed: blue = aminopropanediol , red = acetamide , green = methanesulfonamide .

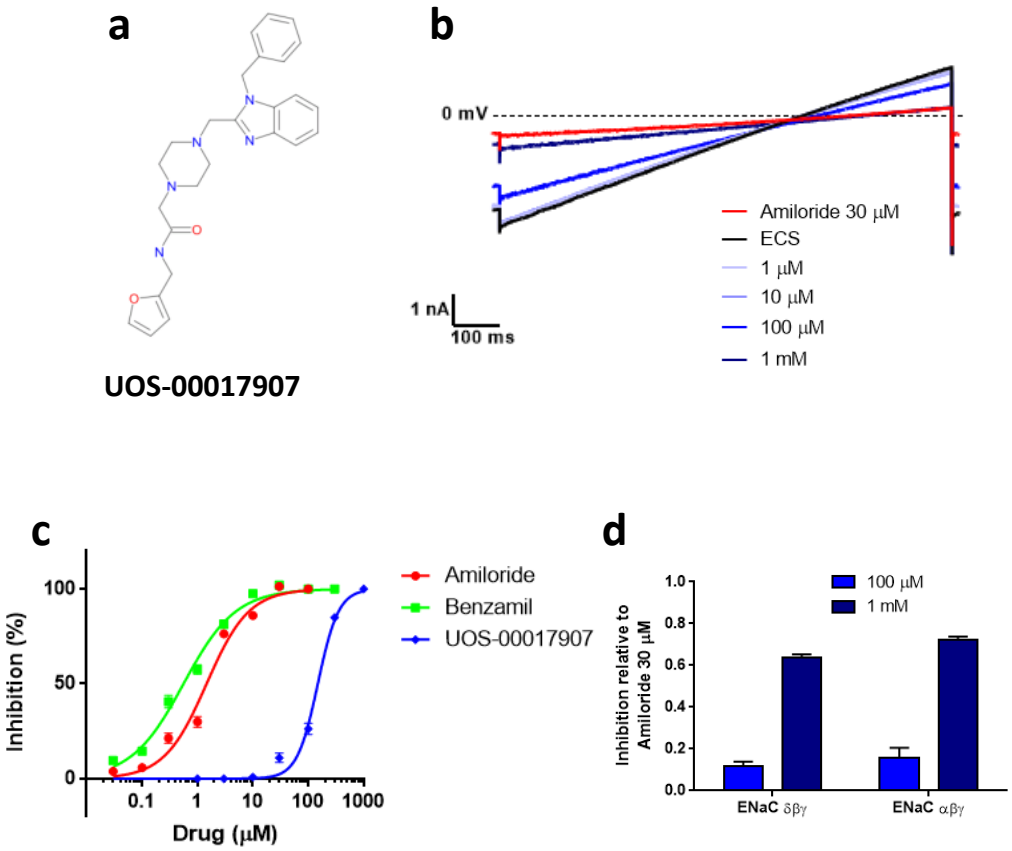

Figure 34. Potency and selectivity of hit compound, confirmed using patch clamp. a Chemical structure of hit compound, UoS-00017907. **b** Raw traces of amiloride-sensitive current when cells are ramped between -50 and +50 mV, over 1 s in the presence of ECS (black), 30 µM amiloride (red), or increasing concentrations of UoS-00017907 (blue). **c** Dose-response curves of amiloride (red), benzamil (green) and UoS-00017907 (blue) in HEK293 cells expressing the ENaC δβ*γ* channel (amiloride: IC_{50} = 1.46 ± 0.08 µM (n=3); benzamil: IC_{50} = 0.56 ± 0.03 µM (n=5); Uos-00017907: IC_{50} = 149.2 ± 5.01 µM (n=8)). **d** Inhibition of the two ENaC channels, relative to complete channel block by amiloride, by UoS-00017907 at 100 µM and 1mM.

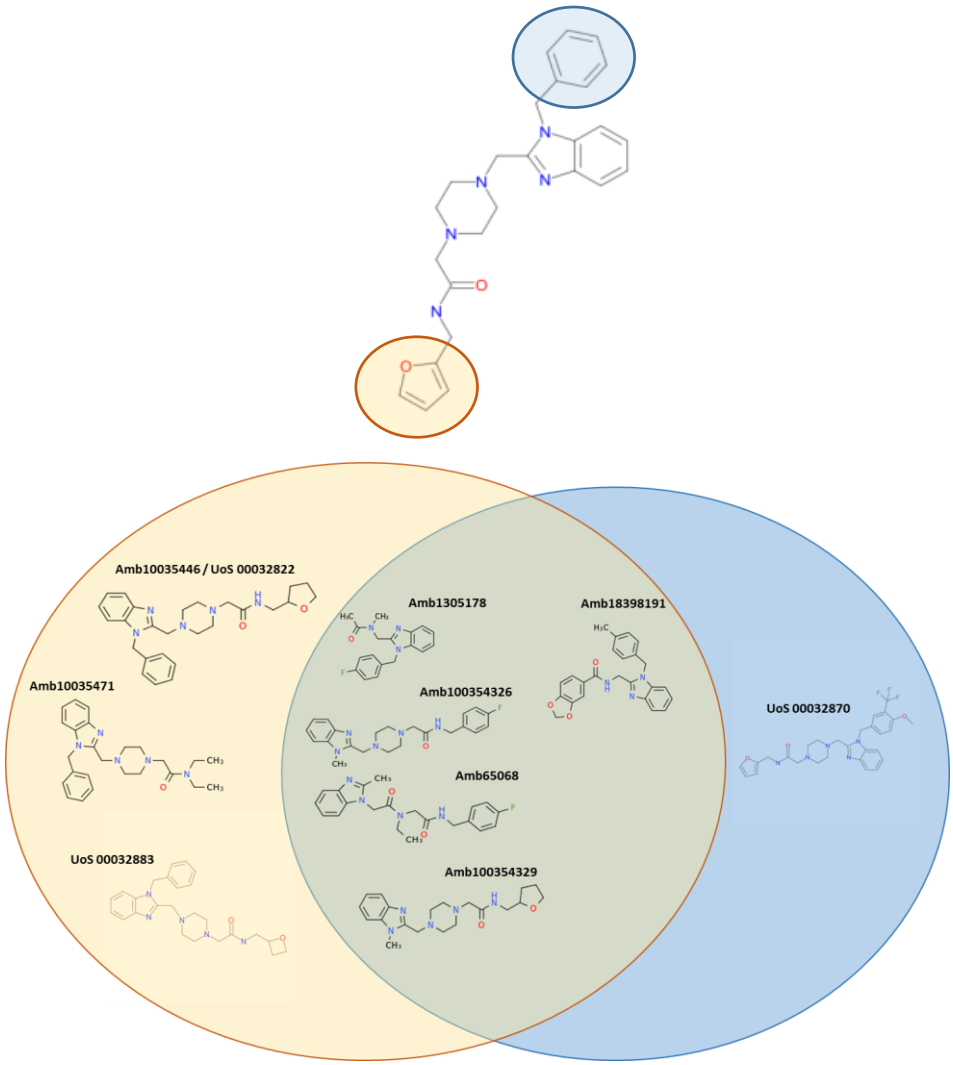

Figure 35. SAR study of hit compound using commercially available and in-house medicinal chemistry capabilities. Chemical structure of hit compound, UoS-00017907 (top) with a Venn diagram to represent the collection of analogues studied and whether they involved alterations made to the furan (orange), phenyl (blue) or both groups either side of the molecule's benzimidazole core.

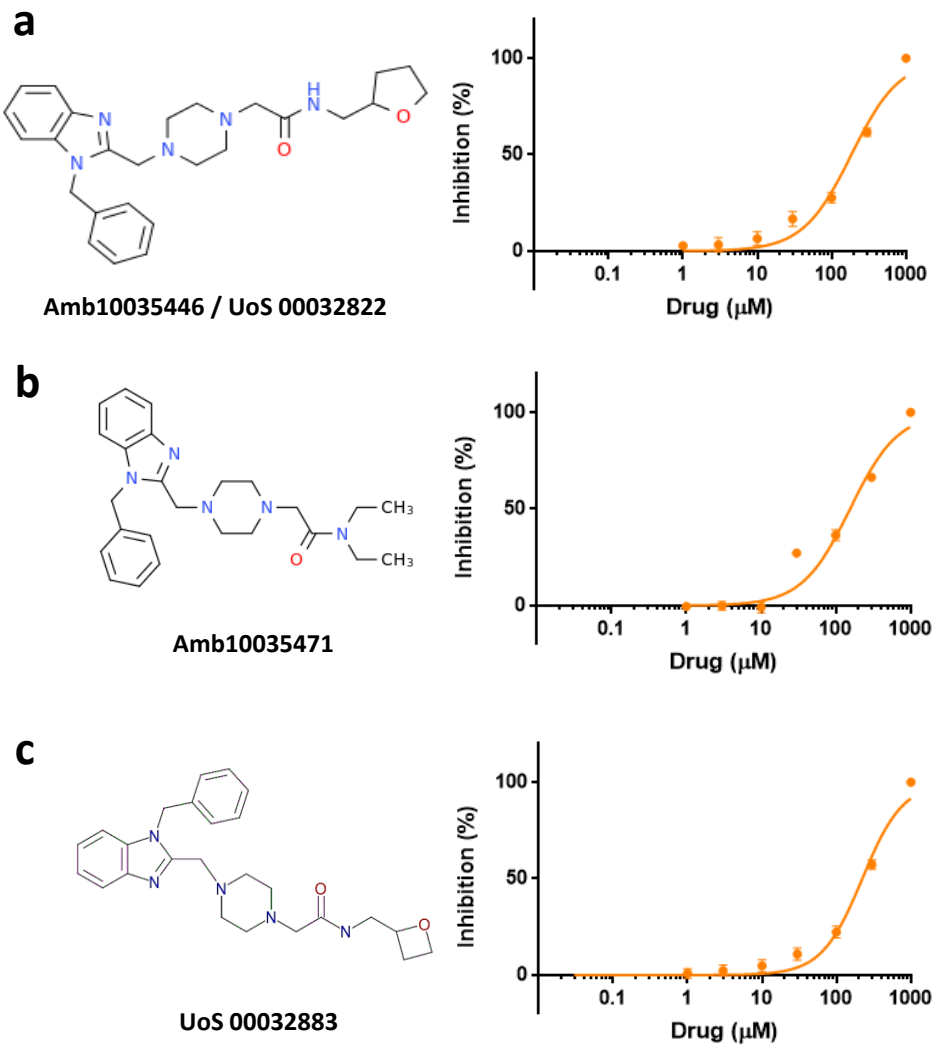

Figure 36. Potency of three analogues of UoS-00017907, which were still able to inhibit the ENaC δ channel. **a** Amb10035446 / UoS-00032822 (IC_{50} = 184.8 ± 11.8 µM (n=12)). **b** Amb10035471 (IC_{50} = 155.1 ± 9.9 µM (n=5)). **c** UoS-00032883 (IC_{50} = 223.1 ± 13.8 µM (n=5)).

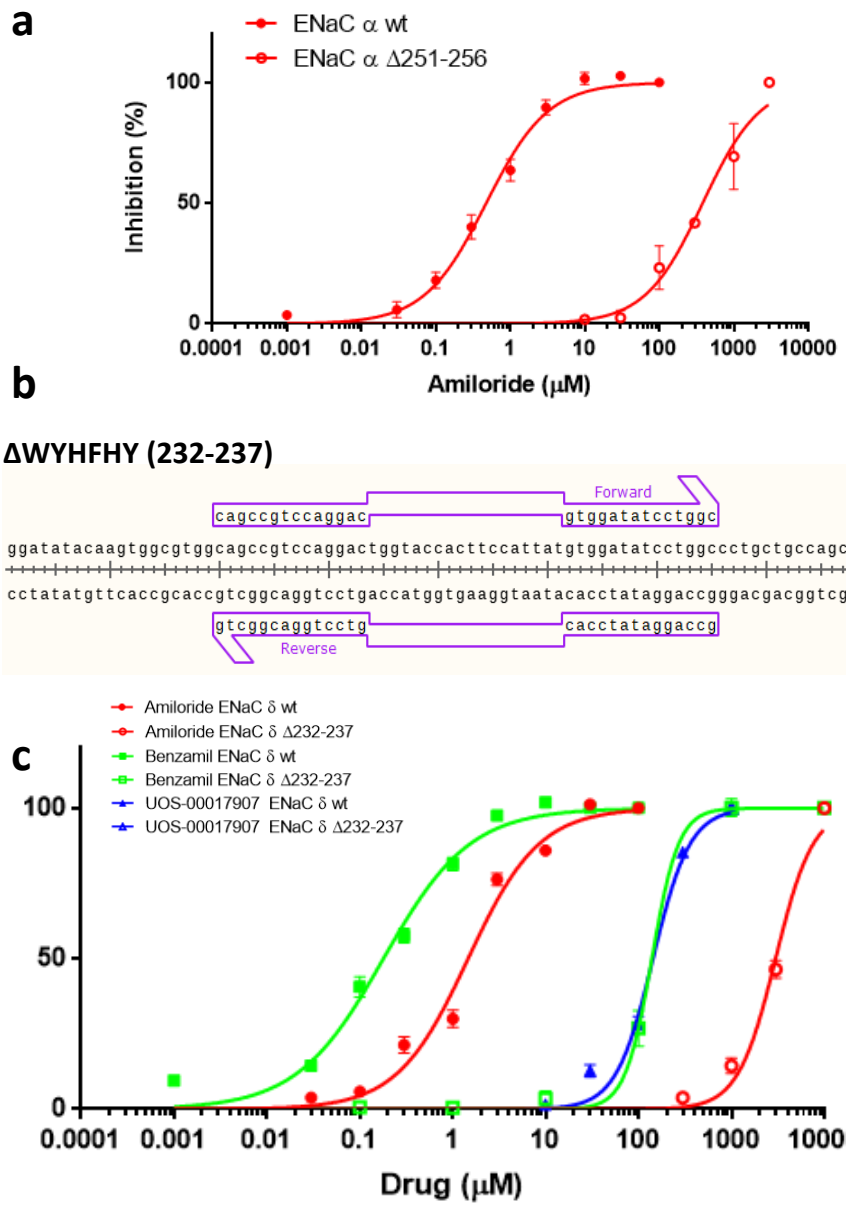

Figure 37. Effect of mutating the WYHFHY motif of the ENaC δ subunit on the potency of amiloride, benzamil and UoS-00017907. a The effect was first validated by mutating the homologous motif of the ENaC α subunit. Amiloride dose-response curve at the ENaC α channel containing the ENaC α wt and ENaC α Δ251-256 (WYRFHY motif) subunit. **b** The position of the base pairs, corresponding to the WYHFHY motif in the ENaC δ subunit with the forward and reverse primers used to introduce a deletion mutation to this subunit. **c** Dose-response curves of amiloride, benzamil and UoS-00017907 at the ENaC δ channel containing the ENaC δ wt and the ENaC δ Δ232-237 subunit.

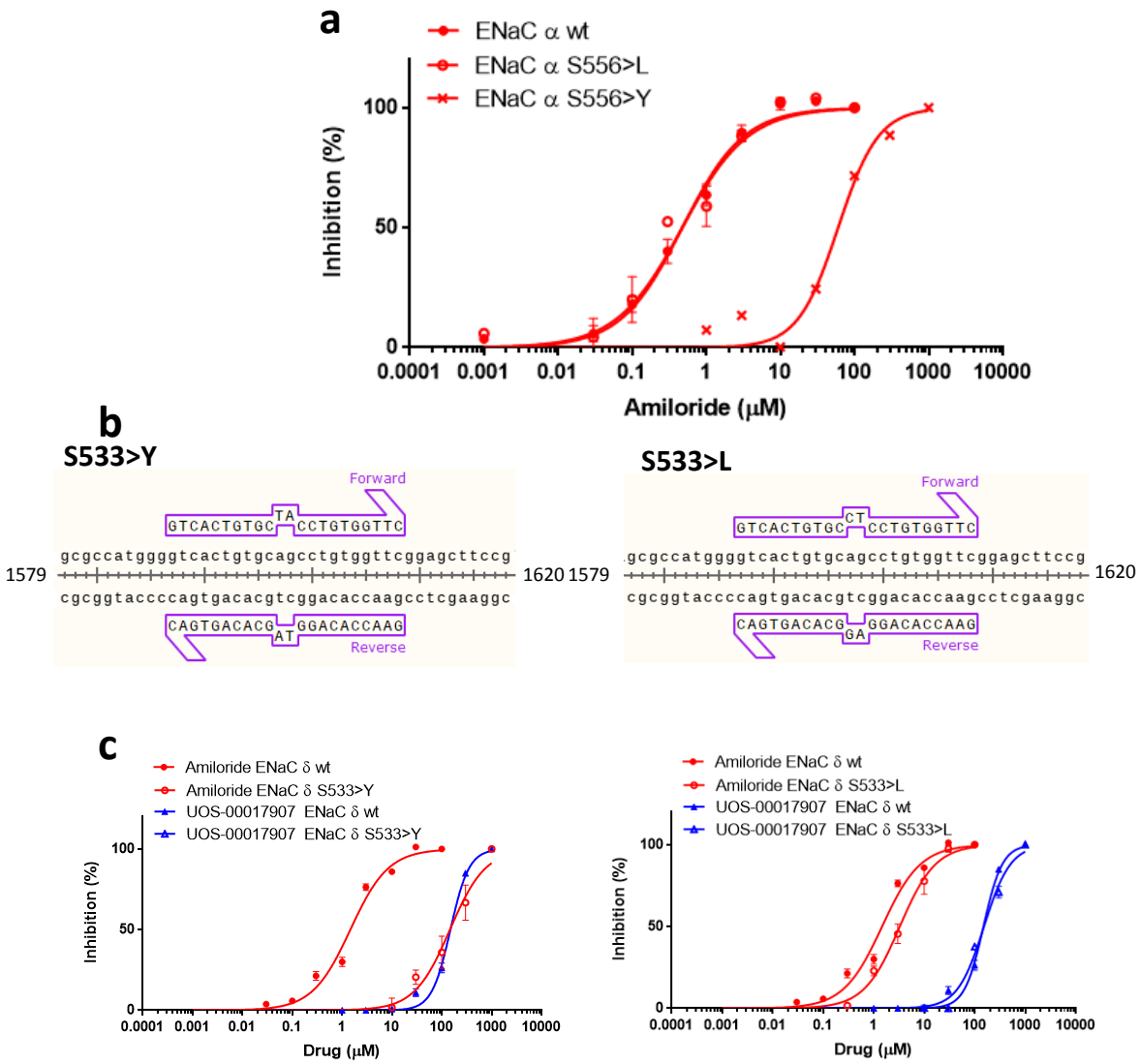

Figure 38. Effect of mutating the serine residue at position 533 of the ENaC δ subunit on the potency of amiloride, benzamil and UoS-00017907. a The effect was first validated by mutating the homologous serine residue at position 556 of the ENaC α subunit. Amiloride dose-response curve at the ENaC α channel containing the ENaC α wt, ENaC α S556>Y and ENaC α S556>L subunit. **b** The position of the base pairs, corresponding to the serine residue in the ENaC δ subunit with the forward and reverse primers used to introduce a single point mutation to either tyrosine (left) or leucine (right). **c** Dose-response curves of amiloride and UoS-00017907 at the ENaC δ channel containing the ENaC δ wt, ENaC δ S533>Y (left) and ENaC δ S533>L (right) subunit.

6

RESULTS: AUTOMATED ELECTROPHYSIOLOGY SCREEN

Chapter 6

6.1. Background:

6.1.1. Automated electrophysiology:

The patch clamp technique, first described by Neher and Sakmann (1976), remains the gold standard for studying ion channel function as it provides high quality and physiologically relevant data of ion channel function at the single cell or single channel. For drug discovery programs, the automation of this technique over the last 10 years now permits electrophysiology to be used as a frontline primary screening technology. Pivotal to this was the development of a planar glass chip containing perforations homologous to the hole at the end of a glass patch pipette, whereby successful recordings of cells or bilayers could be performed (Fertig, et al., 2002). Initially the glass substrate used was quartz for its ability to decrease the electric field as a poor conductor; however the glass now used more commonly in both automated and conventional setups is borosilicate, due to its low capacitance and noise. Systems using this planar patch clamp either provide a GΩ seal quality of data comparable to a conventional recordings, or they rely on the use of a perforated patch clamp technique that increases throughput without compromising data quality and pharmacology.

As with conventional patch clamp, the application of negative pressure can be used to attract a cell to the perforation, followed by a high-resistance seal formation between the glass and the cell membrane, and then rupturing of the membrane to gain electrical access to the inside of the cell. The planar design helps to avoid any need for the skilful microscope and micromanipulator handling, allowing these step to become fully automised. Although the glass chips initially contained one aperture, chips

containing multiple holes are now routinely used to allow for multiple recordings per experiment to increase throughput.

A range of planar patch clamp systems that allow for single cell (e.g. Port-a-Patch, Nanion Technologies), medium throughput (e.g. IonWorks HT/Quattro™, Molecular Devices; QPatch, Sophion Bioscience), and high throughput (e.g. Qube, Sophion Bioscience) recordings are available. Each differs in the types of experimental protocols, throughput and data quality that they offer, for which the IonWorks Quattro™ and QPatch will be the focus of this Chapter.

6.1.2. The IonWorks Quattro™ platform:

The IonWorks platform was the first commercially available automated electrophysiology platform to gain widespread utility that utilised the planar patch clamp technique (Fertig, et al., 2002) before being superseded by the IonWorks Quattro™. This second generation automated electrophysiology system, produced by Molecular Devices (Sunnydale, USA), is capable of generating multiple of thousands of data points per day. It is a low resistance, discontinuous recording system that can measure from 96 or 384 wells in parallel.

The system operates in two modes, single-hole (HT) mode and population patch clamp™ mode (PPC). HT mode records from one cell per well whereas PPC mode, currents from up to 64 cells per well are measured and reported as an average. PPC mode helps to increase the success rate and decrease well-to-well variability (Finkel, et al., 2006). For these reasons, this platform is ideally suited to transiently expressed channels, like the ENaC channel, which display variable expression levels from cell to cell.

The use of plastic material in the plates has been seen to interfere with the potencies of lipophilic compounds, reporting them as less active (Gillie, et al., 2013). However, good assay optimisation has enabled IonWorks assays to replicate compound potencies obtained with manual patch clamp electrophysiology within acceptable levels (Bridgland-Taylor, et al., 2006). The major limitation for this system is its inability to establish GΩ seals.

6.1.3. The QPatch platform:

The QPatch, developed by Sophion Bioscience (Copenhagen, Denmark) aims to address the need for GΩ levels of seals to deliver precision and accuracy comparative to manual electrophysiology recordings, but compromises its throughput (Mathes, et al., 2009). The system has a number of unique features. Firstly, the system includes an automated cell preparation station, permitting several hours of unattended operation and therefore data collection outside of normal working hours. Secondly, the QPlate or multichannel electrode arrays, includes glass-coated microfluidic channels, which limit compound adsorption for increase accuracy in the reporting of compound potencies. Furthermore these channels allow for a rapid solution exchange time (50–100 ms), making them amenable for ligand-gated ion channel investigations, and require only very small volumes of compound (~ 5 µL per addition), lowering the cost per run.

Patch clamp recordings with the QPatch are able to recapitulate the quality of conventional patch clamp. Since the introduction of the QPatch 16, which acquires 16 individual recordings per run, the 48-channel (QPatch HT) upgrade extends its throughput by three-fold without sacrificing data quality. Finally the QPatch HTX takes

this one step further by recording from 48 wells, with each well containing 10 apertures for a combined current recording from 10 cells per well, for each run to maintain throughput and further reduce variability.

6.2. Methods:

6.2.1. IonWorks Quattro™ assay:

HEK293 ENaC β*γ* cells were seeded in T175 cm^2 the day before transduction. Cells were transduced overnight with the BacMam baculovirus for assay (Section 2.2.8.2.).

During assay development, optimisation of buffers, cell preparation and assay protocol parameters was assessed using a compound plate containing 8-point amiloride and benzamil concentration-response curves (300 µM top concentration, 1 in 3 dilution curve) in ECS at 3-times the test concentration. The left half of the compound pate contained amiloride, and the right half contained benzamil.

Immediately prior to screening, all test compounds (Section 2.1.5.2 and 2.1.5.3.) were suspended in the required volume of ECS in their 96-well (CUTE Ion Channel library) or 384-well (Diverse 12K library) source plate at 3-times higher than the test concentration (Section 2.2.8.1.). Controls (100 µM amiloride, 100 % channel block; 3 µM amiloride, 50 % channel block; ECS (v/v) 0.5 % DMSO, vehicle; and an 8-point amiloride concentration-response curve, 300 µM top concentration, 1 in 3 dilution curve) were added to the remaining wells at 3-times the test concentration (see plate layout; Section 2.2.3.2.). DMSO concentration was kept uniform across the plate. A second compound plate was prepared to 4-times the test concentration (100 µM amiloride) for both the 96- and 384-well screens.

On assay, cells were harvested in ECS (Section 2.2.8.2.) and loaded into the cell boat for immediate use. Whole-cell currents were recording using the IonWorks v2.0.3.4 (Molecular Devices) software (Section 2.2.8.4.). Cells were ramped between -100 mV and +30 mV over a 100 ms period after amphotericin B treatment pre-compound addition, post compound addition 1, and post-compound addition 2 (Section 2.2.8.3.).

Data from assay development steps were plotted using GraphPad Prism version 6.04 for Windows (GraphPad Software, La Jolla California USA). All data are reported as mean ± SEM (number). Screening data were exported from the IonWorks v2.0.3.4 software, uploaded onto the Dotmatics database (Hertfordshire, UK) and analysed using Vortex v2015.11.46033 [© Dotmatics Ltd. 2007-2015] (Section 2.2.8.4.).

6.2.2. The QPatch HTX assay:

HEK293 ENaC β*γ* cells were seeded in T175 cm^2 the day before transduction. Cells were transduced overnight with the BacMam baculovirus for assay (Section 2.2.9.2.).

All test solutions (with or without compounds) were held in glass inserts placed in 96-well plates. Immediately prior to assay, 3 concentrations of each test compound (top concentration of 30 µM) (Section 2.2.9.1.) were loaded into the 96-well plate (see plate layout; Section 2.2.9.1.). The DMSO concentration was maintained across every well. The reservoir was filled with ECS, ICS, and 100 µM amiloride in their respective compartments (Section 2.2.9.1.).

All experiments were conducted in the unattended mode of the QPatch, which automatically executes cell wash, solution priming, delivery and positioning of cells to measurement sites, gigaseal and whole-cell formation, voltage clamp, liquid (control,

reference, test compound, and wash solutions) applications to each cell. On assay, cells were harvested in serum-free media containing 100 µM amiloride (Section 2.2.9.2.) and after 30 min under constant agitation, cells were loaded into the on-board centrifuge at a density of 4-6 × 10^6/mL. Newly harvested cells were used for each run.

Whole-cell currents were recording using the QPatch Assay Software v5.6.4 (Sophion Bioscience). Cells were ramped between -100 mV and +30 mV over a 500 ms period (Section 2.2.9.3.) throughout the application protocol. Data were exported and plotted using GraphPad Prism v7.0 (Section 2.2.9.4.). All data are reported as mean ± SEM (number).

6.2.3. Hit confirmation using patch clamp:

Follow-up studies of compounds that show dose-dependent activity at the ENaC δ channel were performed using the patch-clamp technique (Section 2.2.6.). Cells were transduced 24 hr prior to patching and were harvested in serum free media (Section 2.2.6.2.). Cells were kept for up to 4 hr in a reservoir under constant agitation. Standard solutions were used (Section 2.2.6.1.), and test compounds (Section 2.1.5.3.) were prepared from stock (10 mM in 100 % (v/v) DMSO) immediately prior to assay in fresh ECS buffer. To each well of the Dynaflow® Resolve System (Figure 28.) 80 µl of ECS, vehicle control (ECS with standardised DMSO), positive control (30 µM amiloride) or test compound were loaded. The DMSO concentration was kept at 0.3 %.

Whole-cell recording was performed using the Axon™ pCLAMP® 9 Software. Cells were clamped at -30 mV throughout recording. Every cell was exposed to the vehicle and the positive control before testing any compound. Cells were washed out with

ECS between each test compound. Data were analysed using Axon™ pCLAMP® 9 Software (Section 2.2.6.4.) and plotted using GraphPad Prism v7.0.

6.3. Results:

6.3.1. Assay development of an IonWorks Quattro™ automated electrophysiology assay for the ENaC δ channel:

6.3.1.1. Extracellular buffer:

The ICS used for the ENaC δ assay was potassium gluconate-based, as per the published paper describing an IonWorks ENaC α assay (Chen, et al., 2015). Here, Chen, et al. used a sodium gluconate (NaGluc)-based ECS. For ease of use during screening with the IonWorks Quattro, PBS (+/+), which required no preparation, was compared to the NaGluc-based ECS, in single-cell recording (HT) mode. It was immediately apparent during priming and cell sealing steps of the experiment that the combination of gluconate intra- and extra- cellular solutions should be used for all future work (number of 'no seal' wells: NaGluc = 3/384; PBS+/+ = 141/384; Figure 39.a).

It was also apparent that optimisation was required when observing the size of the amiloride-sensitive currents (Figure 39.b), regardless of using gluconate-based buffers (amiloride-sensitive current amplitude= 191.7 ± 0.03 pA (n=384)). This was not comparable to previously described currents in the nA range using conventional patch clamp (Chapter 3.). Looking at the distribution graph of the amiloride-sensitive current amplitude (Figure 39.c) it was clear that although a few wells had a good level of functional ENaC expression, there was very low ENaC expression in the majority of

wells, with ~50 % of wells reporting an ENaC current of less than 100 pA (25 % percentile = -24 pA; median = 106 pA; 75 % percentile = 339 pA).

6.3.1.2. Optimising the MOI of a new baculovirus stock:

Given the small current amplitudes and low ENaC expression levels observed during buffer optimisation experiments, a new batch of baculovirus was used in all subsequent experiments. Before progressing, transduced cells were run in parallel to 3 other populations of cells: untransduced HEK293 cells, untransduced HEK293-ENaC β*γ* cells, and HEK293 cells transduced with the ENaC δ subunit. Amiloride-sensitive currents were only present in the cells expressing all three ENaC subunits (current amplitude = 372 ± 83 pA (n=96); Figure 40.a), which was consistent with our findings using conventional patch clamp (Chapter 3.).

On titration of the virus MOI, the amiloride-sensitive current amplitudes were overall higher than they had been with the previous baculoviral batch, and the highest current amplitudes reported using an MOI 10 (538 ± 67 pA (n=96); Figure 40.b). The current size decreased upon higher viral MOI of 25 and 50, in addition to a reduction in the mean seal resistances at these higher MOIs (MOI 5: 42.95 ± 2.74 MΩ (n=96); MOI 10: 40.72 ± 2.65 MΩ (n=96); MOI 25: 30.19 ± 2.13 MΩ (n=96); MOI 50: 37.23 ± 1.91 MΩ (n=96); Figure 40.c). For all subsequent experiment, HEK293-ENaC β*γ* cells were transduced with the ENaC δ subunit at an MOI 10.

6.3.1.3. 'Half-at-once' vs. 'All-at-once':

The scanning parameters on the IonWorks allows you to select how much of the PatchPlate™ to apply compound to before scanning. The options available include one eighth, one quarter, half or the entire plate. The compound is added to the chosen

fraction of the plate and scanned before the successive addition/scanning cycle, until the entire plate has seen compound and been scanned.

Using dose-response plates containing amiloride and benzamil, and the 'half-at-once' scan in HT mode, it was observed that there was a pattern of 'no seal's across the PatchPlate™ which corresponded to the second half-plate addition (Figure 41.a). This meant no current was measured, interfering with the reported 'block' by amiloride. This can be seen when plotting the dose-response curves (Figure 41.b), whereby the data points for the lowest concentrations for amiloride show two populations of data points, those reporting the correct inhibition (%) values, and those reporting complete channel block (Figure 41.b, top). Changing the scanning parameters to an 'all-at-once' scan greatly improved this problem and allowed for the determination of amiloride's potency (IC_{50} = 7.04 ± 2.59 µM (n=24); Figure 41.b, bottom).

6.3.1.4. Single cell recording vs. population patch clamp:

The IonWorks Quattro™ technology can use 64 holes in the base of each PatchPlate™ well (PPC mode) as opposed to just a single hole (HT mode). This modification increases the probability of achieving a successful recording from each well and in turn the throughput of the assay.

The 'all-at-once' scan in PPC mode produced much less variable data than in HT mode (IC_{50} = 2.10 ± 0.15 µM (n=24); Figure 42.a), and seal resistances (Figure 42.b) and amiloride-sensitive current amplitudes (Figure 42.c) were also less variable (HT mode: seal resistance = 18.29 ± 0.60 MΩ (n=384), current amplitude = 1.00 ± 0.06 nA (n=384); PPC mode: seal resistance = 13.11 ± 0.07 MΩ (n=384), current amplitude = 0.93 ± 0.01

nA (n=384)). This suggested that the IonWorks Quattro™ technology was more adequate to set up a robust ENaC screening assay.

6.3.1.5. Cell density in cell boat:

Cell density needed to be optimised to balance the risk of ligand depletion whilst retaining good quality seals. The effect of cell densities between 0.5 and 2 x 10^6/mL was assessed. Current amplitudes (Figure 43.a) and seal resistances (Figure 43.b) were unaffected at densities between 1-2 x 10^6/mL, however at 0.5 x 10^6/mL both parameters were notably lower. Amiloride potency was unaffected by cell density (Figure 43.c). Subsequent experiments were all performed at a cell density of ~2 x 10^6/mL.

6.3.1.6. DMSO tolerance:

The DMSO tolerance of the assay was assessed to ensure the compounds could be well solubilised without causing cell toxicity. The effect of DMSO on seal resistances, current amplitudes, and pharmacology, at a range of 0.1-5 % (v/v), was determined.

Seal resistances (Figure 44.a) were unaffected but current amplitudes (Figure 44.b) were decreased a DMSO concentration of 5% (0 % DMSO = 472 ± 214 pA (n=48), 5 % DMSO = 54 ± 224 pA (n=48). Amiloride potency was unaffected within this range (Figure 44.c). As this assay would be run within a DMSO range of 0.4-2 % (v/v) to allow for the compounds to be tested at 40 µM, these findings confirmed that the assay would be unaffected up to 2 % DMSO.

6.3.1.7. Compound incubation time:

On implementation of a second compound addition (complete amiloride block) to the assay protocol, the minimum incubation time for the first compound had to be increased. This was to allow for the pipette to cycle through the dispensing, mixing and washing sequence before completing the second compound addition. Whereas all assay development experiments up to this point had included a single compound addition, with an incubation time of 180 s, the minimum incubation time for 2 compound additions was 223 s.

To ensure the increased compound incubation time had no effect on pharmacology reported for the compounds, the effect of repetitive addition of amiloride was tested using the QPatch 16 (Figure 45.a), and the IC_{50} of amiloride was determined using the IonWorks assay for three different incubation times (Figure 45.b). Successive additions of 3 µM amiloride on the QPatch showed no change in the level of amiloride block, however the potency of amiloride in the IonWorks assay was marginally right-shifted with the shorter 180 s incubation time, with no difference in potency report with a 223 s and 300 s incubation (180 s: IC_{50} = 2.10 ± 0.15 µM (n=24); 223 s: IC_{50} = 0.64 ± 0.06 µM (n=48); 300 s: IC_{50} = 0.54 ± 0.07 µM (n=48)). This slight decrease in potency using 180 s was only just outside of the accepted ½-log error for IC_{50} values, suggesting that 223 s compound incubation for screening purposes would have no real effect on the reporting of 'hits'.

6.3.1.8. Pharmacological validation:

IonWorks Quattro™ data for both amiloride and benzamil at the ENaC δ channel (amiloride: IC_{50} = 2.10 ± 0.15 µM (n=24); benzamil: IC_{50} = 0.12 ± 0.01 µM (n=24); Figure 46.) was consistent with both experimental data using conventional patch clamp

(Chapter 3.) and the literature (Yamamura, et al., 2006). This gave confidence that the reporting of false positives and negatives would be minimised during screening.

6.3.2. Identification of potential ENaC δ inhibitors using the IonWorks Quattro™ assay:

Two libraries of compounds were screened using the IonWorks Quattro™ platform in either a 96-well format (CUTE Ion Channel library, Life Chemcials) or 384-well format (Diverse 12k library, BioAscent). All compounds were prepared immediately prior to assay to be tested at a final screening concentration of 40 µM. Controls were included in every plate and at the start of each screening day the second compound plate, containing a uniform concentration of amiloride (test concentration = 100 µM), was prepared.

A total of 9321 compounds were tested screened against the ENaC δ channel at 40 µM and analysed two ways. Initially data were processed using both compound additions, calculating the reduction (%) of the inward current after test compound addition, relative to the reduction (%) in current on 100 µM amiloride addition. Wells were excluded from analysis if the second compound addition of amiloride failed to decrease the inward current by at least 25 % of the uninhibited inward current. Plates were repeated if the control wells did not give the expected data.

Assay quality remained high across all plates (all Z' values > 0.5; Figure 47. b) and the distribution of sample data was narrow (Sample standard deviation ($SD_{samples}$) = 11.791 (n = 9321); Figure 47. a). 'Hits' were considered as any compound reported as giving a positive inhibition of greater than 3-times the standard deviation of the samples (=

35.34 %). This reported a 0.25% hit rate, identifying 23 compounds to be considered as giving a significant level of inhibition, relative to that by 100 µM amiloride.

As 23 compounds was a relatively small number to progress through to validation studies, the data was reanalysed using data from the first compound addition only. The reduction (%) of the inward current after test compound addition was calculated and similarly, plates were repeated if the control wells did not give the expected data. Assay quality remained high across all plates (all Z' values > 0.5; Figure 48. b) and the distribution of sample data was still narrow ($SD_{samples}$ = 9.186 (n = 9388); Figure 48. b). This analysis method reported a 0.49% hit rate (≥ 27.56% inhibition), identifying 46 compounds for further investigation.

On comparison of the data obtained from the CUTE Ion Channel library screened in the membrane potential assay and in the IonWorks Quattro™, there is no correlation between the data (R^2 = 0.0004, 95% CI -0.07 to 0.04; Figure 49.). 'Hits' identified from the IonWorks assay using both analysis methods were collated, and 38 were commercially available to reorder for validation studies using the QPatch HTX.

6.3.3. Hit confirmation:

The aim was to perform hit confirmation using the QPatch HTX platform (Sophion Biosciences. Preliminary studies on the QPatch were performed on the QPatch 16 at ApconiX, Alderley Park, UK (Figure 50.). The assay performance was good, with 100 % of wells achieving whole-cell configuration, and 13 out of 16 wells recording a complete dose-response curve for amiloride. Stable and reproducible amiloride-sensitive currents were recorded (Figure 50.a) and there was good consistency in the amiloride potency reported from well to well. The potency of amiloride was

consistence with values using the IonWorks assay, conventional patch clamp (Chapter 3.), and the literature (Yamamura, et al., 2006) (IC_{50} = 4.05 ± 0.28 µM (n=13); Figure 50.b).

For convenience, the remainder of the QPatch experimental work was performed at the Sussex Drug Discovery Centre (University of Sussex), however the data collected at ApconiX could not be replicated at Sussex. Initial experiments at Sussex aimed to generate a dose-response curve for amiloride, using the same protocol that had been used at ApconiX (Figure 51.). Although some wells gave data that were consistent with what had been measured at ApconiX (amiloride: IC_{50} = 2.29 ± 0.84 µM (n=2); benzamil: IC_{50} = 0.33 ± 0.09 µM (n=2) Figure 51.c), the assay performance was below acceptable levels. Although a high percentage of wells were able to achieve whole-cell configuration, only a low percentage of wells completed the run, of which the data were extremely variable in those that did. Figure 52. is representative of the instability that was observed during the assay. Despite whole-cell configuration being achieved, almost all of the cells were unstable, which reflected a loss of seal resistance during the course of the experiment.

Due to a lack of time to re-optimise this assay at Sussex, the hit compounds from the IonWorks Quattro™ assay were taken into conventional patch clamp studies (Figure 53.). Cells were clamped at a holding potential of -30 mV to insure a submaximal inward Na^+ current, before exposure to 30 µM amiloride to establish the size of the ENaC current, followed by subsequent exposure to the test compounds (Figure 53.a). 17 of the compounds were tested at 30 µM (chemical structures are found in Appendix

1.), of which 8 gave a positive inhibition (%) of the ENaC current, 4 of which were over 30 %. 21 hits remain to be tested.

6.4. Discussion:

A 384-well automated electrophysiology assay using IonWorks Quattro™ technology has been developed, which can assess for ENaC δ channel inhibition in HEK293 cells. The IonWorks Quattro™ assay allows for the rapid and robust assessment of a relatively large number of compounds in a quantitative and sensitive manner. Pharmacological validation showed that data were in agreement with our own findings of those using the gold standard conventional patch clamp, which had not been possible to replicate using the membrane potential assay.

The assay was developed so as it could be run on 4 days per week, with up to 7 runs per day, allowing for an average weekly screen of up to 9000 compounds. The medium to high- throughput capability of this assay, with the reduced possibility of false-positive data, has been exploited by pharmaceutical companies. Automated electrophysiology is often put at the forefront of screening campaigns, replacing other technologies for use as a primary screen. However, the main drawback remains the high cost of consumables, when compared to the membrane potential assay.

Important considerations during assay development included the buffer composition, the IonWorks scanning parameters, single cell or population patch clamp mode and DMSO tolerance. Although literature had recommended gluconate-based buffers both intra- and extra-cellularly (Chen, et al., 2015), initial experiments tried to simplify these buffers. They revealed that using a combination of a potassium gluconate (KGluc)-

based ICS with PBS (+/+) as the ECS, a large number of well were reported as 'no seals'. A 'no seal' is defined as having a seal resistance of less than 20 MΩ or greater than 1500 MΩ. The primary ion constituent of PBS (+/+) is sodium chloride (NaCl) at ~140 mM (Dulbecco & Vogt, 1954), whereas the gluconate-based ECS contained 120 mM NaGluc, and only 20 mM NaCl. The inability to form high resistance seals can be attributed to the differences in the main ionic species of the buffers.

K Gluconate-based ICS is used for stability of recordings as it blocks certain K^+ channels which may be endogenously expressed (Velumian, et al., 1997). Pairing this with a NaCl-based ECS results in a large difference in chloride concentration across the cell membrane. This causes a large liquid junction potential to form at the tip of the micropipette, or in the case of the IonWorks, at the opening of each aperture of the PatchPlate™. A liquid junction potential arises between two solution that are in contact, have ions present at different concentrations and contain ions of different mobilities (Demirel, 2014). This is only a consideration before a high resistance seal is formed, whereby the two solutions are no longer in direct contact. When two solutions are in contact, ions will move down their concentration gradients. In the case of a NaCl-based ECS with KGluc-based ICS, among the anions, the Cl^- will be more mobile than the gluconate in moving into the pipette. If these are not corrected for on the IonWorks system, it can result in absolute voltage errors and poor performance (Molecular Devices, 2005). Therefore upon cell addition, as no correction was specified, this could has caused the reporting of 'no seal's. The pairing of gluconate-based buffers both inside and out worked well, and therefore buffers were not experimented with any further.

This platform was amenable for use with BacMam technology to reconstitute functional ENaC channel. Although transient expression of recombinant protein is often met with low reproducibility, heterogeneity and high variability (Hopkins, et al., 2012), the option of PPC mode on the IonWorks reduces data variability by averaging currents from 64 cells in every well. This in turn increases the usable number of wells, reduces the number of lost data point, overall increasing the assay throughput. The platform also enables two compound additions into each well. As with the membrane potential assay, a double-addition protocol was implemented to include an in-well control (maximum concentration of amiloride) which was used to normalise the response of each well to the test compound to its response upon complete amiloride block of ENaC. This step again acted to reduce the variability of the data.

The IonWorks Quattro™ screen performed with HEK293-ENaCβ*γ*, was robust and reproducible, identifying 38 compounds, which showed a significant inhibition of the ENaC δ channel at 40 µM. The compound libraries selected for screening included, firstly those compounds which had already been screened through the membrane potential assay (CUTE Ion Channel library, Life Chemicals), to ensure compounds had not missed, and a much larger Diverse 12k (BioAscent) to give higher chance of identifying new and novel series' of ENaC blocker. The hit rate of the IonWorks assay was much lower than had been for the membrane potential assay, owing to the decrease in the number of false positives reported using patch clamp (Yu, et al., 2016).

Validation of compound activity was due to be performed using a second automated electrophysiology platform, the QPatch (Sophion Bioscience). This bridges the gap between conventional patch clamp and higher throughput technologies such as the

IonWorks Quattro™ (Mathes, 2006). Although preliminary experiments using the QPatch 16 at ApconiX had been promising it terms of GΩ seal formation and pharmacological validation with amiloride, trying to replicate this on an equivalent machine at the SDDC was unsuccessful. Seal formation and achieving whole-cell formation remained effective, with high success rates aided by the presence of amiloride in the ECS solution throughout these steps. Amiloride was used both during transduction and in the seal and whole-cell formation to block the constitutively active ENaC at the membrane, preventing toxicity and stabilising the membrane (Chen, et al., 2015). Amiloride also readily dissociates from ENaC (Kellenberger, 2003) and can therefore be washed off before the test compound is applied. Unfortunately at the SDDC, the recordings were unstable over time, preventing the measurement of compound activity on the ENaC current.

Several elements of the assay were changed to try and improve the stability of the currents. Firstly, parameters surrounding the cell culture and preparation were investigated. It is well documented in any cell-based assay optimal cell preparation is key (Maddox, et al., 2008). The MOI of the virus was lowered to ensure the driving force of Na^+ into the cell was not too great; the cells were given a longer period of recovery post-harvest to ensure cells were not affected by treatment with TryplE Express or membrane shearing that may results from pipetting; and finally the ECS was altered to maintain the same sodium concentration (140 mM) but in a ratio of NaCl to NMDG (20 mM NaCl, 120 mM NMDG) to similarly reduced the driving force of Na^+. None of these showed any improvements to the assay.

Other areas that were investigated included the DMSO concentration. The concentration of the test compound was lowered to in turn reduce the DMSO concentration, and the osmolarity of the ECS with DMSO of the same concentration of the test compound was measured. Although DMSO tolerance on the cells had already been investigated, the presence of DMSO in ECS can alter the osmolarity of the solution (Sandborn, et al., 1975). The balance in osmolarity between the ICS and ECS solution is vital to preventing cells and organelles from either swelling or shrinking (Mollema, 2003). Adjustments, using sucrose, were made to balance the ICS osmolarity to the ECS containing DMSO. Neither of these two changes improved the assay.

Due to a lack of time, and the cost per plate of the QPatch, the assay was not pursued any further. Although it had been demonstrated at ApconiX that, using the cell line and BacMam technology for transient ENaC expression, it was possible to successfully record stable and robust ENaC currents, more optimisation at the SDDC was required in order for the hit compounds from the IonWorks assay to be validated by this means. Consequently, the interrogation of the 38 compounds by conventional patch clamp was pursued.

Initial observation of 17 of the 38 compounds showed a number of the compounds which inhibited the amiloride-sensitive current. This work demonstrates a far greater translation of hits from the IonWorks Quattro™ assay into conventional patch clamp, compared to the membrane potential assay. In the immediate future, the remaining compounds need to be tested, and any hits should be followed up with complete dose-response curves to ensure the initial data is true. None of the compounds shared any

structural similarity to amiloride, its analogues, or the hit identified from the membrane potential assay. This present new opportunities for medicinal chemistry-assisted SAR studies. Any further studies may require the QPatch assay development to be revisited, depending on their scale, as conventional patch clamp still remains inefficient for large ion channel drug discovery campaigns.

6.5. Conclusion:

Automated patch clamp instruments deliver high-throughput and high quality ion channel assays to meet the demand both for ion channel safety profiling and for ion channel-targeted drug discovery. It has been demonstrated that the IonWorks Quattro™ technology can deliver a robust and reproducible ENaC δ channel assay, identifying a number of novel hits (hit rate of 0.25 - 0.5 %, dependent on analysis method) that require follow-up studies to validate their activity and determine their potency and selectivity. The QPatch platform is a higher throughput and less demanding method of performing hit confirmation and lead generation studies over conventional patch clamp. Preliminary studies show that the existing cell line is amenable for use on this platform and, following optimisation, can be used to progress this project and identify a novel ENaC δ blocker. In the meantime, a small number of hits from the IonWorks Quattro™ assay have been confirmed on the conventional patch clamp, which require further investigation.

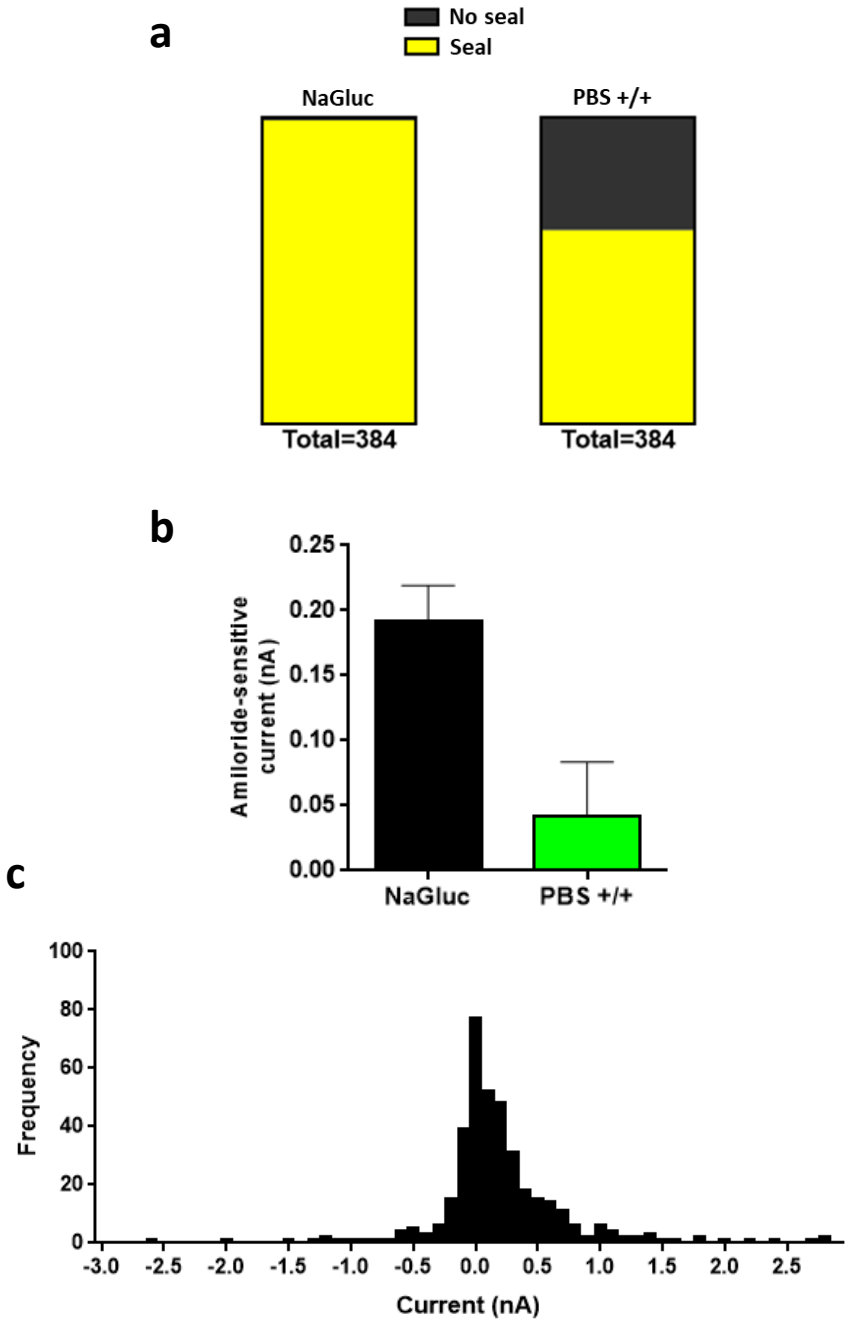

Figure 39. Comparison of extracellular buffers used on the IonWorks platform with the HEK293-ENaC β*γ* cell line. **a** The proportion of wells in the 384 well HT PatchPlate™ which reported as 'no seal' (< 20 MΩ seal resistance). **b** Mean amiloride-sensitive current amplitude (nA) recorded when using either NaGluc- or PBS+/+ -based ECS. **c** Frequency distribution of amiloride-sensitive current amplitudes (nA) when using the NaGluc-based ECS.

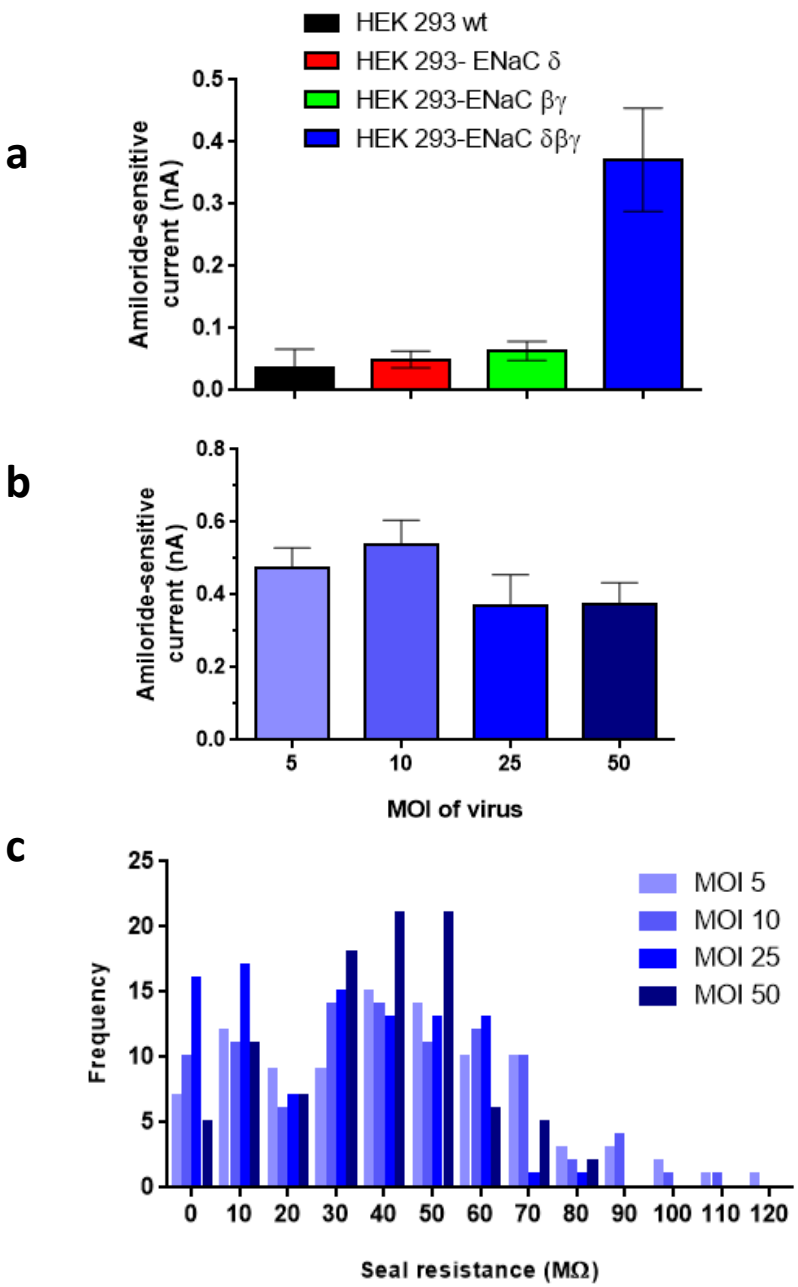

Figure 40. The effect of titrating the baculoviral MOI on the performance of the cell line on the IonWorks platform. **a** The mean amiloride-sensitive current amplitude (nA) measured across 4 different cell lines: HEK 293 wt cells, HEK 293 cells transduced with baculovirus encoding the ENaC δ subunit, HEK 293-ENaC β*γ* cells, and HEK 293-ENaC β*γ* cells transduced with baculovirus encoding the ENaC δ subunit. **b** Mean amiloride-sensitive current amplitude (nA) measured in HEK 293-ENaC β*γ* cells transduced with baculovirus encoding the ENaC δ subunit at different MOIs. **c** Frequency distribution of seal resistances (MΩ) using different viral MOIs.

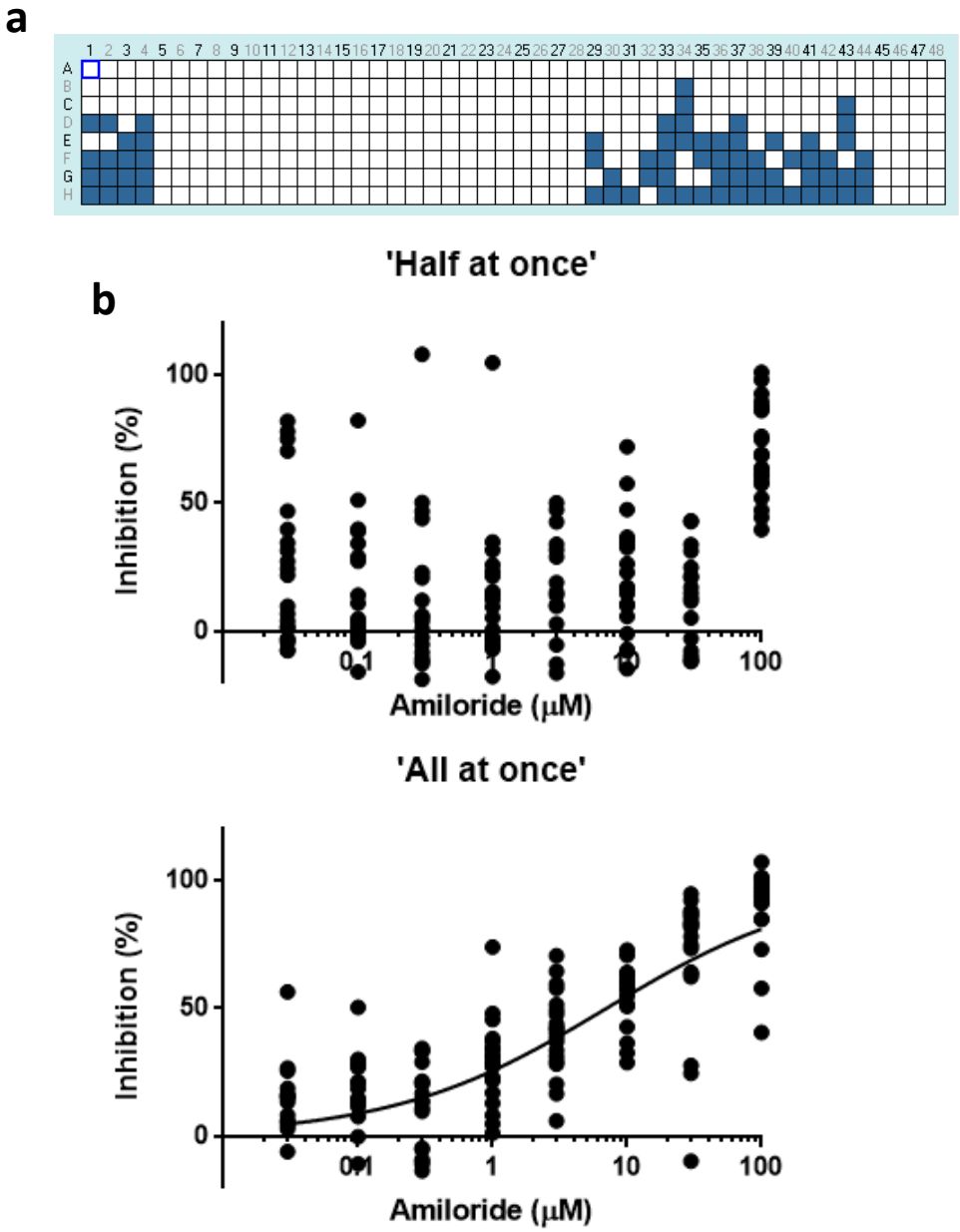

Figure 41. The effect of the scanning parameters of the IonWorks on the data reproducibility across the PatchPlate™. a Screenshot of the PatchPlate™ displayed on the computer screen during an experiment using the 'Half-at-once' scanning mode. Blue wells represent those which are considered to have a seal resistance < 20 MΩ (i.e. no seal). **b** Dose-response curves for amiloride generated by two separate experiments in HT mode, using either the 'Half-at-once' (top) or 'All-at-once' (bottom) scanning mode. Data are plotted as individual replicates, within the plate, for each concentration of amiloride.

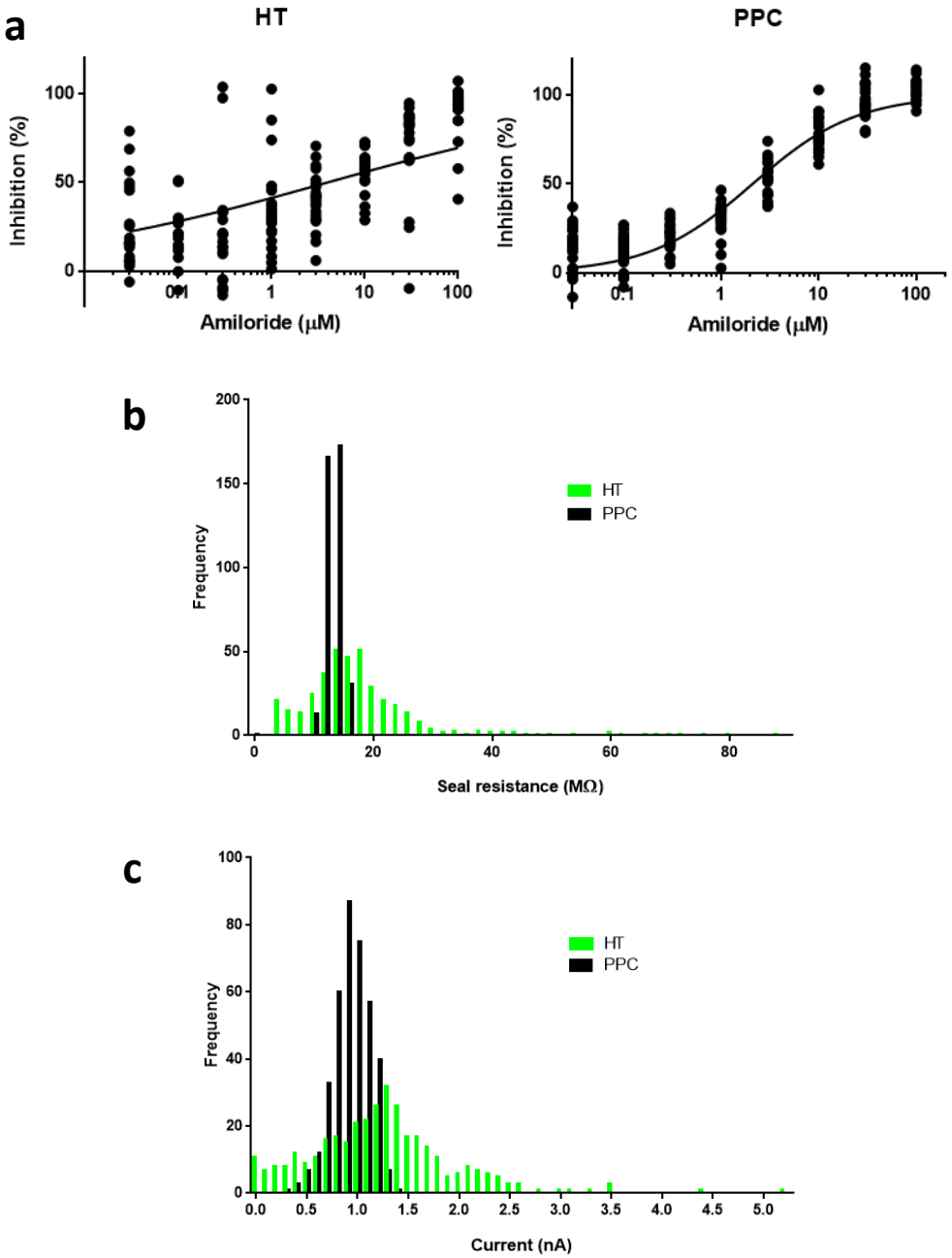

Figure 42. Recording in single- hole (HT) mode and Population Patch Clamp™ (PPC) mode. a Dose-response curves for amiloride generated by two separate experiments in HT or PPC mode, using the 'All-at-once' scanning mode. Data are plotted as individual replicates, within the plate, for each concentration of amiloride. **b** Frequency distribution of seal resistances (MΩ) in HT and PPC mode. **c** Frequency distribution of current amplitudes (nA) in HT and PPC mode.

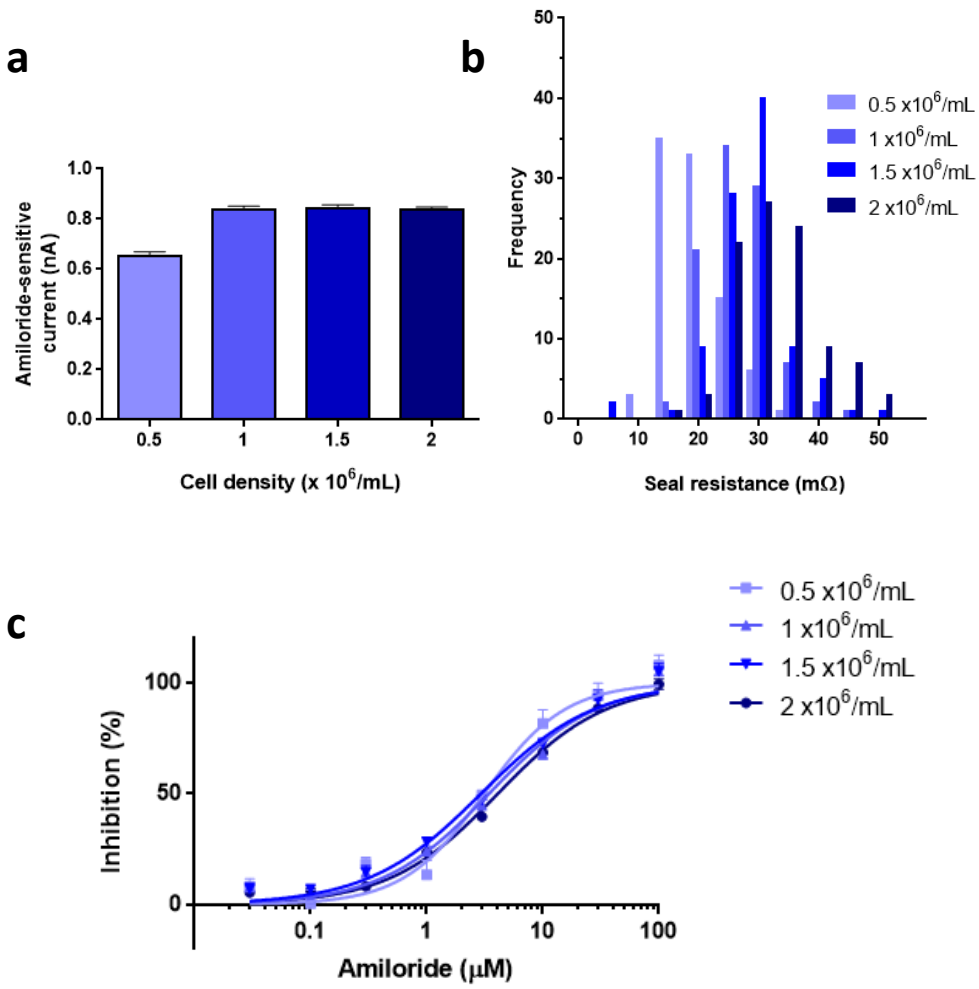

Figure 43. The effect of the cell density in the cell bath on the IonWorks assay. a Mean amiloride-sensitive current amplitude (nA) measured upon loading the cell bath with solution containing cells at different densities. **b** Frequency distribution of seal resistances (MΩ) for different cell densities. **c** Dose-response curves for amiloride generated using cells prepared to different cell densities.

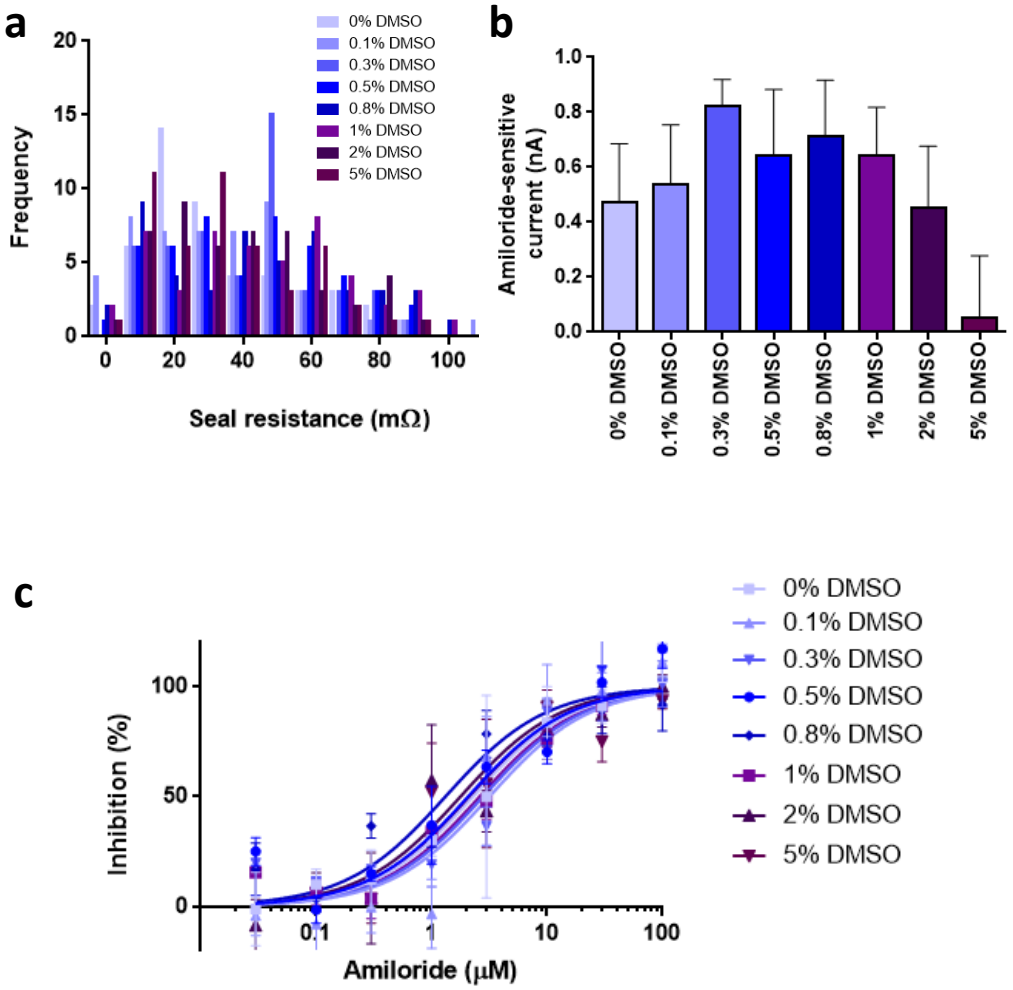

Figure 44. DMSO tolerance of the IonWorks assay. a Frequency distribution of seal resistances (MΩ) for different DMSO concentrations (0-5%). **b** Mean amiloride-sensitive current amplitude (nA) measured upon addition of amiloride in ECS containing different DMSO concentrations. **c** Dose-response curves for amiloride generated using amiloride in ECS containing different DMSO concentrations.

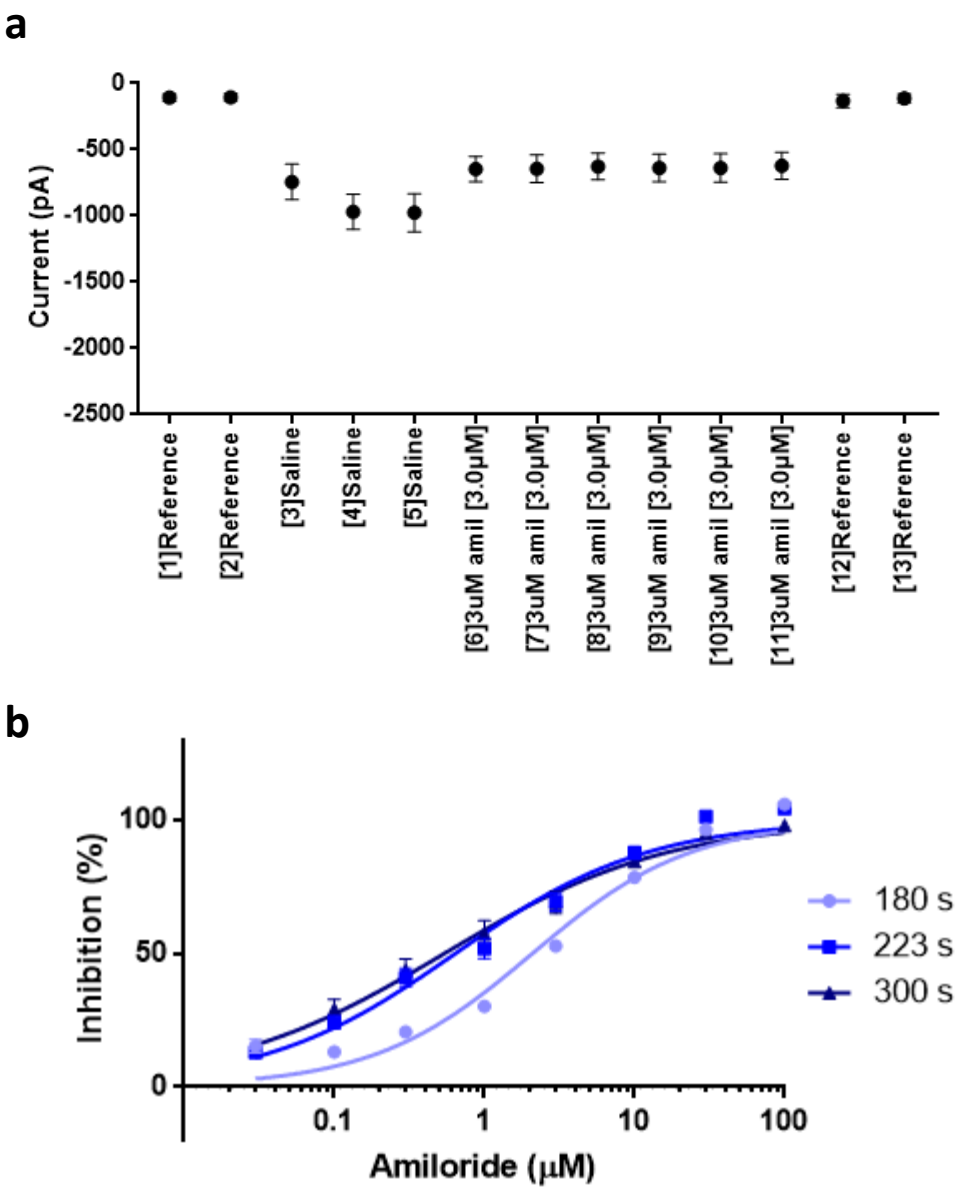

Figure 45. The effect of compound incubation time on pharmacology. **a** Inward currents (pA) measured using the QPatch 16 upon going whole-cell in the presence of amiloride (reference), washing out the blocker, and then repetitively adding amiloride at an IC_{50} concentration (3 µM). **b** Dose-response curves for amiloride after different lengths of exposure time to the drug.

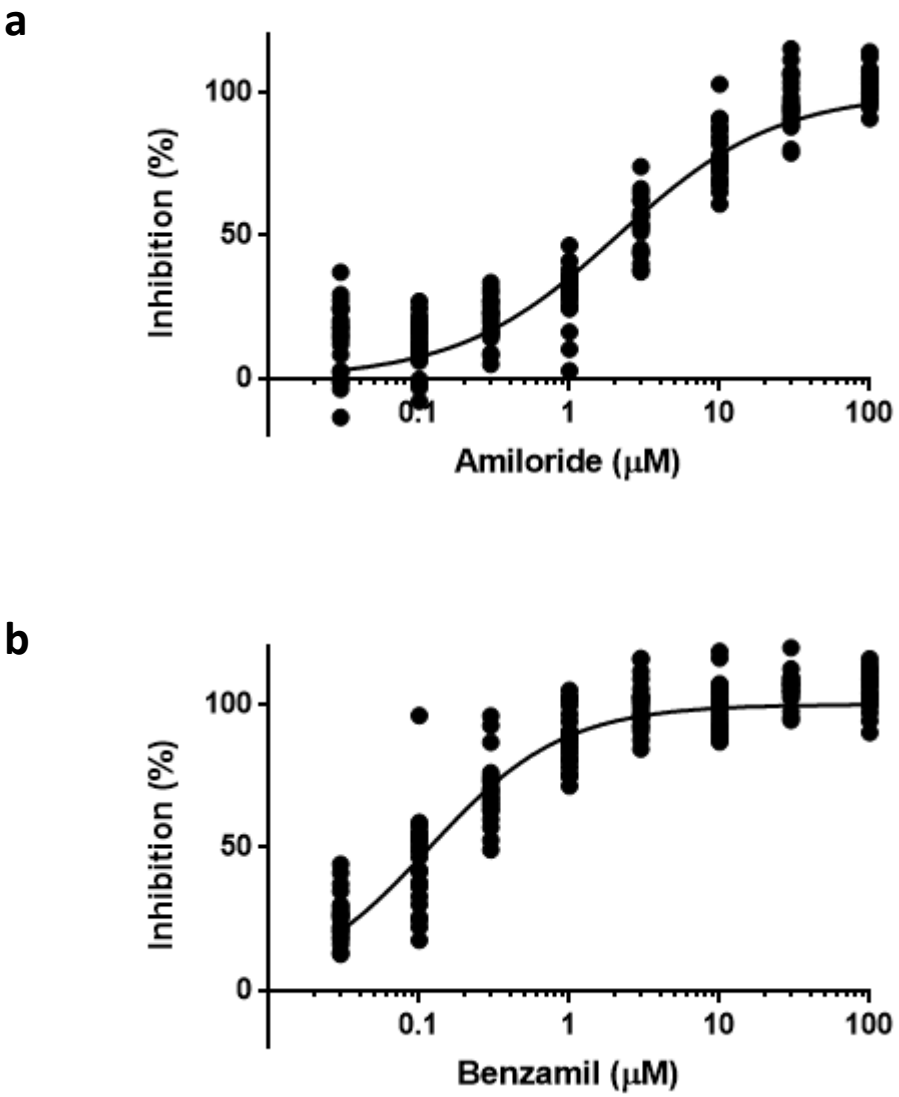

Figure 46. Pharmacological validation of IonWorks assay. Dose-response curves for amiloride (**a**) and benzmail (**b**) run in PPC mode, with an 'All-at-once' scanning mode, and a compound incubation time of 223 s. HEK 293-ENaC β*γ* cells were transduced with the ENaC δ baculovirus at MOI 10 and cells were harvested and loaded onto the platform at a density of $2x10^6$ cell/mL. Data are plotted as individual replicates, within the plate, for each concentration of the drug.

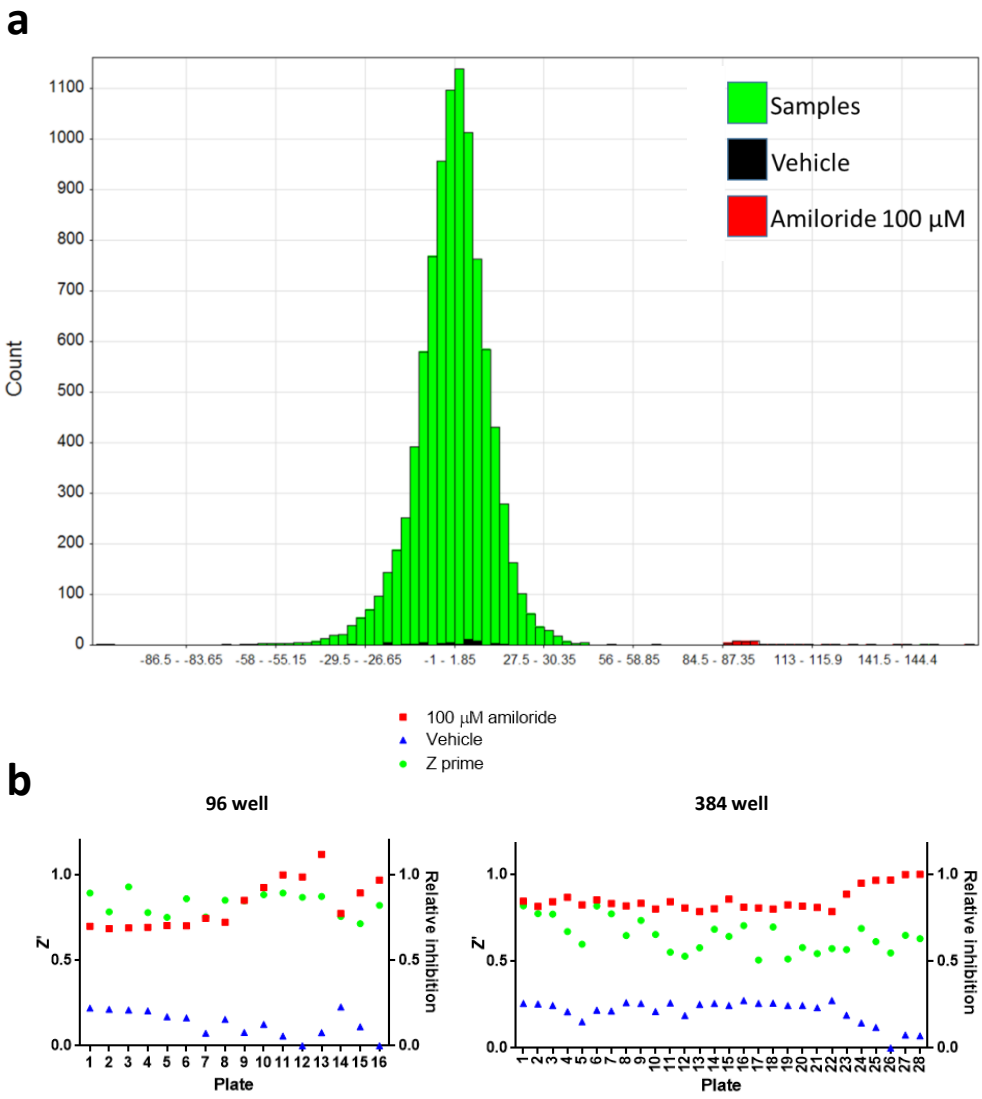

Figure 47. Data from the IonWorks screen of compounds at 40 µM against the ENaC δβ*γ* channel, analysed using both compound additions for normalisation of each well. **a** Distribution of inhibition (%) measured from compounds screened at 40 µM (n=1) in ENaC δβ*γ* cells. Inhibition is normalised to the amiloride-sensitive current (nA). Black = vehicle, red = maximum control (100 µM amiloride), green = samples. **b** Z' values (green), and high (red) and low (blue) channel inhibition, for all assay plates (left = 96 well, right = 384 well).

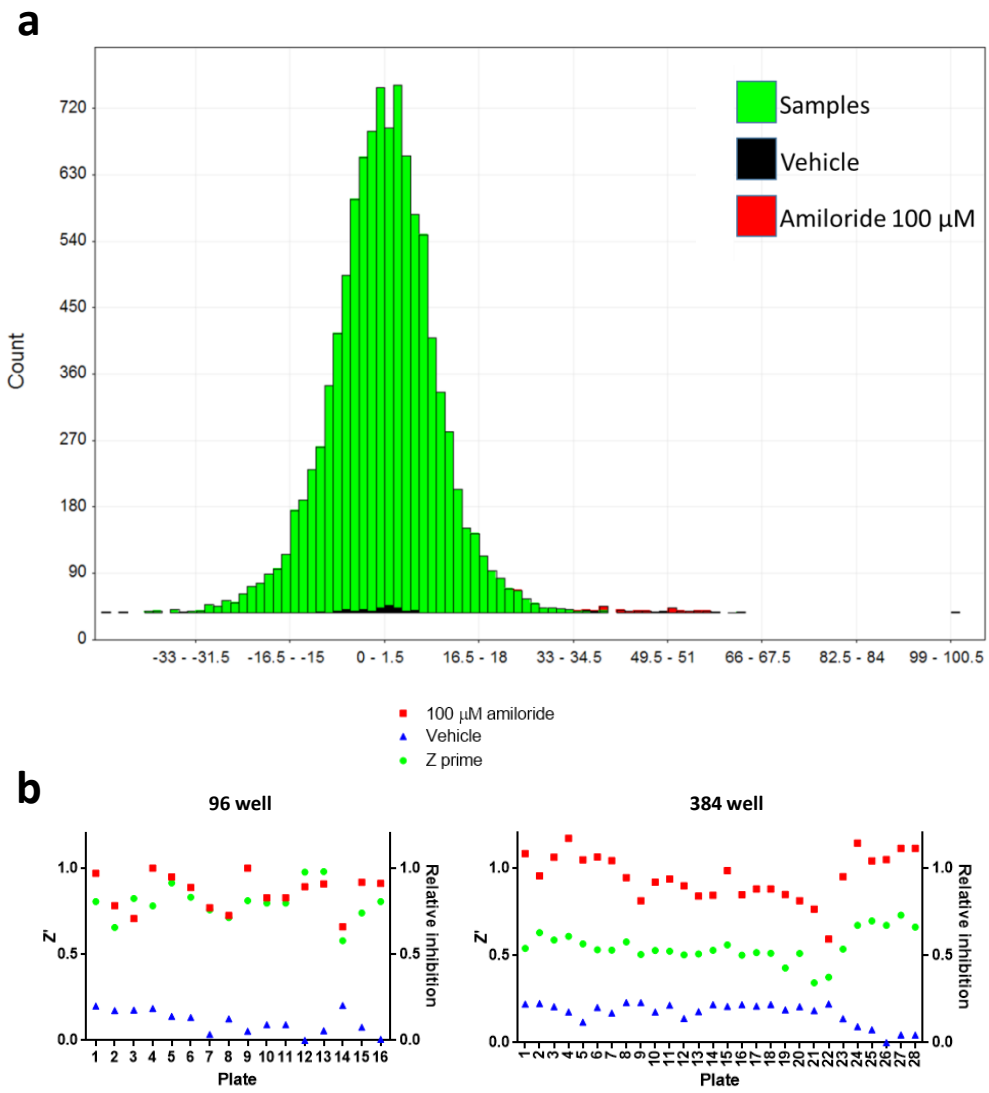

Figure 48. Data from the IonWorks screen of compounds at 40 µM against the ENaC δβ*γ* channel, analysed using just the first test compound addition. **a** Distribution of inhibition (%) measured from compounds screened at 40 µM (n=1) in ENaC δβ*γ* cells. Inhibition is measured as a percentage of block compared to the current measured with just vehicle. Black = vehicle, red = maximum control (100 µM amiloride), green = samples. **b** Z' values (green), and high (red) and low (blue) channel inhibition, for all assay plates (left = 96 well, right = 384 well).

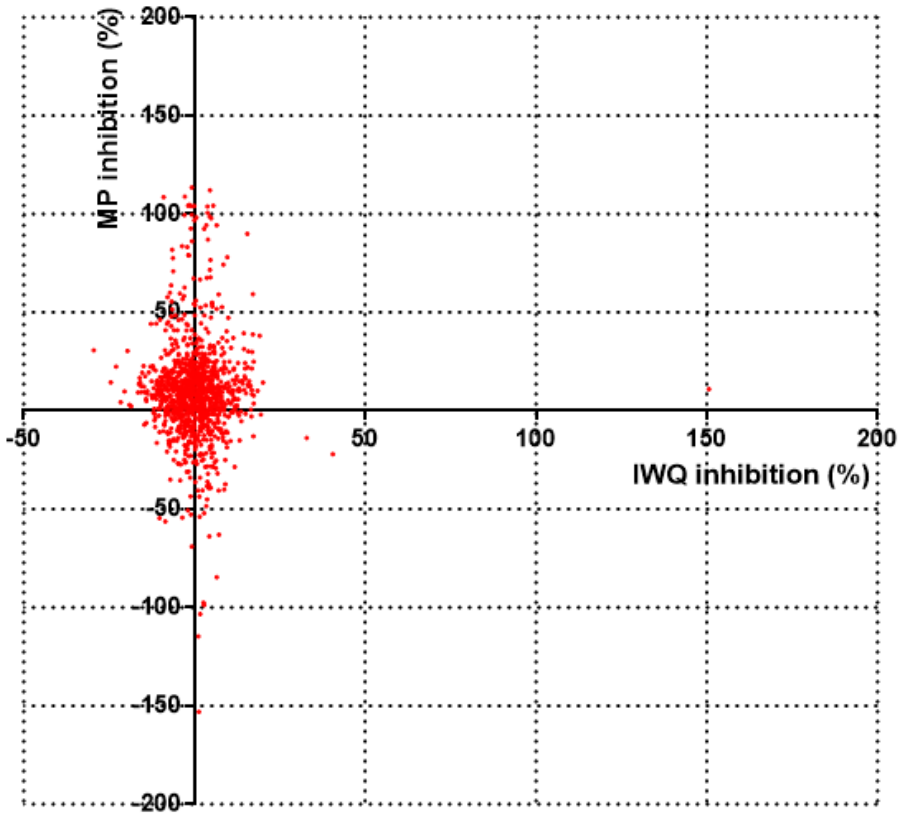

Figure 49. Correlation of inhibition (%) for each compound from the CUTE Ion Channel library screened using the MP assay and the IonWorks assay. No correlation is observed (R^2 = 0.0004, 95% CI -0.07 to 0.04).

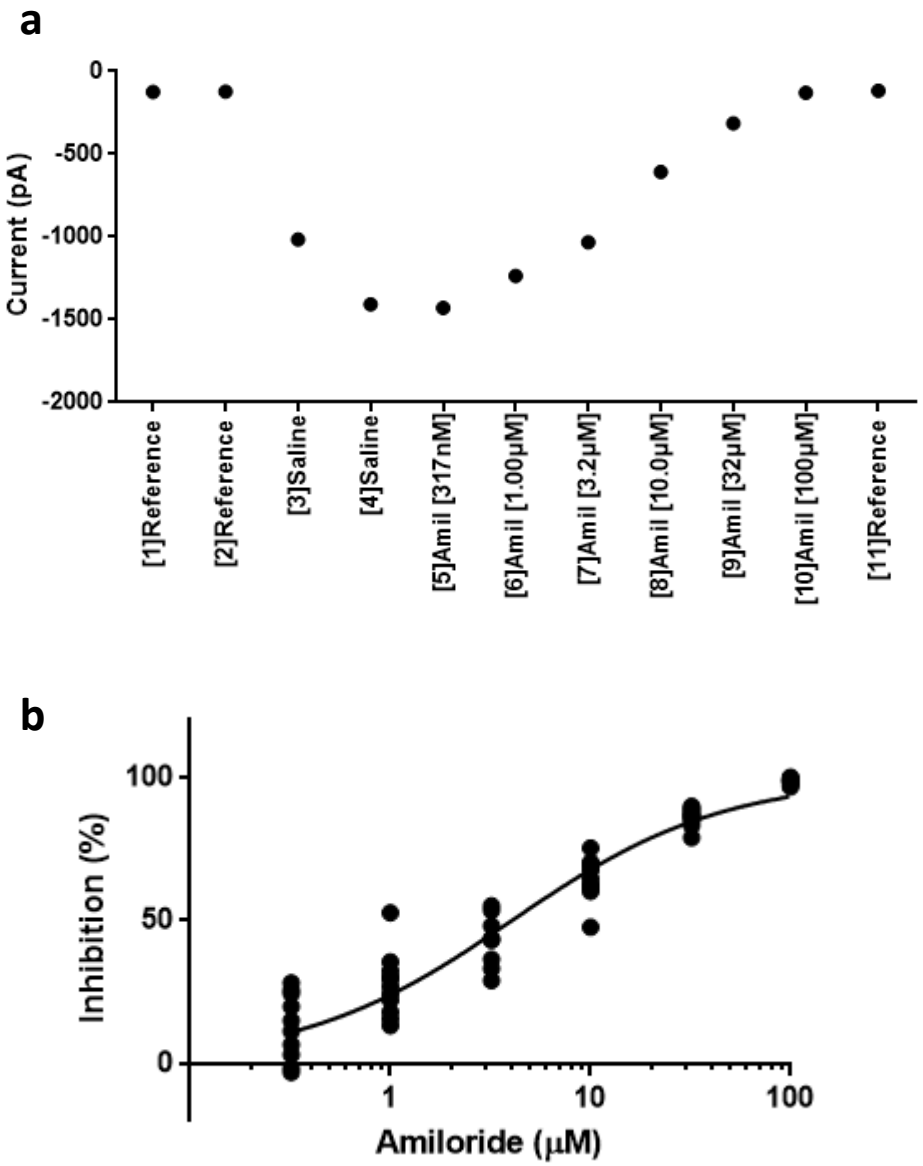

Figure 50. Pharmacological validation of the QPatch assay using the QPatch 16, ApconiX Ltd. **a** Inward currents (pA) measured using the QPatch 16 upon achieving whole-cell configuration in the presence of amiloride (reference), washing out the blocker, and then adding increasing concentrations of amiloride. **b** Dose-response curves for amiloride using HEK 293-ENaC β*γ* cells transduced with the ENaC δ baculovirus at MOI 10. Data are plotted as individual replicates, for each concentration of amiloride.

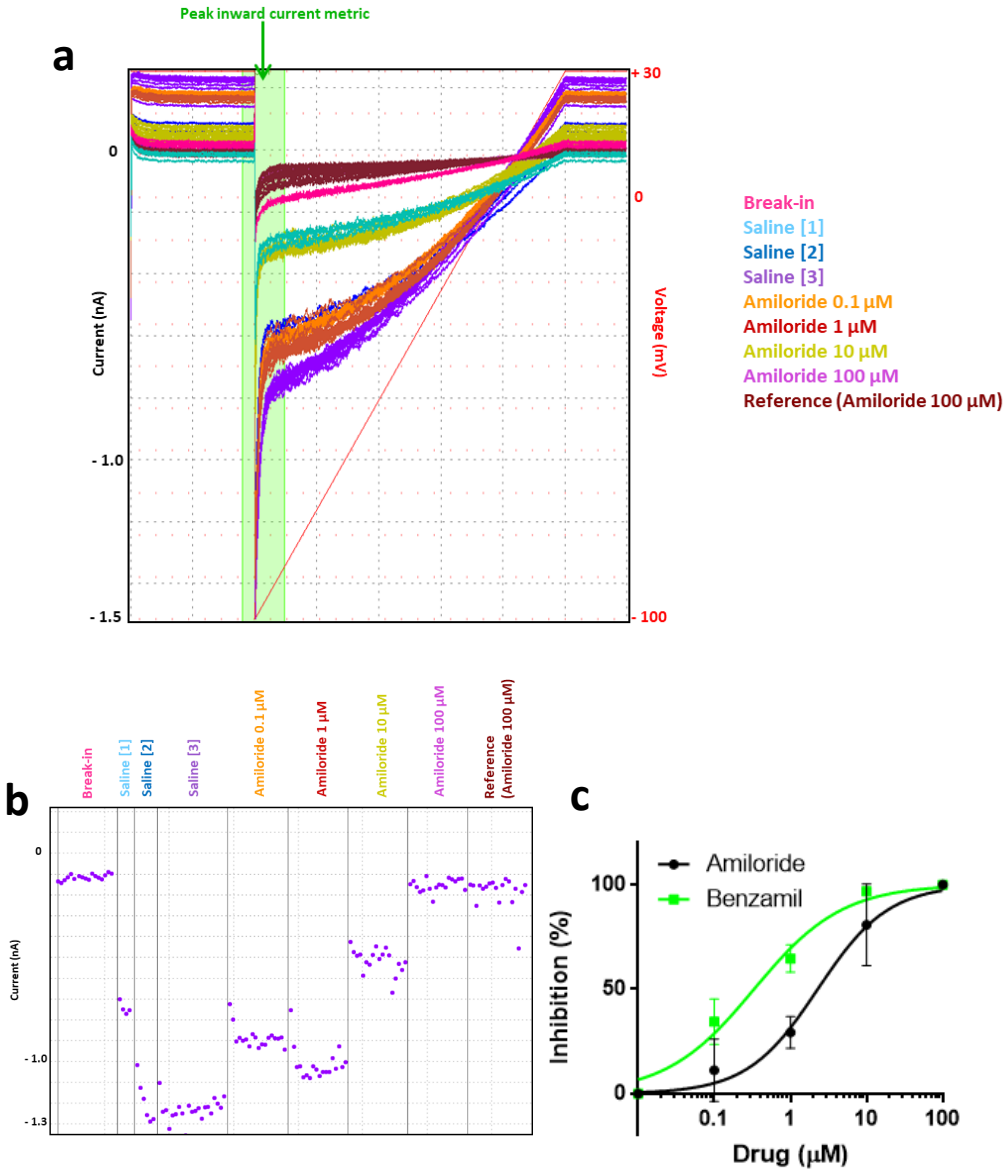

Figure 51. Pharmacological validation of the QPatch assay using the QPatch 16, SDDC. a Raw trace of currents (nA) measured using the QPatch 16 during liquid handling additions, upon achieving whole-cell configuration in the presence of amiloride (break-in), washing out the blocker (saline), and then adding increasing concentrations of amiloride. **b** Peak inward current (nA) at -100 mV for each liquid handling step. Highlighted in green in **a** represents the time period of the voltage ramp, whereby the peak inward current is measured. **c** Dose-response curves for amiloride and benzamil using HEK 293-ENaC β*γ* cells transduced with the ENaC δ baculovirus at MOI 10. Data are plotted as mean ± SEM.

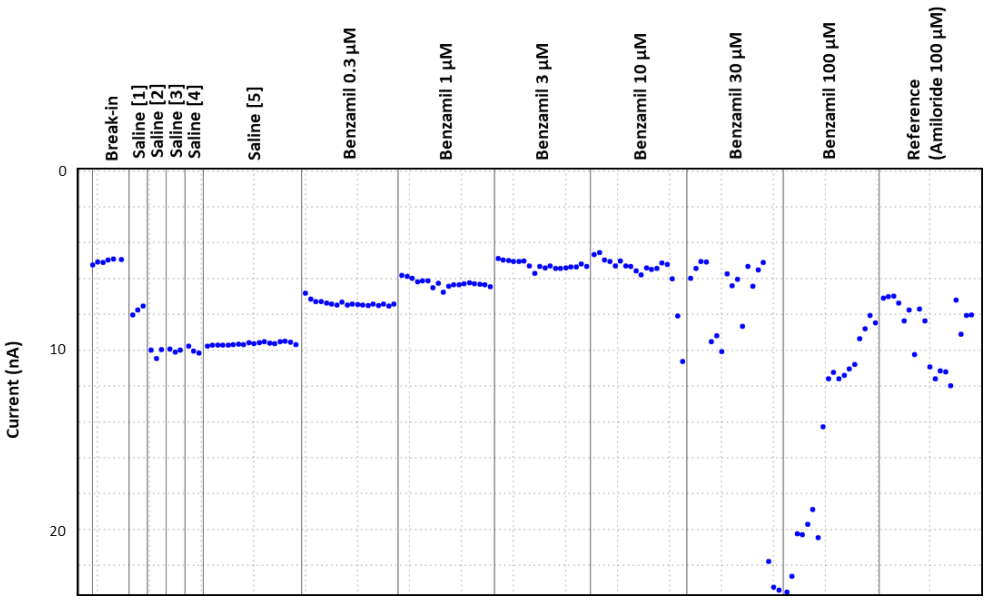

Figure 52. Example of instability of assay, observed across both the QPatch 16 and QPatch HTX, SDDC. a Peak inward current (nA) at -100 mV for each liquid handling step. Example of currents measured on the QPatch HTX upon benzamil addition. Currents become unstable during the addition period of 10 µM Benzamil.

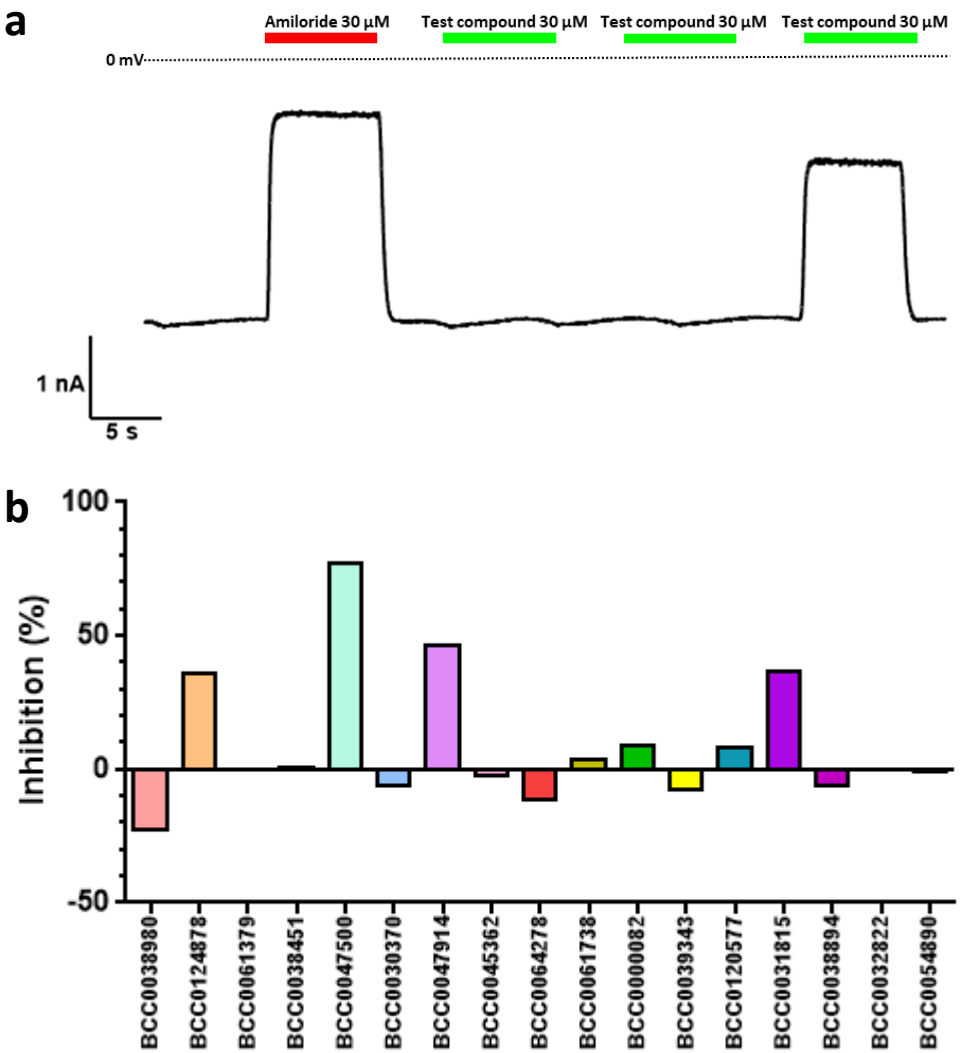

Figure 53. Hit validation using conventional patch clamp. **a** Raw trace of hit validation screen using conventional patch clamp, whereby cells were kept at a holding potential of –30 mV, and first exposed to a 5 sec amiloride addition, before subsequent additions of test compounds, separated by a 3 sec washout with ECS. This trace represents currents measured upon addition of a test compound confirmed as inhibiting the inward ENaC current. **b** Inhibition (%) of the amiloride-sensitive current by 17 of the compounds identified during the IonWorks Quattro™ screening campaign. Data represented was from n=1, with compounds tested at 30 µM.

7

GENERAL DISCUSSION

Chapter 7

Results presented in this investigation outline an ion channel drug discovery campaign, which spans from cell line generation and characterisation, to primary screening, hit validation and hit optimisation. This approach and the techniques used, although shown here to be specific to the ENaC δ channel, can be employed across different ion channel drug discovery projects, reflecting the increased knowledge and technological advancements in this field.

Chapter 3. demonstrates, via fluorescent microscopy and patch clamp electrophysiology, that BacMam technology can be implemented effectively in the reconstitution of the ENaC α or δ channels, circumventing toxicological problems associated with long term overexpression of the channels (Chen, et al., 2015). This method, used to introduce a third ENaC subunit (α or δ) to HEK293 cells that stably express two ENaC subunits (β and γ), results in a cell line which is amenable to studying ENaC channel modulation by conventional patch clamp electrophysiology (Chapter 3.), a membrane potential assay (Chapters 4. and 5.), and automated electrophysiology (Chapter 6.).

Chen, et al. (2015) had previously shown that by stably expressing ENaC β and γ subunits harbouring Liddle's Syndrome mutations, there is a higher level of functional channel activity compared to the wild-type equivalent. This lends to an improved performance in functional assays. On basic characterisation of some of the biophysical and pharmacological properties of these ENaC channels using patch clamp, Chapter 3. ratifies that the ENaC δ channel should be considered distinct from the α variant. In addition to its differential pattern of tissue distribution (Waldmann, et al., 1995; Yamamura, et al., 2006), our findings replicated previous work showing the two

channels differ in their cation permeabilities, proton sensing capacities, and amiloride sensitivity (Ji, et al., 2004; Ji, et al., 2006). Notably, the proton sensitivity observed in the ENaC δ, can be likened to the ASIC channel subfamily, which have previously been described for their role in hypoxia-induced neuronal damage (Siesjo, et al., 1995; Keung Tai & Truong, 2013).

Chapter 4. shows how this cell line was used to develop a robust medium throughput primary screen, in the form of a membrane potential assay. The chapter delineates key steps in the transduction optimisation, and therefore assay development process, of which transferring this assay from the FlexStation® to the FDSS/µCELL platform proved to be pivotal. This assay was able to report differential pharmacology and selectivity of known ENaC blockers at the ENaC α and δ channels, however it lacked the sensitivity of conventional patch clamp. Although the assay reported blockers to be less potent, data were consistent with published values using this platform (Chen, et al., 2015). This was therefore taken into consideration when performing the primary screening campaign (Chapter 5.). The primary screen met acceptable performance criteria (Z' all > 0.5) and had a primary hit rate approaching 5%. Although these fluorescence-based assays are the mainstay of ion channel screening, they suffer from high false positive and negative hit rates (Hughes, et al., 2011), exemplified by confirmation of only one of these primary hits in patch clamp electrophysiology.

This single hit lacked the suitable potency or selectivity to be considered a tool compound. Therefore an SAR-based electrophysiological study that was supported by in-house medicinal chemistry capabilities was pursued. Results from the SAR study, although unsuccessful in improving the potency, indicated regions of the molecule

which were integral to the interaction with the ENaC α/δ subunits. Most significantly, changes in the phenyl moiety removed inhibition of the ENaC current. Phenyl groups are involved in π-stacking interactions, of which a large number are observed between the ligand and the amino acids phenylalanine, tyrosine (Y) (36.8%), tryptophan (W) (8.7%) and histidine (H) (5.1%) (Ferreira de Freitas & Schapira, 2017), all of which are present in the proposed amiloride binding site, WYHFHY (Ismailov, et al., 1996). Mutagenic analysis of this site confirmed that this hit compound was likely to bind at the same site.

In order to identify a second series of compound, an academic-industrial collaboration (SDDC & Apconix Limited) was established to exploit the IonWorks Quattro™ automated electrophysiology platform. Chapter 6. corroborates the value of such platforms at the forefront of drug discovery programs. It was demonstrated that the IonWorks Quattro™ can deliver a robust and reproducible ENaC δ channel assay using Population Patch Clamp™ technology, with a hit rate approaching 0.5 %. Although such platforms would always be the first choice for frontline screening, the cost of interrogating large decks can mean this option is unviable. Their use in triaging compounds that have been identified by a cheaper alternative is the more common application. For example, with fluorescence-based screening methods, secondary screening is crucial to eliminate falsely reported compounds, and is executed on a much smaller scale. Therefore despite the known limitations of fluorescence-based technologies, they can be used relatively cost effectively to screen very large numbers of compounds, if access to automated electrophysiology platforms for triage is possible. This suggest a limitation of the membrane potential primary screen, whereby

a much larger number of compounds could have been assessed and triaged, increasing its likelihood of identifying more than one hit series

Following the IonWorks. Quattro™ screen, preliminary work was performed on the QPatch to demonstrate its potential to be used as a surrogate for conventional patch clamp for hit confirmation and optimisation steps. Although this was met with some success, financial and time restraints prohibited completion of assay optimisation and was not pursued further. Instead, given the limited timeframe, a portion of the hits were examined using conventional patch clamp. A small number of compounds inhibited the channel, indicating that the IonWorks Quattro™ assay had reported a much lower number of false positives.

If, on further investigation, these compounds do prove to exhibit the required affinity and efficacy for the ENaC δ channel, they would also be required to have a number a physicochemical properties required to investigate the channel *in situ*. For example, neuronal expression of the channel would mean the compound would have to be able to cross the blood-brain barrier (BBB). Substances can cross the BBB by a variety of mechanisms but the two most common mechanisms exploited in drug delivery include transmembrane diffusion and transporters (Banks, 2009). Although in recent years, there has been some focus on drug delivery strategies which target proteins that have known transporters, most drugs to date rely on transmembrane diffusion (Pajouhesh, et al., 2005; Banks, 2009). This non-saturable process depends largely on the substances physicochemical properties.

For this reason early assessment of these characteristics for potential CNS drugs is extremely important, and by analysing known CNS drugs retrospectively, guidelines for predicting and designing CNS efficacy have been outlined. Drugs tend to be small (usually ≤ 400 kDa) and lipid soluble, of which the latter is a balancing act (Pajouhesh, et al., 2005; Banks, 2009). The concentration of the drug in the blood can be lowered as lipid solubility favours uptake into peripheral tissues, and if the drug manages to cross the BBB must be able to partition into the aqueous environment of the brain's interstitial fluid. This lipophilicity of the compound, defined by the partition coefficient (LogP) has been shown to be optimal activity is at LogP = 2 (Hansch, et al., 1967). Furthermore, the acid-base dissociation constant (pK_a) is also considered important when defining CNS drugs. It specifies the pH at which 50% of the drug is ionised and 50% is non-ionised. Fischer et al. (1998) estimated pK_a limits for CNS penetration is between 4 and 10.

Overall the results from this investigation emphasise the complexity of studying ion channels as drug targets, despite the increased in knowledge and technologies available. Where possible, automated electrophysiological platforms should be used as the primary screening methodology to eliminate the high attrition rate on hit confirmation, as demonstrated by this project. The ENaC channel has been notoriously hard to pursue as a drug target. ENaC inhibitors which block the channel directly, such as amiloride or its derivatives, have nanomolar affinity for ENaC but lack the desired metabolic stability to be efficacious, for example in the CF airway. As such, the identification of chemotypes in this project, which are distinct from amiloride but

demonstrate the ability to inhibit ENaC current, is a considerable step in the right direction in the search of a tool compound for the ENaC δ channel and must be explored further.

REFERENCE LIST

Abriel, H., Loffing, J. & Rebhun, J., 1999. Defective regulation of the epithelial Na+ channel by Nedd4 in Liddle's Syndrome. *Journal of Clinical Investigations,* 103(5), pp. 667-673.

Aidley, D. & Standfield, P., 1996. Ion channels: molecules in action. *Cambridge University Press*, p. 307.

Altmann, F., Staudacher, E., Wilson, I. & März, L., 1999. Insect cells as hosts for the expression of recombinant glycoproteins. *Journal of Glycoconjugate,* 16(2), pp. 109-123.

Anantharam, A., Tian, Y. & Palmer, L., 2006. Open probability of the epithelial sodium channel is regulated by intracellular sodium. *Journal of Physiology,* 574(2), pp. 333-347.

App, E. et al., 1990. Acute and long-term amiloride inhalation in cystic fibrosis lung disease: a rational approach to cystic fibrosis therapy. *American Review of Respiratory Diseases,* 141(3), pp. 605-612.

Arun, T. et al., 2013. Targeting ASIC1 in primary progressive multiplesclerosis: evidence of neuroprotection with amiloride. *Brain,* 136(1), pp. 106-115.

Ashcroft, F., 2006. From molecule to malady. *Nature,* Volume 440, pp. 440-447.

Baconguis, I. et al., 2014. X-ray structure of acid-sensing ion channel-snake toxin complex reveals open state of a Na+-selective channel. *Cell,* 156(4), pp. 717-729.

Baer, J., Jones, C., Spitzer, S. & Russo, H., 1967. The potassium-sparing and natriuretic activitiy of N-amidino-3,5-diamino-6-chloropyrazinecarboxamide hydrochlorise dihydrate (amiloride hydrochloride). *Journal of Pharmacology: Expert Therapeutics,* 157(2), pp. 472-485.

Bagal, S. et al., 2013. Ion channels as therapeutic targets: a drug discovery perspective. *Journal of Medicinal Chemistry,* 56(3), pp. 593-624.

Balamurugan, V., Sen, A., Saravanan, P. & Singh, R., 2006. Biotechnology in the production of vaccine or antigen for animal health. *Journal of Animal Veterinary Advances,* 5(6), pp. 487-495.

Bangel-Ruland, N. et al., 2010. Characterization of the epithelial sodium channel d-subunit in human nasal epithelium. *American Journal of Respiratory Cell and Molecular Biology,* 42(4), pp. 498-505.

Banks, W., 2009. Characteristics of compounds that cross the blood-brain barrier. *BMC Neurology,* 9.

Barker, P. et al., 1998. Role of γENaC subunit in lung liquid clearance and electrolyte balance in newborn mice. Insights into perinatal adaptation and pseudohypoalosteronism. *Journal of Clinical Investigations,* Volume 102, pp. 1634-1640.

Battaglia, A., 2005. Del 1p36 syndrome: a newly emerging clinical entity. *Brain Development,* 27(5), pp. 358-361.

Beacham, D., Blackmer, T., O' Grady, M. & Hanson, G., 2010. Cell-based potassium ion channel screening using the FluxOR assay. *Journal of Biomolecular Screening,* 15(4), pp. 441-446.

Beneyx, F., 1999. Recombinant protein expression in Escherichia coli. *Current Opinions in Biotechnology,* 10(5), pp. 411-421.

Berdiev, B. et al., 1998. Subunit stoichiometry of a core conduction element in a cloned epithelial amiloride-sensitive Na+ channel. *Biophysical Journal,* 75(5), pp. 2292-2301.

Bernstein, J., 1902. Untersuchungen zur thermodynamik der bioelektrischen ströme: erster theil. *European Journal of Physiology,* Volume 92, pp. 521-562.

Berry, S., 2002. The chemical basis of membrane bioenergetics. *Journal of Molecular Ecology,* 54(5), pp. 595-613.

Bianchi, L. & Driscoll, M., 2002. Protons at the gate: DEG/ENaC ion channels help us feel and remember. *Neuron,* 34(3), pp. 337-340.

Biasio, W., Chang, T., McIntosh, C. & McDonald, F., 2003. Identification of murr1 as a regulator of the human δ epithelial sodium channel. *Journal of Biological Chemistry,* 279(7), pp. 5429-5434.

Bonny, O. & Hummler, E., 2000. Dysfunction of epithlial sodium transport: from human to mouse. *Kidney International,* Volume 57, pp. 1313-1318.

Boshart, M. et al., 1985. A very strong enhancer is located upstream of an immediate early gene of human cytomegalovirus. *Cell,* 41(2), pp. 521-530.

Bridgland-Taylor, M. et al., 2006. Optimisation and validation of a medium-throughput electrophysiology-based hERG assay using IonWorks HT. *Journal of Pharmacological and Toxicological Methods,* 54(2), pp. 189-199.

Brooker, D., Kozak, C. & Kleyman, T., 1995. Epithlial sodium channel genes scnn1b and scnn1g are closely linked on distal mouse chromosome 7. *Genomics,* Volume 29, pp. 784-786.

Brown, T., 2006. *Gene cloning and DNA analysis, an introduction.* s.l.:Blackwell Publishing.

Canessa, C., Horisberger, J. & Rossier, B., 1991. Epithelial sodium channel related to proteins involved in neurodegeneration. *Nature,* Volume 361, pp. 467-470.

Canessa, C., Merillat, A. & Rossier, B., 1994. Membrane topology of the epithelial sodium channel in intact cells. *American Journal of Physiology,* Volume 267, pp. 1682-1690.

Carattino, M., Hughey, R. & Kleyman, T., 2008. Proteolytic processing of the epithelial sodium channel γ subunit has a dominant role in channel activation. *Journal of Biological Chemistry,* Volume 283, pp. 25290-25295.

Carattino, M. et al., 2008. Defining an inhibitory domain in the α-subunit of the epithelial sodium channel. *American Journal of Renal Physiology,* Volume 294, pp. 47-52.

Carter, P., 1986. Site-directed mutagenesis. *Journal of Biochemistry,* 237(1), pp. 1-7.

Catterall, W., 1984. The molecular basis of neuronal excitability. *Science,* Volume 223, p. 653.

Catterall, W., 1993. Structure and modulation of Na+ and Ca2+ channels. *ANNALS,* Volume 707, pp. 1-19.

Catterall, W., 2000. From ionic currents to molecular mechanisms: the structure and function of voltage-gated sodium channels. *Neuron,* 26(1), pp. 13-25.

Cestèle, S. & Catterall, W., 2000. Molecular mechanisms of neurotoxin action on voltage-gated sodium channels. *Biochimie,* 82(9-10), pp. 883-892.

Chalfie, M. & Wolinsky, E., 1990. The identification and suppression of inherited neurodegeneration in Caenorhabditis elegans. *Nature,* Volume 345, pp. 410-416.

Champigny, G., Voilley, N., Waldmann, R. & Lazdunski, M., 1998. Mutations causing neurodegeneration in Caenorhabditis elegans drastically alter the pH sensitivity and inactivation of the mammalian H+-gated Na+ channel MDEG1. *Journal of Biological Chemistry,* 273(25), pp. 15418-15422.

Cheng, C. & Shuman, S., 2000. Recombinogenic flap ligation pathway for intrinsic repair of topoisomerase IB-induced double-strand breaks. *Molecular Cell Biology,* 20(21), pp. 8059-8068.

Chen, M. et al., 2015. Validation and optimization of novel high-throughput assays for human epithelial sodium channels. *Journal of Biomolecular Screening,* 20(2), pp. 242-253.

Choi, D. & Rothman, W., 1990. The role of glutamate neurotoxicity in hypoxic-ischemic neuronal death. *Annual Review of Neuroscience,* Volume 13, pp. 171-182.

Chraibi, A. et al., 1998. Protease modulation of the activity of the epithelial sodium channel expressed in Xenopus oocytes. *Journal of General Physiology,* 111(1), pp. 127-138.

Clare, J., 2010. Targeting ion channes for drug discovery. *Discovery Medicine,* 19(104).

Clare, J., Chen, M. & Downie, D., 2009. Use of planar array electrophysiology for the development of robust ion channel cell lines.. *Combinatorial Chemistry & High Throughput Screening,* 12(1), pp. 96-106.

Cole, K., 1949. Dynamic electrical characteristics of the squid axon membrane. *Archives Des Sciences Physiologiques (Paris),* Volume 3, pp. 253-258.

Coscoy, S. & Barbry, P., 2004. The ENaC/Deg family of cation channels. *Advances in Molecular and Cell Biology,* Volume 32, pp. 303-329.

Crabbé, J., 1961. Stimulation of active sodium transport by the isolated toad bladder with aldosterone in vitro. *The Journal of Clinical Investigation,* Volume 40, pp. 2103-2110.

Cragoe, E. et al., 1967. Pyrazine diuretics. I. N-amidino-3amino-6-halopyrazine-carboxamides. *Journal of Medicinal Chemistry,* 10(1), pp. 66-75.

Cronk, D., 2001. Cell-based high-throughput screening of ion channels using FLIPR and VIPR membrane potential assay technology. *Society for Biomolecular Screening 7th Annual Conference.*

David, E., Tramontin, T. & Zemmel, R., 2009. Pharmaceutical R&D: the road to positive returns. *Nature Reviews Drug Discovery,* 8(8), pp. 609-610.

Deamer, D. et al., 2002. The first cell membranes. *Astrobiology,* 2(4), pp. 371-381.

Debonneville, C. et al., 2001. Phosphorylation of Nedd4-2 by Sgk1 regulates epithelial Na(+) channel cell surface expression. *The EMBO Journal,* 20(24), pp. 7052-7059.

Demirel, Y., 2014. Transport and rate processes in physical, chemical and biological systems. In: *Nonequilibrium Thermodynamics.* Lincoln: Elsevier Science, pp. 75-118.

Di Paolo, G. & De Camilli, P., 2006. Phosphoinositides in cell regulation and membrane dynamics. *Nature,* 443(7112), pp. 651-657.

Diakov, A. & Kormacher, C., 2004. A novel pathway of epithelial sodium channel activation involved serum- and glucocorticoid-inducible kinase consensus motif in the C terminus of the channel's alpha subunit. *Journal of Biological Chemistry,* 279(37), pp. 38134-38142.

Dib-Hajj, S., Cummins, T., Black, J. & Waxman, S., 2007. From genes to pain: Nav1.7 and human pain disorders. *Trends in Neuroscience,* 30(11), pp. 555-563.

Diochot, S. et al., 2007. Peptde inhibitors of acid-sensing ion channels. *Toxicon,* 49(2), pp. 271-284.

Doyle, D. et al., 1998. The structure of potassium channel: molecular basis of K+ conduction and selectivity. *Science,* 280(5360), pp. 69-77.

Driscoll, M. & Chalfie, M., 1991. The mec-4 gene is a member of a family of Caenorhabditis elegans genes that can mutate to induce neuronal degeneration. *Nature,* Volume 349, pp. 588-593.

Driscoll, M. & Chalfie, M., 1992. Developmental and abnormal cell death in C. elegans. *Trends in Neuronscience,* 15(1), pp. 15-19.

Duc, C. et al., 1994. Cell-specific expression of epithelial sodium channel alpha, beta and gamma subunits in the aldestorone-responsive epithlia from the rate: localisation by in situ hybridisation and immunocytochemistry. *Journal of Cell Biology,* 127(6), pp. 1907-1921.

Dudek, A., Arodz, T. & Gálvez, J., 2006. Computational methods in developing quantitative structure-activity relationships (QSAR): a review. *Combinatorial Chemistry & High Throughput Screening,* 9(3), pp. 213-228.

Dulbecco, R. & Vogt, M., 1954. Plaque formation and isolation of pure lines with poliomyelitis viruses. *Journal of Experimental Medicine,* 99(2), pp. 167-182.

Dunlop, J. et al., 2008. High-throughput electrophysiology: an emerging paradigm for ion channel screening and physiology. *Nature Reviews Drug Discovery,* 7(4), pp. 358-368.

Eastwood, A. & Goodwood, M., 2012. Insight into DEG/ENaC channel gating from genetics and structure. *Physiology,* 27(5), pp. 282-290.

Eldeheit, O. et al., 2014. Conserved charged residues at the surface and interface of epithelial sodium channel subunits-roles in cell surface expression and sodium self-inhibition response. *The FEBS Journal,* 281(8), pp. 2097-2111.

Fenwick, E., Marty, A. & Neher, E., 1982. A patch-clamp study of bovine chromaffin cells ad their sensitivity to acetylcholine. *Journal of Physiology,* Volume 331, pp. 577-597.

Ferreira de Freitas, R. & Schapira, M., 2017. A systematic analysis of atomic protein–ligand interactions in the PDB. *MedChemComm,* 8(10), p. 1970–1981.

Fertig, N., Blick, R. & Behrends, J., 2002. Whole cell patch clamp recording performed on a planar glass chip. *Biophysical Journal,* 82(6), pp. 3056-3062.

Finkel, A. et al., 2006. Population patch clamp improves data consistency and success rates. *Journal of Biomolecular Screening,* 11(5), pp. 488-496.

Firsov, D. et al., 1998. The heterotetrameric architecture of the epithelial sodium channel (ENaC). *The EMBO Journal,* 17(2), pp. 344-352.

Fischer, H., Gottschlich, R. & Seelig, A., 1998. Blood-brain barrier permeation: molecular parameters governing passive diffusion. *Journal of Membrane Biology,* 165, pp. 201–211.

Fornwald, J., Lu, Q., Wang, D. & Ames, R., 2007. Gene expression in mammalian cells using BacMam, a modified baculovirus system. *Methods in Molecular Biology,* Volume 388, pp. 95-114.

Frelin, C. et al., 1988. Amiloride and its analogs as tools to inhibit Na+ transport via the Na+ channel, the Na+ /H+ antiport and the Na+/Ca 2+ exchanger. *Biochimie,* 70(9), pp. 1285-1290.

Friese, M. et al., 2007. Acid-sensing ion channel-1 contributes to axonal degeneration in autoimmune inflammation of the central nervous system. *Nature Medicine,* 13(12), pp. 1483-1489.

Fuchs, W., Larsen, E. & Lindemann, B., 1977. Current-voltage curve of sodium channels and concentration dependence of sodium permeability in frog skin. *Journal of Physiology,* 267(1), pp. 137-166.

Garcia-Anoveros, J., Ma, C. & Chalfie, M., 1995. Regulation of Caenorhabditis elegans degenerin proteins by a putative extracellular domain. *Current Trends in Biology,* 5(4), pp. 441-448.

Garcia-Caballero, A. et al., 2009. SPLUNC1 regulates airway surface liquid volume by protecting ENaC from proteolytic cleavage. *PNAS,* 106(27), pp. 11412-11417.

Garcia, M. & Kaczorowski, G., 2005. Potassium channel as target for therapeutic intervention. *Science Signalling,* 2005(302), p. 46.

Garcia, M. & Kaczorowski, G., 2006. Critical success. *European Pharmaceutical Review,* Volume 11, pp. 42-45.

Garcia, M. & Kaczorowski, G., 2016. Ion channels find a pathway for therapeutic success. *PNAS,* 113(20), p. 5472–5474.

Geisse, S., Gram, H., Kleuser, B. & Kocher, H., 1996. Eukaryotic expression systems: a comparison. *Protein Expression and Purification,* 8(3), pp. 271-282.

Gellissen, G., 2005. *Production of recombinant proteins: novel microbial and eukaryotic expression systems.* s.l.:Wiley VCH.

Gillie, D. et al., 2013. Development of a high-throughput electrophysiological assay for the human ether-a-go-go related potassium channel hERG. *Journal of Pharmacological and Toxicological Methods,* 67(1), pp. 33-34.

Giraldez, T., Afonso-Oramas, D., Cruz-Muros, I. & Garcia-Marin, V., 2007. Cloning and functional expression of a new epithelial sodium channel delta subunit isoform differentially expressed in neurons of the human and monkey telencephalon. *Journal of Neurochemistry,* 102(4), p. 1304–1315.

Giraldez, T. et al., 2012. The epithelial sodium channel delta subunit: new notes for an old song. *American Journal of Physiology. Renal Physiology.,* 303(3), pp. 328-338.

Golubovic, A. et al., 2007. A peptide-gated ion channel from the freshwater polyp Hydra. *Journal of Biological Chemistry,* 282(48), pp. 35098-35103.

Gomes, A., Byregowda, S., Veeregowda, B. & Balamurugan, V., 2016. An overview of heterologous expression host systems for the production of recombinant proteins. *Advances in Animal and Veterinary Sciences,* 4(4), pp. 346-356.

Gonzales, E., Kawate, T. & Gouaux, E., 2009. Pore architecture and ion sites in acid-sensing ion channels and P2X receptors. *Nature,* 460(7255), pp. 599-604.

Gonzalez, J. et al., 1991. Cell-based assays and instrumentation for screening ion-channel targets. *Drug Discovery Today,* 4(9), pp. 431-439.

Graham, A. et al., 1993. No added benefit from nebulized amiloride in patients with cystic fibrosis. *The European Respiratory Journal,* 6(9), pp. 1243-1248.

Gregory, S. et al., 2006. The DNA sequence and biological annotation of human chromosome 1. *Nature,* 441(7091), pp. 315-321.

Gründer, S., Chang, S., Lifton, R. & Rossier, C., 1998. PHA-1: a novel thermosensitive mutation in the ectodomain of α-ENaC. *Journal of the American Society of Nephrology,* Volume 9.

Gründer, S. et al., 1997. A mutation causing pseudohypoaldosteronism type 1 identifies a conserved glycine that is involved in the gating of the epithelial sodium channel. *The EMBO Journal,* 16(5), pp. 899-907.

Gründer, S. & Pusch, M., 2015. Biophysical properties of acid-sensing ion channels (ASICs). *Neuropharmacology,* Volume 94, pp. 9-18.

Guha, R., 2013. On exploring structure activity relationships. *Methods in Molecular Biology,* Volume 993, pp. 81-94.

Guharay, F. & Sachs, F., 1984. Stretch-activated single ion channel currents in tissue-cultured embryonic chick skeletal muscle. *Journal of Physiology,* 352(1), pp. 685-701.

Haerteis, S., Krueger, B., Korbmacher, C. & Rauh, R., 2009. The delta-subunit of the epithelial sodium channel (ENaC) enhances channel activity and alters proteolytic ENaC activation. *Journal of Biological Chemistry,* 284(42), pp. 29024-29040.

Haines, J., Inglese, M. & Casaccia, P., 2011. Axonal damage in multiple sclerosis. *The Mount Sinai Journal of Medicine,* 78(2), pp. 231-243.

Hansch, C., Steward, A., Anderson, S. & Bentley, D., 1967. The parabolic dependence of drug action upon lipophilic character as revealed by a study of hypnotics. *Journal of Medicinal Chemistry*, 11, pp. 1–11.

Hanukoglu, A., 1991. Type I pseudohypoaldosteronism includes two clinically and genetically distinct enities with either renal or multiple target organ defects. *Journal of Clinical Endocrinology and Metabolism,* 73(5), pp. 936-944.

Hanukoglu, I. & Hanukoglu, A., 2016. Epithlial sodium channel (ENaC) family: phylogeny, structure-function, tissue distribution, and associated inherited diseases. *Gene,* 579(2), pp. 95-132.

Hanwell, D., Ishikawa, T. & Saleki, R., 2002. Trafficking and cell surface stability of the epithelial Na+ channel expressed in epithelial madin-darby canine kidney cells. *Journal of Biological Chemistry,* 277(12), pp. 9772-9779.

Hernandez-Gonzalez, E. et al., 2006. Sodium and epithelial sodium channels participate in the regulation of the capacitation-associated hyperpolarization in mouse sperm. *Journal of Biological Chemistry,* 281(9), pp. 5623-5633.

Herrington, J., McManus, O. & Kiss, L., 2005. The road ahead and how to get there. *European Pharmaceutical Review,* 10(3), pp. 79-84.

Hille, B., 1992. *Ion channels of excitable membranes.* Sunderland(MA): Sinauer Associates, Inc.

Hiroshi, I., 2011. Proton-binding sites of acid-sensing ion channel 1. *Plos One,* 6(2).

Hirsh, A. et al., 2004. Evaluation of second generation amiloride analogs as therapy for cystic fibrosis lung disease. *Journal of Pharmacology and Experimental Therapeutics,* 311(3), pp. 929-938.

Hobbs, C. et al., 2013. Identification of the SPLUNC1 ENaC-inhibitory domain yields novel strategies to treat sodium hyperabsorption in cystic fibrosis airway epithelial cultures. *American Journal of Physiology-Lung Cellular and Molecular Physiology,* 305(12), pp. 990-1001.

Hodgkin, A. & Huxley, A., 1939. Action potentials recorded from inside a nerve fiber. *Nature,* Volume 144, pp. 710-711.

Hodgkin, A. & Huxley, A., 1952. A quantitative description of membrane current and its application to conduction and excitation in nerve. *Journal of Physiology,* 117(4), pp. 500-544.

Hopkins, R., Wall, V. & Esposito, D., 2012. Optimizing transient recombinant protein expression in mammalian cells. *Methods in Molecular Biology,* Volume 801, pp. 251-268.

Hughes, J., Rees, S., Kalindjuan, S. & Philpott, K., 2011. Principles of early drug discovery. *British Journal of Pharmacology,* 162(6), pp. 1239-1249.

Hughey, R. et al., 2004. Epithelial sodium channels are activated by furin-dependent proteolysis. *Journal of Biological Chemistry,* 279(18), pp. 18111-18114.

Hummler, E. et al., 1996. Early death due to defective neonatal lung clearance in alpha-ENaC-defective mice. *Nature Genetics,* 12(3), pp. 325-328.

Hunt, T. et al., 2012. Discovery of a novel chemotype of potent human ENaC blockers using a bioisostere approach. Part 1: Quaternary amines. *Bioorganic & Medicinal Chemistry Letters,* 22(2), pp. 929-932.

Hunt, T. et al., 2012. Discovery of a novel chemotype of potent hyman ENaC blockers using a bioisostere approach. Part 2: alpha-branched quaternary amines. *Bioorganic Medicinal Chemistry Letters,* 22(8), pp. 2877-2879.

Hüser, A. & Hofmann, C., 2003. Baculovirus vectors: novel mammalian cell gene-delivery vehicles and their applications. *American Journal of Pharmacogenomics,* 3(1), pp. 53-63.

Invitrogen, 2012. *pENTR™ Directional TOPO® Cloning Kits.* [Online] Available at: https://assets.thermofisher.com/TFS-Assets/LSG/manuals/pentr_dtopo_man.pdf [Accessed 15th December 2014].

Invitrogen, 2014. *ViraPower™ BacMam Expression System and BacMam pCMV-DEST Vector Kit.* [Online] Available at: https://assets.thermofisher.com/TFS-Assets/LSG/manuals/virapower_BacMam_express_SystDEST_Kit_man.pdf [Accessed 15th December 2014].

Ismailov, I. et al., 1996. Identification of an Amiloride Binding Domain within the α-Subunit of the Epithelial Na+ Channel. *The Journal of Biological Chemistry,* 272(34), pp. 21075-21083.

Isom, L., 2001. Sodium channel beta subunits: anything but auxiliary. *Neuroscientist,* 7(1), pp. 42-54.

Jan, L. & Jan, Y., 1992. Tracing the roots of ion channels. *Cell,* 69(5), pp. 715-718.

Jasti, J., Furukawa, H., Gonzales, E. & Gouaux, E., 2007. Structure of acid-sensing ion channel 1 at 1.9 A resolution and low pH. *Nature,* 449(7160), pp. 316-323.

Ji, H. & Benos, D., 2004. Degenerin sites mediate proton activation of δβγ-epithelial sodium channel. *Journal of Biological Chemistry,* Volume 279, p. 26939–26947.

Ji, H. et al., 2004. The role of Pre-H2 domains of α- and δ-epithelial Na+ channels in ion permeation, conductance, and amiloride sensitivity. *Journal of Biological Chemistry,* 279(9), pp. 8428-8440.

Ji, H. et al., 2000. The cytosolic termini of the β- and γ-ENaC subunits are involved in the functional interactions between cystic fibrosis transmembrane conductance regulator and epithelial sodium channel. *Journal of Biological Chemistry,* Volume 275, p. 27947–27956.

Ji, H. et al., 2006. δ-subunit confers novel biophysical features to αβγ-human epithelial sodium channel (ENaC) via a physical interaction. *Journal of Biological Chemistry,* 281(12), pp. 8233-8241.

Ji, H. et al., 2012. δ ENaC: a novel divergent amiloride-inhibitable sodium channel. *American Journal of Physiology: Lung Cell Molecuar Physiology,* 303(12), pp. 1013-1026.

John, V. et al., 2007. Novel 384-well population patch clamp electrophysiology assays for Ca2+-Activated K+ channels. *Journal of Biomolecular Screening,* 12(1), pp. 50-60.

Kaczorowski, G., McManus, O., Priest, B. & Garcia, M., 2008. Ion channels as drug targets: the next GPCRs. *Journal of General Physiology,* 131(5), pp. 399-405.

Kashlan, O. et al., 2010. Allosteric inhibition of the epithelial Na+ channel (ENaC) through peptide binding at peripheral finger and thumb domains. *Journal of Biological Chemistry,* 285(45), p. 35216–35223.

Kashlan, O. et al., 2006. Distinct structural elements in the first membrane-spanning segment of the epithalial sodium channel. *Journal of Biological Chemistry,* 281(41), pp. 30445-30462.

Kellenberger, S. et al., 2001. Permeability properties of ENaC selectivity filter mutants. *Journal of General Physiology,* 118(6), pp. 679-692.

Kellenberger, S., Gautschi, I. & Schild, L., 1999. A single point mutation in the pore region of the epithelial Na+ channel changes ion selectivity by modifying sieving. *PNAS,* 96(7), pp. 4170-4175.

Kellenberger, S., Gautschi, I. & Schild, L., 2002. An external site control closing of the epithelial Na+ channel ENaC. *Journal of Physiology,* 543(2), pp. 413-424.

Kellenberger, S. & Schild, L., 2002. Epithelial sodium channel/degenerin family of ion channels: a variety of functions for a shared structure. *Physiological reviews,* 82(3), pp. 735-767.

Kelly, O. et al., 2003. Characterisation of an amiloride binding region in the a-subunit of ENaC. *American Journal of Renal Physiology,* 285(6), pp. 1279-1290.

Keppler-Noreuil, K., Carroll, A., Finley, W. & Rutledge, S., 1995. Chromosome 1p terminal deletion: report of new findings and confirmation of two characteristic phenotypes. *Journal of Medicine: Genetics,* 32(8), p. 619–622.

Keung Tai, K. & Truong, D., 2013. Amiloride but not memantine reduces neurodegeneration, seizures and myoclonic jerks in rats with cardiac arrest-induced global cerebral hypoxia and reperfusion. *Plos One,* 8(4), pp. 1-8.

Khan, K., 2013. Gene expression in mammalian cells and its applications. *Advanced Pharmaceutical Bulletin,* 3(2), pp. 257-263.

Kleyman, T., Carattino, M. & Hughey, R., 2009. ENaC at the cutting edge: regulation of epithelial sodium channels by proteases. *Journal of Biological Chemistry,* 284(31), pp. 20447-20451.

Kleyman, T. & Cragoe, E., 1988. Amiloride and its analogues as tools in the study of ion transport. *Journal of Membrane Biology,* 105(1), pp. 1-21.

Knight, K., Olson, D. & Zhou, R., 2006. Liddle's Syndrome mutations increase Na+ transport through dual effects on epithelial Na+ channel surface expression and proteolytic cleavage. *PNAS,* 103(8), pp. 2805-2808.

Knight, K., Wentzlaff, D. & Snyder, P., 2008. Intracellular sodium regulates proteolytic activation of the epithelial sodium channel. *Jounal of Biochemistry,* 283(41), pp. 27477-27482.

Knowles, M. et al., 1990. A pilot study of aerosolized amiloride for the treatment of lung disease in cystic fibrosis. *New England Journal of Medicine,* 322(17), pp. 1189-1194.

Koefoed-Johnsen, V. & Ussing, H., 1958. On the nature of the frog skin potential. *Acta Physiologica Scandinavica,* 42(3-4), pp. 298-308.

Kost, T. & Condreay, J., 1999. Recombinant baculoviruses as expression vectors for insect and mammalian cells. *Current Opinions in Biotechnology,* 10(5), pp. 428-433.

Lachnit, W., Xie, M., Curtis, R. & Castle, N., 2001. Drug discovery technology for ion channels. *Drug Discovery Today,* 6(1), pp. S17-S18.

Landro, J. et al., 2000. HTS in the new millennium: the role of pharmacology and flexibility. *Journal of Pharmacological and Toxicological Methods,* 44(1), pp. 273-289.

Landy, A., 1989. Dynamic, structural and regulatory aspects of lambda site-specific recomobination. *Annual Reviews: Biochemistry,* Volume 58, pp. 913-949.

Lefèvre, C. et al., 2014. Pharmacological and electrophysiological characterization of the human bile acidsensitive ion channel (hBASIC). *European Journal of Physiology,* 466(2), pp. 253-263.

Li, J., Cragoe, E. & Lindemann, B., 1985. Structure-activity relationship of amiloride analogs as blockers of epithelial Na channels: I. Pyrazine-ring modifications. *The Journal of Membrane Biology,* 83(1-2), pp. 45-56.

Lingueglia, E., Champigny, G., Lazdunski, M. & Barbry, P., 1995. Cloning of the amiloride-sensitive FMRFamide peptide-gated sodium channel. *Nature,* 378(6558), pp. 730-733.

Lingueglia, E. & Lazdunski, M., 2013. Pharmacology of ASIC channels. *WIREs Membrane Transport and Signaling,* 2(4), pp. 155-171.

Lipinski, C., Lombardo, F., Dominy, B. & Feeney, P., 2001. Experimental and computational approaches to estimate solubility and permeability in drug discovery and development settings. *Advanced Drug Delivery Reviews,* 46(1-3), pp. 3-26.

Li, T., Yang, Y. & Canessa, C., 2011. Outlines of the pore in open and closed conformation descrive the gating mechanism of ASIC1. *Nature Communications,* Volume 2, p. 399.

Liu, M. et al., 2016. Acid-sensing ion channel 1a contributes to hippocampal LTP inducibility through multiple mechanisms. *Scientific Reports,* 6(23350).

Lu, C. et al., 2007. The PY motif of ENaC, mutated in Liddle's Syndrome, regulates channel internalization, sorting and mobilization from subapical pool. *Traffic,* 8(9), pp. 1246-1264.

Ludwig, M. et al., 1998. Structural organisation of the gene encoding the alpha-subunit of the human amiloride-sensitive epithelial sodium channel. *Human Genetics,* 102(5), pp. 576-581.

Macarron, R. et al., 2011. Impact of high-throughput screening in biomedical research. *Nature Reviews Drug Discovery,* 10(3), pp. 188-195.

MacCoss, M. & Baillie, T., 2004. Organic chemistry in drug discovery. *Science,* 303(5665), pp. 1810-1813.

Maddox, C., Rasmussen, L. & White, E., 2008. Adapting cell-based assays to the high throughput screening platform: problems encountered and lessons learned. *JALA Charlottesv Va,* 13(3), pp. 168-173.

Mall, M. et al., 2004. Increased airway epithelial Na+ absorption produces cystic fibrosis-like lung disease in mice. *Nature Medicine,* 10(5), pp. 487-493.

Malys, N., Wishart, J., Oliver, S. & McCarthy, J., 2011. Protein production in Saccharomyces cerevisiae for systems biology studies. *Methods in Enzymology,* Volume 500, pp. 197-212.

Mansouri, M. et al., 2016. Gene expression in mammalian cells using BacMam, a modified baculovirus system. *Nature Communications,* 11529(1350), pp. 95-116.

Mathes, C., 2006. QPatch: the past, present and future of automated patch clamp. *Expert Opinion on Therapeutic Targets,* 10(2), pp. 319-327.

Mathes, C., Friis, S. & Finley, M., 2009. QPatch: the missing link between HTS and ion channel drug discovery. *Combinatorial Chemistry & High Throughput Screening,* 12(1), pp. 78-95.

McManus, O., 2014. HTS assays for developing the molecular pharmacology of ion channels. *Current Opinion in Pharmacology ,* 15(1), pp. 91-96.

Meuwis, K. et al., 1995. Photophysics of the fluorescent K+ indicator PBFI. *Biophysical Journal,* 68(6), pp. 2469-2473.

Minta, A. & Tsien, R., 1989. Fluorescent indicators for cytosolic sodium. *Journal of Biological Chemistry,* 264(32), pp. 19449-19457.

Mohamed, R., Degac, J. & Helms, V., 2015. Composition of overlapping protein-protein and protein-ligand interfaces. *Plos ONE,* 10(10).

Mollema, A., 2003. *Patch clamping: an introductory guide to patch clamp electrophysiology.* s.l.:John Wiley & Sons, Ltd.

Monnard, P. & Deamer, D., 2002. Memrbane self-assembly processes: steps toward the first cellular life. *The Anatomical Record,* 268(3), pp. 196-207.

Murer, H., Hopfer, U. & Kinne, R., 1976. Sodium/proton antiport in brush-border-membrane vesicles from rat small intestine and kidney. *Journal of Biochemistry,* 154(3), pp. 57-604.

Nakayama, Y., Yoshimura, K. & Iida, H., 2012. Organellar mechanosensitive channels in fission yeast regulate the hypo-osmotic shock response. *Nature Communications,* 3(1020).

Nassar, M., Levato, A., Stirling, L. & Wood, J., 2005. Neuropathic pain develops normally in mice lacking both Nav1.7 and Nav1.8. *Molecular Pain: SAGE Journals,* 1(24).

Neher, E. & Sakmann, B., 1976. Single-channel currents recorded from membrane of denervated frog muscle fibres. *Nature,* 260(5554), pp. 799-802.

Nernst, W., 1888. On the kinetics of bodies: the theory of diffusion. *Zeitschrift für Physikalische Chemie,* Volume 2, pp. 613-637.

Nicolotti, O., Giangreco, I., Miscioscia, T. & Carotti, A., 2009. Improving quantitative structure-activity relationships through multiobjective optimization. *Journal of Chemical Information and Modeling,* 49(10), pp. 2290-2302.

Olaharski, A. et al., 2006. The histone deacetylase inhibitor trichostatin a has genotoxic effects in human lymphoblasts in vitro. *Toxicological Sciences,* 93(2), pp. 341-347.

Olsen, R. & Sieghart, W., 2008. International Union of Pharmacology. LXX. Subtypes of γ-aminobutyric acid (A) receptors: classification on the basis of subunit composition, pharmacology, and function. *Pharmacological Reviews,* 60(3), pp. 243-260.

Overington, J., Al-Lazikani, B. & Hopkins, A., 2006. How many drug targets are there?. *Nature Reviews Drug Discovery,* 5(12), pp. 993-996.

Pajouhesh, H., Lenz, G., 2005. Medicinal chemical properties of successful central nervous system drugs. *NeuroRX,* 2(4), pp. 541-553.

Payandeh, J. et al., 2012. Crystal structure of a voltage-gated sodium channel in two potentially inactivated states. *Nature,* Volume 486, pp. 135-139.

Payandeh, J., Scheuer, T., Zheng, N. & Catterall, W., 2011. The crystal structure of a voltage-gated sodium channel. *Nature,* 475(7356), pp. 353-358.

Perniss, A. et al., 2015. Evans Blue is not a suitable inhibitor of the epithelial sodium channel δ-subunit. *Biochemical and Biophysical Research Communications,* 466(3), pp. 468-474.

PharmaFactz, 2018. *Drug design: structure activity relationships.* [Online] Available at: https://pharmafactz.com/drug-design-structure-activity-relationships/ [Accessed 18th July 2018].

Phorille, A., 2002. From organic molecules in space to the origins of life and back. *Advances in Space Research,* 30(6), pp. 1509-1520.

Pogozheva, L., Mosberg, H. & Lomie, A., 2014. Life at the border: adaption of proteins to anisotropic membrane environment. *Protein Science,* 23(9), pp. 1165-1196.

Pons, G. et al., 2000. French multicenter randomized double-blind placebo-controlled trial on nebulized amiloride in cystic fibrosis patients. *Pediatric Pulmonology,* 30(1), pp. 25-31.

Prakash, S. et al., 2010. Rare copy number variants disrupt genes regulating vascular smooth muscle cell adhesion and contractility in sporadic thoracic aortic aneurysms and dissections. *American Journal of Human Genetics,* 87(6), pp. 743-756.

PubChem, 2018. *PubChem CID 5951.* [Online] Available at: https://pubchem.ncbi.nlm.nih.gov/compound/L-serine [Accessed 28 August 2018].

PubChem, 2018. *PubChem CID 6106.* [Online] Available at: https://pubchem.ncbi.nlm.nih.gov/compound/6106 [Accessed 28 Aug 2018].

Ringer, S., 1983. A further contribution regarding the influence of the different constituents of the blood on the contraction of the heart. *Journal of Physiology,* 4(1), pp. 29-42.

Robinson, R. & Siegelbaum, S., 2003. Hyperpolarization-activated cation currents: from molecules to physiological function. *Annual Reveiw of Physiology,* Volume 65, pp. 453-480.

Rossier, B., 2002. Hormonal regulation of the epithelial sodium channel ENaC. *Journal of Genetic Physiology,* 120(1), pp. 67-70.

Rossier, B. & Stutts, M., 2009. Activation of the epithelial sodium channel (ENaC) by serine proteases. *Annual Review of Physiology,* Volume 71, pp. 361-379.

Ruppersberg, J. et al., 1990. Heteromultimeric channels formed by rat brain potassium-channel proteins. *Nature,* 345(6275), pp. 535-537.

Russ, T., Reid, W., Ullrich, F. & Mutschler, E., 1992. Preparation and diuretic properties of novel amiloride analogues. *Archiv der Pharmazie,* 325(12), pp. 761-767.

Sakai, H. et al., 1999. Cloning and functional expression of a novel degenerin-like Na+ channel gene in mammals. *Journal of Physiology,* 519(2), pp. 323-333.

Sandborn, E., Stephens, H. & Bendayan, M., 1975. The influence of dimethyl sulfoxide on cellular ultrastructure and cytochemistry. *ANNALS,* 243(1), pp. 122-138.

Saxena, A. et al., 1998. Gene structure of the human amiloride-sensitive epithelial sodium channel beta subunit. *Biochemical and Biophysical Research Communications,* 252(1), pp. 208-213.

Scannell, J. & Bosley, J., 2016. When quality beats quantity: decision theory, drug discovery, and the reproducibility crisis. *Plos One,* 11(2).

Schild, L., 1996. The ENaC channel as the primary determinant of two human diseases: Liddle syndrome and pseudohypoaldosteronism. *Nephrologie,* 17(7), pp. 395-400.

Schild, L., 2010. The epithelial sodium channel and the control of sodium balance. *Biochimica et Biophysica Acta (BBA) - Molecular Basis of Disease,* 1802(12), pp. 1159-1165.

Schild, L., Schneeberger, E., Gautschi, I. & Firsov, D., 1997. Identification of amino acid residues in the alpha, beta and gamma subunit of the epithelial sodium channel (ENaC) involved in amiloride block ad ion permeation. *Journal of Genetic Physiology,* 109(1), pp. 15-26.

Schroeder, K., Neagle, B., Trezise, D. & Worley, J., 2003. Ionworks HT: a new high-throughput electrophysiology measurement platform. *Journal of Biomolecular Screening,* 8(1), pp. 50-64.

Scott, D. et al., 2017. SPX-101 is a novel epithelial sodium channel–targeted therapeutic for cystic fibrosis that restores mucus transport. *American Journal of Respiratory and Critical Care Medicine,* 196(6), pp. 734-745.

Sheng, S., Bruns, J. & Kleyman, T., 2004. Extracellular histidine residues crucial for Na+ self-inhibition of epithelial Na+ channels. *Journal of Biological Chemistry,* 279(11), pp. 9743-9749.

Sheng, S. et al., 2006. Furin cleavage activates the epithelial Na+ channel by relieving Na+ self-inhibition. *American Journal of Renal Physiology,* 290(6), pp. 1488-1496.

Sheng, S., McNulty, K., Harvey, J. & Kleyman, T., 2001. Second transmembrane domains of ENaC subunit contribute towards ion permeation and selectivty. *Journal of Biological Chemistry,* 276(47), pp. 44091-44098.

Sheng, S., Perry, C., Kashlan, O. & Kleyman, T., 2004. Side chain orientation of residues lining the selectivity filter of epithelial Na+ channels. *Journal of Biological Chemistry,* 280(9), pp. 8513-8522.

Shen, H. et al., 2017. Structure of a eukaryotic voltage-gated sodium channel at near-atomic resolution. *Science,* 355(6328).

Siesjo, B. et al., 1995. Glutamate, calcium, and free radicals as mediators of ischemic brain damage. *The Annals of Thoracic Surgery,* 59(5), pp. 1316-1320.

Silver, I. & Erecinska, M., 1992. Ion homeostasis in rat brain in vivo: intra- and extracellular Ca2+ and H+ in the hippocampus during recovery from short-term, transient ischemia. *Journal of Cerebral Blood Flow and Metabolism,* 12(5), p. 759–772.

Simon, R., Swan, J., Griffiths, T. & Meldrum, B., 1984. Blockade of N-methyl-D-aspartate receptors may protect against ischemic damage in the brain. *Science,* 226(4676), pp. 850-852.

Smith, J., Karp, P. & Welsh, M., 1994. Defective fluid transport by cystic fibrosis airway epithelia. *The Journal of Clinical Investigation,* 93(3), pp. 1307-1311.

Snyder, P. et al., 1998. Electrophysiological and biochemical evidence that DEG/ENaC cation channels are composed of nine subunits. *Journal of Biological Chemistry,* 273(2), pp. 681-684.

Snyder, P. et al., 2004. cAMP and serum and glucocorticoid-inducible kinase (SGK) regulate the epithelial Na(+) channel through convergent phosphorylation of Nedd4-2. *Journal of Biological Chemistry,* 279(44), pp. 45753-45758.

Snyder, P. et al., 1995. Mechanism by which Liddle's syndrome mutations increase activity of a human epithelial Na+ channel. *Cell,* 85(6), pp. 969-978.

Staruschenko, A., Adams, E., Booth, R. & Stockand, J., 2005. Epithelial Na+ channel subunit stoichiometry. *Biophysical Journal,* 88(6), pp. 3966-3975.

Staub, O. et al., 1997. Regulation of stability and function of the epithelial Na+ channel (ENaC) by ubiquitination. *The EMBO Journal,* 16(21), pp. 6325-6336.

Stockand, J. et al., 2008. Insight toward epithelial Na+ channel mechanism revealed by the acid-sensing ion channel 1 structure. *IUBMB Life,* 60(9), pp. 620-628.

Studer, R., Person, E., Robinson-Rechavi, M. & Rossier, B., 2011. Evolution of the epithelial sodium channel and the sodium pump as limiting factors of aldosterone action on sodium transport. *Physiological Genomics,* 43(13), pp. 844-854.

Sudol, M., 1998. From Src Homology domains to other signaling modules: proposal of the `protein recognition code'. *Oncogene,* Volume 17, pp. 1467-1474.

Syberg, S., 2016. *RDMag: reducing the edge effect in cell culture microplates.* [Online] Available at: https://www.rdmag.com/article/2016/10/reducing-edge-effect-cell-culture-microplates
[Accessed July 2018].

Tapper, A. & George Jr, A., 2003. Heterologous expression of ion channels. In: *Neurogenetics.* New York: Springer, pp. 285-294.

Tarran, R. et al., 2001. The CF salt controversy: in vivo observations and therapeutic approaches. *Molecular Cell,* 8(1), pp. 149-158.

Tarran, R. & Redinbo, M., 2014. Mammalian short palate lung and nasal epithelial clone 1 (SPLUNC1) in pH-dependent airway hydration. *The International Journal of Biochemistry & Cell Biology,* Volume 52, pp. 130-135.

Thomas, C., Doggett, N., Fisher, R. & Stokes, J., 1996. Genomic organistaion of the 5' flanking region of the gamma subunit of the human amiloride-sensitive epithelial sodium channel. *Journal of Biological Chemistry,* Volume 271, pp. 26062-26066.

Tikhonov, D. & Zhorov, B., 2017. Mechanism of sodium channel block by local anesthetics, antiarrhythmics, and anticonvulsants. *Journal of General Physiology,* 149(4), pp. 465-481.

Tousson, A. et al., 1989. Immunochemical localisation of amiloride-sensitive sodium channels in transporting epithelia. *Journal of Cell Science,* Volume 93, pp. 349-362.

Valler, M. & Green, D., 2000. Diversity screening versus focused screening in drug discovery. *Drug Discovery Today,* 5(7), pp. 286-293.

van De Sluis, B. et al., 2002. Identification of a new copper metabolism gene by positional cloning in a purebred dog population. *Human Molecular Genetics,* 11(2), pp. 165-173.

van der Zwaag, B. et al., 2009. Gene-network analysis identifies susceptibility genes related to glycobiology in autism. *Plos ONE,* 4(5), p. 5324.

Velumian, A., Zhang, L., Pennefather, P. & Carlen, P., 1997 . Reversible inhibition of IK, IAHP, Ih and ICa currents by internally applied gluconate in rat hippocampal pyramidal neurones.. *Pflügers Archiv: European Journal of Physiology,* 433(3), pp. 343-350.

Venanzi, C., Plant, C. & Venanzi, T., 1992. Molecular recognition of amiloride analogs: a molecular electrostatic potential analysis. 1. Pyrazine ring modifications. *Journal of Medicinal Chemistry,* 35(9), pp. 1643-1649.

Vergo, S. et al., 2011. Acid-sensing ion channel 1 is involved in both axonal injury and demyelination in multiple sclerosis and its animal model. *Brain,* 134(2), pp. 571-584.

Verrey, F., 1999. Early aldosterone action: toward filling the gap between transcription and transport. *American Journal of Physiology,* 277(3), pp. 319-327.

Vidt, D., 1981. Mechanism of action, pharmacokinetics, adverse effects, and therapeutic uses of amiloride hydrochloride, a new potassium-sparing diuretic. *Pharmacotherapy,* 1(3), pp. 179-187.

Voilley, N. et al., 1994. The lung amiloride-sensitive Na+ channel: biophysical properties, pharmacology, ontogenesis, and molecular cloning. *PNAS,* 91(1), p. 247–251.

von Heijne, G., 1992. Membrane protein structure prediction. Hydrophobicity analysis and the positive-inside rule. *Journal of Molecular Biology,* 225(2), pp. 487-494.

Vukicevic, M. et al., 2006. Trypsin cleaves acid-sensing ion channel 1a in a domain that is critical for channel gating. *Journal of Biological Chemistry,* 281(2), pp. 714-722.

Vukicevic, M. et al., 2006. Trypsin cleaves acid-sensing ion channel 1a in a domain that is critical for channel gating. *Journal of Biological Chemistry,* 281(2), pp. 714-722.

Vyacheslavova, A. et al., 2012. Expression of heterologous genes in plant systems: New possibilities. *Russian Journal of Genetics,* 48(11), pp. 1067-1079.

Waggoner, A., 1976. Optical probes of membrane potential. *Journal of Membrane Biology,* 27(1), pp. 317-334.

Waldmann, R. et al., 1995. Molecular cloning and functional expression of a novel amiloride-sensitive Na+ channel. *Journal of Biological Chemistry,* 270(46), pp. 27411-27414.

Waldmann, R., Champigny, G. & Lazdunski, M., 1995. Functional degenerin-containing chimeras identify residues essential for amiloride-sensitive Na+ channel function. *Journal of Biological Chemistry,* 270(20), pp. 11735-11737.

Waldmann, R. et al., 1991. H+-gated cation channels. *ANNALS,* Volume 868, pp. 67-76.

Waugh, D., 2005. Making the most of affinity tags. *Trends in Biotechnology,* 23(6), pp. 316-320.

Wemmie, J. et al., 2002. The acid-activated ion channel ASIC contributes to synaptic plasticity, learning, and memory. *Neuron,* 34(3), pp. 463-477.

Wesch, D. et al., 2012. Differential N termini in epithelial Na+ channel δ-subunit isoforms modulate channel trafficking to the membrane. *American Journal of Physiology: Cell Physiology,* Volume 302, pp. 868-879.

Wesch, D. et al., 2010. The neuronal-specific SGK1.1 kinase regulates {delta}-epithelial Na+ channel independently of PY motifs and couples it to phospholipase C signaling. *American Journal of Physiology Cell physiology ,* 299(4), pp. 779-790.

Wiemuth, D. et al., 2012. BASIC—a bile acid-sensitive ion channel highly expressed in bile ducts. *Federation of American Societies for Experimental Biology,* 26(10), pp. 4122-4130.

Yamamoto-Hino, M. et al., 1994. Cloning and characterization of human type 2 and type 3 inositol 1,4,5-trisphosphate receptors. *Receptors Channels,* 2(1), pp. 9-22.

Yamamura, H. et al., 2004. Protons activate the δ-subunit of the epithelial Na+ channel in humans. *Journal of Biological Chemistry,* 279(13), p. 12529–12534.

Yamamura, H. et al., 2006. A novel spliced variant of the epithelial Na+ channel δ-subunit in the human brain. *Biochemical and Biophysical Research Communications,* 349(1), pp. 317-321.

Yamamura, Y., Ugawa, S., Ueda, T. & Shimada, S., 2005. Evans blue is a specific antagonist of the human epithelial Na+ channel delta-subunit. *Journal of Pharmacology and Experimental Therapeutics,* 315(2), pp. 965-969.

Yang, S., 2010. Pharmacophore modeling and applications in drug discovery: challenges and recent advances. *Drug Discovery Today,* 15(11-12), pp. 444-450.

Yu, H., Li, M., Wang, W. & Wang, X., 2016. High throughput screening technologies for ion channels. *Acta Pharmacologica Sinica,* 37(1), pp. 34-43.

Zelle, K., Lu, B., Pyfrom, S. & Ben-Shahar, Y., 2013. The genetic architecture of degenerin/epithelial sodium channel in Drosophila. *G3: Genes, Genomes, Genetics,* 3(3), pp. 441-450.

Zhanga, Z. et al., 2012. Quality control of cell-based high-throughput drug screening. *Acta Pharmaceutica Sinica B,* 2(5), pp. 429-438.

Zhao, R. et al., 2012. Characterization of a novel splice variant of δ ENaC subunit in human lungs. *American Journal of Physiology: Lung Cellular and Molecular Physiology,* 302(12), pp. 1262-1272.

Zhorov, B. & Tikhonov, D., 2004. Potassium, sodium, calcium and glutamate-gated channels: pore architecture and ligand action. *Journal of Neurochemistry,* 88(4), pp. 782-799.

Zhou, Z. et al., 2008. Preventive but not late amiloride therapy reduces morbidity and mortality of lung disease in bENaC-overexpressing mice. *American Journal of Respiratory and Critical Care Medicine,* 178(12), pp. 1245-1256.

Appendix 1. Chemical structure of hits from IonWorks Quattro™ assay. Hits showing above 30% inhibition relative to amiloride are highlighted in yellow.

Structure	Compound ID	MWt
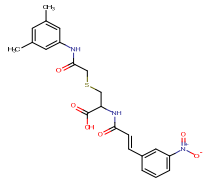	BCC0038980	457.4995
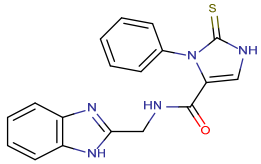	BCC0124878	349.4172
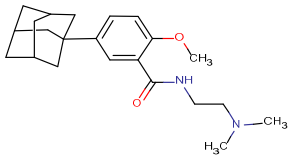	BCC0061379	356.5017
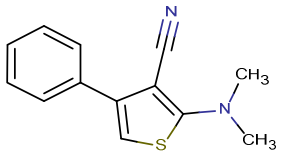	BCC0038451	228.3128
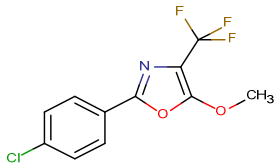	BCC0047500	277.627
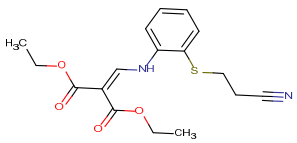	BCC0030370	348.4167
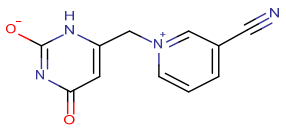	BCC0032822	229.2148

Structure	Compound ID	MWt
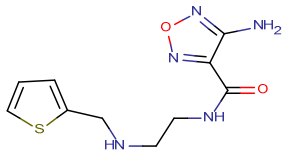	BCC0061738	267.3075
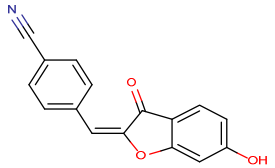	BCC0000082	263.255
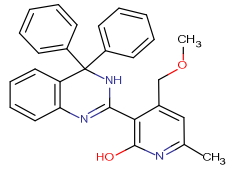	BCC0039343	435.517
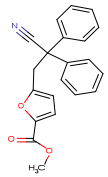	BCC0120577	331.3745
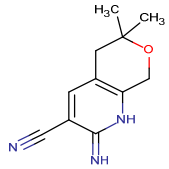	BCC0031815	203.2404
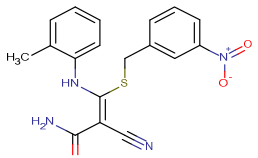	BCC0038894	368.4096
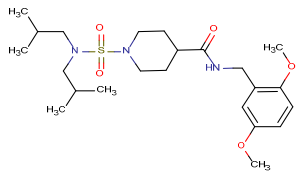	BCC0054890	469.6379